Proteomic Characterisation of Patient Samples Diagnosed with Haematological Malignancies

Ciara Tierney, BSc.

January, 2020.

Maynooth University
National University of Ireland Maynooth

Thesis submitted to Maynooth University for the degree of Doctor of Philosophy

Supervisor.
Dr. Paul Dowling,
Dept. of Biology,
Maynooth University,
Maynooth,
Co. Kildare,
Ireland

Co-Supervisor
Prof. Peter O Gorman
Dept of Haematology,
Mater Misericordiae Hospital,
Dublin 7,
Ireland

Head of Department
Prof. Paul Moynagh
Dept. of Biology
Maynooth University,
Maynooth,
Co. Kildare,
Ireland

Table of Contents

Declaration

This thesis has not previously been submitted in whole or part to this, or any other University, for any other degree. This thesis is original work of the author, except where stated otherwise.

Signed:

_____

Ciara Tierney, B.Sc.

Date:

_____

Abbreviations

1D-GE	One-dimensional Gel Electrophoresis
2D-GE	Two-Dimensional Gel Electrophoresis
Ab	Antibody
AGE	Advanced Glycation Endproducts
AML	Acute Myeloid Leukaemia
ANOVA	Analysis of variance
ASCT	Autologous Stem-Cell Transplantation
Asp	Aspartate
AUC	Area under the curve
BM	Bone Marrow
BMT	Bone Marrow Trephine
BSA	Bovine serum albumin
Bz	Bortezomib
BzR	Bortezomib Resistance
CA	Carbonic Anhydrase
Cfz	Carfilzomib
CML	Chronic Myeloid Leukaemia
CNS	Central Nervous System
CR	Complete Response
CRAB	Hypercalcaemia, Renal Impairment, Anaemia, Lytic Bone Lesions
CysC	Cystatin C
Da	Dalton
DFCI	Dana-Farber Cancer Institute
dH_2O	Distilled water
DIGE	Fluorescence Difference In-Gel Electrophoresis
DSRT	Drug sensitivity and resistance testing
DSS	Drug Sensitivity Screening
DSSS	Durie-Salmon Staging System
DTT	Dithiothreitol
Dx	Diagnosis
ECM	Extracellular matrix
EGF	Epidermal Growth Factor
ELISA	Enzyme linked immunosorbent assay
ELN	European LeukemiaNet
EMW	European Myeloma Network

FAB	French-American British classification system
FABP	Fatty Acid Binding Protein
FASP	Filter aided sample preparation
FIMM	Institute of Molecular Medicine, Helsinki, Finland
FISH	Fluorescent in Situ Hybridisation
FLC	Free Light Chain
g	Grams
g/dL	Grams Per Decilitre
G	g force
GO	Gene Ontology
Gt	Goat
H	Hour(s)
HCl	Hydrochloric acid
HDACi	Histone deacetylase inhibitor
His	Histidine
HSP	Heat Shock Protein
HR	High Risk
HRP	Horse radish peroxidase
IAA	Iodoacetamide
IHC	Immunohistochemistry
IL	Interleukin
IMiD	Immunomodulator (Lenalidomide/ Thalidomide)
IMWG	International Myeloma Working Group
ISS	International Staging System
IV	Intravenous
Kb	Kilobase
kDa	Kilo Daltons
KEGG	Kyoto encyclopaedia of gene and genomes
L1CAM	L1 Cell Adhesion Molecule
LC-MS/MS	Liquid chromatography tandem mass spectrometry
Len	Lenalidomide
LFQ	Label-free quantification
M	Molar
mAb	Monoclonal Antibody
MSC	Mesenchymal Stromal Cells

MGUS	Monoclonal Gammopathy of Undetermined Significance
Min	Minute(s)
MIP-1α	Macrophage Inflammatory Protein-1α
Ml	Millilitre(s)
Mm	Millimetre(s)
mM	Millimolar
MM	Multiple Myeloma
M-protein	Monoclonal Protein
MR	Minimal response
MRD	Minimum residual disease
Ms	Mouse
MS	Mass spectrometry
MW	Molecular weight
m/z	Mass/charge ratio
NFκB	Nuclear factor-kappaB
nM	Nanomolar
Nx	Navitoclax
OC	Oral Cancer
OS	Overall survival
OSCC	Oral Squamous Cell Carcinoma
pAb	Polyclonal antibody
PANTHER	Protein analysis through evolutionary relationships
PBS	Phosphate buffered saline
PD	Progressive Disease
p*I*	Isoelectric point
PI	Proteasome inhibitor
PO_4	Phosphate group
Ppm	Parts per million
PR	Partial Response
Pt.	Patient
PTM(s)	Post-translations Modification(s)
Quiz	Quizinostat
Rb	Rabbit
RISS	Revised International Staging System
ROC	Receiver operating characteristic

RsqVD	Treatment using Revlimid (Lenalidomide) and subcutaneous Velcade (Bortezomib) and Dexamethasone.
RRMM	Relapse/refractory multiple myeloma
RVD	Revlimid (Lenalidomide), Velcade (Bortezomib), Dexamethasone
S	Second(s)
SD	Stable Disease
SDF	Stromal Derived growth Factor
SDS	Sodium dodecyl sulphate
SDS-PAGE	Sodium dodecyl sulphate polyacrylamide gel electrophoresis
Ser	Serine
SMM	Smouldering multiple myeloma
SP	Solitary Plasmacytoma
SR	Standard Risk
STRING	Sequential window acquisition of all theoretical fragment ion spectra
sq	Subcutaneous
TCP4	Activated RNA polymerase II transcriptional
TFA	Trifluororacetic acid
TGM3	Transglutaminase-3
Thr	Threonine
Tyr	Tyrosine
V	Volts
VDR	Velcade (Bortezomib) and Dexamethasone resistant (also MM.1VDR)
VEGF	Vascular Endothelial Growth Factor
VGPR	Very good partial response
WHO	World Health Organisation
β2M	β_2-microglobulin
µg	Micrograms
µl	Microlitre
µm	Micrometre

Index of Figures

Index of Tables

Publications

Research Papers

Tierney, C., Bazou, D., Majumder, M.M., Anttila, P., Silvennoinen, R., Heckman, C.A., Dowling, P. and O'Gorman P. Combining Next Generation Proteomics Platforms with Drug Sensitivity Screening allows Identification of Physiologically Distinct Sub-clones that can inform Therapeutic and Drug Development Strategies for patients with Multiple Myeloma. *Scientific Reports*. **Submitted as of 11/05/2020.**

Tierney, C., Bazou, D., Lê, G., Dowling, P. and O'Gorman, P. Saliva-Omics in Plasma Cell Disorders- Proof of Concept and Potential as a Non-Invasive Tool for Monitoring Disease Burden. *Journal of Proteomics*. **In review as of 23/04/2020**.

Tierney, C., Dowling, P., Bazou, D., Heckman C.A. and O'Gorman, P. Evaluation of Cellular and Secreted Proteins Associated with Different Prognostic Risk Groups in Acute Myeloid Leukemia. *European Journal of Cell Biology*. **Manuscript prepared for submission.**

Silva, L.P., Frawley, D., José da Silva, L., **Tierney, C**., Fleming, A.B., Bayram, O. and Goldman, G. Membrane receptors contribute to activation and efficient signalling of Mitogen-Activated Protein Kinase cascades during adaptation of Aspergillus fumigatus to different stressors and carbon sources. *mBio*. **In review as of 29/04/2020.**

Conferences

2019	17th International Myeloma Workshop, International Myeloma Society, Boston, MA, USA. **Two Poster Presentations.**
2019	Irish Mass Spectrometry Society Annual Conference, Dublin, Ireland. **Attended.**
2018	60TH ASH Annual Meeting and Exposition, American Haematology Society, San Diego, CA, USA. **Two Poster Presentation.**

2017 HUPO 2017: 16th Annual Human Proteome Organization World Congress, Convention Centre, Dublin, Ireland. **Poster Presentation.**

Presentations

Poster Presentations

Saliva-Omics in Plasma Cell Disorders- Proof of Concept and Potential As a Non-Invasive Tool for Monitoring Disease Burden and MRD Status. **Ciara Tierney,** Despina Bazou, Giao Le, Paul Dowling and Peter O'Gorman. 17th International Myeloma Workshop, International Myeloma Society, Boston, MA, USA.

Combining Next Generation Proteomic Platforms with Drug Sensitivity Resistance Testing allows Identification of Physiologically Distinct Sub-clones that can inform Therapeutic and Drug Development Strategies. Despina Bazou, Muntasir M. Majumder, **Ciara Tierney,** Sinead O'Rourke, Pekka Anttila, Raija Silvennoinen, Caroline A. Heckman, Paul Dowling and Peter O'Gorman. 17th International Myeloma Workshop, International Myeloma Society, Boston, MA, USA.

Salivaomics-based Biomarker Discovery for Disease Progression in Multiple Myeloma. **Ciara Tierney,** Despina Bazou, Giao Le, Paul Dowling and Peter O'Gorman. 60TH ASH Annual Meeting and Exposition, American Haematology Society, San Diego, CA, USA.

Discovery Proteomics, in Combination with Drug Sensitivity Scoring, for the Identification of Distinct Sub-clones that can inform Therapeutic and Drug Development Strategies. Despina Bazou, Muntasir M. Majumder, **Ciara Tierney,** Sinead O'Rourke, Pekka Anttila, Raija Silvennoinen, Caroline A. Heckman, Paul Dowling and Peter O'Gorman. 60TH ASH Annual Meeting and Exposition, American Haematology Society, San Diego, CA, USA.

Combatting Drug Resistance in Multiple Myeloma. **Ciara Tierney**, Muntasir M. Majumder, Despina Bazou, Caroline A. Heckman, Paul Dowling and Peter O'Gorman. HUPO 2017: 16th Annual Human Proteome Organization World Congress, Convention Centre, Dublin, Ireland.

Acknowledgements

Firstly, I would like to my supervisor Dr. Paul Dowling. Thank you for believing in my abilities enough to agree to be my supervisor, for your endless support, advice, wisdom and especially your encouragement over the last three years. Thank you for everything PhD related but, most importantly, thank you for being a friendly face to chat to when things just weren't working out. You're knowledge of proteomics is endless, I will never not be impressed by your ability to pick a random protein from a list of thousands and know its exact function or your ability to remember the details of my project, even when I couldn't. It has been an absolute pleasure working under your guidance, I am eternally grateful for everything!

Thank you to Professor Peter O'Gorman for co-supervising me throughout my project. I really appreciate all of your guidance and encouragement over the last three years.

A huge thank you to Dr. Despina Bazou. You have been my mentor over the last three years, even if you didn't realise you were, and I am eternally grateful for everything you have done for me. Your advice has been amazing, you've always had a word of wisdom to help me. It was a pleasure working with you.

Thank you to Prof. Kevin Kavanagh and Dr. James Carolan for agreeing to be on my assessment team and for all of your advice throughout my PhD. Thank you to all members of the Biology Department at Maynooth University for all of your help throughout the years, it's been a pleasure. A big thank you to Dr. Annemarie Larkin for allowing me to use the auto-stainer in DCU and your hospitality for the couple of weeks that I spent there.

To all the other labs, thank you all so much for all the laughs at tea and lunch and, of course, nights out! You all have made doing a PhD a little easier. Special thanks to Sarah, Merissa, and Anatte for all the laughs and all the tea!! To Felipe, you're kind words and support, even from Brazil, have always put a smile on my face. Thank you for being great. Thank you Dr. Sandra for showing me the ropes in the lab and never getting sick of my constant questions.

To Laura (AKA Toby, AKA Tobs), your support has been endless throughout my PhD and I can't thank you enough for that. Thank you for telling me that I'm fab and I CAN

do it when I doubted myself, for always being up for a shopping trip or a notions day in town, for always being a source of laughter and thank you for just being great. Couldn't have done it without you, Girl!
Claire, Sarah and Rachel, thank you for always being there, no matter what.
Thank you to Conor and Adrian for all of your support over the last couple of years. I promise I will finally start to pay attention to our FF league, the comeback is on Lads!

To the dearest, best friends a girl could ever ask for, Dean and Peter!! Thank you, from the bottom of my heart, for absolutely everything you have both done for me. I can't begin to put into words how much you both mean to me. You have made the final year of my PhD an absolute pleasure. Thank you for supporting me through everything, making me cry with laughter, cheering me up constantly, being my cheerleaders, roast chicken rolls for dinner, saving me from spiders (by punching them), all our movie nights and sleepovers, supplying me with all the fun(gal) facts and a place to run to when I just needed the chats and to procrastinate. I don't know if I could have survived my PhD without a fun fact of the day. I attribute finally getting this thesis written to midnight batch toast with loads of Kerrygold butter!! I couldn't love either of you more than I do! You better not replace me when I'm gone. Xoxo Tierno!

Finally, thank you to my amazing family. To my grandad, if it wasn't for all that change I took on you as a kid I wouldn't be where I am today!! To my gran, thank you for always having the kettle on and listening to all of my problems. To my Brother, Antoinette, Max, Ava and Ruby Mae, thank you for all of your support and always making me laugh. To my mam and dad, your support throughout this PhD has been endless and I can't thank you both enough for that. Your wisdom, love and constant sense of fun have kept me going through all the twists and turns that have been the last 3 years! Thank you for being fantastic parents, for always encouraging me and thank you, most importantly, for being amazing friends! I love you both so much and I couldn't have done this without you both!

Abstract

Multiple myeloma (MM) is the second most commonly diagnosed lymphoid cancer worldwide, after non-Hodgkin's lymphoma, and is characterised by the uninhibited proliferation of terminally differentiated B-lymphocytes. The proliferation of these mutated plasma cells leads to the secretion of monoclonal proteins, resulting in mutated heavy/light chain immunoglobulin formation. Characterised by serum albumin levels, serum beta-2-microglobulin levels and hypercalcemia, renal impairment, anaemia, bone lesions (CRAB criteria), MM is diagnosed as stage Ⅰ, Ⅱ or Ⅲ. Even with a multitude of new, novel treatments developed for MM, although OS has increased significantly, MM is considered an incurable disease as the vast majority of patients go into relapse. With the use of label-free liquid chromatography mass spectrometry, proteomic analysis was carried out on MM patient samples with varying drug resistance. Vinculin, talin-1, filamin A and integrin β3 were identified as having an increased abundance in drug resistance in 4 of the 6 drugs tested. Activated RNA polymerase II transcriptional coactivator p15 118 phosphoserine and heat shock protein 27 phosphoserine 78 were identified as having a changed abundance between sensitive and resistant patients. Fatty acid binding protein 5 was detected in saliva as having a significant increase in abundance throughout disease progression of MM. Macrophage inflammatory protein 1α is predicted to play a significant role in the development of adverse side effects, after Rsq-VD treatment, with an observed increased abundance in all patients who developed toxicity throughout the clinical trial. CD44 is also predicted to have potential as a biomarker for poor outcome after Rsq-VD treatment. Multiple proteins were identified as differentially abundant in Group 1 (favourable) to Group 3 (Adverse) in acute myeloid leukaemia (AML), stromal derived growth factor 1 being of particular interest in this study. Overall this work shows proteomic techniques can be used to identify potential biomarkers for haematological malignancies.

Chapter 1

Introduction

1.1 Overview of Multiple Myeloma

1.1.1 Introduction

With an estimated rate of diagnosis of 159,985 cases globally in 2018 (Bray et al., 2018), Multiple Myeloma (MM) is thought to be the second most highly diagnosed lymphoid cancer, after non-Hodgkin Lymphoma (Becker, 2011). It has been observed that approximately 5 in every 100,000 cancer cases diagnosed in Ireland are MM cases, with approximately 240 cases diagnosed annually. MM is included in a spectrum of disease ranging from monoclonal gammopathy of undetermined significance (MGUS) to plasma cell leukaemia. The rate of diagnosis accounts for roughly 1% of all newly diagnosed cancer cases annually and has a 5 year survival rate of 45% (Rajkumar, 2016). Characterised by anaemia, renal failure, infection and commonly bone disease, MM most commonly affects patients over the age of 60, with only 2% of reported cases affecting those under the age of 40. MM is known as a cancer of unrestrained proliferation of terminally differentiated B-lymphocytes (plasma cells), accumulating in the bone marrow. The cancer cells have been known to crowd healthy blood cells and instead of producing normal antibodies, monoclonal proteins (M proteins) are produced. The production of these leads to the inability to fight infection and kidney damage. These M proteins are secreted by the mutated plasma cells, resulting in mutated heavy and/or light chain immunoglobulin formation. This formation causes differing isotopes of MM. These isotypes are IgG kappa myeloma, IgA kappa myeloma, IgA lambda myeloma, light chain myeloma or IgD myeloma. Light chain MM is diagnosed by the presence of free light chain kappa or lambda detection in serum or urine.

1.1.2 Monoclonal Gammopathy of Unknown Significance

MGUS, the early indolent form of monoclonal plasma cell proliferation which leads to the development of MM, is characterised by the detection of a monoclonal protein in the blood of a patient without any other signs and symptoms of MM. MGUS is considered the premalignant form of MM, with approximately 1% of MGUS patients progressing to MM annually (Kyle et al., 2006), and 93% of MM patients exhibiting M protein production associated with MGUS within 7 years before MM diagnosis (Kyle et al., 2004). It has been observed that approximately 6% of "well" people between the ages of 60 to 80 years account for the incidence of MGUS (Crawford et al., 1987). In 1984 it was predicted that approximately 3.2% of the white general population, over 50 years of age, in western countries have MGUS (Kyle, 1984). MGUS is distinguished from MM on the percentage of monoclonal plasma cells in the bone marrow (BM) of patients, with <10% diagnosed as MGUS and ≥10% diagnosed as MM. A serum concentration of M protein of <3g/dL and no anaemia, lytic bone lesions, hypercalcemia and renal failure are also associated with MGUS (Group, 2003) (Table 1.1).

1.1.3 Smouldering (Asymptomatic) Multiple Myeloma

Smouldering MM (SMM) is considered the intermediate form of MM, being characterised by a high level (3g/dL or more) of M protein in serum or urine and a ≥10% monoclonal plasma cells in the bone marrow (BM) (Kyle et al., 2004) (Table 1.1). SMM patients exhibit no additional MM defining characteristics. The risk of SMM progressing to MM is significantly higher than that of MGUS, with approximately 10% of SMM disease progression per year (Lisch et al., 2016). 80% to 90% of SMM patients progress to active MM within two years, and therefore require treatment. There has, however, been a subset of SMM patients identified as a higher risk group

with a median time to disease progression less than 2 years (Cherry et al., 2013). The three subtypes of SMM are IgA, IgG and light chain SMM, with median time to progression as 27, 75 and 159 months respectively. Treatment strategy for SMM is currently a strategy of “watch and wait”, with initial blood tests taken every 2-3 months for the first year after SMM diagnosis, every 4-6 months for the following year and 6-12 if clinical stability is established (Kyle et al., 2010). Solitary Plasmacytoma (SP) is a malignant monoclonal plasma cell spectrum with a low concentration of M protein in serum and urine, an absence of MM related characteristics (CRAB features) and no evidence of monoclonal plasma cells in the BM but with a bone lesion with monoclonal plasma cell proliferation.

1.1.4 CRAB Criteria, MM Biomarkers and Clinical Presentation

MGUS and SMM are both diagnosed according to the level of M protein in serum by serum protein electrophoresis, along with the percentage of monoclonal plasma cells in the BM. However, calcium, creatine, haemoglobin, Bence-Jones proteins and serum free light chain levels are also taken into account during diagnosis. Through disease progression, a change in the levels of the aforementioned, along with exhibiting CRAB criteria are used to restage disease. In 2005, serum β_2-microglobulin (β2M) and serum albumin were used to develop the International Staging System (ISS), allowing the prediction of disease stage and long-term prognosis of patients by clinicians (Greipp et al., 2005). Patients with a serum albumin measurement greater than or equal to 3.5g/dL and a serum β2M lower than 3.5mg/L are by definition stage 1 disease. Stage 3 disease is defined as having a serum β2M level greater than 5.5mg/L. Stage 2 disease is defined as a serum albumin or β2M level not fulfilling either stage 1 or stage 3 disease. In 2014 the criteria for diagnosis of MM changed from **CRAB** features (hyper**c**alcemia, **r**enal failure, **a**naemia and osteolytic **b**one

lesions) to include specific biomarkers defining the disease (Rajkumar et al., 2014). The three biomarkers used for diagnosis of MM are “clonal bone marrow plasma cells greater than or equal to 60%, serum free light chain (FLC) ratio greater than or equal to 100 provided involved FLC level is 100 mg/L or higher, or more than one focal lesion on MRI”, according to Rajkumar et al (Table 1.1). These features manifest as fatigue due to anaemia, bone pain, fractures and weakening due to bone lesions, anuria (failure of the kidneys to produce urine) or oliguria (significant decrease in the volume of urine produced) due to renal impairment occasionally leading to a dialysis requirement, perioral paraesthesia due to hypercalcaemia, altered immunity causing frequent infection and autonomic neuropathy causing numbness, loss of strength and tingling.

Although the identification of CRAB criteria, along with previously mentioned biomarkers in serum, have vastly improved the speed of diagnosis of MM and is considered the most useful predictor of disease progression, these identifiers are not reliable in 100% of cases. Some patients have been noted as presenting active MM symptoms without previous diagnosis of MGUS/SMM. Patients have been recorded as presenting to clinic with the presence of M protein levels in serum or urine, >10% monoclonal plasma cells in the BM, along with the presence of end organ damage i.e. CRAB criteria. Patients have also been diagnosed with MM due to hypercalcaemia or loss of renal function which are unexplained. Liver profile testing has also aided in the diagnosis, leading to the identification of increased serum protein, with a significant globulin-to-total protein ratio.

Table 1.1: Diagnosis Criteria for MGUS, SMM and MM as outlined by the International Myeloma Working Group (IMWG).

*Table was adapted from (Kumar et al., 2017)

Disorder	Disease Definition
Non-IgM MGUS	• Serum monoclonal protein <3g/dL (non-IgM) • Clonal BM plasma cells <10% • Absence of end-organ damage e.g. CRAB criteria
IgM MGUS	• Serum IgM monoclonal protein <3g/dL • BM lymphoplasmacytic infiltration <10% • No anaemia, constitutional symptoms, hyperviscosity, lymphadebopathy or hepatosplenomegaly caused by underlying lymphoproliferative disorder.
Light-chain MGUS	• Abnormal free light chain ratio (<0.26 or >1.65) • Increases level of light chain (increased kappa free light chain with ratios >1.65 and lambda free light chain with ratio <0.26) • No immunoglobulin heavy chain or immunofixation • No end-organ damage e.g. CRAB criteria • Clonal BM plasma cells <10% • Urinary M protein <500 mg/24h
SMM	• Serum M protein >3g/dL or urinary M protein >500mg/24h and/or clonal BM plasma cells 10%-60% • No myeloma defining symptoms e.g. CRAB criteria
MM	• Clonal BM plasma cells >10% or biopsy proven bony or extramedullary plasmacytoma

	One or more: • End organ damage due to plasma cell proliferation • Hypercalcemia • Renal impairment • Anaemia • Bone lesions • Clonal BM plasma cells>60% • Involved : uninvolved serum free light chain ratio >100 (involved free light chain levels must be >100mg/L) • More than one focal lesion greater than 5mm

1.1.5 Management/Treatment of MM

In 2014, the European Myeloma Network (EMN) established guidelines for the maintenance of newly diagnosed MM. Initial staging should be carried out as the International Staging System and the cytogenetic profile of the patient should be identified using fluorescent in situ hybridisation (FISH), to distinguish between high risk (HR) and standard risk (SR) patients. After patient staging, induction therapy is recommended using a triple regime, including a proteasome inhibitor (PI) such as bortezomib, a glucocorticoid such as dexamethasone and one of adriamycin /thalidomide/cyclophosphamide. Autologous stem cell transplant (ASCT), a process in which healthy blood stem cells are taken from the patient and used to replace diseased bone marrow, is recommended directly after induction therapy with the prerequisite that the patient must be deemed fit to undergo the procedure. Subsequent thalidomide or lenalidomide based therapy must be administered as a

form of maintenance therapy, provided that a satisfactory response is achieved. Following a less than excellent response after ASCT, bortezomib is recommended. Patients who are deemed unfit or ineligible for ASCT are generally treated with bortezomib/thalidomide, along with melphalan and prednisolone. When ineligible patients achieve satisfactory response to treatment, lenalidomide alone or in combination with low dosage dexamethasone is recommended for maintenance of MM.

1.1.6 MM Staging

The Durie-Salmon Staging System (DSSS) and the International Staging System (ISS) have both been established to aid in consistency of staging MM worldwide. The DSSS was established in 1975 and was commonly used to stage MM (Durie and Salmon, 1975) until, with developing technologies and knowledge of the disease, the ISS was established in 2005 with much more in-depth, updated criteria for staging (Figure 1.1). The DSSS is used to predict overall survival, tumour mass and therefore disease stage, by measuring the levels of immunoglobulin and haemoglobin from serum. This information is combined with calcium concentration and the prevalence and amount of bone lesions (Hari et al., 2009). The ISS identified serum β_2-microglobulin and serum albumin were identified by this study as potential prognostic factors due to the reproducibility, the inexpensive testing and the statistical significance of both in various models. Stage Ⅰ, Ⅱ, Ⅲ are distinguishable by the levels of these markers, stage Ⅰ exhibiting levels of serum β_2-microglobulin <3.5 mg/l and serum albumin ≥ 3.5 g/dL, stage Ⅱ exhibiting levels of serum β_2-microglobulin <3.5mg/L but serum albumin <3.5g/dL or serum β_2-microglobulin levels of 3.5 to <5.5mg/L and stage Ⅲ exhibiting serum β_2-microglobulin ≥5.5 mg/L. These staging

groups exhibit a median overall survival of 62 months, 44 months and 29 months respectively (Greipp et al., 2005). The ISS has been widely adapted due to the validation in subsequent studies, ease to compute and the even distribution of patients in the three established staging (Hungria et al., 2008).

In 2016 an updated version of the ISS (RISS) was established to combine the criteria established by the ISS (serum β_2-microglobulin and serum albumin levels along with other elements of tumour burden) with MM biology, including the cytogenetic factors and abnormalities associated with HR disease and elevated lactate dehydrogenase level. This combination of factors have shown a 5-year survival rate of 82%, 62% and 40% for stage Ⅰ, Ⅱ and Ⅲ respectively using the RISS (Rajkumar, 2016).

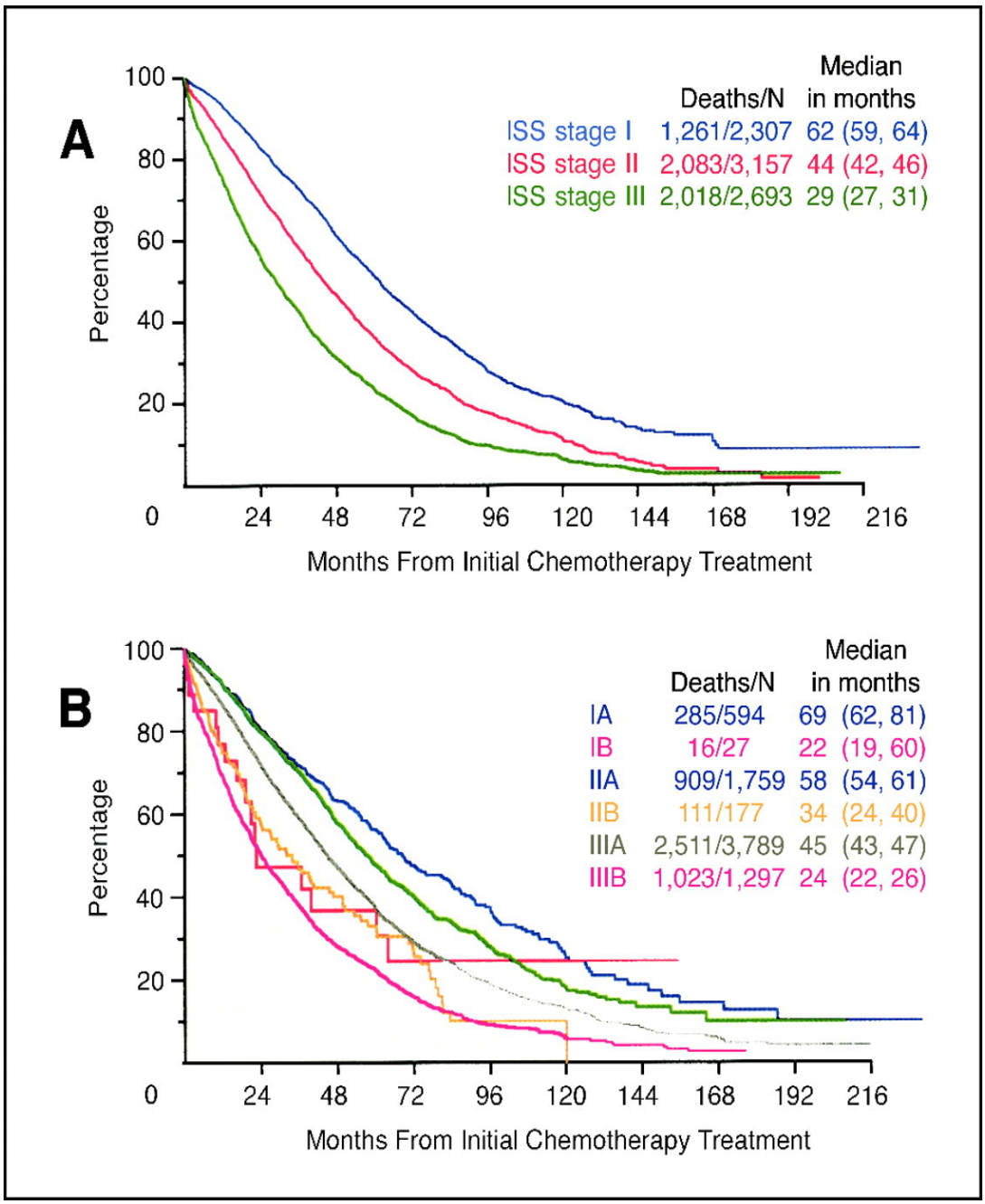

Figure 1.1: Comparison of both ISS and DSSS comparing OS of patients in with varying stage diagnosis.

A is the overall survival by ISS staging system and B is overall survival by DSSS staging system. ISS staging provides a more equal distribution across the three staging groups, making this method of staging more desirable.

*Figure 1.1 was taken from (Greipp et al., 2005)

1.1.7 Relapse and Refractory MM

Along with CRAB criteria for newly diagnosed MM and in-depth guidelines for the diagnosis of MGUS and SMM, specific criteria have been established for the diagnosis of relapse and refractory MM (RRMM). Although vast improvements in the treatment of MM have been observed since the introduction of these novel drugs, vastly high rates of relapse and refractory disease have been recorded and linked to resistance to these novel drugs. It has been recorded that, although large numbers of patients experience long periods of remission, RRMM is imminent for high-risk MM. To establish patient response, MM is staged by clinicians after treatment, ranging from complete response (CR), very good partial response (VGPR), partial response (PR), stable disease (SD), minimal response (MR) and progressive disease (PD). Staging is carried out after in-depth analysis of reduction of BM clonal plasma cells numbers, reduction of M-protein levels in serum or urine, free light chain assay reduction and lack of soft tissue plasmacytomas. These response guidelines were established by the IMWG to ensure consistency worldwide.

Relapsed MM is diagnosed due to increased disease burden and/or new or worsening CRAB criteria. This is generally diagnosed after remission or lessening symptoms of MM response to treatment. This is quantified as one or more of ≥25% difference between involved and uninvolved serum-free light chain, ≥25% M protein increase in serum, evidence of newly developed hypercalcaemia/ extramedullary plasmacytoma or >10% absolute percentage increase of BM plasma cells (Sonneveld, 2017). Relapse can be divided into three separate categories, symptomatic relapse, biochemical relapse and aggressive relapse, defined by the IMWG. Biochemical relapse is diagnosed in the case that there are no symptoms defining criteria present other than an increased concentration of M proteins. Symptomatic relapse is diagnosed due to disease progression along with significant

organ compromise and slow progression of MM criteria, along with a slowly increasing concentration of M proteins. Both biochemical and symptomatic relapse are considered non-aggressive relapse. Aggressive relapse is diagnosed by high lactate dehydrogenase, high serum β_2-microglobulin or low serum albumin, presence of extramedullary disease and circulating plasma cells. Along with this isoform transformation, adverse cytogenetic abnormalities, ISS staging of Ⅱ or Ⅲ at relapse and showing signs of rapid onset of symptoms are considered aggressive relapse symptoms. Finally, extensive MM related finding by radiography, laboratory or pathology examination and organ impairment related to MM are determining factors or aggressive relapse (Laubach et al., 2016).

RRMM is defined as the case where MM patients become unresponsive to therapy or, in patients who achieve MR or better to prior treatment, show signs of disease progression while receiving therapy or within 60 days of last treatment (Anderson et al., 2008). Chemotherapy can be used to salvage patients response to previous treatment, however, in RRMM, response is negligible or MM symptoms progress during the 60 days prior to treatment.

RRMM is a common problem in MM patients, bringing its own set of further complications in the disease. Although massive advances have been made in recent years in the treatment of MM, with the introduction of new novel agents for treatment, the vast majority of MM patients will eventually reach a stage of RRMM. It was observed, in a study totalling 286 patients, that the average event free survival for patients with RRMM who were refractory to bortezomib and/or resistant to immunomodulatory drugs (IMiD) or with intolerance/ineligibility to IMiD drugs was 5 months. These patients were observed to have an average overall survival of 9 months, with survival from diagnosis averaging at 4.7 years. 9 months was the overall survival for both refractory to bortezomib patients and refractory/intolerant to IMiD drugs (Kumar et al., 2012) (Figure 1.2).

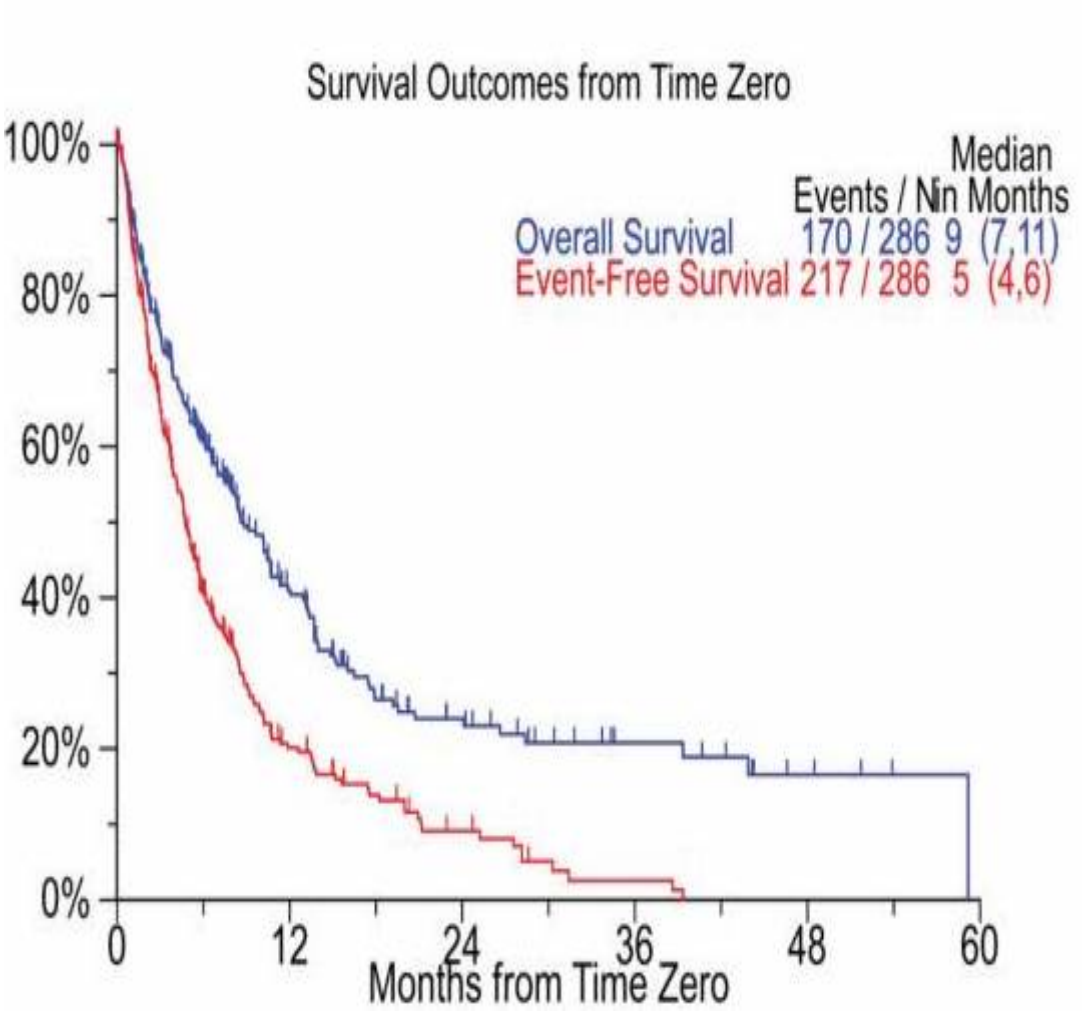

Figure 1.2: Overall survival outcomes of patients with refractory disease to bortezomib and immunomodulatory drugs.

The mean overall survival was observed to be 9 months for refractory disease for each treatment regime. Time zero is defined as the patient was i) refractory to bortezomib and/or ii) resistant to an IMiD or iii) intolerant or ineligible to treatment using an IMiD.

*Figure 1.2 was taken from (Kumar et al., 2012)

1.1.8 Overview of Cytogenetic Factors Associated with MM

With varying OS time for patients ranging from 6 months to greater than 15 years, it has been observed that this variability has arisen from the heterogeneity in monoclonal plasma cell biology along with varying genetic factors of subcategories of patients. In-depth analysis of CD138+ monoclonal plasma cells from MM samples has been carried out to establish genetic abnormalities to aid in the evaluation of patient response to treatment and, also, to predict disease susceptibility using standard cytogenetic or FISH. Two distinct genetic groups were established: hyperdiploid or hypodiploid. Translocations such as t(4:14) and t(14;16) are considered hypodiploid translocations and are both associated with an overall worse prognosis, whereas t(11;14) translocations are known as hyperdiploid translocations (Sawyer, 2011). MM has also been associated with secondary aberrations, generally involving deletions such as del13q and del1p or the amplification of 1q. Del17p has been strongly associated with very poor prognosis, therefore, require an aggressive clinical treatment course it has been suggested that this deletion is a prerequisite for clonal expansion of MM tumours (Fonseca et al., 2009).

Whole genome sequencing was carried out on 38 MM patients to evaluate the genetic aberrations related to the pathogenesis of MM. 11 distinct mutations implicated the activation of NF-κB in the pathogenicity of MM, along with the demonstrated mutations of BRAF kinase in 4% of patients (Chapman et al., 2011). This mutation had not, previously, been implicated in the pathogenicity of MM and predicts that BRAF kinase targeting using BRAF inhibitors has high potential as a possible MM target, a treatment which is a currently used for metastatic malignant melanoma (Bollag et al., 2012).

1.2 The Bone Marrow Microenvironment in MM Pathogenesis

The bone marrow (BM) microenvironment and its role in MM proliferation has been studied extensively due to the nature of the disease. The BM has been observed to have a protective effect on clonal plasma cells in MM, specifically the protection stromal cells and osteoclasts provide, aiding in the survival of these MM cells. Stromal cells directly interact with clonal plasma cells via adhesion molecules on the cell surface, subsequently inducing the activation of NF-κB and upregulation of interleukin-6. Both of these have previously been implicated in malignant plasma cell clone survival (Zhou et al., 2005).

Osteoclasts have been observed to be one of the leading causes of lytic lesions in MM. In normal bone, osteoclasts breakdown or remodel damaged bone, leading to the activation of osteoblasts and allowing the repair of bone damage. Osteoblast activity is suppressed in MM, leading to the breakdown of bony tissue by osteoclasts and the inability to remodel and repair by osteoblasts and the formation of the MM characteristic of lytic lesions (Hideshima et al., 2007). MM cells attach to osteoclasts by adhesion molecules, such as vascular cell adhesion molecule-1 (VCAM-1), resulting in osteoclastogenesis (Michigami et al., 2000). A subsequent reduction in osteoprotegerin results in the increased survival of myeloma cells and the increased production of osteoclasts. As osteoprotegerin promotes the remodelling of bone tissue via osteoblasts, the reduced production of this molecule results in the inhibition of bone repair after osteoclast bone degradation (Pearse et al., 2001). It has also been observed that co-culturing MM cells with osteoclasts in-vitro reduces MM cell apoptosis and increases MM cell viability, in comparison to cultured MM cells in isolation (Yaccoby et al., 2004).

1.3 Proteomics

OMICs based approaches for analysis of unknowns is a vastly expansive field with unlimited potential. Proteomics, a wide scale study of proteins, has become a key technology in the analysis of biofluid, cells, tissue or organisms. Proteomic analysis identifies protein abundance, localisation, structure, protein-protein interactions and post-translational modifications. The study of proteins is a direct result of wide scale nucleotide sequencing of genomic DNA and expressed sequence tags. The identification of the 20,700 approx. protein coding genes present in the human genome led to the identification of over 100,000 protein isoform translations (Lander, 2011). After establishing this, it became apparent that proteomics allows a deeper insight to organism, cellular and tissue response to changing environments, stimuli, stress and disease, therefore proving just as important as genomics.

Proteomic workflows generally rely on the separation of proteins from an original source, either by the means of gel or gel free separation, leading to either targeted or discovery mass spectrometry (MS) of the protein or peptide fragments. Identification of these isolated proteins/peptide fragments is then carried out by searching against a Uniprot database of protein sequences, allowing protein identification (Figure 1.3). A plethora of analytical software programs have been established to identify protein abundance, post-translational modifications (PTMs) and protein interactions. Two possible MS approaches can be used for protein identification, top-down identification and bottom-up identification. Top-down identification analyses intact proteins, leading to a superior sequence coverage as biochemical properties and PMTs are preserved (Catherman et al., 2014). Allowing full characterisation of proteoforms and 100% sequence coverage, top-down proteomics has been considered a viable approach to protein identification. However, top-down proteomic through put, proteome coverage and sensitivity has fallen behind

bottom-up approaches. Generally, a bottom-up, mass spectrometry based method is employed for proteomic analysis. Bottom-up proteomics depends on the enzymatic cleavage of protein samples to simplified peptides, which are then analysed by liquid chromatography mass spectrometry (LC-MS/MS). The resulting output relies heavily on the LC-MS/MS instrument and the database search engine, which evaluates the mass spectra and converts to peptide sequences. This evaluation allows the identification of proteins from which the peptide has been cleaved (Lane, 2005). Although the most commonly used approach, a number of disadvantages are apparent from the use of bottom-up proteomics. As large sections of proteins may not be identified by MS, this may omit valuable information such as PMTs or sequence variants.

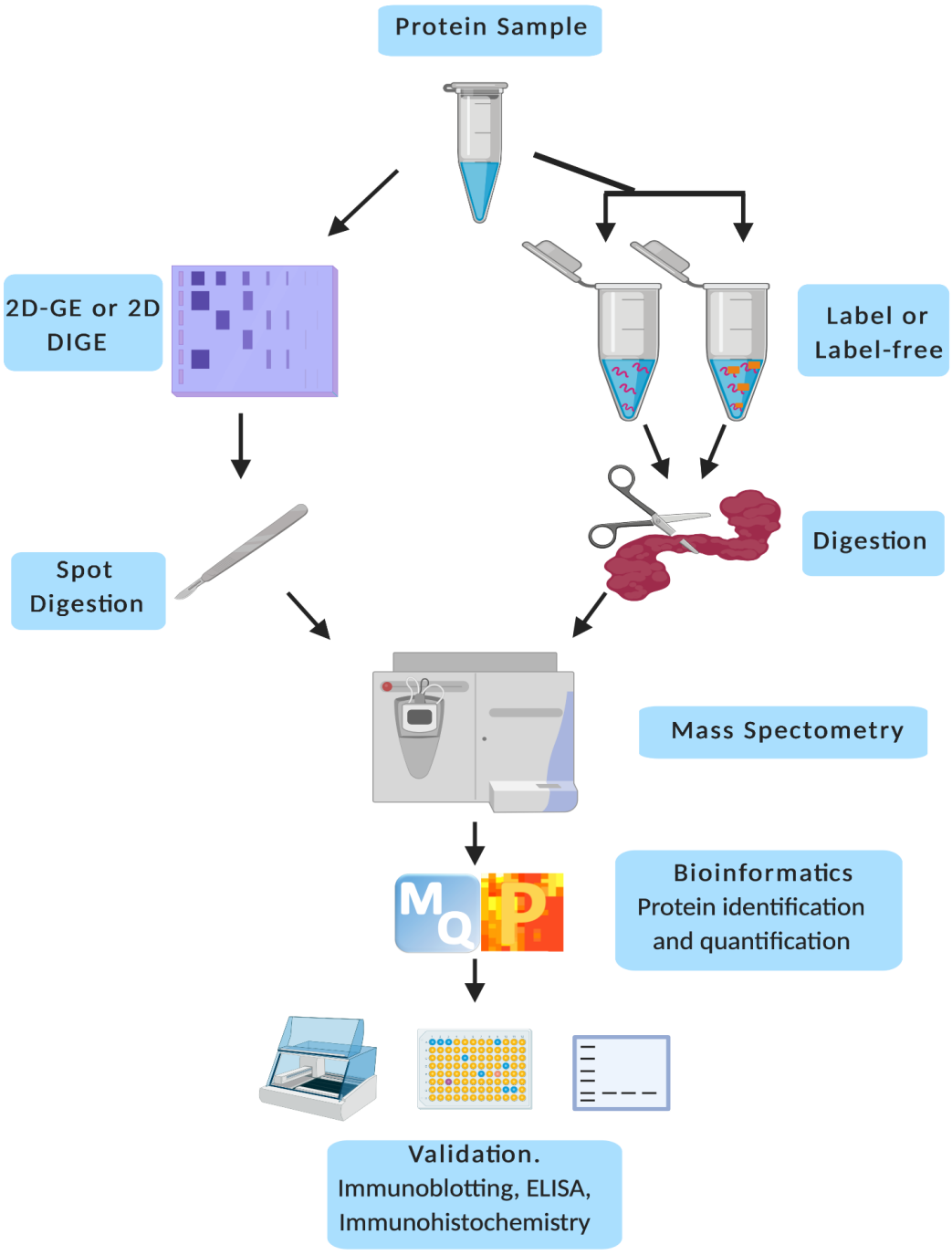

Figure 1.3: Overview of gel-free versus gel mass spectrometric analysis.

The flow chart above depicts the main steps involved in the proteomic analysis of samples. Samples can be processed using either gel based or gel-free method. Gel-free approaches require either label or label-free methods. Figure was created with Biorender.

1.3.1 Gel Electrophoresis

Gel electrophoresis was the origin of the first form of proteomic analysis carried out. The proteomic profiles of *E. coli* (O'Farrell, 1975), mouse (Klose, 1975) and guinea pig (Scheele, 1975) were identified in 1975, using two dimensional gel electrophoresis (2D-GE), allowing the visualisation and separation but the identification of each individual protein was not possible. 2D-GE combines isoelectric focusing with gel electrophoresis, separating proteins firstly by isoelectric point (p*I*) and, secondly, by molecular mass. By loading samples onto a thin strip of polyacrylamide gel, with a fixed pH, and subjecting the gel to isoelectric focusing, proteins will migrate through the gel to their p*I* value (Rabilloud and Lelong, 2011). A *pI* value is the pH at which the net charge of the protein is 0. The strips are then reduced, alkylated and loaded onto a polyacrylamide slab for molecular mass separation, the second dimension. The gel is subjected to an electrical current (polyacrylamide gel electrophoresis or PAGE), allowing proteins with a smaller molecular mass to migrate further through the gel and proteins with a larger molecular mass to migrate less (Ohlendieck, 2011). To visualise this protein migration the gel must be stained, pre- or post-electrophoresis, which is dependent on i) the sensitivity of detection required, ii|) the concertation of protein initially loaded onto the gel and iii) the downstream application. These stained, migrated proteins can be excised from this gel, digested into peptides and mass spectrometry identification can be carried out. One dimensional gel electrophoresis (1D-GE) separates proteins purely based on their molecular mass, in a similar process to the second dimension mentioned above in 2D-GE. The initial samples are loaded onto a polyacrylamide gel and the gel is subjected to an electrical current, allowing the proteins to migrate through the gel based on their molecular mass. Larger proteins will not migrate as far through the

gel as smaller proteins. Again, these proteins can be excised, digested and further identified by mass spectrometry analysis.

Standard 2D-GE approaches to protein separation has been observed to under represent particular protein classes, such as highly hydrophobic membrane proteins, proteins with a high molecular mass and low copy number of proteins, along with noted variations from gel-to-gel, making reproducibility increasing difficult. Fluorescence difference in-gel electrophoresis (DIGE) was developed in 1997 to combat the variation that arises in gel-to-gel when using 2D-GE (Unlü et al., 1997). Fluorescent tags are added to the samples prior to isoelectric focusing, using two different cyanine CyDye DIGE fluor dyes, allowing the quick identification of proteins (Lewis et al., 2012). As the dyes are different colours, samples can be run on the same gels, therefore reducing variability and increasing reproducibility. The addition of a pooled internal standard, labelled with a third CyDye, allows the accurate quantification of protein expression changes as well as assessment of experimental and biological variation (Tannu and Hemby, 2006).

1.3.2 Label-free Liquid Chromatography Mass Spectrometry (LC-MS/MS)

One of the most important events in the field of proteomics was the development of mass spectrometry. MS technological advances, along with growing bioinformatic platforms, have increased sensitivity and protein detection, reliability, efficiency and reproducibility. As opposed to gel based protein detection, LC-MS/MS utilises in-solution protein digestions to identify an extensively vast array of proteins. Proteins with high molecular mass, low copy number proteins, proteins with an extreme p*I*, integral membrane proteins and PTMs are all easily detectable and identified using LC-MS/MS, leading to the subsequent replacement of gel-based approaches in many

areas of proteomics (Dowling et al., 2014b). LC-MS/MS separates digested peptides by liquid chromatography and analyses this by tandem mass spectrometry.

Two possible quantitative LC-MS/MS methods can be used: labelled and label-free. Labelled methods, such as ICAT (Isotope-Coded Affinity Tag), SILAC (Stable Isotope Labelling with Amino acids in Cell culture) and iTRAQ (isobaric Tags for Relative and Absolute Quantitation), incorporate metabolic and chemical labelling of proteins/peptides in advance of MS analysis. The quantity of these peptides/proteins is analysed by the mass increase of relative signal intensities and labels between the labelled and unlabelled proteins. Label-free methods quantify protein abundance based on the difference between MS peptide ion intensities or spectral counts from varying samples (Ramasamy et al., 2014). Label-free methods give bias free proteomic analysis as there is an absence of labelled peptides, the reduction of sample contamination and handling, therefore increasing through put. To quantify peptides, identify peptides to proteins and carry out statistical testing on the differently abundant proteins, a plethora of different bioinformatic software packages are available. All the above technologies are combined to form a comprehensive platform for proteomic analysis, used for biomarker discovery for diagnosis and prognosis of disease and understanding disease systems (Dowling et al., 2014a).

1.4 Biomarkers

According to the National Institute of Health Biomarkers Definition Working Group, biomarkers, or biological markers, are defined as characteristic molecules or genes that can be objectively quantified as a marker of standard biological processes, response to therapeutics for disease or pathological processes. These are reproducible and can be accurately quantified (Group., 2001). Biomarkers have potential to be used for situations such as diagnosis and prognosis of disease,

monitoring of response and disease progression, giving greater insight into potential personalised medicine and a measurement of clinical endpoint. Clinical endpoints are considered endpoints to any clinical research and are variables that encompass a patients overall wellbeing and health at the end of clinical research e.g. overall survival, as opposed to biomarkers which quantify a characteristic of disease but do not account for subject wellbeing (Group, 2016). A broader definition was coined by the World Health Organisation (WHO), the United Nations and International Labour Organization, which stated that biomarkers are defined as "any substance, structure, or process that can be measured in the body or its products and influence or predict the incidence of outcome or disease" (Strimbu and Tavel, 2010). This extended definition not only focuses on disease related outcomes but includes interventions, effects from treatment and environmental factors and is considered to encompass all measurable interactions involving a biological system and potential hazard. This measurable interaction includes cellular level biochemical interactions, functional and physiological integrations or molecular interactions (Strimbu and Tavel, 2010).

Biomarkers have been considered as surrogates endpoints, especially in the case of use in clinical trials. Biomarkers focus solely on the physiological and molecular changes of disease without accounting for patient wellbeing changes. For consideration as a biomarker, the specific characteristic of disease must accurately and consistently predict change and clinical outcome in the vast majority of the population, therefore allowing a biomarker to act as an alternative to clinical endpoints (Califf, 2018). As an alternative to clinical endpoints, biomarkers can predict more information about disease progression and treatment strategies, therefore reducing long term harm to the subjects. Biomarkers as surrogate biomarkers must prove relevance, referring to the ability to provide clinical applicability to disease, and validity, referring to the effectiveness of the potential biomarker, before consideration as an endpoint alternative. Biomarkers should be, ideally, highly sensitive, non-invasive, diagnostically conclusive, characteristic of specific disorders, disease

progression specific and be cost sensitive, enabling worldwide testing for the specific disease (Ohlendieck, 2013).

Biomarkers can be classified into four types: diagnostic, prognostic, predictive, and therapeutic.

· A diagnostic biomarker allows the early detection of the cancer in a non-invasive way and thus the secondary prevention of the cancer.

· A predictive biomarker allows predicting the response of the patient to treatment (targeted) and identify cohorts of patients that are likely going to benefit from a specific therapeutic intervention.

· A prognostic biomarker is a clinical or biological characteristic that provides information on the likely course of the disease and will provide information about the outcome of the patient (may be associated with cancer grade, low-high).

· A therapeutic biomarker is generally a protein that could be used as target for a therapy.

1.4.1 Biomarker Discovery via Proteomics

Proteomics has become an established and reliable tool for high through put discovery of protein changes in disease and health, due to its unbiased nature. The establishment of the Human Proteome Organisation (HUPO) in 2001 has greatly advanced the field of proteomics for human health, with particular emphasis on the human proteome project. The human proteome project was formed to map the entire human proteome, aiding in the understanding of disease and increasing the ability to fight disease. Urine and serum were a primary focus of the human proteome project

as non-invasive biofluids as a source of potential biomarkers (Farrah et al., 2014). As proteomics is considered an unbiased, high throughput, large scale method of the detection of proteins, the identification of particular protein targets or biomarkers in the fight against disease has become a topic of great interest. Serum, plasma, urine and saliva are the ideal source of protein biomarkers, due to the less-invasive sample collection methods, although tissue samples (biopsies) and proximal fluid may also be a source of biological markers. Due to the invasive nature of sample collection of both tissue samples and proximal fluid, both are deemed less suitable than the aforementioned biofluids.

Protein biomarker discovery involves four stages before a predicted biomarker is considered for clinical use. Stage 1 is known as the discovery stage. This is the stage at which potential protein biomarkers are identified, generally through the use of mass spectrometry. Stage 2 is considered the qualification stage, where differentially abundant proteins of interest are identified from all of the quantified proteins from mass spectrometry using specific targeted methods. Stage 3 is known as the verification stage. At this stage the identified potential protein biomarkers are examined in a population derived cohort of human samples. Stage 4 is the validation stage. This stage is where the potential protein biomarkers are examined with emphasis on disease specificity and sensitivity. If these criteria are fulfilled then the development of a clinical assay can be optimised for clinical use (Paulovich et al., 2008) (Figure 1.4). Protein biomarker discovery has been recorded as being largely successful until stage 3, verification, where a large variation in protein abundance is evident due to a general human population of samples (Rifai et al., 2006). The “bottleneck” effect that occurs at stage 3 of biomarker discovery may be overcome by the use of multiple reaction monitoring, which enables the quantitative analysis of hundreds of proteins at once (Whiteaker et al., 2007a).

Although proteomic biomarker discovery seems very promising for early detection of disease, prediction of prognosis and drug response, a number of challenges must be

overcome. Biofluids are vastly complex and dynamic, with an abundance of information to be discovered in minimum amounts of sample. As mentioned above, variation in the human population causes great disparity between samples, making the discovery of one single protein/group of proteins characteristic for a specific disease in the majority of the population almost impossible, especially as it is considered that there is a low abundance of disease specific protein biomarkers. Biomarker discovery is also faced with limited resources, with minimal high-quality antibody assays available. ELISA assay are generally used in evaluating potential biomarkers, limiting the selection of potential biomarkers to assays available. ELISA can be relatively high-throughput and sensitive in targeting analytes but developmental costs and long assay development times can provide another limiting factor in the validation of potential biomarkers (Whiteaker et al., 2007b). Generally an emphasis is put on a biomarker that is known to relate to the disease in question, however, this biological information may be limited for a vast number of conditions. However, with considering these limiting factors, proteomic based biomarker discovery is still a relatively new field of discovery. As proteomic based research progresses, technology and resource availability will increase, leaving infinite room from improvement in diagnosis, prognosis and therapeutic evaluation.

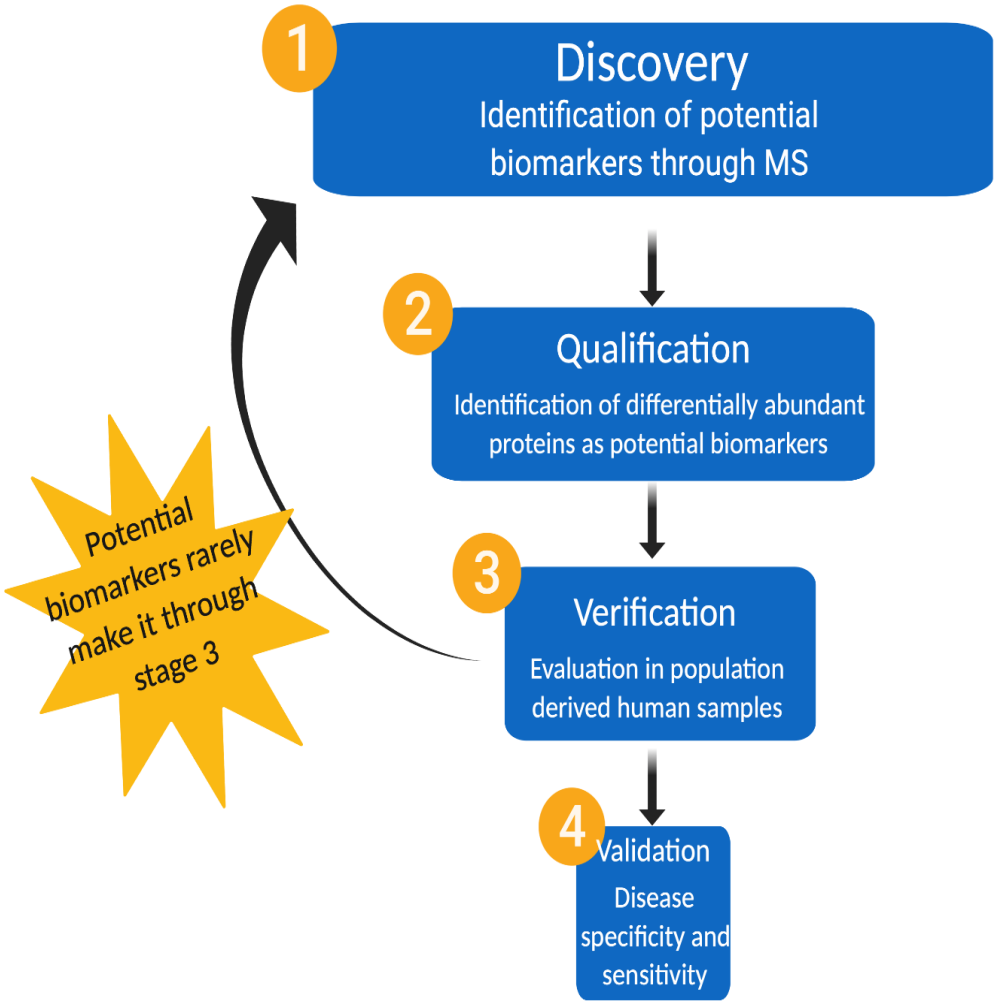

Figure 1.4: Overview of Protein Biomarker Discovery Stages.

Depicted above is a guide to the workflow involved in protein biomarker discovery, stage 1-4, and the process carried out for each step. The majority of protein biomarkers do not make it through the verification as they fail to show significance in a population derived human study. Figure was created using Biorender.

1.5 Aims of the Project

To:

- Compare and contrast the proteomic signatures of the 10 most and 10 least sensitive MM patients to a panel of 6 therapeutic regimes. These include novel, conventional and investigative therapies.

- Identify potential targets to predict positive/negative outcomes during treatment, allowing a strategy of a more personalised treatment regime to be prescribed.

- Determine the influence of phosphorylation involved in drug sensitivity and drug resistance for MM patients.

- Examine the difference between quantitative and qualitative proteomic approaches in potential marker discovery.

- Examine and evaluate the potential use of saliva as a source of biomarkers for the transformation from pre-malignant MGUS to newly diagnosed MM.

- Determine the potential of saliva as a source of protein biomarkers for MM disease progression, monitor disease burden and minimal residual disease statues.

- Determine the potential use of proteomics to monitor disease progression and clinical response to CAR-T cell therapy.

- Identify the changes in proteomic signatures between Group Ⅰ, Ⅱ and Ⅲ of Acute Myeloid Leukaemia (AML) patients.

- Compare and contrast different proteomic approaches, discovery and targeted, in potential marker discovery.

Chapter 2

Materials and Methods

2.1 Materials

2.1.1 General chemicals and reagents

Distilled H_2O, (dH_2O), was purified using a Millipore Milli-Q apparatus to obtain Milli-Q water 18MΩ. Complete mini tablets containing protease inhibitors were supplied by Roche Diagnostics (Mannheim, Germany). Bradford reagent for protein quantification was obtained from Biorad Laboratories (Hemel-Hempstead, Hertfordshire, UK). All other general chemicals used were of analytical/electrophoretic/proteomic grade and were purchased from Sigma Chemical Company (Dorset, UK), unless stated otherwise.

2.1.2 1D Gel Electrophoresis

4-12% Bis-Tris Plus precast gels were obtained from Invitrogen by Thermo Fisher Scientific (UK). 20X MOPS SDS Running Buffer was obtained from Novex by Life Technologies (Carlsbad, CA, USA). Protein molecular mass markers and Laemmli-type buffer were obtained from Biorad Laboratories (Hemel-Hempstead, Hertfordshire, UK).

2.1.3 Mass Spectrometry

Filter Aided Sample Preparation (FASP) vivacon 500 spin filters were obtained from Sartorius (Gottingen, Germany) and C18 spin filters were obtained from Thermo Fisher Scientific (UK). Mass Spectrometry grade modified trypsin was obtained from Thermo Scientific (IL, USA). Formic acid and acetonitrile were obtained from Fluka (Dorset, UK). LC-MS/MS vials and vial caps were purchased from VWR (PA, USA). The remaining analytical grade chemicals for mass spectrometry were obtained from Sigma Chemical Company (Dorset, UK), Thermo Fisher Scientific (UK) and Biorad Laboratories (Hemel-Hempstead, Hertfordshire, UK).

2.1.4 Immunoblotting

Whatman nitrocellulose transfer membrane was obtained from Invitrogen (Carlsbad, CA, USA). Chemiluminescence substrate was obtained from Thermo Scientific (IL, USA). Ponceau S-Red staining solution was obtained from Sigma Chemical Company (Dorset, UK). Commercially available antibodies used for this research were obtained from different sources, listed below in Table 2.1. peroxidase-conjugated secondary antibodies were supplied by Merck (Kenilworth, NJ, USA).

Table 2.1: Antibodies used for Immunoblotting

List of all commercially available antibodies used for this project with antibody specificity, host species, company and catalogue number.

Antibody	Species	Specificity	Company	Catalogue Number	Dilution
Fatty acid binding protein 5	Gt	pAb	R&D Systems	AF3077	1:1000

2.1.5 ELISA

ELISA kit (FABP5) was obtained from AssayPro (USA).

2.1.6 Phosphopeptide Enrichment Kit

A Pierce® Magnetic Titanium Dioxide Phosphopeptide Enrichment Kit was obtained from Thermo Fisher Scientific (UK).

2.1.7 Human Phospho-Kinase Array

The Human Phospho-Kinase Array was obtained from R&D Systems (MN, USA).

2.1.8 Luminex Technology

MILLIPLEX MAP Human Circulating Cancer Biomarker Panel 4 cancer multiplex assay, Cytokine/Chemokine Magnetic Bead Panel, premixed 29 plex and Cytokine/Chemokine Magnetic Bead Panel II, premixed 23 plex were purchased from Merck (Kenilworth, NJ, USA).

2.1.9 Immunohistochemistry

Formalin-fixed paraffin-embedded bone marrow trephine biopsies were provided by the pathology team at the Mater Misericordiae University hospital pathology laboratory. Paraffin blocks were cut using a Microtome in combination with MX35 Premier+ microtome blades and Superfrost Ultra Plus slides were obtained from Thermo Fischer Scientific (UK). DAKO Wash buffer 10x, DAKO Citrate Target Retrieval Solution pH6.1, DAKO REAL Peroxidase-Blocking Solution, DAKO REAL EnVision Detection System Peroxidase/DAB+, Rabbit/Mouse, DAKO Hematoxylin and DAKO antibody diluent were obtained from Agilent (Santa Clara, CA, USA). DPX Mountant for histology was obtained from Sigma Chemical Company (Dorset, UK).

Table 2.2: Antibodies used for IHC

List of all commercially available antibodies used for this project with antibody specificity, host species, company and catalogue number.

Antibody	Species	Specificity	Company	Catalogue Number	Dilution Used
CD44	Rb	mAb	Cell Signalling Technology	37259	1:220
CD48	Rb	mAb	Cell Signalling Technology	29499	1:150
CD68	Rb	mAb	Cell Signalling Technology	76437	1:600
Fatty Acid Binding Protein 5	Rb	mAb	Cell Signalling Technology	39926	1:250
Talin-1	Rb	mAb	Cell Signalling Technology	4021	1:50
Vinculin	Rb	mAb	Cell Signalling Technology	13901	1:300
Integrin β3	Rb	mAb	Cell Signalling Technology	13166	1:300

2.2 Methods

2.2.1 Patient Samples

A total of 35 bone marrow (BM) aspirates were collected from 10 diagnostic and 25 relapse patients. No exclusion criteria were applied to the patients and the samples were collected prospectively. Data collection was continued at successive relapses to follow disease progression. The ethics committees of the participating hospitals approved the study in compliance with the Declaration of Helsinki. These samples were obtained from the Institute of Molecular Medicine, Helsinki, Finland (FIMM).

A total of 91 saliva samples from patients at varying diagnosis stage were obtained from the Mater Misericordiae University Hospital, Dublin 7, Ireland. Ethical approval was obtained sitewide by both the Mater Misericordiae University Hospital and Maynooth University in compliance with the declaration of Helsinki. The GBO Saliva Collection System was used for saliva sample collection (Greiner Bio-One International GmbH, Kremsmünster, Upper Austria).

Both plasma cell and serum AML samples were collected from 49 patients with varying grade of disease, ranging from grade 1 to grade 3. This grading was carried out by the participating hospitals and the study was approved in compliance with the Declaration of Helsinki. These samples were obtained from the Finnish Haematology Registry and Clinical Biobank (FHRB).

A total of 69 patient samples were received from The Dana Farber Cancer Institute, Boston, Massachusetts.

42 pre-paraffin embedded histology blocks containing bone marrow trephines were obtained from the Histology Department, Mater Misericordiae University Hospital, Dublin 7, Ireland. These samples corresponded to patients involved in the saliva study (Chapter 5), with varying diagnosis throughout disease progression.

2.2.2 Cell lysis

Harvested CD138+ plasma cells were resuspended in 8M urea PTMscan lysis buffer (Cell Signalling Technologies, Massachusetts, USA), sonicated using a Sonoplus HD 2200, Bandelin (Berlin, Germany), for three cycles for 30 seconds at a power setting of 50%. Samples were centrifuged at 20,800 x g for 20 mins at 4ºC.

2.2.3 Acetone Precipitation

Prior to mass spectrometric analysis, samples were purified by acetone precipitation. 5 times the sample volume of cold 100% acetone was added to each sample and stored overnight at -20℃. Samples were centrifuged at 15,000 x g for 15 min at 4℃. The supernatant was decanted, and samples centrifuged again at 15,000 x g for 5 min. The supernatant was discarded, excess supernatant was removed using a Gilson P20 pipette and the resulting pellet was allowed to air-dry for 10 min. The pellets were re-suspended in appropriate volume of label-free solubilisation buffer (6 M urea, 2 M thiourea, 10 mM Tris, pH 8.0 in LCMS grade water) and vortexed and sonicated, using a Sonoplus HD 2200, Bandelin (Berlin, Germany), to ensure full re-suspension.

2.2.4 2D CleanUp (BioRad)

The commercially available Ready Prep 2D clean up kit from Bio-Rad Laboratories (Hemel-Hempstead, Hertfordshire, UK) was used as an alternative to acetone precipitation. The kit removes contaminants from protein extracts which may otherwise interfere with downstream mass spectrometric analysis. The purification was carried out as per the manufacturer's guidelines.

2.2.5 Protein quantification using the Bradford assay system

Protein quantification was carried out using the method of Bradford (Bradford, 1976). A standard curve was generated using a 1:1 serial dilution of a stock solution of 2 mg/ml BSA to give the following standards: 2 mg/ml, 1 mg/ml, 0.5 mg/ml, 0.25 mg/ml, 0.125 mg/ml and 0 mg/ml. Protein samples were appropriately diluted prior to quantification. Both standards and samples were constituted in the protein buffer. 5 µl of sample and standards were added to a 96-well plate. 250 µl of diluted Bradford reagent (diluted 1:4) was added to each well. The plate was left to incubate for 10 min at room temperature in the dark to allow for complete binding and the associated colour development. Absorbance of standards and samples was read at λ=595 nm using a Synergy HT BIO-TEK unit and KC4 software from Mason Technology Ltd. (Dublin, Ireland). Protein concentrations were determined using the standard curve, whilst multiplying by the dilution factor. Standards were analysed in duplicate while protein samples were analysed in triplicate.

2.2.6 Sample preparation for label-free liquid chromatography mass spectrometry

Following the determination of protein concentration using the Bradford assay system, sample volumes were equalised with label-free solubilisation buffer. Protein samples were reduced with 10 mM dithiothreitol (DTT) for 30 min at room temperature with gentle shaking and alkylated with 25 mM Iodoacetamide (IAA) in 50 mM ammonium bicarbonate for 20 min at room temperature in the dark (Dowling et al., 2014a). To quench any unreacted IAA and thus prevent the alkylation of trypsin, a further 10 mM DTT was added to each sample and samples were incubated for 15 min at room temperature in the dark. Proteolytic digestion was achieved using a combination of the enzymes Lys-C and trypsin. Samples were initially digested with sequencing grade Lys-C at a ratio of 1:100 (protease: protein) and incubated at 37°C

for 4 h. Samples were then diluted with four times the initial sample volume using 50 mM ammonium bicarbonate to dilute the urea molarity to a range at which trypsin is active (Proc et al., 2010). Samples were then incubated with sequencing grade modified trypsin at a ratio of 1:25 (protease: protein) overnight at 37℃. The proteolytic digestion was halted by the addition of 2% trifluoroacetic acid (TFA) in 20% acetonitrile (ACN) (3:1 (v/v) dilution). The peptides were purified using Pierce C18 spin columns from Thermo Fisher Scientific (Dublin, Ireland), dried through vacuum centrifugation and re-suspended in loading buffer (2% ACN, 0.05% TFA in LC-MS grade water) (Murphy et al., 2015a). Peptide suspensions were vortexed and sonicated to aid full re-suspension. Samples were centrifuged briefly at 14,000 x g and the supernatant transferred to mass spectrometry vials. Any remaining peptide suspension was stored at -80℃.

2.2.7 Filter Aided Sample Preparation for Label-Free Liquid Chromatography Mass Spectrometry

Protein concentrations were equalised with label-free solubilisation buffer and 30 µg of protein was processed by the filter aided sample preparation (FASP) method (Wiśniewski et al., 2009) using a trypsin to protein ratio of 1:25 (protease: protein). Following overnight digestion and elution of peptides from the spin filter, 2% TFA in 20% ACN was added to the filtrates (3:1 (v/v) dilution). The peptides were then purified using Pierce C18 spin columns from Thermo Fisher Scientific (Dublin, Ireland), dried through vacuum centrifugation and re-suspended in mass spectrometry loading buffer (2% ACN, 0.05% TFA in LC-MS grade water). Peptides were vortexed, sonicated and briefly centrifuged at 14,000 x g and the supernatant transferred to mass spectrometry vials for label-free LC-MS/MS.

2.2.8 Label-free liquid chromatography mass spectrometry

An Ultimate 3000 NanoLC system (Dionex Corporation, Sunnyvale, CA, USA) coupled to a Q-Exactive mass spectrometer (Thermo Fisher Scientific) in the Proteomics Suite at Maynooth University was used for all mass spectrometry-based analysis carried out. Re-suspended peptide mixtures (a maximum load of the equivalent 1 µg pre-digested protein) were loaded by an autosampler onto a C18 trap column (C18 PepMap, 300 µm id × 5 mm, 5 µm particle size, 100 Å pore size; Thermo Fisher Scientific). The trap column was switched on-line with an analytical Biobasic C18 Picofrit column (C18 PepMap, 75 µm id × 500 mm, 2 µm particle size, 100 Å pore size; Dionex). The peptides generated were eluted over either 65 min or 180 min using the following binary gradients: solvent A [2% (v/v) ACN and 0.1% (v/v) formic acid in LC-MS grade water] and 0-90% solvent B [80% (v/v) ACN and 0.1% (v/v) formic acid in LCMS grade water]. The column flow rate was set to between 0.25 – 0.3 µL/min (Murphy et al., 2015a, Murphy et al., 2016b). The Q-Exactive was operated in positive, data dependent mode and was externally calibrated. Survey MS scans were conducted in the 300-1700 m/z range with a resolution of 140,000 (m/z 200) and lock mass set to 445.12003. CID (collision-induced dissociation) fragmentation was carried out with the fifteen most intense ions per scan and at a resolution of 17,500. A dynamic exclusion window was applied within 30 s. An isolation window of 2 m/z and one micro-scan were used to collect suitable tandem mass spectra.

2.2.9 Quantitative proteomic profiling of mass spectrometric data using MaxQuant and Perseus Software

For quantitative analysis mass spectrometry, files were analysed in MaxQuant (version 1.6.1.0), with the Andromeda search engine used to search the detected

features against the UniProtKB-SwissProt database for *Homo sapiens*. The following search parameters were used: i) first search peptide tolerance of 20 ppm, ii) main search peptide tolerance of 4.5 ppm, iii) cysteine carbamidomethylation set as a fixed modification, iv) methionine oxidation set as a variable modification, v) a maximum of two missed cleavage sites and vi) a minimum peptide length of seven amino acids. The FDR was set to 1% for both peptides and proteins using a target-decoy approach (Grassl et al., 2016). Relative quantification was performed using the MaxLFQ algorithm (Cox et al., 2014). The "proteinGroups.txt" file produced by MaxQuant was further analysed in Perseus (version 1.5.1.6). Proteins that matched to the reverse database or a contaminants database or that were only identified by site were removed. The label-free quantification (LFQ) intensities were log2 transformed, and only proteins found in all replicates in at least one group were used for further analysis. Data imputation was performed to replace missing values with values that simulate signals from peptides with low abundance chosen from a normal distribution specified by a downshift of 1.8 times the mean standard deviation of all measured values and a width of 0.3 times this standard deviation (Deslyper et al., 2016). A two sample t-test was performed using $p \leq 0.05$ on the post imputated data to identify statistically significant differentially abundant proteins.

2.2.10 Qualitative proteomic profiling of mass spectrometric data

Qualitative data analysis was used for protein identification. Mass spectrometry raw files were processed using the Proteome Discoverer 1.4 (Thermo Fisher Scientific) software with Sequest HT as the search engine and the UniProt sequence database. The following search parameters were used for protein identification: (i) peptide mass tolerance set to 10 ppm, (ii) MS/MS mass tolerance set to 0.02 Da, (iii) up to two missed cleavages, (iv) carbamidomethylation set as a fixed modification and (v) methionine oxidation set as a variable modification. Mass spectrometry raw files were

searched against the UniProtKB-SwissProt *Homo sapiens* database. Peptides were filtered using a minimum XCorr score of 1.5 for +1, 2.0 for +2, 2.25 for +3 and 2.5 for +4 charge states, with peptide probability set to high confidence.

2.2.11 Generation of heat maps using Perseus

Heat maps illustrating protein abundances for statistically significant differentially abundant proteins were designed using Perseus software. The normalised abundances of differentially abundant proteins determined were loaded as a .txt file into Perseus and the data was log2 transformed. Hierarchical clustering was then performed on Z-score normalised intensity values by clustering both samples and proteins using Euclidean distance and average linkage.

2.2.12 Bioinformatics analysis of proteomic data

A number of bioinformatics software packages were used to give comprehensive analyses of identified proteins with differential abundance. Such bioinformatics tools were used to i) classify the types of proteins identified, ii) give meaningful insights into the potential roles of identified proteins in disease pathophysiology and iii) identify potential associations between identified proteins. The PANTHER database of protein families (http://pantherdb.org; version 10.0) was used to group proteins based on their protein class (Mi et al., 2013). Differentially abundant proteins were also analysed by version 10.5 of the STRING database (http://string-db.org/) for medium (0.4) or high confidence (>0.7) interactions using the evidence view. STRING analysis clusters proteins based on known and predicted protein interactions that include direct physical and indirect functional protein associations (Szklarczyk et al., 2017). The DAVID bioinformatics resource (https://david.ncifcrf.gov/) was used to identify enriched functionally related protein groups and KEGG pathway (http://www.genome.jp/ kegg/pathway.html) was employed to map proteomic data

onto pathway maps to enable biological interpretation of large proteomic datasets. The web-based gene set analysis toolkit (http://www.webgestalt.org/) was also used to interrogate proteomic datasets. Over-representation enrichment analysis was performed, with genome_protein-coding as the reference list, non-redundant gene ontology terms, a minimum of 2 genes for a category, an FDR ≤ 0.05 and with the Benjamini & Hochberg method used for multiple test adjustment. The ClueGO app in the Cytoscape bioinformatics package was used to identify enriched GO categories, using a two-sided hypergeometric test and a Benjamini-Hochberg p value correction.

2.2.13 Comparative immunoblot analysis

Comparative immunoblot analysis was carried out for the independent verification of a number of important protein hits identified by LC-MS/MS. Immunoblotting was performed under routine conditions (Holland et al., 2013), typically using 25 µg protein per lane. Proteins were first separated on hand-cast 10% polyacrylamide gels by SDS-PAGE and were subsequently transferred by the method of Towbin (Towbin et al., 1979) to Whatman nitrocellulose membranes in a Trans-Blot cell from Bio-Rad laboratories by wet transfer (transfer buffer: 25 mM tris, 192 mM glycine, 20% methanol) at 100 V for 70 min at 4℃. Transfer efficiency was assessed using Ponceau reversible stain (0.1% PonceauS, 5% acetic acid). To prevent non-specific binding, membranes were blocked for 1 h at room temperature using a milk protein solution (2.5% (w/v) fat-free milk powder in 10% PBS), and then incubated with appropriately diluted primary antibodies overnight at 4℃ with gentle agitation. The following day, membranes were washed twice in the milk protein solution for 10 min, and then incubated with appropriately diluted peroxidase-conjugated secondary antibodies for 1.5 h at room temperature with gentle agitation (Murphy et al., 2015a). Membranes were washed with the milk protein solution for 10 min twice and with 10% PBS for 10 min twice, and enhanced chemiluminescence was used for the

visualisation of immuno-decorated protein bands (O'Connell and Ohlendieck, 2009). Densitometric scanning and statistical analysis of immunoblots was performed using a HP PSC-2355 scanner and ImageJ software (NIH, Bethesda, MD, USA) along with Graph-Pad Prism software (San Diego, CA, USA), in which a p value ≤ 0.05 was deemed to be statistically significant.

2.2.14 Phosphopeptide Enrichment

CD138+ lysed plasma cells were enriched for phosphopeptides using a Pierce Magnetic Titanium Dioxide Phosphopeptide Enrichment Kit to identify potential phosphopeptide biomarkers for treatment resistance using label-free LC-MS/MS. Peptides were initially purified using Pierce C18 spin columns from Thermo Fisher Scientific (Dublin, Ireland), dried through vacuum centrifugation and re-suspended in 80% acetonitrile/2% formic acid. 10μl of magnet capture beads were resuspended in 190μl binding buffer per sample, which was vortexed to uniform suspension for 30 secs. 200μl magnetic bead solution was placed in a clean, labelled eppendorf and 100μl per sample was added, pipetting up and down to ensure mixing. Beads were separated from solution using a magnetic separator rack, allowing beads to separate from solution for a minimum of 1 minute. The magnetic rack was tilted 90º and the supernatant was removed, ensuring no beads were removed. 200μl of binding buffer was added per sample and supernatant was removed after allowing the beads to settle in the magnetic separator rack for 1 min, repeating three times. 200μl wash buffer was added quickly after removing samples from the magnetic separator and supernatant was removed using the magnetic separator after allowing to incubate for 1 minute. All wash buffer was ensured to be removed before elution step. 30μl Elution buffer was added to each sample, ensuring that samples were well mixed by pipetting multiple times and samples were allowed to incubate for 10 mins at room temperature. Samples were placed on the magnetic separator for 1 minute, ensuring

all beads had separated from solution and eluted phosphopeptides were removed from the eppendorfs and placed in clean, labelled eppendorfs. Samples were dried through vacuum centrifugation at high heat and re-suspended in loading buffer (2% ACN, 0.05% TFA in LC-MS grade water) (Murphy et al., 2015a). Peptide suspensions were vortexed and sonicated to aid full re-suspension. Samples were centrifuged briefly at 14,000 x g and the supernatant transferred to mass spectrometry vials. Any remaining peptide suspension was stored at -80℃.

2.2.15 Human Phospho-Kinase Array

A Human Phospho-Kinase Array was used to validate potential target phosphopeptide biomarkers as identified by label-free LC-MS/MS after phosphopeptide enrichment. 100μg of protein was used for analysis. The array was carried out as per the manufacturer's guidelines using two highly sensitive and two highly resistant lysed CD138+ plasma cell samples to treatment (Chapter three).

2.2.16 Enzyme linked immunosorbent assay

ELISA assays were employed to verify some potential circulatory protein markers as identified by label-free LC-MS/MS. 50μl of crude saliva and serum samples were added to antibody-coated microtiter wells and incubated at room temperature as directed by the manufacturers' recommendations (2 h for FABP5). After the incubation period wells were washed and a HRP labelled secondary detector antibody was added. After incubation at room temperature for 2 hours in the dark, TMB chromogen substrate was added. The reaction was stopped after exactly 15 mins and absorbance was measured at 450 nm on a microplate reader (Cynthia Martin et al., 2014). The quantity of protein in the test samples was interpolated from a generated standard curve and was corrected for sample dilution. All test samples

were assayed in triplicate. The intra-plate % coefficient of variation (CV) was calculated and was found to be less than 10% for all assays (Murphy et al., 2017b).

2.2.17 Luminex Technologies

Luminex was employed to carry out a targeted investigation into both circulating cancer biomarkers and cytokine and chemokine biomarkers in AML and RsqVD samples. 96 well plate was washed with 200μl wash buffer and was mixed for 10 mins at 25°C. Standard curve was set up according to manufacturer's guidelines. Wash buffer was removed and 25μl of standard or control was loaded according to manufacturer's protocol, followed by 25μl of assay buffer. 25μl of crude sample was added to each well, according to experimental design. 15μl of vortexed beads were added to each well, ensuring to mix bead matrix regularly to ensure beads didn't settle, and plates were sealed and mixed for 18hrs at 4°C. Plate was placed in plate magnet and content of the wells was emptied. 200μl wash buffer was added to each well, removed and 14μl detection antibody with 14μl assay buffer was added to each well, with incubation for 1hr. 14μl Streptavidin-Phycoerythrin combined with 14μl assay buffer was added to each well, with incubation for 30mins while wrapped in tinfoil on plate shaker. Plate content was removed, ensuring plate was secure in plate magnet, and 150μl of sheath fluid was added to each well to resuspend beads using the plate shaker for 5 mins. Plates were read and analysed using a Guava EasyCyte Plus platform (Millipore, Merck KGaA, Darmstat, Germany).

2.2.18 Immunohistochemistry

Immunohistochemistry was employed as a method of validation for potential biomarkers for both drug sensitivity (Chapter 3) and potential salivary biomarkers (Chapter 4) as identified by label-free LC-MS/MS.

2.2.18.1 Histology

Blocks with paraffin embedded bone marrow trephines were stored overnight at -20°C, to ensure more efficient sectioning. Temperature of these blocks was maintained by storing them on the cold plate of the embedding station. The water bath was maintained at 52.6°C to float sections, allowing easy mounting on slide. Each block was cut in initially using a fresh microtome blade until tissue was at full face, ensuring a full representation of all the tissue embedded in the block. After a full face was obtained, block was returned to the cold plate to allow further cooling. Further cooling also eliminates tissue wasting when taking a section. A fresh blade was used to cut a maximum of 3 blocks. Each section of tissue was taken with a thickness of 5 microns.

2.2.18.2 Section Staining

Slides were initially heated for antigen retrieval at 95°C in pH 6.1 citrate buffer for 20 minutes using a PT Link Pre-Treatment Module (DAKO, Agilent, Santa Clara, CA, USA). DAKO REAL EnVision Detection System (DAKO) was used for immunohistochemical analysis of the bone marrow trephines according to manufacturer's instructions. Briefly slides were blocked for endogenous peroxidase activity and subsequently washed with DAKO wash buffer. Next slides were treated with primary antibodies listed in Table 2.2, diluted in DAKO antibody diluent, or negative controls treated with DAKO antibody diluent alone. Slides were again washed with DAKO wash buffer. Slides were then stained with DAKO Real Envision Detection system and stained with DAB chromogen. Finally slides were counter-stained using haematoxylin. This staining was carried out using a DAKO AutostainerPlus (Agilent, Santa Clara, CA, USA). Slides were dehydrated by treatment using 70% Ethanol for 3 mins twice, 90% Ethanol for 3 mins twice, 100%

ethanol for 3 mins twice and 100% xylene for 5 mins twice. Slides were then cover slipped using a glass coverslip, ensuring tissue did not dry out after xylene and that tissue was completely covered by the coverslip.

All slides were analysed by light microscopy, and images acquired at 10x and 40x magnification. Slides were scored semi-quantitatively according to the intensity of the staining: negative (-), weakly positive (+1), positive (+2) or strongly positive(+3).

Chapter 3

Proteomic Profiling of Most Sensitive/ Least Sensitive Patients After Treatment Using a Panel of Six Drugs Used for the Treatment of Multiple Myeloma.

3.1 Introduction

Over the last number of years multiple novel drugs have been developed and approved for the treatment of MM, leading to an increase in OS in patients with MM from approximately 5 years to an expected median of 15 years (Guang et al., 2018). These novel drugs are now considered the first point of call for treatment of newly diagnosed MM including proteasome inhibitors (PI), monoclonal antibodies and immunomodulatory drugs (IMiDs). Although vast improvements in the treatment of MM have been observed since the introduction of these novel drugs, vastly high rates of relapse and refractory disease have been recorded and linked to resistance to these novel drugs. It has been recorded that, although large numbers of patients experience long periods of remission, relapse/refractory disease (RRMM) is imminent for high-risk MM. RRMM is “defined as progression of therapy in patients who achieve minor response or better, or who progress within 60 days of their last therapy” (Nooka et al., 2015).

Bortezomib, a first class, reversible boronic acid dipeptide PI with high selectivity for inhibition of the 26S proteasome, has been associated with the induction of mitochondrial depolarization and apoptosis. Bortezomib binds to the catalytic site of the 26S proteasome, resulting in an increased abundance of p53 and p27 and an inhibition of NF-κB transcriptional activity (Adams et al., 1998), leading to increased cell stress and apoptosis (Obeng et al., 2006). A direct result of this inhibition is the activation of c-Jun N-terminal kinase, the accumulation of misfolded proteins (Obeng et al., 2006) and the stabilization of cell cycle inhibitors. Bortezomib is broadly used as the primary treatment for MM as renal insufficiency (Leal et al., 2011) and hepatic function impairment doesn’t affect it’s efficacy (LoRusso et al., 2012) but has been linked with a significant increased risk of varicella zoster virus infection.

Carfilzomib, a second generation PI, is used primarily after patients have received at least two prior therapies, generally including an IMiD and bortezomib (Nooka et al.,

2015). Carfilzomib binds to the N-terminal threonines irreversibly, which prolongs proteasome inhibition (Manasanch and Orlowski, 2017). Inhibition of the chymotrypsin-like subunit in the constitutive proteasome and the immunoproteasome by carfilzomib causes cytotoxic effects in MM cells, leading to MM cell apoptosis (Parlati et al., 2009). Good full body penetration is recorded during treatment with carfilzomib and, as opposed to treatment using bortezomib, it is metabolized extra-hepatically and is therefore not dependent on liver function (Yang et al., 2011).

Lenalidomide, an IMiD, is used to inhibit angiogenesis and induce apoptosis of established neovasculature (Nooka et al., 2015) and is a less toxic and more potent analog of Thalidomide (Zou et al., 2013). The use of this IMiD has been observed as having a significantly better effect in combination with another form of treatment, such as a PI (Wang et al., 2013), cytotoxic agent (Reece et al., 2015) or antibodies (Plesner et al., 2016), increasing overall response rate from 65% to 95%. Lenalidomide has been noted to increase T cell proliferation (Corral et al., 1999) and by inhibiting TNFα-induced endothelial cell migration, bFGF and VEGF (Dredge et al., 2005) exhibits anti-angiogenic properties. These properties are a partial result of Akt phosphorylation inhibition caused by the inhibition of bFGF (D'Amato et al., 1994).

Navitoclax is a high affinity small molecule BH3 mimetic known to inhibit BCL-2 and BCL-XL which leads to the inhibition and apoptosis in MM (Tse et al., 2008). BCL-2 members control the outer mitochondrial membrane integrity and lead to cell apoptosis susceptibility (Vogler et al., 2009), showing either antiapoptotic and proapoptotic properties. BCL-2 binding to Ca^{2+} endoplasmic reticulum channels, inositol 1,4,5-triphosphate receptors (IP_3Rs), prevent the triggering of cell death by docking Ca^{2+}-activated phosphatase calcineurin and calcineurin-regulated inhibitor of protein phosphatase 1 (DARPP-32) to IP_3Rs. Forming a negative feedback loop, an excess of Ca2+ is sensed by the complex and decreases IP_3Rs phosphorylation. This, in turn, decreases Ca^{2+} mediated by IP_3R and thus, inhibiting apoptosis (Chang et al., 2014) Antiapoptotic BCL-2 members are inhibited by BH3 mimetic Navitoclax,

which induces apoptosis by binding in hydrophobic pockets formed by BH domains 1-3 and dislocating pro-apoptotic proteins (Chipuk et al., 2010).

Quizinostat is a histone deacetylase inhibitor (HDACi) that specifically targets HDAC6. HDAC6 is an enzyme that aids in the transport of misfolded proteins to protein storage sites, known as aggresomes (Rodriguez-Gonzalez et al., 2008) and has been hypothesised as a factor in maintaining MM cell growth (Imai et al., 2016). The administration of Quizinostat has been linked to blocked transport of misfolded proteins to the aggresome leading to the apoptosis of MM cells. It has also been suggested that advanced MM cells exhibit a high abundance of PPP3CA, aiding in cell growth and proliferation of MM cells. Treatment with Quizinostat reduces the abundance of PPP3CA, leading to a reduction in HSP90, a known protein that deacetylates HDAC6, maintaining its chaperone function (Kovacs et al., 2005).

PF-04691502 is an experimental drug that is known to be a PI3K/mTOR inhibitor that has been observed to result in antiproliferative activity in cultured cells (Yuan et al., 2011) and antitumor activity in xenograft models (Mallon et al., 2011). The PI3K/mTOR signalling pathway has been implicated in cancer cell proliferation, motility, growth and survival (Courtney et al., 2010).

Although there have been vast improvements in the treatment of MM and RRMM, using both singular drug treatment and combinational therapy, a vast number of experimental drugs are still in early phase clinical trials or early development to find a comprehensive cure for MM and RRMM.

Personalised medicine is predicted to be the future of treatment of MM patients. Myeloma cell phenotyping and genotyping, along with a proteomic signature for individual patients to form a personal course of treatment to combat the proliferation of MM plasma cells, will increase the overall survival (OS) of patients and in the long term lead to the cure of MM. To date, clinicians must combine a number of the multiple available treatment regimens to determine the best line of treatment for MM patients including proteasome inhibitors (PI), monoclonal antibodies and

immunomodulatory drugs (IMiDs). The idea that each patient is different and a personalised course of treatment for maintenance of the disease, along with a more aggressive search for an overall cure, is becoming more apparent over time (Russell and Rajkumar, 2011).

A hallmark of MM is the sequel development of drug resistant phenotypes, which may be present initially or emerge during the course of treatment. These drug resistant phenotypes reflect the intra-tumor and inter-patient heterogeneity of this cancer. Most MM cells are sensitive to PIs, which have become the standard of care in the treatment of newly diagnosed and relapsed MM. However, resistance develops (intrinsic/acquired) (Nooka et al., 2015). Although several novel drugs have recently been approved or are in development for MM, there are few molecular indicators to guide treatment selection. To address this limitation, we have combined mass spectrometry-based proteomics analysis together with ex vivo drug response profiles and clinical outcome to elucidate a best possible accurate phenotype of the resistant sub-clones, thus yielding a theranostic profile that will inform therapeutic and drug development strategies.

3.1.1 Experimental Design

3.1.1.1 Patients and Samples

The ethics committees of the participating hospitals approved the study in compliance with the Declaration of Helsinki. A total of 35 bone marrow (BM) aspirates were collected from 10 diagnostic and 25 relapse patients. Patient characteristics and associated treatments are detailed in Tables 3.1 and 3.2. Patients cytogenetics are shown in Figure 3.1. No exclusion criteria were applied to the patients and the samples were collected prospectively. Data collection was continued at successive relapses to follow disease progression.

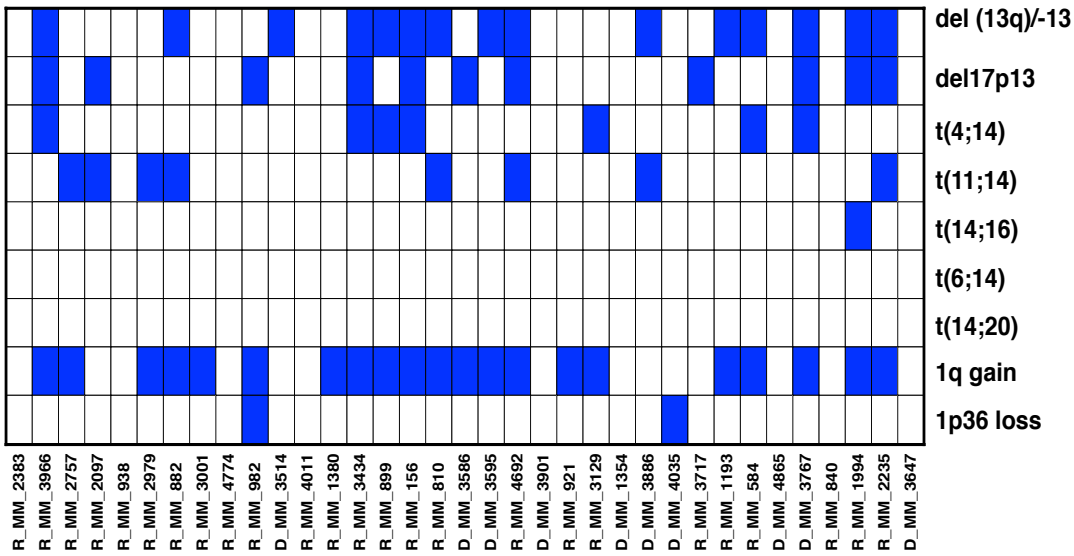

Figure 3.1: Cytogenetics of the patient cohort.

Heatmap showing the cytogenetics status of the patient cohort. Blue indicates the presence of genetic abnormality.

Table 3.1: MM patient cohort characteristics.

Table illustrating the gender, age at diagnosis, gender, paraprotein and light chain of the MM patient cohort. Patient identifiers beginning with R indicates remission samples and D indicates diagnosis samples. Paraprotein indicates the specific monoclonal heavy chain, light chain or intact immunoglobulins present in serum/urine of patients.

Patient ID	Gender	Age at Diagnosis	Paraprotein	Light Chain
R_MM_2383	Male	58	Unknown	Lambda
R_MM_3966	Female	65	IgA	Lambda
R_MM_2757	Male	59	IgA	Lambda
R_MM_2097	Female	59	Unknown	Kappa
R_MM_938	Male	50	IgG	Kappa
R_MM_2979	Female	69	IgA	Kappa
R_MM_882	Female	57	Unknown	Lambda
R_MM_3001	Male	56	Unknown	Kappa
R_MM_4774	Male	78	IgA	Kappa
R_MM_982	Male	56	IgG	Kappa
D_MM_3514	Female	68	IgG	Kappa
R_MM_4011	Male	66	Unknown	Unknown
R_MM_1380	Male	68	IgA	Lambda
R_MM_3434	Male	49	IgG	Kappa
R_MM_899	Male	62	IgA	Lambda
R_MM_156	Female	62	IgA	Kappa
R_MM_810	Male	74	Unknown	Unknown
D_MM_3586	Male	61	Unknown	Kappa
D_MM_3595	Male	67	IgG	Lambda
R_MM_4692	Male	41	IgG	Lambda
D_MM_3901	Male	71	IgA	Kappa
R_MM_921	Female	56	Unknown	Lambda
R_MM_3129	Male	60	IgG	Kappa
D_MM_1354	Male	66	Unknown	Unknown
D_MM_3886	Female	59	IgG	Lambda
D_MM_4035	Female	61	IgG	Kappa
R_MM_3717	Male	51	Unknown	Kappa
R_MM_1193	Male	68	IgA	Lambda
R_MM_584	Male	71	IgA	Kappa
D_MM_4865	Male	66	Unknown	Kappa
D_MM_3767	Female	55	IgA	Lambda
R_MM_840	Female	64	IgA	Kappa
R_MM_1994	Female	68	IgG	Lambda
R_MM_2235	Female	56	IgG	Kappa
D_MM_3647	Male	63	IgG	Kappa

Table 3.2: Patient cohort treatment course.

Table illustrating the 1st next line treatment, all subsequent line treatments and the deepest response in next line treatments.

Patient ID	Name of 1st next line treatment	Names of all next line treatments	Deepest response in next line treatment
R_MM_2383	VAD	VAD	Exitus
R_MM_3966	DR-PACE (Cis/Cpm/Dxm/Dox/Eto/L)	DR-PACE (Cis/Cpm/Dxm/Dox/Eto/Len)	PR
R_MM_2757	Bor/Dxm/Len	Bor/Dxm/Len	PR
R_MM_2097	Len/Dxm	Len/Dxm Bor/Dxm/Len	PR
R_MM_938			
R_MM_2979	Bor/Dxm	Bor/Dxm Bor/Mel/Pred (VMP)	VGPR
R_MM_882	Benda/Bor/Pred	Benda/Bor/Pred	
R_MM_3001	Bor/Dxm/Len	Bor/Dxm/Len	PR
R_MM_4774			
R_MM_982	Bor/Dxm	Bor/Dxm	PR
D_MM_3514	Dxm	Dxm	VGPR
R_MM_4011	Radiotherapy		VGPR
R_MM_1380	Bor/Dxm/Len	Bor/Dxm/Len	SD
R_MM_3434	Bor/Dxm	Bor/Dxm	PR
R_MM_899	Pomal/Dxm	Pomal/Dxm	SD
R_MM_156	Radiotherapy	Radiotherapy Bor/Dxm/Len Len/Dxm	VGPR
R_MM_810	Bor/Dxm	Bor/Dxm Bor/Dxm/Len	Clinical Relapse
D_MM_3586	Dxm	Dxm	PR
D_MM_3595	Bor/Dxm/Len	Bor/Dxm/Len Mobilisation (Cpm/G-CSF) AutoHSCT (HD Mel) Len	Scr
R_MM_4692	Carfilzomib		
D_MM_3901	Bor/Mel/Pred (VMP)	Bor/Mel/Pred (VMP) Bor/Dxm/ Bor/Cpm/Dxm	PR
R_MM_921	Len/Dxm	Len/Dxm Dxm DLI	PR
R_MM_3129	Pomal/Dxm	Pomal/Dxm	SD
D_MM_1354			
D_MM_3886	Bor/Dxm	Bor/Dxm Bor/Cpm/Dxm Bor/Dxm/Len Mobilisation (Cpm) Bor/Dxm/Len	VGPR

		AutoHSCT (HD Mel)	
D_MM_4035	Radiotherapy	Bor/Dxm Bor/Cpm/Dxm Bor/Dxm/Len Mobilisation (Cpm) Bor/Dxm/Len AutoHSCT (HD Mel)	VGPR
R_MM_3717	Bor/Dxm	Bor/Dxm	VGPR
R_MM_1193	Bor/Dxm/Len	Bor/Dxm/Len	VGPR
R_MM_584	No treatment	No treatment	Exitus
D_MM_4865			
D_MM_3767	Bor/Dxm/Len	Bor/Dxm/Len Mobilisation (G-CSF)	PR
R_MM_840	Len/Dxm	Len/Dxm	VGPR
R_MM_1994	Bor/Cpm/Dxm/Len	Bor/Cpm/Dxm/Len	PD
R_MM_2235			
D_MM_3647	Benda/ Bor/Pred	Benda/Bor/Pred	PR

3.1.1.2 Label-free LC-MS/MS Analysis of CD138+ Plasma Cells of Most and Least Sensitive Patients to Treatment.

CD138 enriched plasma cells were initially lysed in RIPA buffer (25mM Tris, pH 7 – 8; 150 mM NaCl; 0.1% SDS; 0.5% sodium deoxycholate and 1% NP-40). The lysates were buffer exchanged using the 'filter aided sample preparation' (FASP) method in a buffer containing 8M urea/50 mM NH4HCO3/0.1% ProteaseMax. The protein amount was estimated using an RC/DC protein assay from Bio-Rad. BSA was used as a standard. After dithiothreitol reduction and iodoacetic acid-mediated alkylation, a double digestion was performed using Lys-C (for 4 hours at 37°C) and Trypsin (overnight at 37°C) on 5µg of protein. Digested samples were desalted prior to analysis using C18 spin columns (Thermo Scientific, UK). 500 ng of each digested sample was loaded onto a Q-Exactive (ThermoFisher Scientific, Hemel Hempstead, UK) high-resolution accurate mass spectrometer connected to a Dionex Ultimate 3000 (RSLCnano) chromatography system (ThermoFisher Scientific, Hemel Hempstead, UK). Peptides were separated using a 2% to 40% gradient of acetonitrile on a Biobasic C18 Picofrit column (ThermoFisher Scientific, Hemel Hempstead, UK) (100mm length, 75mm ID) over 65 min at a flow rate of 250nl/min. Data was acquired

with the mass spectrometer operating in automatic data dependent switching mode. A full MS scan at 140,000 resolution and a range of 300–1700 m/z was followed by an MS/MS scan, resolution 17,500 and a range of 200–2000 m/z, selecting the 10 most intense ions prior to MS/MS.

3.1.1.3 Data Analysis of all statistically significantly proteins with altered abundance for each treatment.

Protein identification and label-free quantification (LFQ) normalisation of MS/MS data was performed using MaxQuant v1.5.2.8 (http://www.maxquant.org). The Andromeda search algorithm incorporated in the MaxQuant software was used to correlate MS/MS data against the *Homo sapiens* Uniprot reference proteome database and a contaminant sequence set provided by MaxQuant. Perseus v.1.5.6.0 (www.maxquant.org/) was used for data analysis, processing and visualisation. Normalised LFQ intensity values were used as the quantitative measurement of protein abundance for subsequent analysis. The data matrix was first filtered for the removal of contaminants and peptides identified by site. LFQ intensity values were log2 transformed and each sample was assigned to its corresponding group. ANOVA-based multisample t-test were performed using a cut-off of $p<0.05$ on the post imputated dataset to identify statistically significant differentially abundant proteins. Receiver-operating characteristic (ROC) curve analysis was performed as it is a useful tool in assessment of biomarker accuracy. The ROC plots were obtained by plotting all sensitivity values (true positive fraction) on the y-axis against their equivalent (100-specificity) values (false positive fraction) for all available thresholds on the x-axis (MedCalc for Windows 8.1.1.0, Medcalc Software, Mariakerke, Belgium). The area under the curve (AUC) was calculated to provide a summary of overall classifier effectiveness. In our study, we consider AUC values ranging from 0.5→0.7 as poor, 0.7→0.8 as average, 0.8→0.9 as good and >0.9 as outstanding.

3.1.1.4 Bioinformatic Analysis of all statistically significantly proteins with altered abundance for each treatment.

In order to group identified proteins based on their protein class and to identify potential protein targets with increased abundance in both most and least sensitive patients, publicly available bioinformatics software programmes were employed. The programs used were the PANTHER database of protein families (http://pantherdb.org/) and the STRING database of known and putative protein interactions that include both direct physical and indirect functional protein associations (http://string-db.org/). KEGG colour pathway analysis was carried out with a focus on proteins increased in abundance in both patient groupings using the Kyoto Encyclopaedia of Genes and Genomes databank (https://www.genome.jp/kegg).

3.1.1.5 Verification of Proteomic Findings by Immunohistochemistry

As a method of validation for a number of potential biomarkers identified by LS-MS/MS, immunohistochemistry was carried out on formalin-fixed paraffin embedded bone marrow trephines with varying diagnosis.

3.2 Results

3.2.1 MM Patients are Stratified into Different Chemoresistance Groups

To determine and examine drug response of the 35 CD138+ plasma cell samples, drug sensitivity scoring (DSS) was used as outlined previously by Pemovska et al. 2013; Majumder et al. 2017. Four distinct chemoresistance groups were formed, ranging from sensitive (Group 1) to resistant (Group 4) to the panel of drugs used (Fig. 3.2). Twelve patients fell in Group 1, nine in Group 2, eight in Group 3 and six in Group 4. Correlating the DSS with the available clinical data we found that although Group 1 is the most sensitive to treatment, the OS of this group is the shortest (Fig. 3.3). In contrast, Group 4, although resistant to treatment, exhibit an OS which is similar to that of Group 3 (diminished response to most drugs) and is slightly decreased in comparison to the OS of Group 2 (moderate sensitivities) (Fig. 3.3).

A

G1	G2	G3	G4
R_MM_2383	R_MM_1380	R_MM_921	D_MM_4865
R_MM_3966	R_MM_3434	R_MM_3129	D_MM_3767
R_MM_2757	R_MM_899	D_MM_1354	R_MM_840
R_MM_2097	R_MM_156	D_MM_3886	R_MM_1994
R_MM_938	R_MM_810	D_MM_4035	R_MM_2235
R_MM_2979	D_MM_3586	R_MM_3717	D_MM_3647
R_MM_882	D_MM_3595	R_MM_1193	
R_MM_3001	R_MM_4692	R_MM_584	
R_MM_4774	D_MM_3901		
R_MM_982			
D_MM_3514			
R_MM_4011			

B

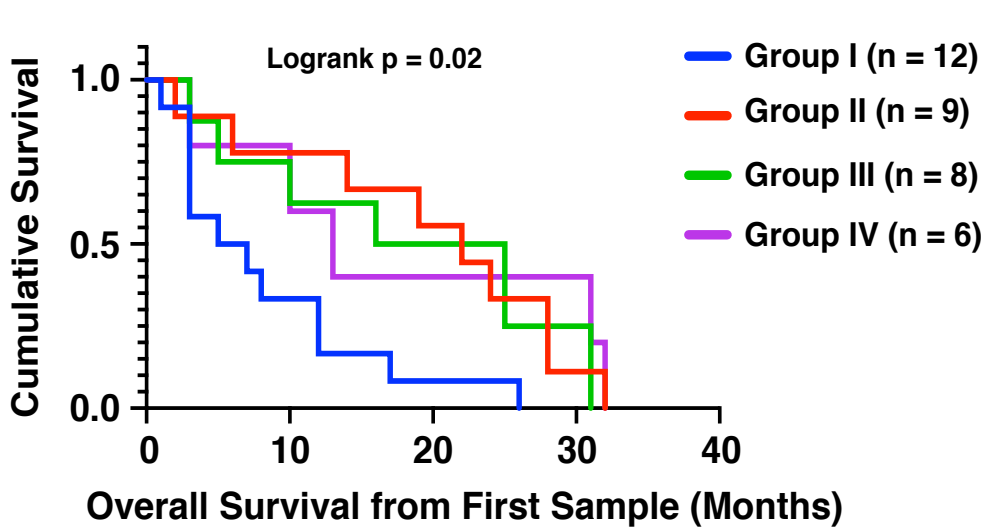

Figure 3.2: Chemoresistance and overall survival of the patient cohort.

A) Four distinct chemoresistance groups were formed, ranging from sensitive (G1) to resistant (G4) to the panel of drugs used. B) G1 is the most sensitive to treatment with the shortest OS. G4, although resistant to treatment, exhibit an OS which is similar to that of G3 (diminished response to most drugs) and is slightly decreased in comparison to the OS of G2 (moderate drug sensitivities).

3.2.2 MM Patients Show Differential Response to Six Different Classes of Drugs

We next investigated the response of the 35 CD138+ plasma cell samples, to six anti-myeloma therapies: Bortezomib and Carfilzomib, Lenalidomide, Navitoclax, Quizinostat and the investigational drug PF-04691502. Patients were stratified into groups of “most sensitive” to “least sensitive” to the six chemotherapeutics used as, although some patients The most sensitive group comprises the ten patients with the highest DSS for each particular drug and the least sensitive group is compiled of the ten patients with the lowest DSS for each drug. The comparison between the most and least sensitive patients to individual drugs is significant across all treatments (Fig. 3.3). Interestingly, when compiling groups of most sensitive and least sensitive patients to the selected six drugs, the least sensitive group was compiled of Group 4 patients whereas the most sensitive group was compiled of patients ranging from Group 1 to Group 3 (Fig.3.3).

A

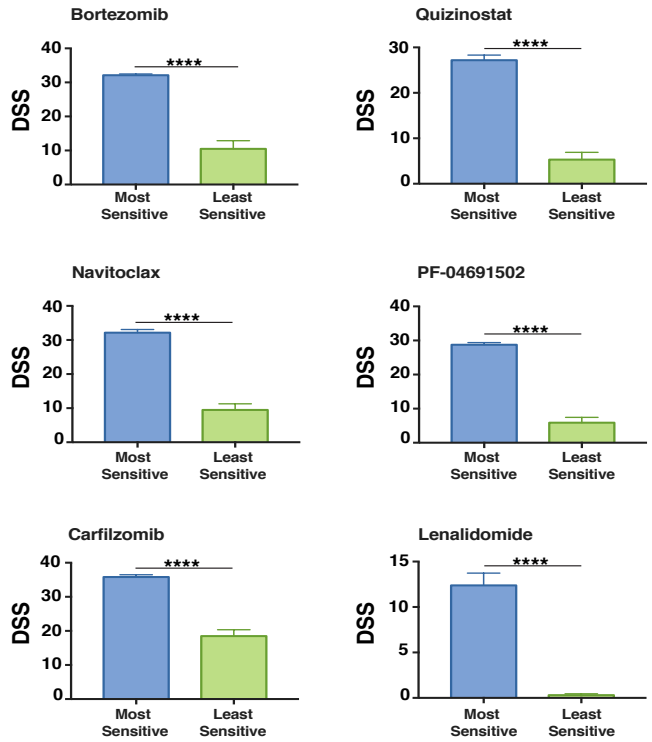

B

Bortezomib Least Sensitive	
Sample ID	DSS Group
D_4865	G4
R_1994	G4
R_840	G4
D_3767	G4
R_3717	G4
R_2235	G2
R_3129	G3
D_1354	G3
R_921	G3
R_1193	G4

Bortezomib Most Sensitive	
Sample ID	DSS Group
R_982	G1
R_2757	G1
R_584	G4
D_3901	G2
R_156	G2
R_3434	G2
R_1380	G2
R_2097	G1
R_2757	G1
R_2383	G1

Quizinostat Least Sensitive	
Sample ID	DSS Group
D_4865	G4
R_921	G3
D_1354	G3
R_1994	G4
R_840	G4
D_3767	G4
R_3717	G4
R_4774	G1
R_2757*	G1
R_982	G1

Quizinostat Most Sensitive	
Sample ID	DSS Group
R_4692	G2
R_810	G2
R_938	G1
R_156	G2
D_3886	G3
R_1193	G4
D_3514	G1
R_584	G4
R_2757*	G1
R_3966	G1

Navitoclax Least Sensitive	
Sample ID	DSS Group
R_2979	G1
D_3767	G4
R_3717	G4
R_1994	G4
R_840	G4
D_4865	G4
R_3001	G1
D_3901	G2
D_3886	G3
R_584	G4

Navitoclax Most Sensitive	
Sample ID	DSS Group
R_2235	G3
R_2383	G1
R_1193	G4
D_4011	G2
D_3647	G2
R_2097	G1
D_3586	G2
R_3434	G2
R_156	G2
R_1380	G2

Carfilzomib Least Sensitive	
Sample ID	DSS Group
D_4035	G3
R_840	G4
R_1994	G4
R_3717	G4
D_3767	G4
D_4865	G2
R_2383	G1
R_2235	G2
D_3886	G3
R_1193	G4

Carfilzomib Most Sensitive	
Sample ID	DSS Group
R_ 982	G1
R_ 584	G4
D_3514	G1
R_3434	G2
D_3586	G2
R_ 156	G2
R_2097	G1
R_ 938	G1
R_2757*	G1
R_2757*	G1

Lenalidomide Least Sensitive	
Sample ID	DSS Group
R_1994	G4
R_ 840	G4
R_2323	G1
R_3001	G1
R_1193	G4
R_2097	G1
R_1380	G2
D_3586	G2
D_3595	G2
R_ 810	G2

Lenalidomide Most Sensitive	
Sample ID	DSS Group
R_ 4692	G2
R_ 938	G1
D_ 3901	G2
R_ 584	G4
R_ 3966	G1
D_ 3514	G1
R_2757*	G1
R_2757*	G1
R_ 4774	G1
R_ 982	G1

PF-04691502 Least Sensitive	
Sample ID	DSS Group
R_1994	G4
R_ 840	G4
D_ 3767	G4
R_3717	G4
D_ 4035	G3
D_ 4865	G4
R_2757*	G1
R_ 882	G1
R_1193	G4
D_ 3886	G3

PF-04691502 Most Sensitive	
Sample ID	DSS Group
R_4692	G2
D_ 3595	G2
R_ 938	G1
D_ 3647	G2
R_2097	G1
D_ 3514	G1
R_ 584	G4
R_2757*	G1
R_3966	G1
R_2383	G1

Figure 3.3: Patients Show Differential Response to Five Different Classes of Drugs.

A) Most and Least Sensitive patients have a significantly different DSS ($p < 0.001$) across all six drug treatments. B) DSS group of most sensitive and least sensitive patients to the selected six drugs. The least sensitive group was compiled of G4 patients whereas the most sensitive group was compiled of patients ranging from G1 to G3.

3.2.3 Proteomic Analysis of Patients Most/Least Sensitive to Bortezomib, Carfilzomib, Quizinostat and PF-04691502 Exhibit Similar Protein Signatures

In-depth proteomic analysis of samples identified statistically significant ($p<0.05$) proteins with changes in abundance. This data was used to compile a heatmap for each individual drug (Figs. 3.4, 3.5, 3.6 and 3.7). Patients exhibited similar protein signatures to Bortezomib, Carfilzomib, Quizinostat and PF-04691502.

Bortezomib and Carfilzomib (Figs. 3.4 and 3.5) show a clear distinction in protein abundance from the ten most sensitive patients and the ten least sensitive patients. Quizinostat (Fig. 3.6) exhibits distinct difference in protein abundance between the two different patient groups, especially in the first seven patients in the least sensitive group in comparison with the most sensitive group. The difference seen in three of the least sensitive patients may be due to the partial positive response seen by the specific three patients in the least sensitive group. With a less apparent distinction between both groups compiled after treatment with PF-04691502 (Fig. 3.7), the slight overlap from four of the least sensitive patients into the most sensitive group is most likely due to a partially positive response recorded from these four patient samples, similar to that seen in Quizinostat.

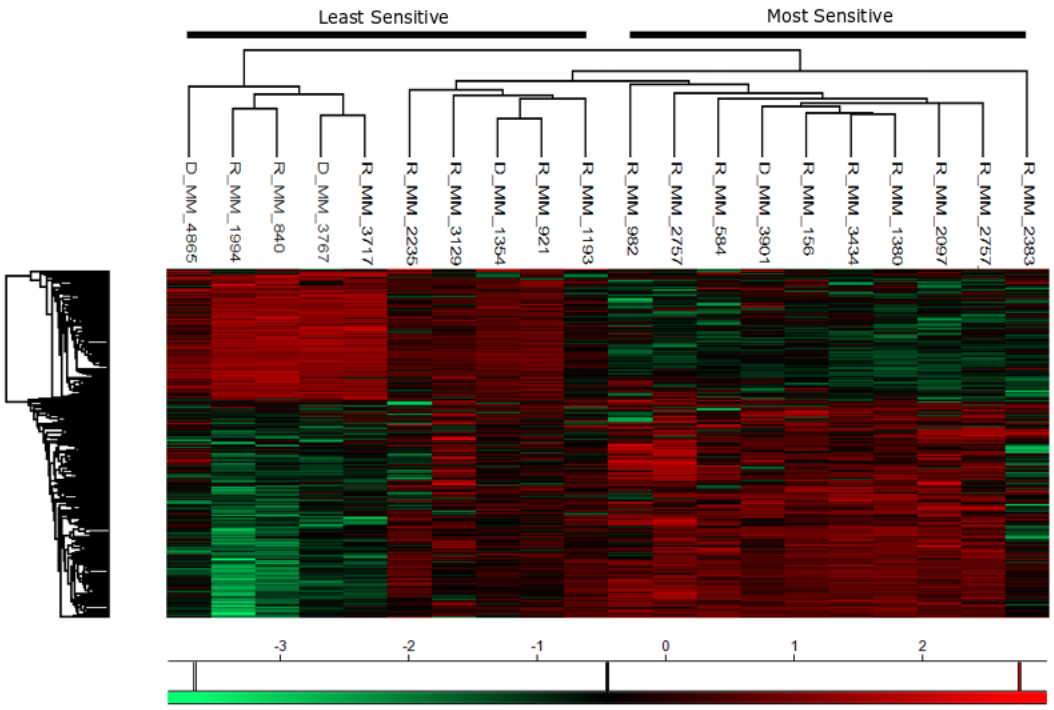

Figure 3.4: Heatmap Depicting the Change in Abundance of Proteins Identified by LC-MS/MS Between Most and Least Sensitive Patients to Treatment using Bortezomib.

Heatmap showing protein abundance changes of the ten most sensitive and the ten least sensitive patients to Bortezomib, individually identified by corresponding patient number above heatmap. Most sensitive and least sensitive patients were determined by drug sensitivity and resistances testing. Red indicates an increased abundance of individual proteins, while green a decrease in protein abundance. Increased and decreased abundance are determined by LFQ intensities from LC-MS/MS analysis.

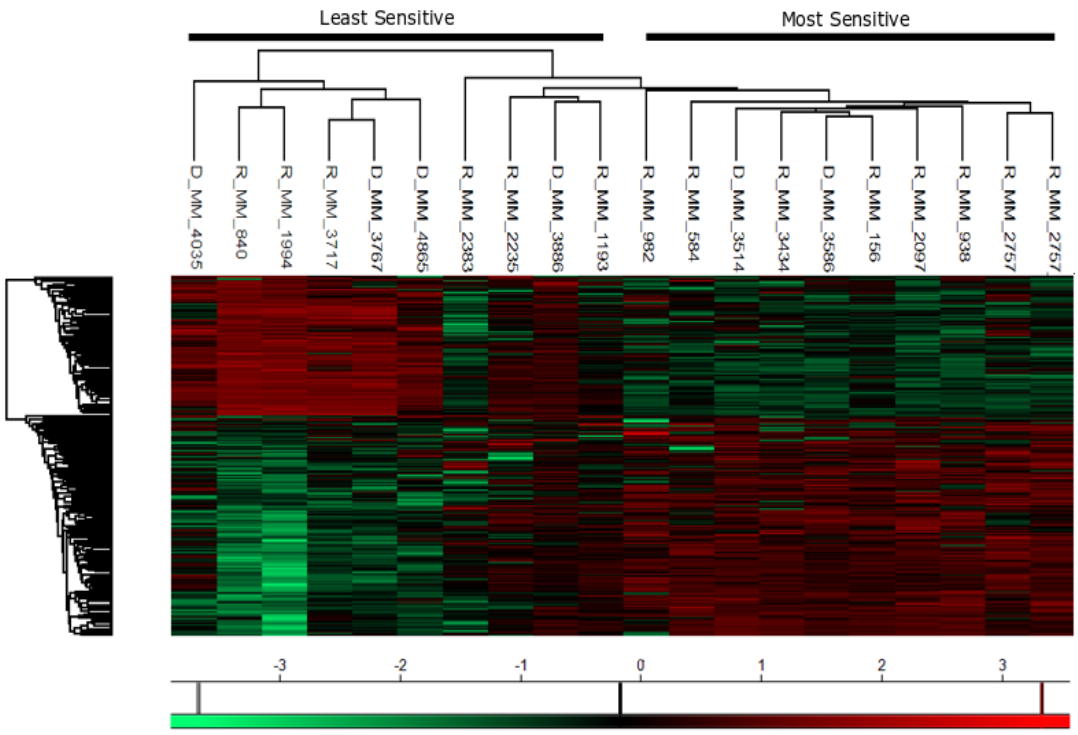

Figure 3.5: Heatmap Depicting the Change in Abundance of Proteins Identified by LC-MS/MS Between Most and Least Sensitive Patients to Treatment using Carfilzomib.

Heatmap showing protein abundance changes of the ten most sensitive and the ten least sensitive patients to Carfilzomib, individually identified by corresponding patient number above heatmap. Most sensitive and least sensitive patients were determined by drug sensitivity and resistances testing. Red indicates an increased abundance of individual proteins, while green a decrease in protein abundance. Increased and decreased abundance are determined by LFQ intensities from LC-MS/MS analysis.

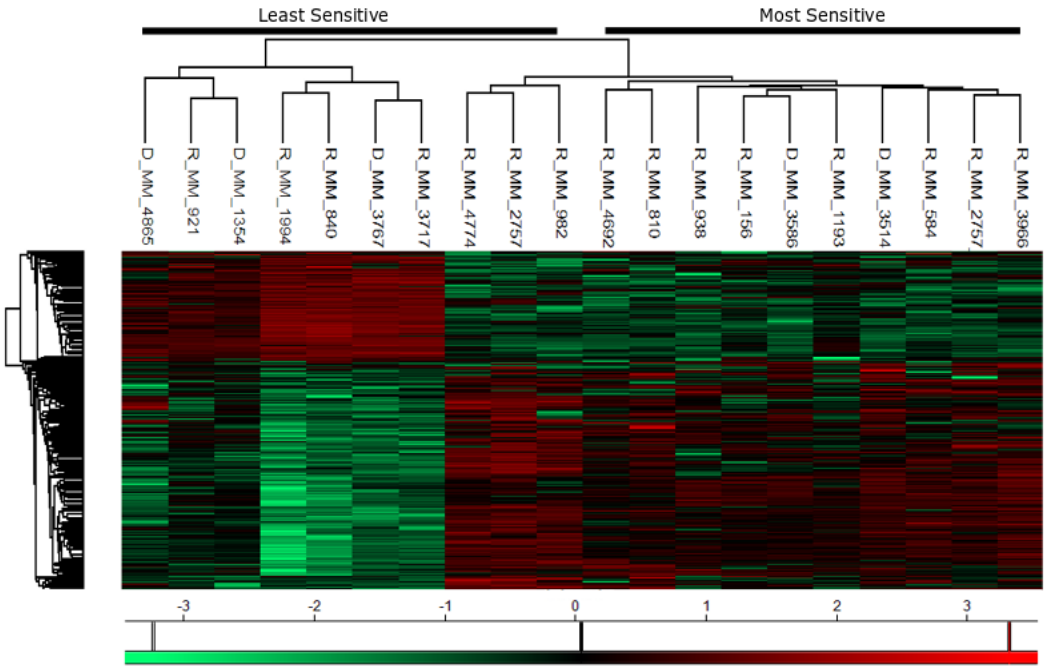

Figure 3.6: Heatmap Depicting the Change in Abundance of Proteins Identified by LC-MS/MS Between Most and Least Sensitive Patients to Treatment using Quizinostat.

Heatmap showing protein abundance changes of the ten most sensitive and the ten least sensitive patients to Quizinostat, individually identified by corresponding patient number above heatmap. Most sensitive and least sensitive patients were determined by drug sensitivity and resistances testing. Red indicates an increased abundance of individual proteins, while green a decrease in protein abundance. Increased and decreased abundance are determined by LFQ intensities from LC-MS/MS analysis.

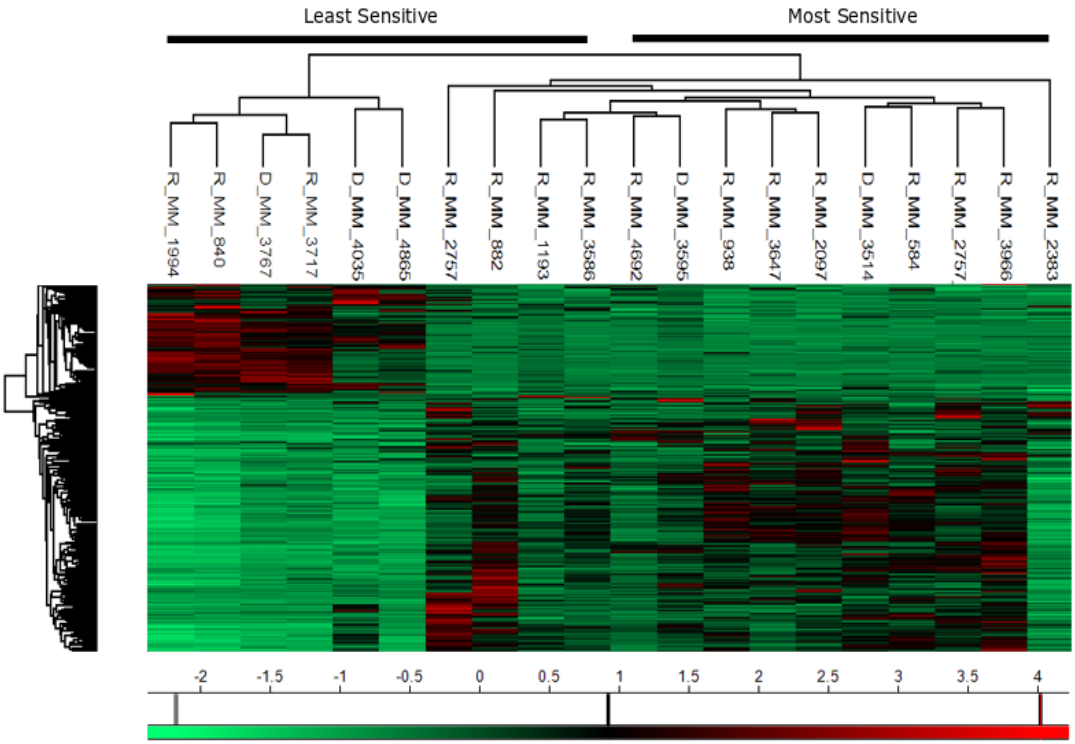

Figure 3.7: Heatmap Depicting the Change in Abundance of Proteins Identified by LC-MS/MS Between Most and Least Sensitive Patients to Treatment using PF-04691502.

Heatmap showing protein abundance changes of the ten most sensitive and the ten least sensitive patients to PF-04691502, individually identified by corresponding patient number above heatmap. Most sensitive and least sensitive patients were determined by drug sensitivity and resistances testing. Red indicates an increased abundance of individual proteins, while green a decrease in protein abundance. Increased and decreased abundance are determined by LFQ intensities from LC-MS/MS analysis.

3.2.4 Proteomic Analysis of Patients Most/Least Sensitive to Lenalidomide and Navitoclax Exhibit Different Protein Signatures

A distinction between least sensitive and most sensitive patients is less apparent in response to Lenalidomide (Fig. 3.8). Navitoclax on the other hand, revealed a stark contrast between most and lease sensitive patients' protein abundance (Fig. 3.9).

3.2.5 Metabolic Pathways are Associated with Most Sensitive Patients while Biological Adhesion is Associated with Least Sensitive Patients

The proteomic dataset was further analysed using PANTHER to identify the biological processes which are associated with these altered proteins for the six selected chemotherapeutics. For both Bortezomib (Fig. 3.10) and Carfilzomib (Fig. 3.11), a significant increase in the abundance of proteins related to metabolic processes in the most sensitive group of patients was identified, whereas an increased abundance of proteins associated with biological adhesion was found in the least sensitive group. For Quizinostat (Fig. 3.12), an increase in metabolic process-related proteins and cellular component organization or biogenesis proteins is recorded in the most sensitive group. Similar results were obtained for PF-04691502 (Fig. 3.13). Biological adhesion associated proteins are increased in abundance in Quizinostat and PF-04691502 in the least sensitive patients.

Metabolic process- related proteins exhibit a higher abundance in the most sensitive patients after treatment using Quizinostat (Fig. 3.12), mirroring the findings observed for Bortezomib, Carfilzomib and PF-04691502. Interestingly, an increased abundance in cellular component organization or biogenesis associated proteins were more abundant in the most sensitive patients than least sensitive patients following Quizinostat treatment, showing a similar increase as for Navitoclax (Fig. 3.15). Again, biological adhesion associated proteins are clearly associated with the least sensitive patients for Quizinostat. A significant increase in metabolic process,

cellular process, biological regulation proteins and cellular component organization or biogenesis proteins can be observed for Lenalidomide in the most sensitive patients (Fig. 3.15); however the larger volume of proteins exhibited in the most sensitive patients may lead to this increased abundance. Furthermore, a significant increase in the abundance of metabolic process proteins was observed in the least sensitive patients for Navitoclax (Fig. 3.14).

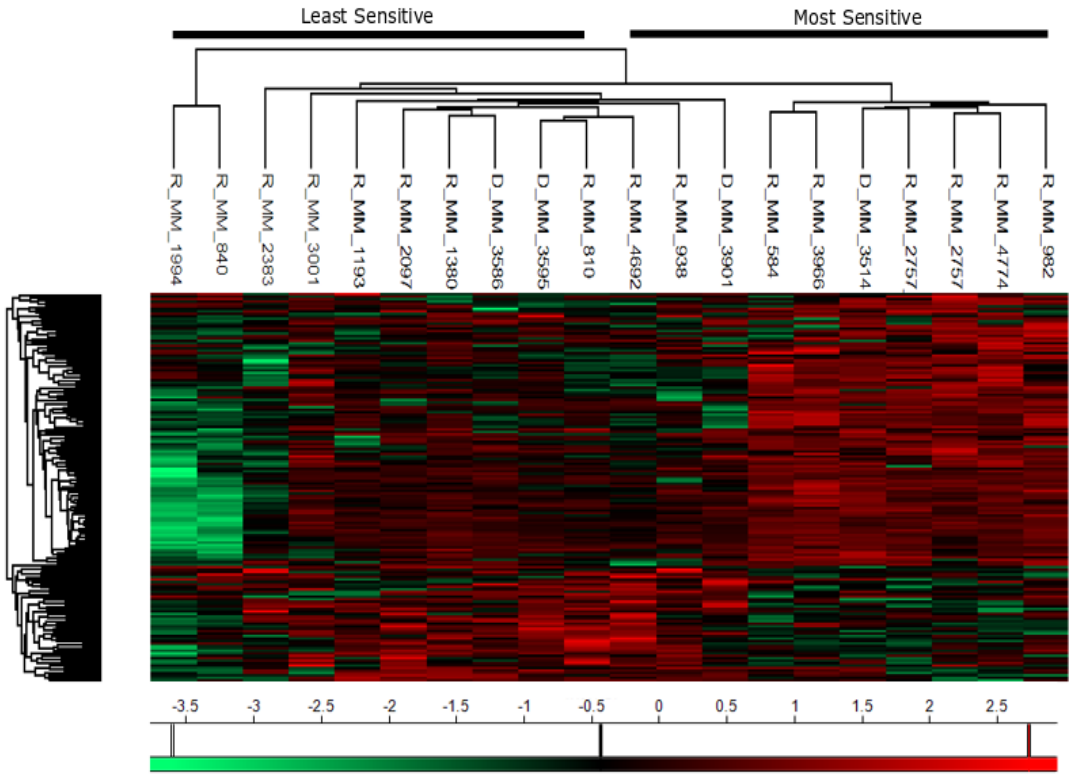

Figure 3.8: Heatmap Depicting the Change in Abundance of Proteins Identified by LC-MS/MS Between Most and Least Sensitive Patients to Treatment using Lenalidomide.

Heatmap showing protein abundance changes of the ten most sensitive and the ten least sensitive patients to Lenalidomide, individually identified by corresponding patient number above heatmap. Most sensitive and least sensitive patients were determined by drug sensitivity and resistances testing. Red indicates an increased abundance of individual proteins, while green a decrease in protein abundance. Increased and decreased abundance are determined by LFQ intensities from LC-MS/MS analysis.

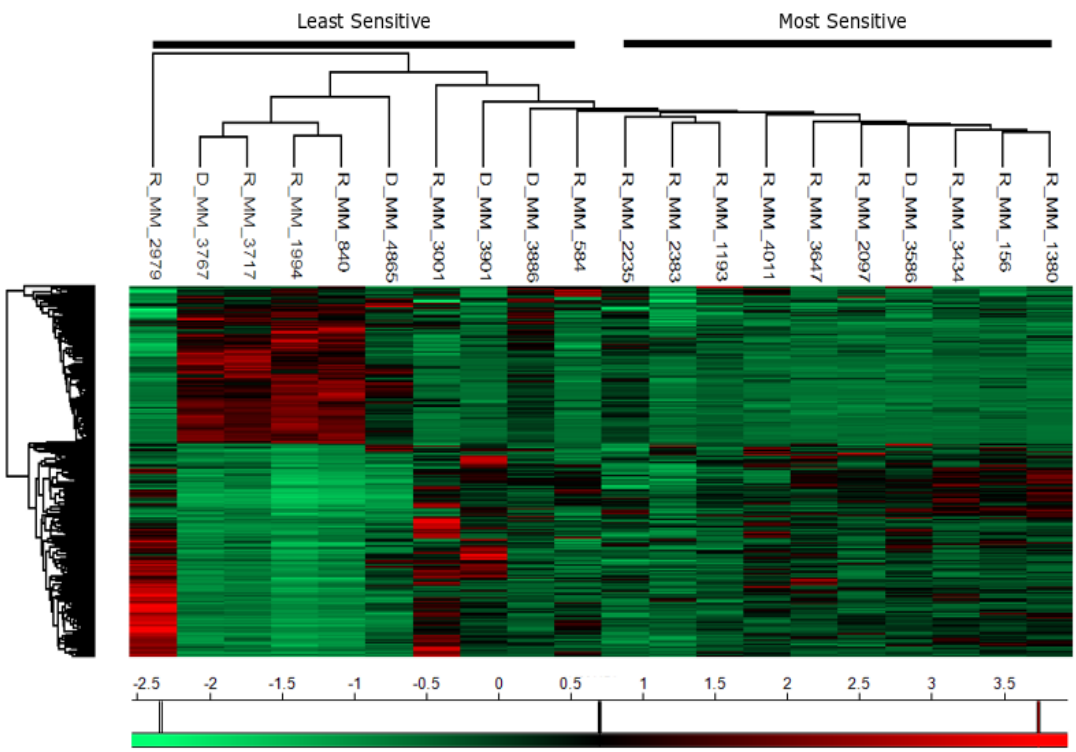

Figure 3.9: Heatmap Depicting the Change in Abundance of Proteins Identified by LC-MS/MS Between Most and Least Sensitive Patients to Treatment using Navitoclax.

Heatmap showing protein abundance changes of the ten most sensitive and the ten least sensitive patients to Navitoclax, individually identified by corresponding patient number above heatmap. Most sensitive and least sensitive patients were determined by drug sensitivity and resistances testing. Red indicates an increased abundance of individual proteins, while green a decrease in protein abundance. Increased and decreased abundance are determined by LFQ intensities from LC-MS/MS analysis.

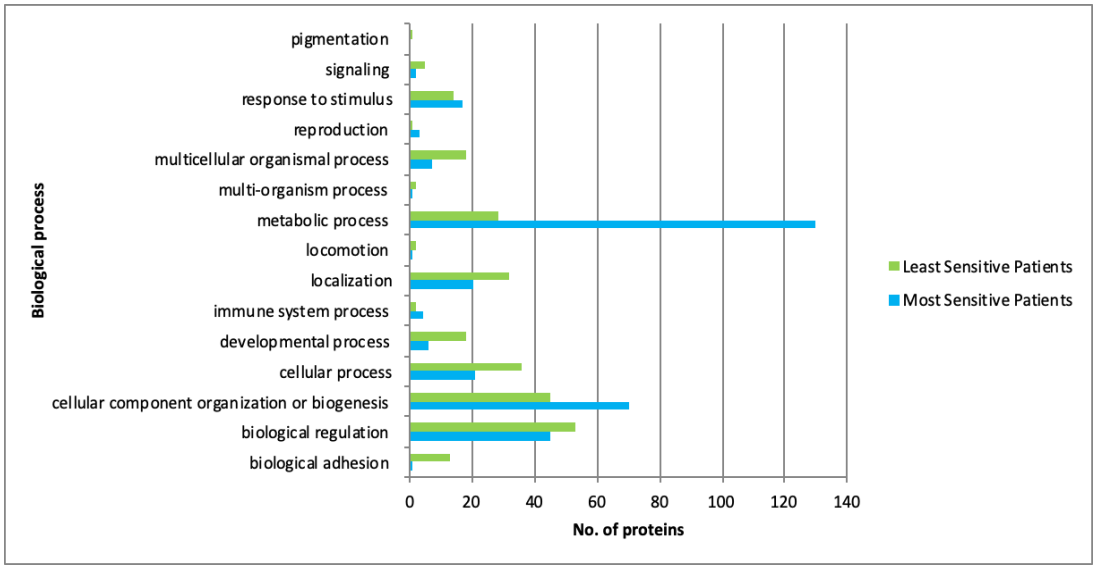

Figure 3.10: PANTHER analysis of Biological Processes Associated with Proteins Identified by LC-MS/MS After Treatment with Bortezomib.

Graphical comparison showing the biological processes associated the most sensitive (blue) and least sensitive (green) patients to treatment using Bortezomib.

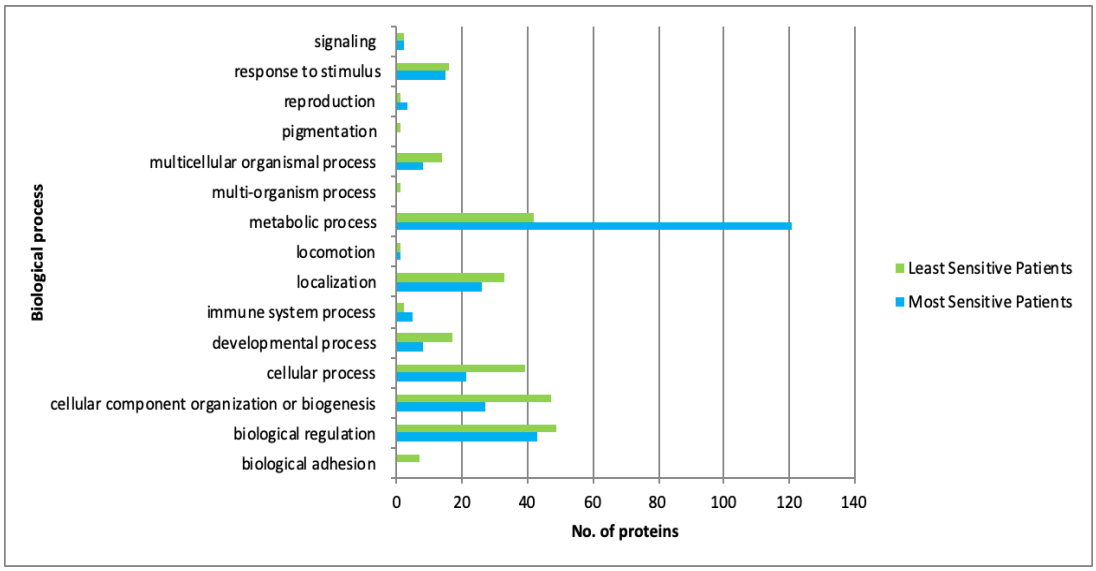

Figure 3.11: PANTHER analysis of Biological Processes Associated with Proteins Identified by LC-MS/MS After Treatment with Carfilzomib.

Graphical comparison showing the biological processes associated the most sensitive (blue) and least sensitive (green) patients to treatment using Bortezomib.

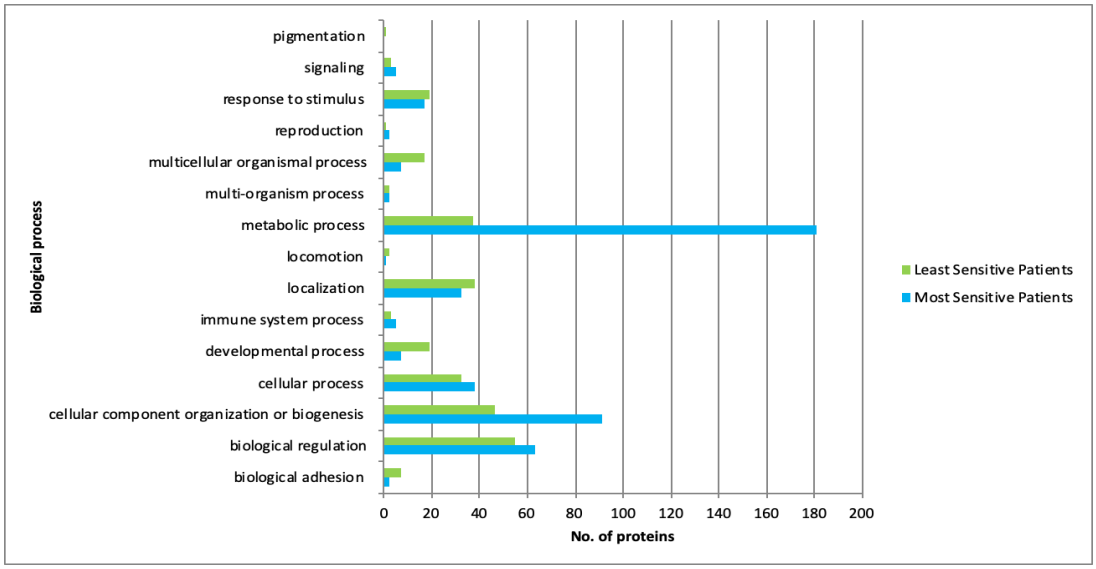

Figure 3.12: PANTHER analysis of Biological Processes Associated with Proteins Identified by LC-MS/MS After Treatment with Quizinostat.

Graphical comparison showing the biological processes associated the most sensitive (blue) and least sensitive (green) patients to treatment using Bortezomib.

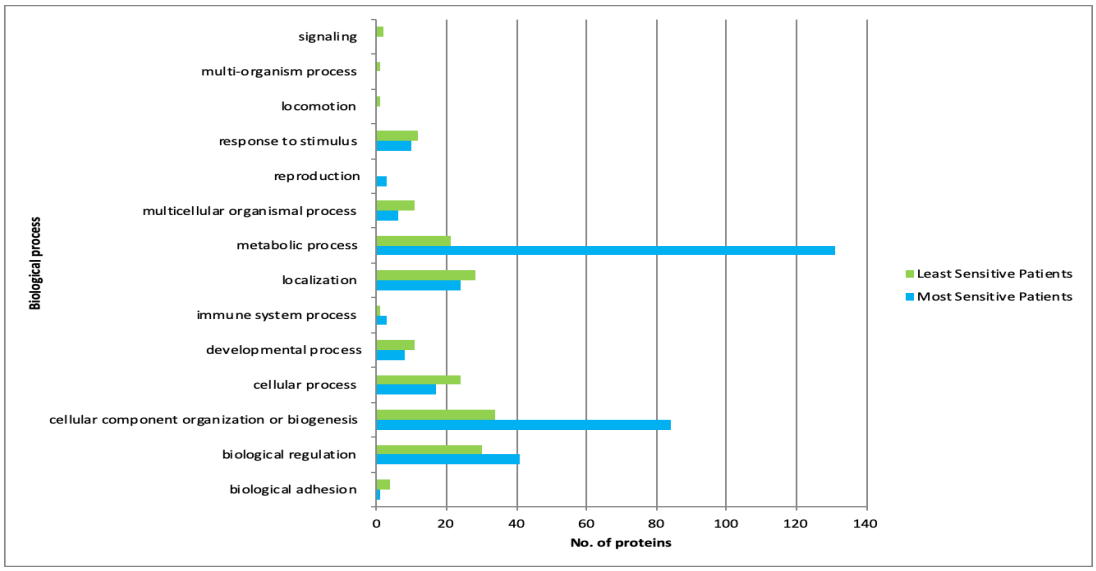

Figure 3.13: PANTHER analysis of Biological Processes Associated with Proteins Identified by LC-MS/MS After Treatment with PF-04691502.

Graphical comparison showing the biological processes associated the most sensitive (blue) and least sensitive (green) patients to treatment using Bortezomib.

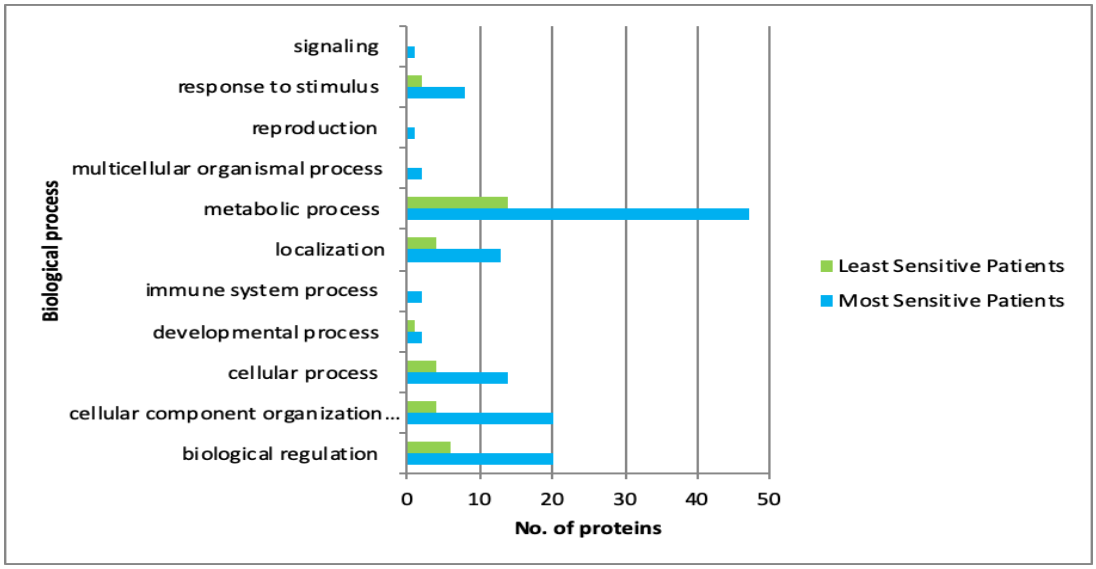

Figure 3.14: PANTHER analysis of Biological Processes Associated with Proteins Identified by LC-MS/MS After Treatment with Lenalidomide.

Graphical comparison showing the biological processes associated the most sensitive (blue) and least sensitive (green) patients to treatment using Bortezomib.

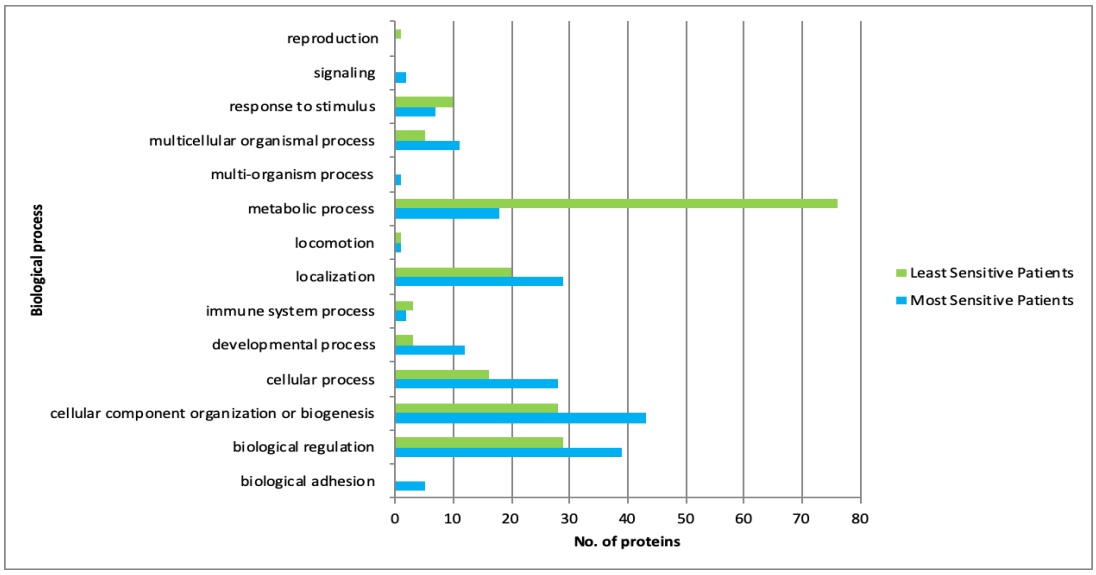

Figure 3.15: PANTHER analysis of Biological Processes Associated with Proteins Identified by LC-MS/MS After Treatment with Navitoclax.

Graphical comparison showing the biological processes associated the most sensitive (blue) and least sensitive (green) patients to treatment using Bortezomib.

3.2.6 Similar Individual Protein Signatures are Exhibited for Patients Treated with Bortezomib, Carfilzomib, Quizinostat and PF-04691502

We then investigated the individual proteins that showed an increased abundance in the most and least sensitive groups across the panel of six drugs. Altered proteins associated with Bortezomib treatment led to the observation of fold changes as high as 12.57 for Phosphoenolpyruvate carboxykinase [GTP] and high statistically significant abundance of Glycine-tRNA ligase and 40S ribosomal protein S24. Vastly more extreme fold changes, as observed for Integrin β3, and high statistically significant abundance of Talin-1, were recorded in the least sensitive group (Table 3.4). Five of the ten most statistically significant proteins in the most sensitive patients were strongly associated with cellular component organization or biogenesis, specifically Glycine-tRNA Ligase, 40S Ribosomal Protein S24, NSFL1 Cofactor p47, 60S Ribosomal Protein L38 and Tryptophan-tRNA Ligase (cytoplasmic) (Table 3.3). As both Carfilzomib and Bortezomib are PIs, there is an unsurprising similarity in both ten most significant protein lists. The fold changes recorded showed a significant change after treatment with Carfilzomib in abundance of biological adhesion and metabolic process proteins in the least sensitive group with fold changes as high as 756 times for Coagulation factor XIII A chain abundance and high statistically significant abundance for Vinculin (Table 3.6). Interestingly, seven of the ten proteins with the highest significance in Bortezomib are similarly recorded in Carfilzomib, however, the fold change of these proteins is recorded as being significantly higher. Five of the seven identical proteins are linked closely with the focal adhesion pathway and, more specifically, with actin polymerization. This is also observed in the proteins with altered abundance in the most sensitive group, with the increased abundance of Glycine-tRNA Ligase, Tryptophan- tRNA Ligase (cytoplasmic), Phosphoenolpyruvate carboxykinase [GTP], Phosphoserine aminotransferase seen with treatment using

both PIs, two of which are cellular component organization or biogenesis associated proteins (Table 3.5).

A list of the ten most significant proteins for each group was compiled for treatment using PF-04691502. Fold changes as high as 13.25 and high statistically significant abundance for D-3-phosphoglycerate dehydrogenase were observed in the most sensitive group of patients (Table 3.9) with fold changes as high as 96.02 for Integrin β3 and high statistically significant abundance for Apolipoprotein A-I in the least sensitive grouping (Table 3.10). Five of the ten proteins observed in the least sensitive patients were also recorded in the least sensitive patients in Bortezomib (Table 3.4), Carfilzomib (Table 3.6) and Quizinostat (Table 3.8). Four of the ten proteins with altered abundance in the most sensitive group of patients were observed in either Bortezomib (Table 3.3) or Carfilzomib (Table 3.5) also, all of which are cellular component organization or biogenesis associated proteins.

From the two lists compiled after Quizinostat treatment, fold increases as high as 5.32 for Cold-inducible RNA-binding protein and high statistically significant abundance for Ubiquitin carboxyl-terminal hydrolase 7 was recorded in the most sensitive group of patients (Table 3.7). Fold changes as high as 481.27 for Integrin alpha-IIb with high statistically significant abundance for Vinculin were recorded in the least sensitive group (Table 3.8). Remarkably, five of the ten proteins with increased abundance in the least sensitive group were recorded as being highly abundant in either of the PIs used in this study (Tables 3.3, 3.5), two of which are also recorded after treatment with PF-04691502.

In four of the six drugs tested there is a very clear increase in the abundance of proteins related to the focal adhesion pathway, specifically actin production leading to cell motility, in the least sensitive groups. Bortezomib (Table 3.4), Carfilzomib (Table 3.6), Quizinostat (Table 3.8) and PF-04691502 (Table 3.10) all showed this statistically significant increased p-values for the abundance of these associated proteins. This indicated that there is a significant change in the production of actin

and, consequently, cell mobility related to poor sensitivity to these varying drug treatments. Vinculin and Integrin β-3 have a significant increase in abundance in all four of the previously mentioned drugs. A very significant fold increase is recorded in the abundance of Vinculin in treatment with Carfilzomib, with the lowest of the fold increase abundances seen in treatment with Bortezomib. Integrin β-3 has a similar fold increase abundance across all four treatments, the highest of which is observed in treatment using Quizinostat and the lowest in treatment with Bortezomib.

Talin-1, Gelsolin, Filamin A are all increased in abundance in the least sensitive patients in three of the six drugs tested, specifically in Bortezomib (Table 3.4), Carfilzomib (Table 3.6), Quizinostat (Table 3.8) and PF-04691502 (Table 3.10). Talin-1 is seen to have an increased abundance in Bortezomib, Carfilzomib and Quizinostat with a fold change increase with highest significance recorded in Carfilzomib, the lowest of the fold change increases is observed in Bortezomib. Interestingly, an increased abundance of Talin-1 is noted in treatment with Navitoclax, which is in contrast to findings for other drugs tested. Gelsolin is observed to be upregulated in treatment with Bortezomib, Carfilzomib and PF-04691502, with the most significant fold increase shown in Carfilzomib and the lowest fold change observed in Bortezomib. Filamin A shows a similar trend in increased abundance to that of previously discussed proteins, with an increased abundance observed in Bortezomib, Carfilzomib and Quizinostat. The largest fold change recorded in Quizinostat with the lowest of the fold changes recorded in treatment with Bortezomib.

Table 3.3: Top 10 Most Significant Proteins with Increased Abundance in the 10 Most Sensitive Patients to Treatment Using Bortezomib.

Top 10 Most Significant Proteins with Increased Abundance in Most Sensitive Patients	Biological Function	Fold Change	p-value
Glycine--tRNA ligase	Cellular component organization or biogenesis	2.14	0.000104
40S ribosomal protein S24	Cellular component organization or biogenesis	5.68	0.000119
NSFL1 cofactor p47	Cellular component organization or biogenesis	1.95	0.000351
Phosphoenolpyruvate carboxykinase [GTP], mitochondrial	Developmental Process	12.57	0.000449
Phosphoserine aminotransferase	Metabolic process	8.56	0.000456
60S ribosomal protein L38	Cellular component organization or biogenesis	2.19	0.000483
Cytosolic non-specific dipeptidase	Metabolic process	1.87	0.000492
Tryptophan--tRNA ligase, cytoplasmic	Cellular component organization or biogenesis	5.57	0.000516
Oxysterol-binding protein 1	Localization	2.32	0.000606
Interferon-inducible double-stranded RNA-dependent protein kinase activator A	Multicellular organismal process	2.07	0.000638

Table 3.4: Top 10 Most Significant Proteins with Increased Abundance in the 10 Least Sensitive Patients to Treatment Using Bortezomib.

Top 10 Most Significant Proteins with Increased Abundance in Least Sensitive Patients	Biological Function	Fold Change	p-value
Talin-1	Biological regulation	10.93	6.48E-06
Vinculin	Biological adhesion	19.04	7.65E-06
Coronin-1C	Cellular component organization or biogenesis	6.37	1.03E-05
Integrin beta-3	Biological adhesion	42.03	1.35E-05
Transgelin-2	Multicellular organismal process	7.65	2.48E-05
Gelsolin	Developmental process	19.01	3.44E-05
Vasodilator-stimulated phosphoprotein	Biological regulation	13.70	4.56E-05
Myotrophin	Biological adhesion	2.87	7.73E-05
Tropomyosin alpha-4 chain	Cellular component organization or biogenesis	6.68	8.17E-05
Filamin-A	Locomotion	15.15	8.84E-05

Table 3.5: Top 10 Most Significant Proteins with Increased Abundance in the 10 Most Sensitive Patients to Treatment Using Carfilzomib.

Top 10 Most Significant Proteins with Increased Abundance in Most Sensitive Patients	Biological Function	Fold Change	p-value
Tryptophan--tRNA ligase, cytoplasmic	Cellular component organization or biogenesis	7.27	5.44E-06
Bifunctional purine biosynthesis protein PURH	Metabolic process	2.02	0.000269
Phosphoenolpyruvate carboxykinase [GTP], mitochondrial	Biological regulation	9.79	0.000274
Phosphoserine aminotransferase	Metabolic process	9.69	0.000371
Elongation factor Tu, mitochondrial	Cellular component organization or biogenesis	1.74	0.000546
Rootletin	Biological regulation	2.91	0.000568
Proteasome-associated protein ECM29 homolog	Biological regulation	3.71	0.000614
Glycine--tRNA ligase	Cellular component organization or biogenesis	2.18	0.00064
Bifunctional 3-phosphoadenosine 5-phosphosulfate synthase 1	Metabolic process	5.33	0.000651
Interferon regulatory factor 4	Biological regulation	3.68	0.000737

Table 3.6: Top 10 Most Significant Proteins with Increased Abundance in the 10 Least Sensitive Patients to Treatment Using Carfilzomib.

Top 10 Most Significant Proteins with Increased Abundance in Least Sensitive Patients	Biological Function	Fold Change	p-value
Vinculin	Biological adhesion	264.90	1.02E-08
Talin-1	Developmental process	19.04	2.33E-07
Integrin beta-3	Biological adhesion	202.88	3.22E-07
Transgelin-2	Multicellular organismal process	14.68	1.11E-06
Gelsolin	Developmental process	68.14	1.18E-06
Coagulation factor XIII A chain	Metabolic process	756.41	1.44E-06
Vasodilator-stimulated phosphoprotein	Biological regulation	39.27	2.73E-06
Filamin-A	Locomotion	42.32	4.12E-06
Integrin alpha-IIb	Biological adhesion	209.46	7.99E-06
Voltage-dependent anion-selective channel protein 3	Localisation	1.86	8.99E-06

Table 3.7: Top 10 Most Significant Proteins with Increased Abundance in the 10 Most Sensitive Patients to Treatment Using Quizinostat.

Top 10 Most Significant Proteins with Increased Abundance in Most Sensitive Patients	Biological Function	Fold Change	p-value
Ubiquitin carboxyl-terminal hydrolase 7	Biological regulation	3.39	2.40E-05
KH domain-containing, RNA-binding, signal transduction-associated protein 1	Metabolic process	3.90	4.94E-05
Nuclear migration protein nudC	Cellular process	2.33	8.86E-05
Cold-inducible RNA-binding protein	Biological regulation	5.33	0.000118
Non-POU domain-containing octamer-binding protein	Biological regulation	4.04	0.000161
60S ribosomal protein L10	Cellular component organization or biogenesis	2.96	0.000168
Phosphoenolpyruvate carboxykinase [GTP], mitochondrial	Biological regulation	5.73	0.000183
Thymocyte nuclear protein 1	Cellular process	2.60	0.000188
Exportin-2	Localisation	3.28	0.000203
BolA-like protein 2	Biological regulation	3.99	0.000248

Table 3.8: Top 10 Most Significant Proteins with Increased Abundance in the 10 Least Sensitive Patients to Treatment Using Quizinostat.

Top 10 Most Significant Proteins with Increased Abundance in Least Sensitive Patients	Biological Function	Fold Change	p-value
Vinculin	Biological adhesion	120.65	1.18E-06
Platelet basic protein	Locomotion	145.90	2.47E-06
Filamin-A	Locomotion	53.53	3.45E-06
Talin-1	Developmental process	17.65	8.70E-06
Fermitin family homolog 3	Biological adhesion	18.00	1.25E-05
Erythrocyte band 7 integral membrane protein	Biological regulation	69.83	1.34E-05
Integrin alpha-IIb	Biological adhesion	481.28	1.86E-05
Integrin beta-3	Biological adhesion	349.10	2.38E-05
Profilin-1	Biological regulation	3.66	2.44E-05
Ras suppressor protein 1	Biological regulation	84.47	2.54E-05

Table 3.9: Top 10 Most Significant Proteins with Increased Abundance in the 10 Most Sensitive Patients to Treatment Using PF-04691502.

Top 10 Most Significant Proteins with Increased Abundance in Most Sensitive Patients	Biological Function	Fold Change	p-value
D-3-phosphoglycerate dehydrogenase	Metabolic process	13.25	2.73E-05
ATP-binding cassette sub-family E member 1	Cellular compartment organization or biogenesis	2.08	6.68E-05
Dedicator of cytokinesis protein 2	Biological regulation	2.53	9.15E-05
26S protease regulatory subunit 10B	Biological regulation	2.31	0.000132
Elongation factor Tu, mitochondrial	Cellular compartment organization or biogenesis	2.14	0.000208
40S ribosomal protein S6	Cellular compartment organization or biogenesis	2.07	0.000269
Glycine--tRNA ligase	Cellular compartment organization or biogenesis	2.19	0.000319
Phosphoenolpyruvate carboxykinase [GTP], mitochondrial	Biological regulation	7.83	0.000387
Heterogeneous nuclear ribonucleoprotein M	Biological regulation	2.48	0.000387
26S protease regulatory subunit 8	Biological regulation	1.85	0.000389

Table 3.10: Top 10 Most Significant Proteins with Increased Abundance in the 10 Least Sensitive Patients to Treatment Using PF-04691502.

Top 10 Most Significant Proteins with Increased Abundance in Least Sensitive Patients	Biological Function	Fold Change	p-value
Apolipoprotein A-I	Biological regulation	5.72	1.98E-05
Platelet endothelial cell adhesion molecule	Biological adhesion	12.01	3.96E-05
Integrin beta-3	Biological adhesion	96.02	7.00E-05
Alpha-1-antitrypsin	Metabolic process	4.77	7.22E-05
Coagulation factor XIII A chain	Metabolic process	49.63	9.31E-05
Vinculin	Biological adhesion	57.81	0.000152
Bridging integrator 2	Cellular compartment organization or biogenesis	13.91	0.000184
Voltage-dependent anion-selective channel protein 3	Localization	1.64	0.000501
Gelsolin	Developmental process	37.73	0.000532
Ras-related protein Rap-1b	Biological adhesion	9.35	0.000766

3.2.7 Different Individual Protein Signatures are Exhibited for Patients Treated with Lenalidomide and Navitoclax

The lack of distinction observed in the heat map from treatment using Lenalidomide (Figure 3.8) is also apparent in the ten most statistically significant proteins in both the most sensitive (Table 3.11) and least sensitive group of patients (Table 3.12) , where the fold changes and p-values of the abundantly changed proteins in both groups is significantly less drastic to that of the fold changes and p-values recorded for Bortezomib (Table 3.3-3.4) and Carfilzomib (Table 3.5-3.6). Both fold changes and p-values are vastly different to that of the generated lists for different drugs within this study, with high statistically significant abundance for Serine/threonine-protein kinase PAK 2 and fold changes as high as 4.74 for DNA replication licensing factor MCM2 in the most sensitive group. High statistically significant abundance for Very long-chain specific acylCoA dehydrogenase, mitochondrial and fold changes as high as 3.96 for Methylmalonate-semialdehyde dehydrogenase [acylating], mitochondrial in the least sensitive group. The proteins with altered abundance associated with this particular drug show no obvious overlap with the altered proteins from previously discussed treatments.

Fold increases as high as 41.97 for Pleckstrin and high statistically significant abundance for Alpha-actinin-1 were recorded in the most sensitive group for Navitoclax (Table 3.13) whereas fold changes as high as 3.45 for Nucleoside diphosphate kinase 3 and high statistically significant abundance for Phosphatidylethanolamine binding protein 1 were recorded in the least sensitive group (Table 3.14), following Navitoclax treatment. Seven out of ten of the most significant proteins changed in abundance in the least sensitive patients are observed to be metabolic process associated proteins whereas the most sensitive group has a less defined involvement in biological processes. Interestingly, trends exhibited after treatment with Navitoclax in altered protein abundance are opposite to those shown

after treatment with Bortezomib, Carfilzomib, Quizinostat and PF-04691502, with proteins exhibited in the most sensitive patients in table 3.13 observed in the least sensitive patients for these treatments and vice versa.

Table 3.11: Top 10 Most Significant Proteins with Increased Abundance in the 10 Most Sensitive Patients to Treatment Using Lenalidomide.

Top 10 Most Significant Proteins with Increased Abundance in Most Sensitive Patients	Biological Function	Fold Change	p-value
Serine/threonine-protein kinase PAK 2	Biological regulation	2.01	0.00016
DNA replication licensing factor MCM7	Cellular process	3.55	0.000507
Ataxin-10	Developmental process	1.63	0.001734
Host cell factor 1	Reproduction	2.42	0.001849
FACT complex subunit SSRP1	Cellular process	1.50	0.00202
Lamina-associated polypeptide 2, isoforms beta/gamma	Biological regulation	2.27	0.002061
Splicing factor 3B subunit 2	Metabolic process	1.78	0.002243
ATP-binding cassette sub-family F member 1	Metabolic process	1.51	0.002361
Heat shock protein HSP 90-alpha	Biological regulation	1.71	0.00237
DNA replication licensing factor MCM2	Cellular process	4.74	0.00304

Table 3.12: Top 10 Most Significant Proteins with Increased Abundance in the 10 Least Sensitive Patients to Treatment Using Lenalidomide.

Top 10 Most Significant Proteins with Increased Abundance in Least Sensitive Patients	Biological Function	Fold Change	p-value
Very long-chain specific acyl-CoA dehydrogenase, mitochondrial	Metabolic process	2.04	0.001889
Nucleobindin-2	Biological regulation	2.50	0.00373
Methylmalonate-semialdehyde dehydrogenase [acylating], mitochondrial	Metabolic process	3.96	0.004655
Protein disulfide-isomerase A3	Response to stimuli	2.13	0.005016
Phosphoacetylglucosamine mutase	Metabolic process	2.04	0.006313
Methylthioribulose-1-phosphate dehydratase	Metabolic process	2.05	0.006362
Protein transport protein Sec23A	Biological regulation	1.62	0.007053
Putative ATP-dependent RNA helicase DHX30	Biological regulation	1.27	0.007567
D-tyrosyl-tRNA(Tyr) deacylase 1	Biological regulation	1.48	0.007882
Annexin A7	Cellular process	1.45	0.011916

Table 3.13: Top 10 Most Significant Proteins with Increased Abundance in the 10 Most Sensitive Patients to Treatment Using Navitoclax.

Top 10 Most Significant Proteins with Increased Abundance in Most Sensitive Patients	Biological Function	Fold Change	p-value
Alpha-actinin-1	Locomotion	20.45	1.11E-05
Talin-1	Developmental process	19.73	1.40E-05
Transgelin-2	Multicellular organismal process	10.50	2.85E-05
Myosin regulatory light chain 12A	Development process	7.20	6.25E-05
Vasodilator-stimulated phosphoprotein	Biological regulation	28.96	7.19E-05
Fermitin family homolog 3	Biological adhesion	14.81	8.02E-05
Bridging integrator 2	Cellular component organization or biogenesis	12.59	8.81E-05
Pleckstrin	Cellular process	41.98	8.96E-05
14-3-3 protein eta	Biological regulation	6.22	0.00013
Tubulin beta-1 chain	Cellular component organization or biogenesis	11.45	0.000158

Table 3.14: Top 10 Most Significant Proteins with Increased Abundance in the 10 Least Sensitive Patients to Treatment Using Navitoclax.

Top 10 Most Significant Proteins with Increased Abundance in Least Sensitive Patients	Biological Function	Fold Change	p-value
Phosphatidylethanolamine-binding protein 1	Biological regulation	2.59	0.000154
NADH dehydrogenase [ubiquinone] 1 alpha subcomplex subunit 5	Metabolic process	1.94	0.000329
Inorganic pyrophosphatase	Metabolic process	2.68	0.000824
NSFL1 cofactor p47	Cellular component organization or biogenesis	1.82	0.000967
Endophilin-B2	Biological adhesion	2.16	0.001021
Nucleoside diphosphate kinase 3	Metabolic process	3.45	0.001304
3-hydroxyisobutyryl-CoA hydrolase, mitochondrial	Metabolic process	3.08	0.001418
ATP synthase subunit delta, mitochondrial	Metabolic process	2.39	0.001434
ATP synthase F(0) complex subunit B1, mitochondrial	Metabolic process	1.69	0.001951
ATP synthase subunit O, mitochondrial	Metabolic process	1.90	0.00203

3.2.8 AUC ROC Exhibited by Most and Least Sensitive Patients Using Treatments Showing Similar Proteomic Signatures.

The area under the receiver-operator characteristic curve (AUC ROC) value for the top five most significant candidate biomarkers was calculated for each drug used in this study. The AUC was found to have good discriminatory power for all potential biomarkers for sensitive patients using Bz, ranging from 0.9 for RS24 and 0.95 for SYG (Fig. 3.16), according to guidelines published by Hosmer and Lemeshow. In the least sensitive patients, grouping AUC values ranged from 0.96 for VINC and TAGL2 to 0.98 for TLN1, exhibiting remarkable discriminatory power for all potential biomarkers (Fig. 3.17). PF-04691502 showed similar notable AUC values ranging from 0.95 for LC7L2 to 0.96 for the remaining four potential biomarkers for the most sensitive patients (Fig. 3.20) and a range of 0.98 for four potential biomarkers to 1 for A1AT (Fig. 3.21) with respect to the least sensitive patients. Quizinostat was found to have a range of AUC values of 0.835 for CIRBP to 1.000 for UBP7 for the most sensitive group of patients (Fig. 3.22) and a range from 0.970 for FLNA and TLN1 to 0.99 for CXCL7 in the least sensitive patient grouping (Fig. 3.23). These values represent excellent discriminatory power.

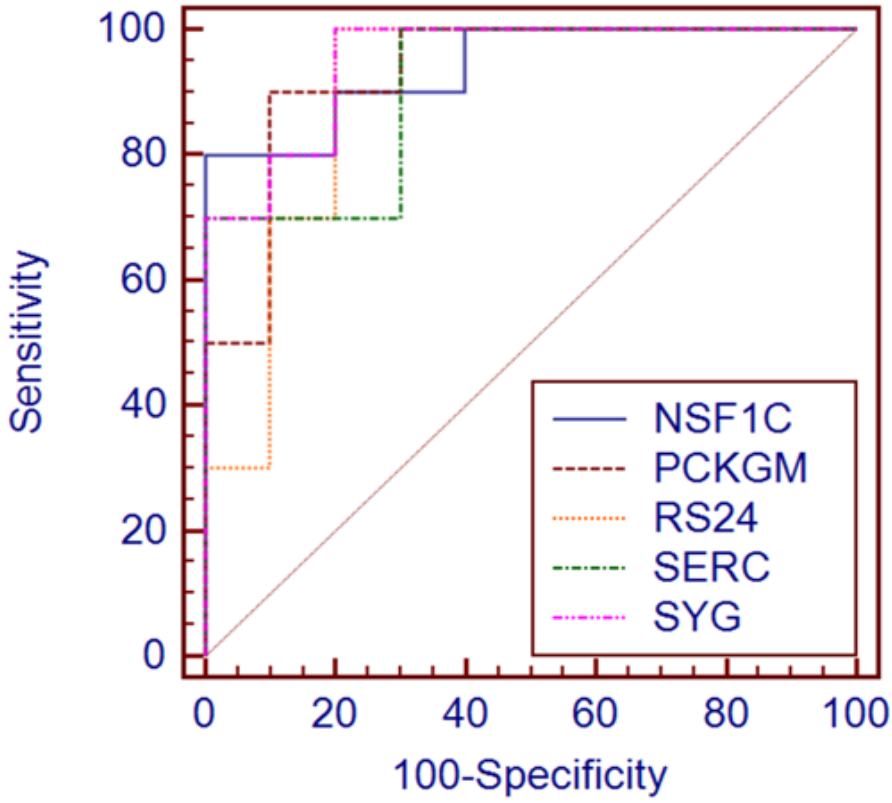

Protein	AUC	SE	95% CI
NSF1C	0.94	0.05	0.737 to 0.997
PCKGM	0.93	0.058	0.723 to 0.996
RS24	0.9	0.078	0.683 to 0.988
SERC	0.91	0.065	0.696 to 0.991
SYG	0.95	0.044	0.751 to 0.999

Figure 3.16: AUC ROC Analysis of the Five Most Significant Proteins with an Increased Abundance in the Most Sensitive Patients After Treatment Using Bortezomib.

ROC analysis for the top five statistically significant proteins for the most sensitive patients to bortezomib, including the calculated AUC, standard error (SE) and 95% confidence interval (CI).

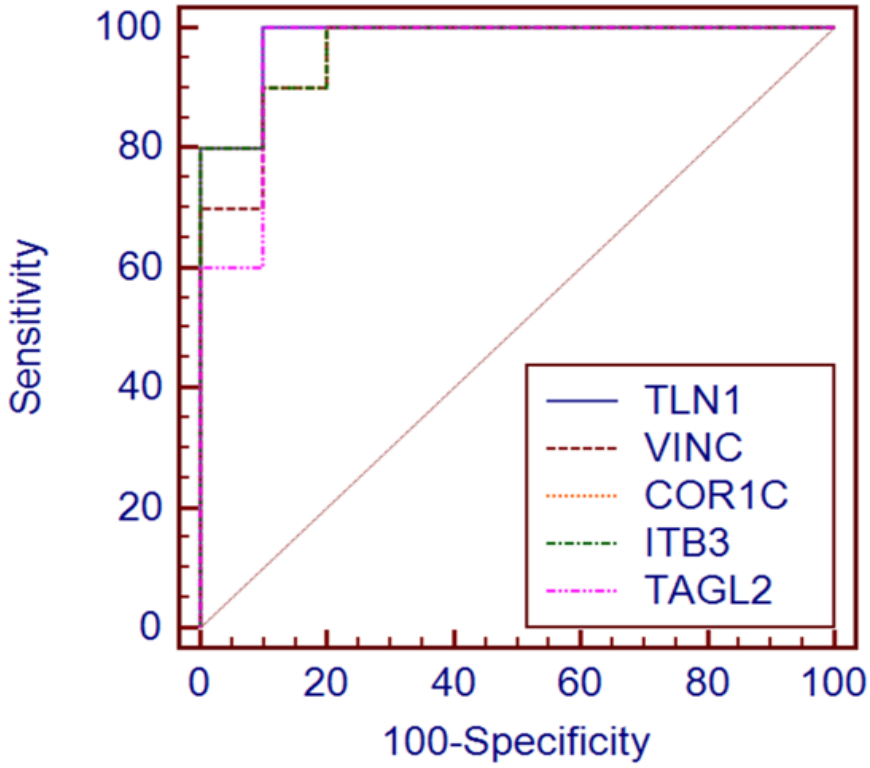

Protein	AUC	SE	95% CI
TLN1	0.98	0.024	0.797 to 1.000
VINC	0.96	0.038	0.766 to 1.000
COR1C	0.97	0.03	0.781 to 1.000
ITB3	0.97	0.03	0.781 to 1.000
TAGL2	0.96	0.043	0.766 to 1.000

Figure 3.17: AUC ROC Analysis of the Five Most Significant Proteins with an Increased Abundance in the Least Sensitive Patients After Treatment Using Bortezomib.

ROC analysis for the top five statistically significant proteins for the least sensitive patients to bortezomib, including the calculated AUC, standard error (SE) and 95% confidence interval (CI).

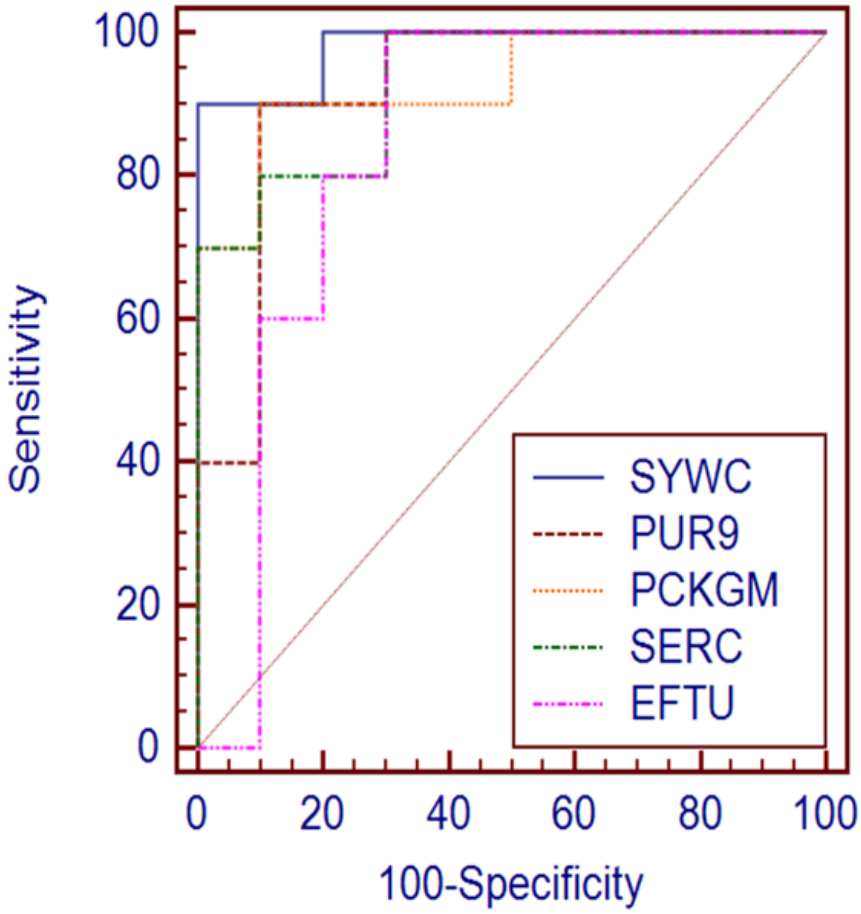

Protein	AUC	SE	95% CI
SYWC	0.98	0.024	0.797 to 1.000
PUR9	0.92	0.066	0.709 to 0.993
PCKGM	0.93	0.0579	0.723 to 0.996
SERC	0.93	0.054	0.723 to 0.996
EFTU	0.84	0.106	0.609 to 0.963

Figure 3.18: AUC ROC Analysis of the Five Most Significant Proteins with an Increased Abundance in the Most Sensitive Patients After Treatment Using Carfilzomib.

ROC analysis for the top five statistically significant proteins for the most sensitive patients to Carfilzomib, including the calculated AUC, standard error (SE) and 95% confidence interval (CI).

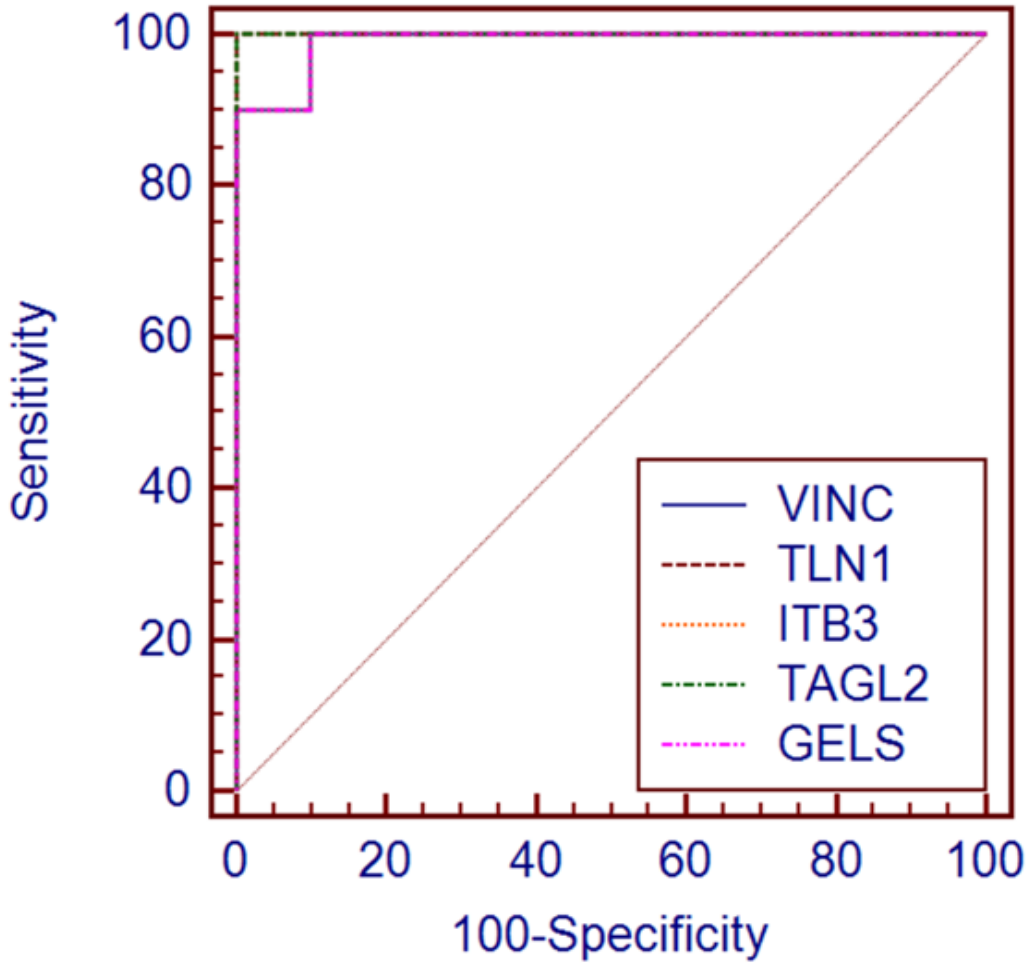

Protein	AUC	SE	95% CI
VINC	0.99	0.0141	0.814 to 1.000
TLN1	1	0	0.832 to 1.000
ITB3	0.99	0.0141	0.814 to 1.000
TAGL2	1	0	0.832 to 1.000
GELS	0.99	0.0141	0.814 to 1.000

Figure 3.19: AUC ROC Analysis of the Five Most Significant Proteins with an Increased Abundance in the Least Sensitive Patients After Treatment Using Carfilzomib.

ROC analysis for the top five statistically significant proteins for the least sensitive patients to Carfilzomib, including the calculated AUC, standard error (SE) and 95% confidence interval (CI).

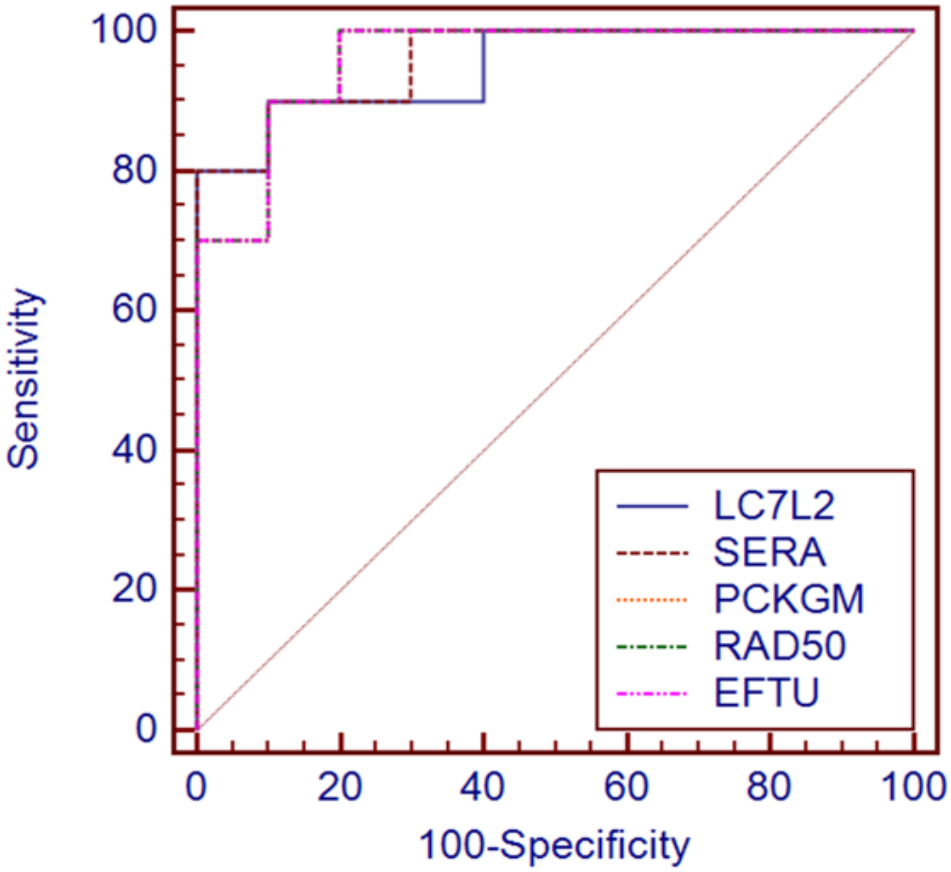

Protein	AUC	SE	95% CI
LC7L2	0.95	0.0459	0.751 to 0.999
SERA	0.96	0.0377	0.766 to 1.000
PCKGM	0.96	0.0377	0.766 to 1.000
RAD50	0.96	0.0377	0.766 to 1.000
EFTU	0.96	0.0377	0.766 to 1.000

Figure 3.20: AUC ROC Analysis of the Five Most Significant Proteins with an Increased Abundance in the Most Sensitive Patients After Treatment Using PF-04691502.

ROC analysis for the top five statistically significant proteins for the most sensitive patients to PF-04691502, including the calculated AUC, standard error (SE) and 95% confidence interval (CI).

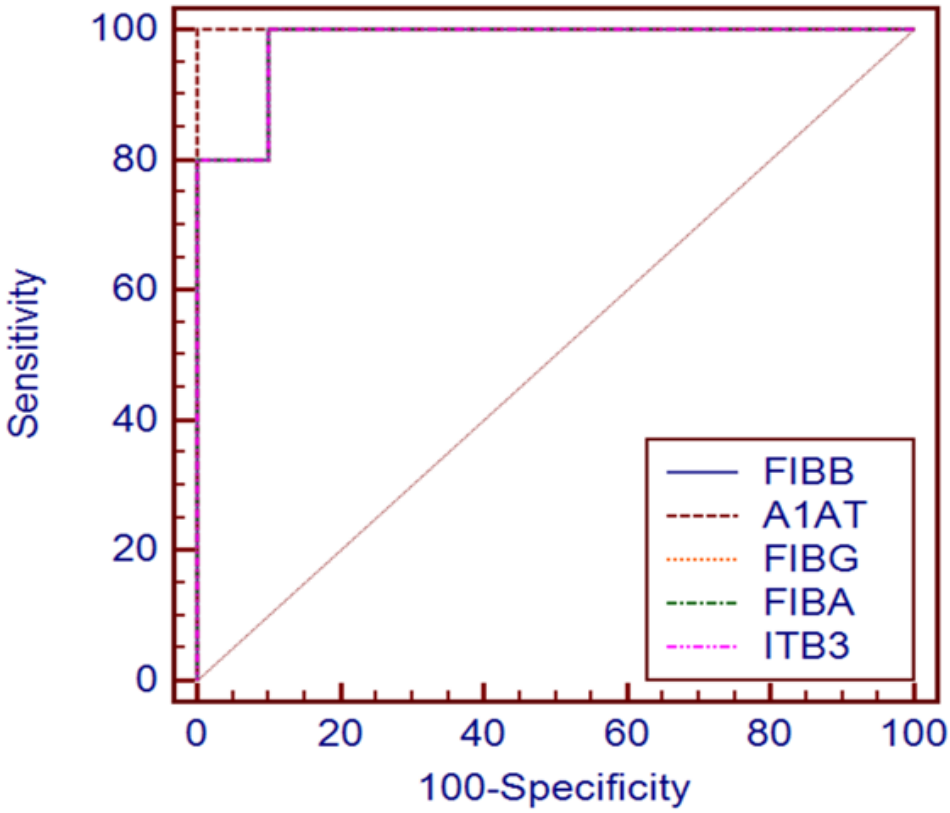

Protein	AUC	SE	95% CI
FIBB	0.98	0.024	0.797 to 1.000
A1AT	1	0	0.832 to 1.000
FIBG	0.98	0.024	0.797 to 1.000
FIBA	0.98	0.024	0.797 to 1.000
ITB3	0.98	0.024	0.797 to 1.000

Figure 3.21: AUC ROC Analysis of the Five Most Significant Proteins with an Increased Abundance in the Least Sensitive Patients After Treatment Using PF-04691502.

ROC analysis for the top five statistically significant proteins for the least sensitive patients to PF-04691502, including the calculated AUC, standard error (SE) and 95% confidence interval (CI).

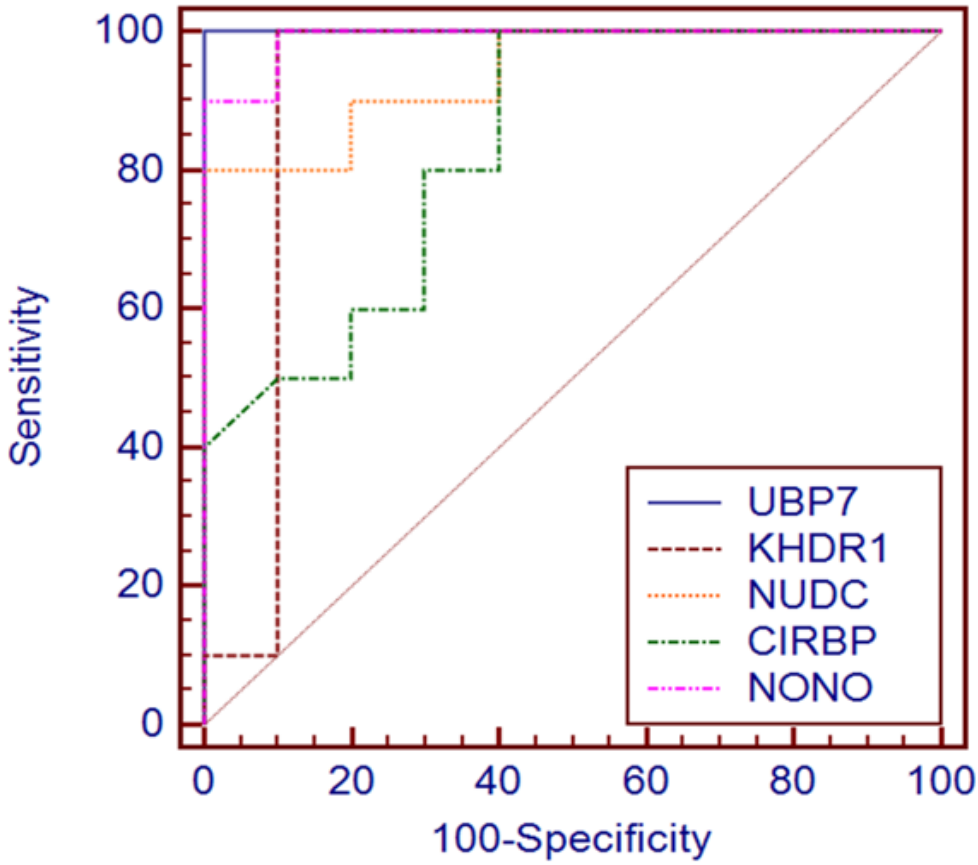

Protein	AUC	SE	95% CI
UBP7	1	0	0.832 to 1.000
KHDR1	0.91	0.0906	0.696 to 0.991
NUDC	0.94	0.0503	0.737 to 0.997
CIRBP	0.835	0.0913	0.603 to 0.961
NONO	0.99	0.0141	0.814 to 1.000

Figure 3.22: AUC ROC Analysis of the Five Most Significant Proteins with an Increased Abundance in the Most Sensitive Patients After Treatment Using Quizinostat.

ROC analysis for the top five statistically significant proteins for the most sensitive patients to Quizinostat, including the calculated AUC, standard error (SE) and 95% confidence interval (CI).

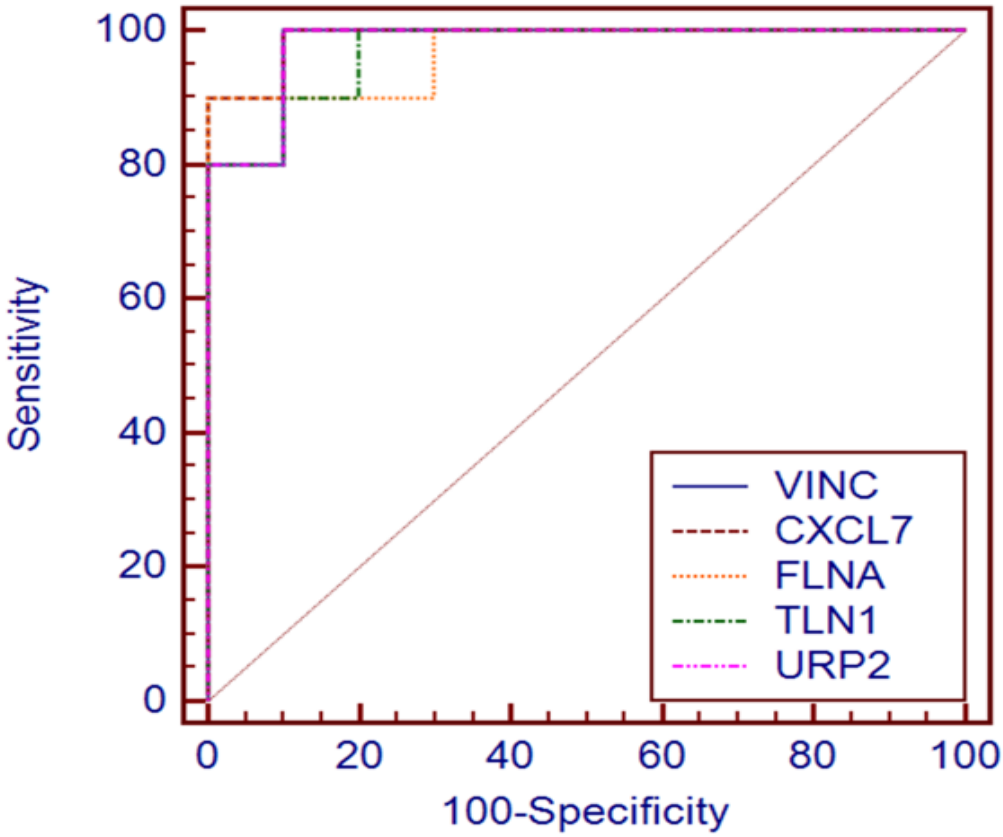

Protein	AUC	SE	95% CI
VINC	0.98	0.024	0.797 to 1.000
CXCL7	0.99	0.0141	0.814 to 1.000
FLNA	0.97	0.0337	0.781 to 1.000
TLN1	0.97	0.0302	0.781 to 1.000
URP2	0.98	0.024	0.797 to 1.000

Figure 3.23: AUC ROC Analysis of the Five Most Significant Proteins with an Increased Abundance in the Least Sensitive Patients After Treatment Using Quizinostat.

ROC analysis for the top five statistically significant proteins for the least sensitive patients to Quizinostat, including the calculated AUC, standard error (SE) and 95% confidence interval (CI).

3.2.9 AUC ROC Using Treatments Showing Different Individual Protein Signatures.

A broader range of AUC values are observed after treatment using Lenalidomide, with values ranging from 0.66 for ATX10 to 0.96 for PAK2 with regards to the most sensitive grouping (Fig. 3.24) and 0.64 for AGM1 to 0.92 for MMSA in the least sensitive group (Fig. 3.25). These values are low and are not considered to be significant. Navitoclax reveals more obvious discriminatory power as a range from 0.9 for MYL9 and 0.96 for DREB in the most sensitive patients (Fig. 3.26) and 0.81 for ECI2 and 0.93 for HEBP2 in the least sensitive patients (Fig. 3.27)

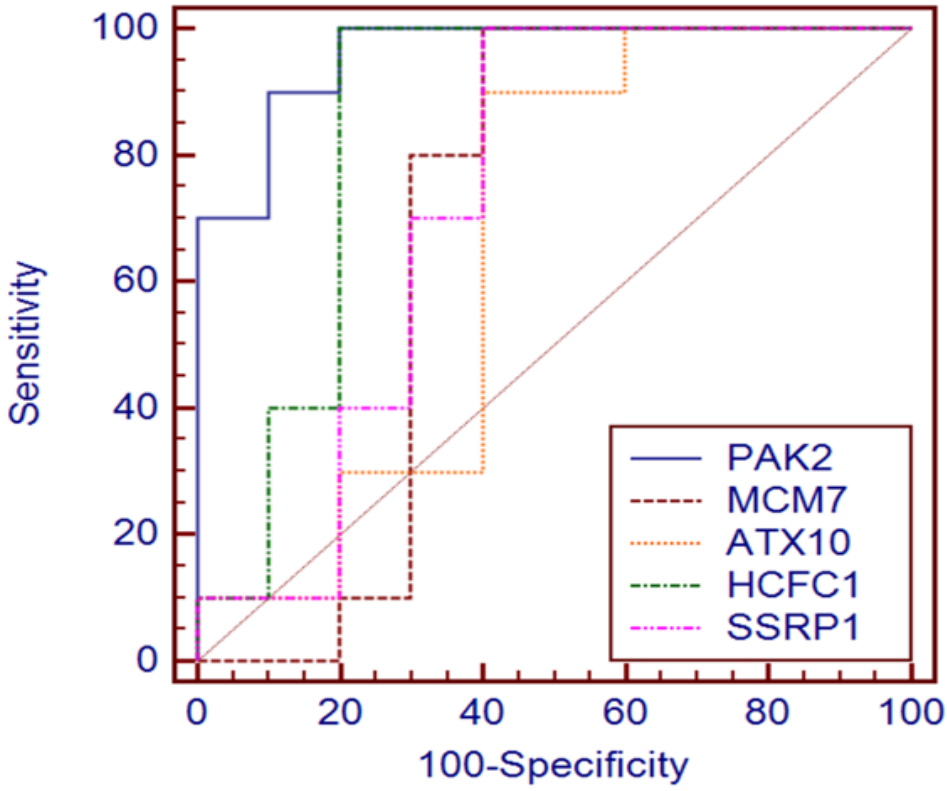

Protein	AUC	SE	95% CI
PAK2	0.96	0.0377	0.766 to 1.000
MCM7	0.69	0.146	0.447 to 0.874
ATX10	0.66	0.138	0.418 to 0.853
HCFC1	0.85	0.105	0.621 to 0.968
SSRP1	0.73	0.128	0.488 to 0.901

Figure 3.24: AUC ROC Analysis of the Five Most Significant Proteins with an Increased Abundance in the Most Sensitive Patients After Treatment Using Lenalidomide.

ROC analysis for the top five statistically significant proteins for the most sensitive patients to Lenalidomide, including the calculated AUC, standard error (SE) and 95% confidence interval (CI).

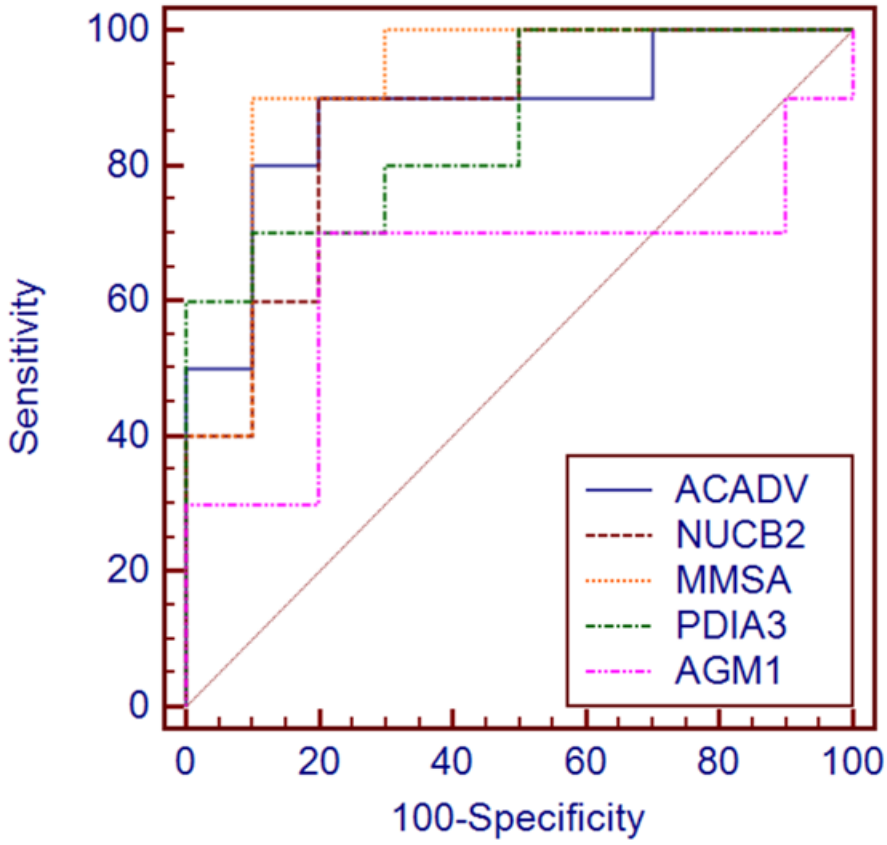

Protein	AUC	SE	95% CI
ACADV	0.88	0.0825	0.658 to 0.981
NUCB2	0.87	0.0818	0.645 to 0.977
MMSA	0.92	0.066	0.709 to 0.993
PDIA3	0.86	0.0835	0.633 to 0.972
AGM1	0.64	0.142	0.398 to 0.839

Figure 3.25: AUC ROC Analysis of the Five Most Significant Proteins with an Increased Abundance in the Least Sensitive Patients After Treatment Using Lenalidomide.

ROC analysis for the top five statistically significant proteins for the least sensitive patients to Lenalidomide, including the calculated AUC, standard error (SE) and 95% confidence interval (CI).

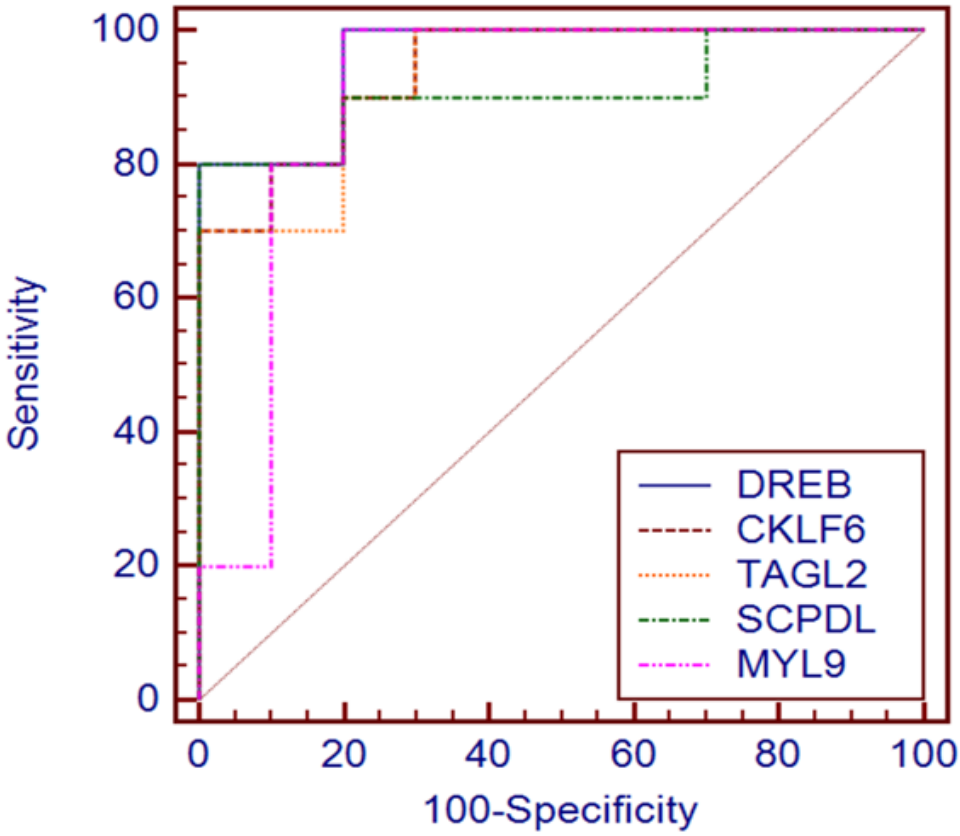

Protein	AUC	SE	95% CI
DREB	0.96	0.0377	0.766 to 1.000
CKLF6	0.94	0.0481	0.737 to 0.997
TAGL2	0.93	0.054	0.723 to 0.996
SCPDL	0.91	0.0744	0.696 to 0.991
MYL9	0.9	0.083	0.683 to 0.988

Figure 3.26: AUC ROC Analysis of the Five Most Significant Proteins with an Increased Abundance in the Most Sensitive Patients After Treatment Using Navitoclax.

ROC analysis for the top five statistically significant proteins for the most sensitive patients to Navitoclax, including the calculated AUC, standard error (SE) and 95% confidence interval (CI).

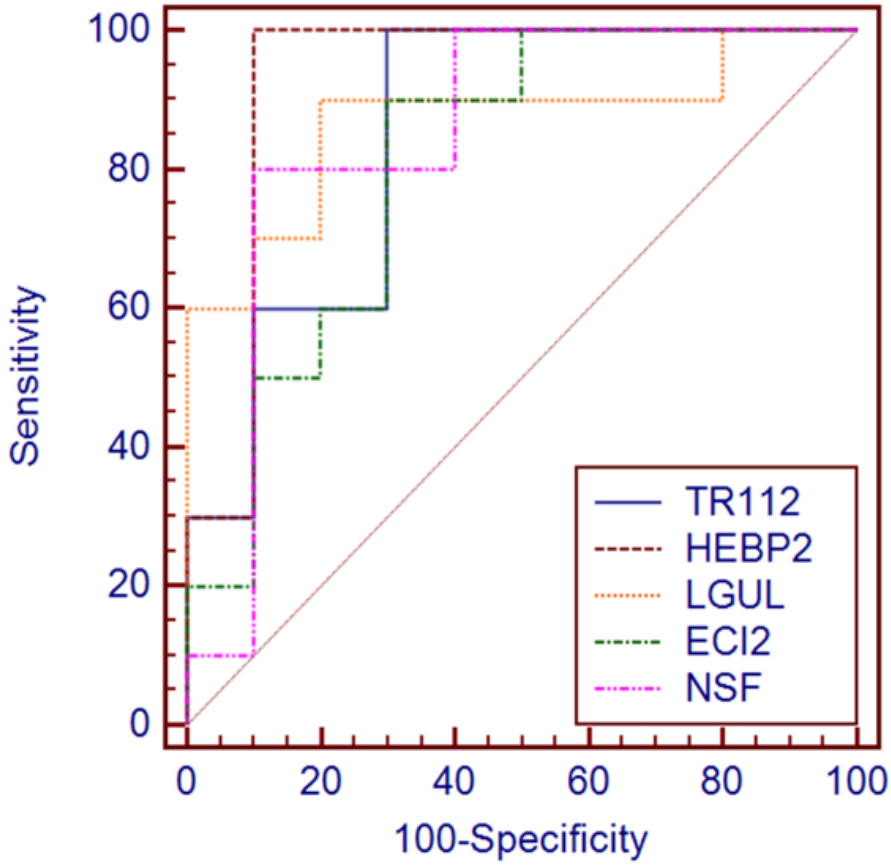

Protein	AUC	SE	95% CI
TR112	0.85	0.0913	0.621 to 0.968
HEBP2	0.93	0.0716	0.723 to 0.996
LGUL	0.87	0.0883	0.645 to 0.977
ECI2	0.81	0.102	0.575 to 0.948
NSF	0.85	0.0983	0.621 to 0.968

Figure 3.27: AUC ROC Analysis of the Five Most Significant Proteins with an Increased Abundance in the Least Sensitive Patients After Treatment Using Navitoclax.

ROC analysis for the top five statistically significant proteins for the least sensitive patients to Navitoclax, including the calculated AUC, standard error (SE) and 95% confidence interval (CI).

3.2.10 Immunohistochemistry of Bone Marrow Trephines from patients with varying disease diagnosis.

Comparative IHC was carried out with the use of multiple potential biomarkers for drug resistance in MM identified from detailed analysis of LC-MS/MS spectra. Vinculin, Integrin β3, CD44, CD68 and Talin-1 were all identified as potential targets, with an increased abundance in each of the potential targets stated being linked to disease progression in MM. Independent, blind scoring of stained slides was carried out, to ensure an unbiased evaluation of the staining intensity. Vinculin staining was observed to be weak positive (+1) for both MGUS bone marrow and active MM, with positive staining (+2) observed in disease maintenance and strong positive staining (+3) observed for newly diagnosed MM and remission. In summary, vinculin abundance was observed as Remission/Newly diagnosed>disease maintenance>Active MM/ MGUS (Figure 3.28). For Integrin β3, staining was determined to be weak positive (+1) in MGUS, newly diagnosed MM, active MM and response to treatment. The strongest amount of staining of Integrin β3 was observed in the remission bone marrow trephine (+3). In summary, the observed staining was greatest in remission, then MGUS and weakest in active MM, although staining in Active MM was similar to that of MGUS (Figure 3.29). Talin-1 exhibited no staining, section wide, with MGUS and Newly diagnosed MM (1). Weak staining (+1) was observed on newly diagnosed MM (2) (Figure 3.30). Very strong staining was generally observed with CD68, the highest of the staining recorded in MGUS and Active MM (+3). Staining was observed to be positive in newly diagnosed MM, maintenance and remission sections (+2) (Figure 3.31). Interestingly, the lowest staining, with negative staining recorded (+1), for CD68 was observed in bone marrow trephines from a patient with progressive disease. This image, however, is not included. CD44 abundance was also evaluated with the use of IHC in bone marrow trephines. Similar to CD68, high levels of staining were recorded section wide

for all samples examined. MGUS, newly diagnosed, post ASCT transplant and remission all exhibited staining with positive intensity (+2), the highest of the staining being recorded in active MM (+3) (Figure 3.32).

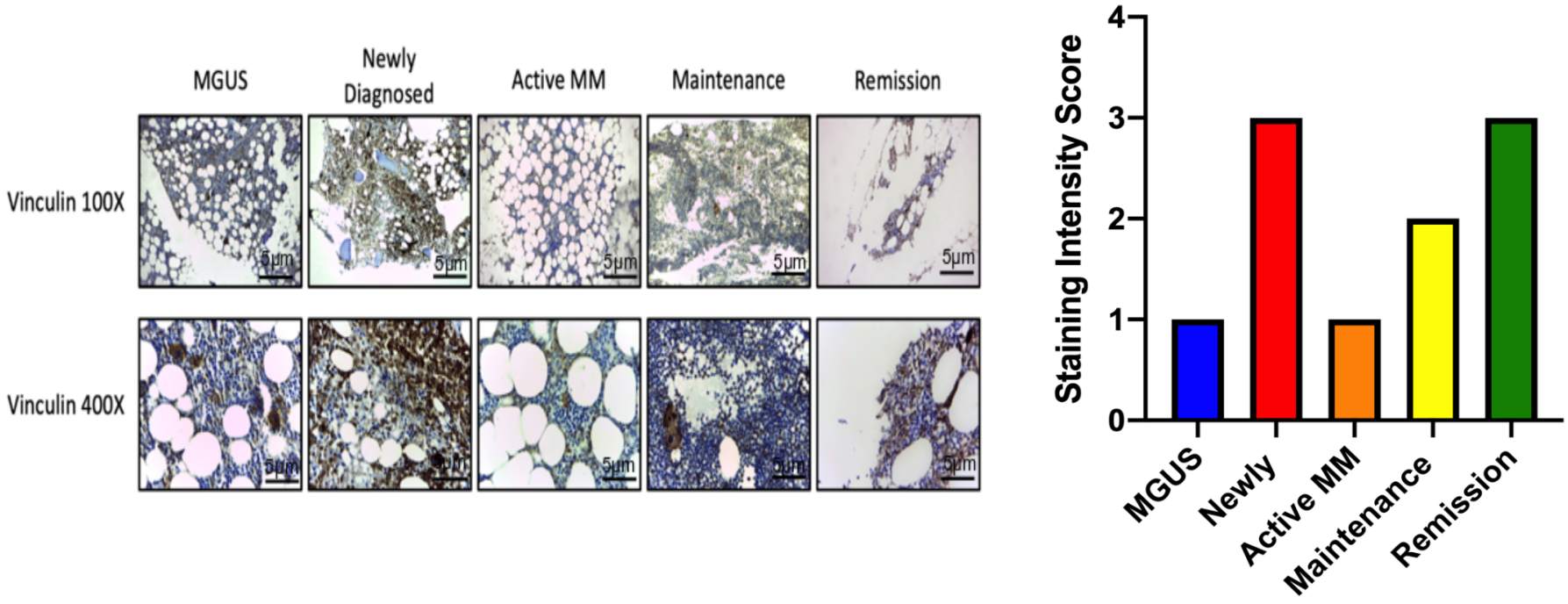

Figure 3.28: Comparative Immunohistochemistry (IHC) Staining of Vinculin in BM trephines for varying stages of disease.

The figure depicts the comparative IHC staining of BMTs using an antibody specific for Vinculin. The increased abundance of Vinculin is noted in staining of the sectioned tissue, the scoring of which is depicted in the corresponding graph.

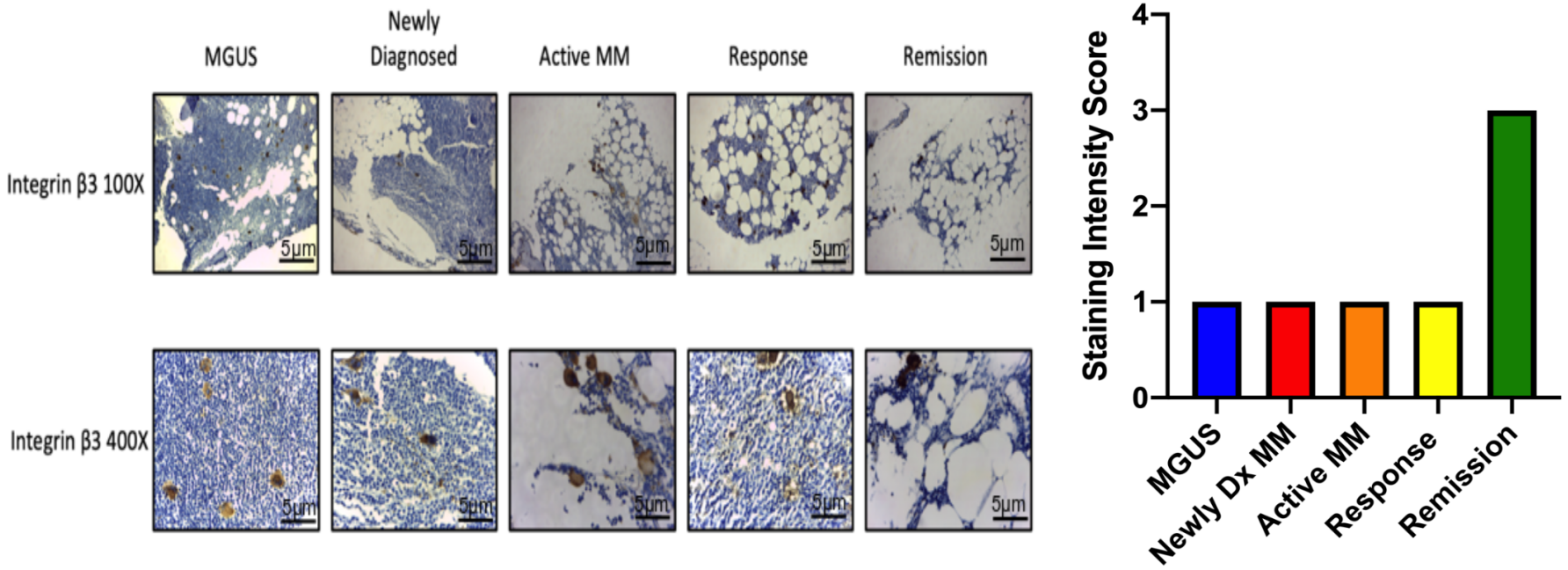

Figure 3.29: Comparative IHC Staining of Integrin β3 in BM trephines for varying stages of disease.
The figure depicts the comparative IHC staining of BMTs using an antibody specific for Integrin β3. The increased abundance of Integrin β3 is noted in staining of the sectioned tissue, the scoring of which is depicted in the corresponding graph.

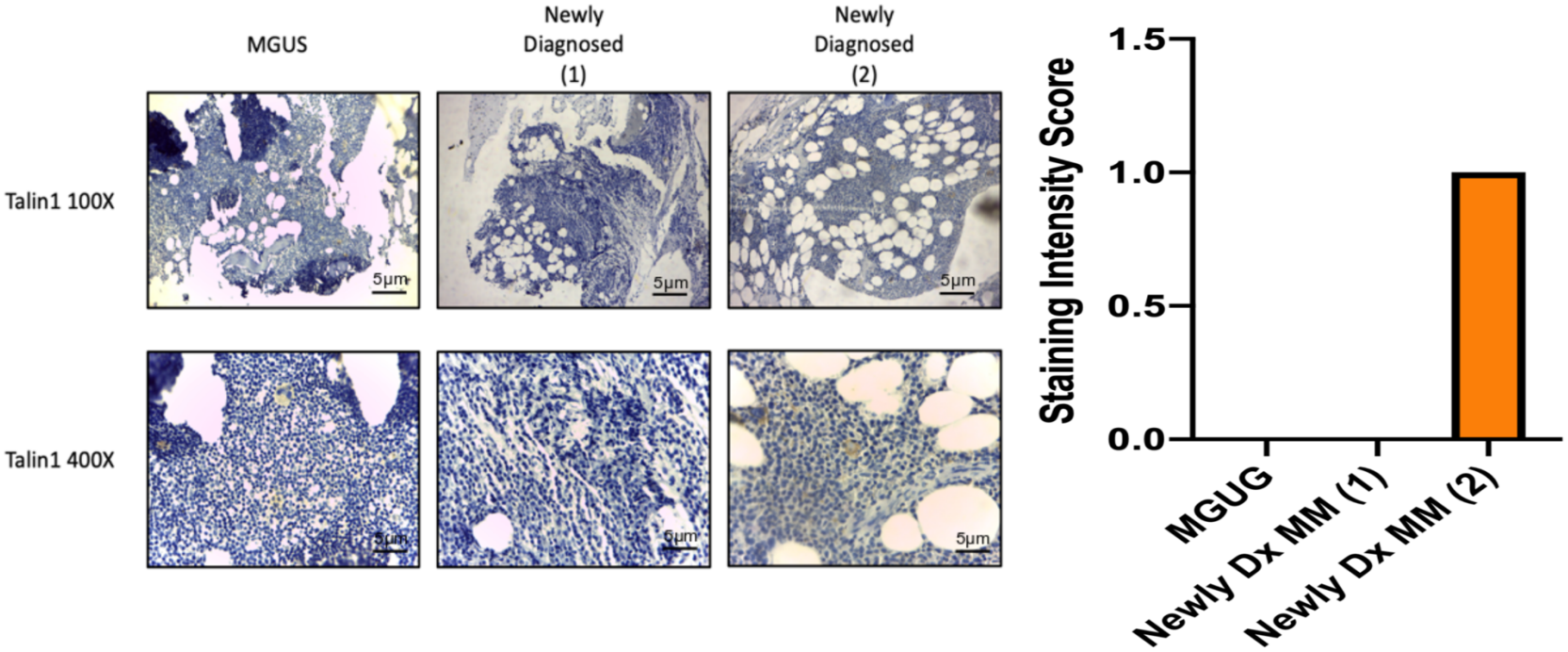

Figure 3.30: Comparative IHC Staining of Talin-1 in BM trephines for varying stages of disease.
The figure depicts the comparative IHC staining of BMTs using an antibody specific for Talin-1. The increase in abundance of staining (weak positive) of the sectioned tissue is noted in one of the two newly diagnosed BMTs, the scoring of which is depicted in the corresponding graph.

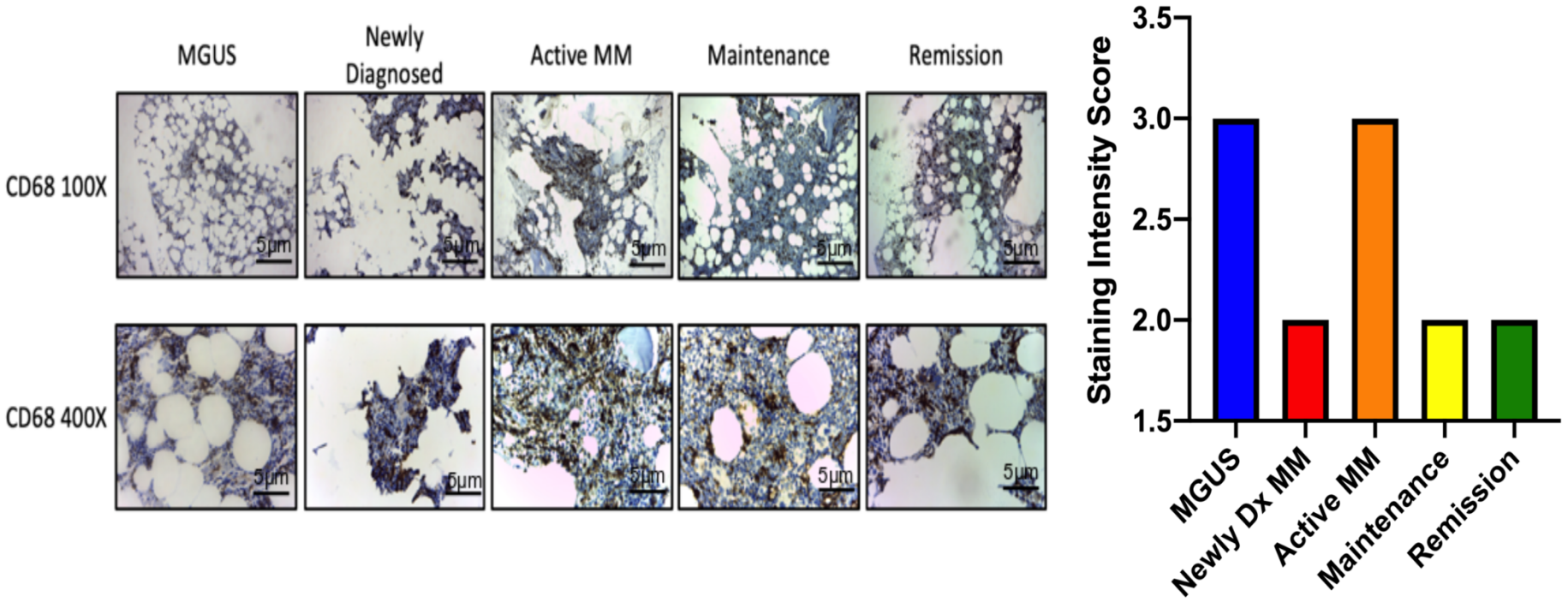

Figure 3.31: Comparative IHC Staining of CD68 in BM trephines for varying stages of disease.
The figure depicts the comparative IHC staining of BMTs using an antibody specific for CD68. The increased abundance of CD68 is noted in staining of the sectioned tissue, the scoring of which is depicted in the corresponding graph.

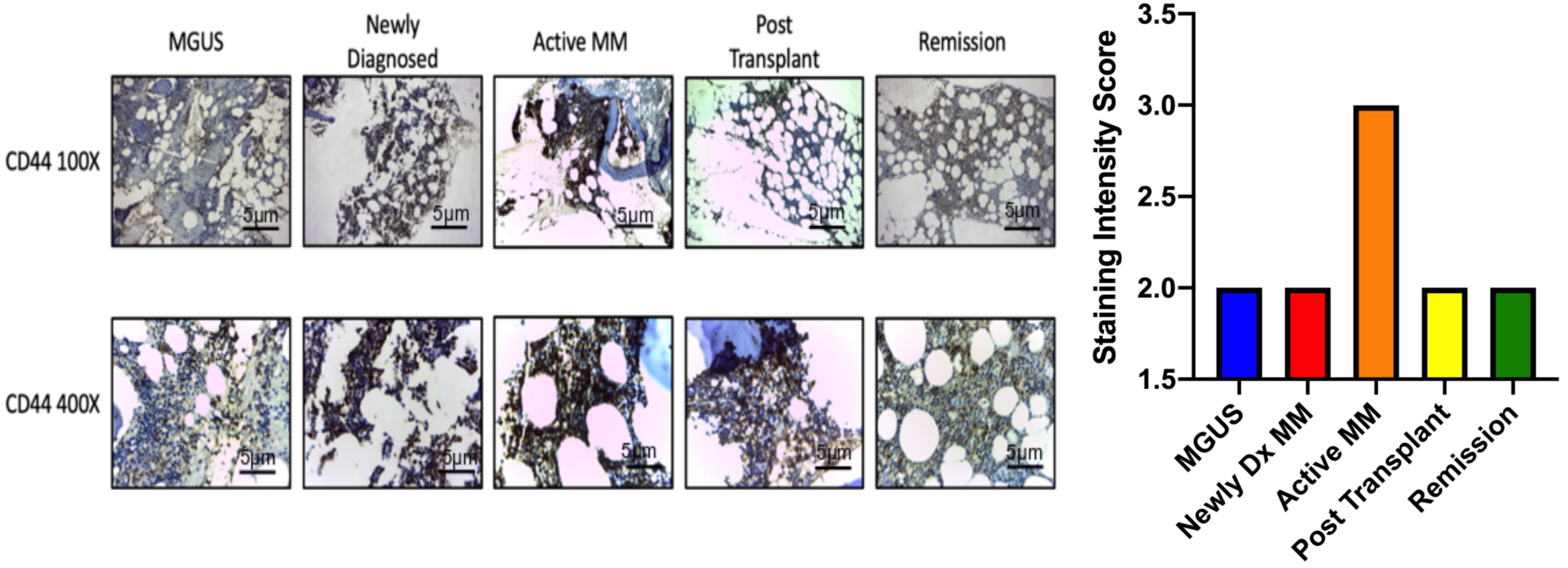

Figure 3.32: Comparative IHC Staining of CD44 in BM trephines for varying stages of disease.
The figure depicts the comparative IHC staining of BMTs using an antibody specific for CD44. The increased abundance of CD44 is noted in staining of the sectioned tissue, the scoring of which is depicted in the corresponding graph.

3.3 Discussion

The changes in protein abundance of 35 CD138+ patients to six MM drug treatments was studied to give a unique insight into drug resistance to these particular treatments from patients at varying stages of disease progression, with the long-term goal of developing individual treatment courses catering to individual patient needs. Four (Bortezomib, Carfilzomib, Quizinostat and PF-04691502) of the six drugs selected exhibited a similar protein signature while the remaining two drugs (Lenalidomide and Navitoclax) exhibited differing signatures. Bortezomib, Carfilzomib, Quizinostat and PF-04691502 lead to an increased abundance of Vinculin and Integrin β-3, with Bortezomib, Carfilzomib, Quizinostat showing an increased abundance of Talin-1, Gelsolin and Filamin A, in the least sensitive patients.

Vinculin is an actin binding, ubiquitously expressed protein noted for its role in focal adhesion formation (Humphries et al., 2007), regulation of actin cytoskeleton (Wen et al., 2009) and cell proliferation (Subauste et al., 2004). An increased abundance has been observed in varying different types of cancer such as breast cancer (Park, 2018). The increased abundance of Vinculin has previously been observed in MM cell lines, stimulating RhoA signalling and therefore leading to cell adhesion-mediated drug resistance (Kobune et al., 2007). These findings further support the claim that increased Vinculin abundance is implicated in drug resistance to four of the six drugs tested in MM.

Integrin β3 is one of two most notable integrins involved in tumour proliferation and has been implicated in multiple types of cancer including ovarian cancer (Cruet-Hennequart et al., 2003), papillary thyroid carcinoma (Trusolino et al., 1998) and lung carcinoma (Peláez et al., 2017). This implication has been associated with proliferation via Integrin Linked Kinase, regulation of epidermal growth factor receptor (EGFR) promoter leading to co-clustering of this receptor on cell surface in ovarian

cancer (Lössner et al., 2008). Cell adhesion mediated drug resistance has been strongly linked with the increased abundance of Integrin β3. Intrinsic and acquired resistance to erlotinib (a treatment commonly used to treat non-small cell lung cancer and pancreatic cancer) and lapatinib (commonly used to treat advanced hormone-related breast cancer) due to increased abundance of integrin β3 after acquired resistance to EGFR inhibitors, driving the NFκB signalling pathway, has been noted in multiple different cancer types, leading to predicted controlled behaviour of cancer stem cells (Seguin et al., 2014). Interestingly, it has been observed in multiple studies that targeting the NFκB signalling pathway when treating MM reduces drug resistance to PIs (Anderson and Carrasco, 2011), suggesting that the significantly increased abundance of Integrin β3 shown in this study may be leading to increased levels of NFκB signalling, causing cell adhesion-mediated drug resistance to four of the six drugs. Previously, clusterin has been implicated in bortezomib resistance in MM (Ting et al., 2017), which is a cancer cell survival protein acting through Akt and NFκB activation (Zoubeidi et al., 2010).

Talin-1, a central component of integrin adhesion and a prerequisite for assembly and maintenance of integrin based cell-extracellular matrix binding (Klapholz and Brown, 2017), has been seen to exhibit binding sites for Actin and Vinculin (Chinthalapudi et al., 2018). Talin-1 has been previously implicated in tumour cell invasion in both mammary tumours and lung metastasis (Gligorijevic et al., 2012). The close association between Talin-1 and the other focal adhesion proteins mentioned in the least sensitive patients in Bortezomib, Carflilzomib, Quizinostat and PF-04691502 further confirms the role of focal adhesions, actin production and subsequently cell motility and has previously been implicated in cell adhesion in MM cells. It has been recorded that Talin-silenced MM cells are notably more susceptible to Bortezomib-mediated cell apoptosis (Martínez-Moreno et al., 2016). Vinculin has previously been observed to require Talin-1 as a binding partner to comprehensively

unmask binding sites for the continuation of Vinculin localisation to focal adhesions (Bakolitsa et al., 2004).

Similar to Talin-1, Gelsolin and Filamin A are associated with actin assembly and actin binding respectively. Gelsolin severs, caps and nucleates actin filaments and sequesters monomers (Nag et al., 2013) and exhibits both inhibitory (Koya et al., 2000) and supportive traits for apoptosis (Geng et al., 1998) depending on surrounding conditions and cells. Overexpression of Gelsolin has been linked to metastasis in breast cancer (Marino et al., 2013) and hepatocellular carcinoma (HCC) (Deng et al., 2015). Interestingly, an increased abundance of Gelsolin has shown a strong correlation to chemoresistance in gynaecological cancers and a decreased OS (Abedini et al., 2014).

Filamin A, a scaffold serving protein in multiple signalling networks (Feng and Walsh, 2004), binds and cross-links actin filaments into three dimensional structures. A close link between increased Filamin A abundance and increased metastasis has been observed in numerous cancer types such as HCC (Ai et al., 2011), prostate cancer (Bedolla et al., 2009), melanoma and breast cancer (Jiang et al., 2013). Filamin A has been previously linked to cancer cell migration and it has been observed that knockdown of Filamin A affects the migration and spreading of MM endothelial cells, as well as inhibiting angiogenic activity in these cells (Berardi et al., 2012).

The increased abundance of Vinculin, Integrin β3 and along with Talin-1, Gelsolin and Filamin A indicates that there is a significant increase in proteins related to focal adhesion, actin assembly and cell motility. All these proteins have a distinct function within the focal adhesion pathway. Firstly, multiple different studies predicted that cell “stiffness”, due to actin production, leads to cancer proliferation and invasion. The significant increased abundance of Vinculin, along with Myosin II and Rho, has been observed to cause increased cell stiffness in chemoresistant cells via mechanical cytoskeleton alterations (Nyongesa and Park, 2018). Cell adhesion-mediated drug resistance has commonly been linked to MM and it has been reported that Wnt3 plays

a crucial role in cell adhesion-mediated drug resistance, which is caused by increased Vinculin abundance and a rearrangement of the actin filament (Kobune et al., 2007). Secondly, the increased activation of NFκB, a transcription factor regularly seen to play a role in tumour progression, growth and chemoresistance (Almeida et al., 2014), from increased levels of Integrin β3 has been reported in multiple studies as a cause for drug resistance in cancer cells. Interestingly, it has been observed that treatment using a PI such as Bortezomib and Carfilzomib has led to decreased NFκB expression in xenograft models of MM (Wilczynski et al., 2011). This, in turn, leads to the hypothesis that NFκB expression is upregulated following Bortezomib, Carfilzomib, Quizinostat and PF-04691502 treatment. The implication that NFκB plays a significant role in drug resistance in MM has been explored in further chapters within this body of work (Chapter 4).

The immunohistochemistry carried out is purely for validation purposes and, due to the small sample size of bone marrow trephines, no strong conclusions can be made from the data provided. The identification of individual plasma cells proved extremely difficult as CD138 staining was not carried out along with the potential target staining. To further validate the findings of IHC, the BMT sections would require CD138 staining to allow the identification of the individual plasma cells, allowing the identification of the precise location of the potential markers (Vinculin, Integrin β3, Talin-1, CD68 and CD44). The increased abundance of Vinculin and Integrin β3 in remission patients may be eluding to the fact that, although the patient is in remission, this must be monitored as RRMM will occur with drug resistance to previously used treatment regimes. As vastly high rates of RRMM occur, the vast majority of patients diagnosed with MM do eventually progress from remission to RRMM. The increased abundance evident from the BMT staining for Vinculin (Figure 3.28) and Integrin β3 (Figure 3.29) indicates less sensitivity to Bortezomib, Carfilzomib, Quizinostat and

PF-04691502, as forms of treatment in RRMM. A decrease in abundance in CD68 (Figure 3.31) and CD44 (Figure 3.32) from active MM to remission indicates that CD44 and CD68 are most active in proliferating MM, and therefore play a role in disease progression. CD44 is a family of single-span transmembrane glycoproteins, with family members differing in the extracellular domain. These proteins act as receptors for hyaluronan, which is a co-receptor for receptor tyrosine kinases (RTKs), which is explored more in Chapter 4. CD44 also acts as a receptor for G-protein-coupled receptors, as well as providing a platform for metalloproteinases (Yan et al., 2015). CD44 has previously been implicated in drug resistance in gastric cancer (Lee et al., 2019), ovarian cancer (Yang et al., 2015), colorectal cancer (Zaytseva et al., 2012) and breast cancer (Wang et al., 2018), to name but a few. An infinite fold increase in sensitive patients in comparison to resistant patients was recorded by LC-MS/MS in this particular study (infinite meaning an absence of CD44 in the resistant cohort of patients). CD68, a heavily glycosylated glycoprotein, is known to be a tumour associated macrophage (TAM) and is highly expressed in macrophages and other mononuclear phagocytes. It has been associated with being a good predictive marker for cancer prognosis (Chistiakov et al., 2017). CD68 has been observed as being highly abundant in hepatocellular carcinoma tissue and is especially associated with stage Ⅳ (Minami et al., 2018), has shown direct links with poor prognosis of head and neck squamous cell carcinoma (Seminerio et al., 2018) and has shown a direct correlation between abundance and poor prognosis in colorectal cancer (Yang et al., 2019). A 5-fold increase in the abundance of CD68 was recorded the least sensitive patients, in comparison to the most sensitive patients. This eludes to the connection between CD68 and disease invasiveness along with drug resistance in MM.

Chapter 4

Phosphoproteomic Analysis of DSS Patient Samples in Four Groups Ranging from Responders to Non-Responders

4.1 Introduction

Protein phosphorylation is a reversible post translational modification (PTM) that occurs through protein kinases. PTMs are considered to play a vital role in processes such as subcellular localisation, stability and protein activity control (Olsen et al., 2006). This PTM involves the addition of a phosphate group (PO_4) to the polar R group of amino acids, modifying the protein from hydrophobic apolar to hydrophilic polar (Sacco et al., 2012). The change in hydrophobicity of the protein allows alterations in confirmation during interactions with other molecules. Phosphorylated amino acids have the ability to bind molecules with protein interaction abilities, allowing the assembly and detachment of protein complexes (Ardito et al., 2017). Protein phosphatases have the opposite function to that of kinases, they remove a phosphate group from a phosphoprotein, restoring the protein to its previous state (Barford, 1996). This phosphorylation/dephosphorylation acts similar to a molecular switch (Figure 4.1).

Kinases are enzymes that transfer a phosphate group from high energy nucleoside triphosphate to specific proteins, carbohydrates, lipids and substrates. This process leads to stability, activity and localization of proteins, playing a crucial role in cell biology. Kinases are activated by cis-/autophosphorylation and, in turn, activate a cascade of phosphorylation events (Roskoski, 2012). As the second largest enzyme family, kinases are noted to encompass 518 family members, with 106 pseudogenes (Lind et al., 2019). Phosphorylation activity is stimulated by cytogenetic alterations, epigenetic modification, genetic alterations or by tumour microenvironment activation. ATP hydrolysis supplies the phosphate group, leading to a PTM formation (Fukami and Lipmann, 1983). This PTM formation can cause carcinogenic effects, leading to oncogenic pathway activation. This activation is generally caused by a phospho-binding protein binding to a phosphate group of an already modified phosphoprotein (Ardito et al., 2017) (Figure 4.1).

Phosphorylation occurs predominantly on the serine (Ser) residues, threonine (Thr) residues and tyrosine (Tyr) residues of proteins, although Ser residues are the most common. Tyr phosphorylation is rare in comparison, with this being typical of the epidermal growth factor receptor family (Schwartz and Murray, 2011). The less stable phosphorylation of histidine (His) and aspartate (Asp) does occur but is much less common than the aforementioned (Nishi et al., 2014). Although most phospho-complexes contain a small amount of phosphorylation sites, it has been observed approximately half of their threonine, serine and tyrosine sites are phosphorylated (Nishi et al., 2011). Approximately 2% of human coding genes are encoding for protein kinases, eluding to the importance of phosphorylation in humans (Manning et al., 2002). The number of phosphatase encoding genes has been recorded as being significantly less, almost ten time less than kinase encoding genes.

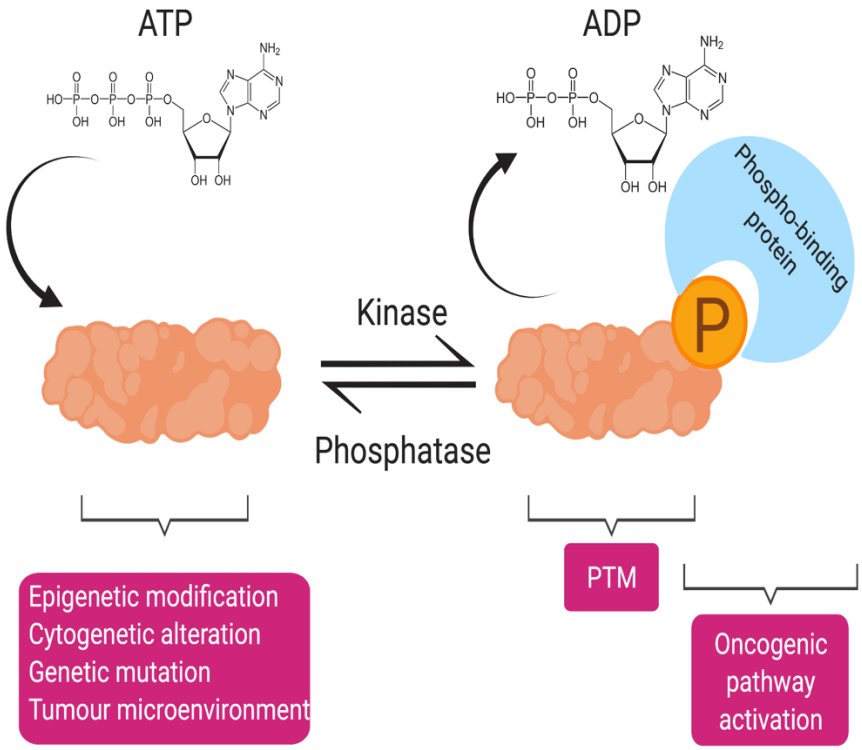

Figure 4.1: Phosphorylation signalling pathway.

The figure above depicts the means in which phosphorylation is regulated.

*Figure was adapted from Ardito et al., 2017 and was created with Biorender.

Phosphorylation has been identified as an extremely important mechanistic event which is known to have an involvement in cell growth, cell division, protein synthesis, signal transduction, development and aging. P53 is known to be activated by phosphorylation, leading to the transcription of cell cycle inhibitory genes, apoptosis and DNA repair activation (Heinrich et al., 2002). Importantly, phosphorylation plays a crucial role in biological processes such as the aforementioned, along with proliferation and differentiation.

In cancer, it has been observed that phosphorylation plays an important role, allowing cancer cells to exploit the “on-off” switch mechanism in which phosphorylation

operates. More than 1,000 protein kinase expression variations have been observed in human tumours, leading to the establishment of the clinical relevance of these variations as biomarkers. Such variations include Her2 for breast cancer (Stephens et al., 2005) and EGFR for colon cancer (Barber et al., 2004). mTOR, a protein kinase is activated by phosphorylation and induces activation of cyclin D and HIF1α, both of which are cell cycle proteins. This activation further activates vascular endothelial growth factor, a signal protein known to promote angiogenesis (Dancey, 2006). The phosphorylation driven activation of mTOR, and the subsequent downstream activation effects leading to promotion of angiogenesis, have been noted as being particularly active in renal cancer (Thomas et al., 2006). Chronic myeloid leukaemia (CML), a disease of haemopoietic stem cells, is known to arise from the translocation t(9;22)(q34;q11) which leads to the generation of a novel kinase, retinoblastoma. This kinase is constantly active, which has been established as one of the leading causes of tumour cell proliferation in CML (Murphree and Benedict, 1984). Acute myeloid leukaemia (AML), discussed in detail in Chapter 7, show that group I mutations result in the activation of pro-proliferation pathways due to the mutation of tyrosine kinase domain mutations (TKD). The increased tyrosine phosphorylation of signal transducer and activator of transcription 3 (STAT3), either due to the TKD mutations or increased production of cytokines eludes to a worse prognosis (Schuringa et al., 2000). This increase in phosphorylation is observed in up to 50% of AML cases (De Kouchkovsky and Abdul-Hay, 2016).

Phosphorylation has, importantly, been previously implicated in MM cell survival. Bruton tyrosin kinase (BTK), a non-receptor tyrosine kinase is expressed through the entire process of B-cell differentiation. This expression plays an important role in B-cell function and development (de Weers et al., 1994). PLC-γ phosphorylation allows BTK signalling, which, in turn, leads to the downstream activation of IκB and the subsequent activation of the NF-κB signalling pathway. The activation of this

signalling pathway further induces MAPK and AKT signalling. All three of the aforementioned are vital for signalling pathways involved in MM cell survival (Gilmore, 2007). Tyrosine phosphorylation of STAT3, a transcription factor which plays a vital role in cell proliferation and growth, has also been implicated in disease progression in MM and unfavourable prognosis.

The identification of the significant role that phosphorylation plays in cancer cell proliferation and survival has led to the development of kinase targeting cancer therapeutics. As it becomes clearer that phosphorylation events are a prevalent cause of cancer proliferation, targeted therapeutics have been developed to manipulate kinase signalling pathways related to cancer proliferation. As of 2013, 17 tyrosine kinase inhibitors were in use as a treatment method for differing cancer types, with approximately 390 potential therapeutics being tested (Gonzalez de Castro et al., 2013). Trastuzumab, a monoclonal antibody, has been developed to target HER2 in breast cancer patients (Carvajal-Hausdorf et al., 2015). Sunitinib has been developed to target VEGF receptors and platelet-derived growth factor receptors, reducing tumour vascularization and stimulating cancer cell apoptosis in renal cell carcinoma (Czarnecka et al., 2016) and gastrointestinal stromal tumour (Demetri et al., 2006). As previously stated in Chapter 3, PF-04691502 is a MM experimental drug that is known to be a PI3K/mTOR inhibitor, targeting PI3K/Akt/mTOR phosphorylation and signalling pathway. PF-04691502 has shown promising results in xenograft models and cultured cells, resulting in antitumor and antiproliferative activity (Mallon et al., 2011). Along with this experimental drug, multiple phosphorylation targeting therapeutics are currently being investigated for the treatment of MM, the most promising of these being small molecules targeting receptor tyrosine kinases (RTKs), BTKS, Ras/Raf/MEK/MAPK pathway, cyclin-dependent kinases (CDKs) and the previously mentioned PI3K/Akt/mTOR pathway (Lind et al., 2019).

4.1.1 Experimental Design

4.1.1.1 Patients and Samples

A total of 32 bone marrow (BM) aspirates were collected from patients with varying sensitivities to treatment (Table 4.1). No exclusion criteria were applied to the patients and the samples were collected prospectively. Data collection was continued at successive relapses to follow disease progression. The ethics committees of the participating hospitals approved the study in compliance with the Declaration of Helsinki. These samples were obtained from the Institute of Molecular Medicine, Helsinki, Finland (FIMM). In-depth patient details are outlined in Chapter 3.

Table 4.1: Sample Number and Drug Sensitivity Screening Group of Phosphopeptide Enriched Samples.

Sample Number	Patient Identifier (As per Chapter 3)	DSS Grouping
MM002	R_MM_3966	Group 1
MM003	R_MM_2757	Group 1
MM004	R_MM_2097	Group 1
MM005	D_MM_3514	Group 1
MM006	R_MM_938	Group 1
MM022	R_MM_2757	Group 1
MM023	R_MM_882	Group 1
MM024	R_MM_3001	Group 1
MM025	R_MM_4774	Group 1
MM027	R_MM_4011	Group 1
MM007	R_MM_1380	Group 2

MM008	R_MM_3434	Group 2
MM009	D_MM_3647	Group 2
MM010	R_MM_899	Group 2
MM011	R_MM_156	Group 2
MM012	R_MM_2979	Group 2
MM028	R_MM_810	Group 2
MM029	R_MM_4011	Group 2
MM030	R_MM_4692	Group 2
MM031	D_MM_3595	Group 2
MM013	R_MM_2235	Group 3
MM014	R_MM_921	Group 3
MM016	D_MM_3901	Group 3
MM017	D_MM_3586	Group 3
MM032	D_MM_4865	Group 3
MM035	D_MM_3886	Group 3
MM018	R_MM_3717	Group 4
MM019	D_MM_3767	Group 4
MM020	R_MM_1193	Group 4
MM021	R_MM_584	Group 4
MM038	R_MM_840	Group 4
MM039	R_MM_1994	Group 4

4.1.1.2 Drug Sensitivity Screening of Patient Samples at Varying Stages of Diagnosis.

CD138+ cells were enriched using the EasySep™ Human CD138 Positive Selection kit (StemCell Technologies, Grenoble, France) from the mononuclear cell fraction of BM aspirates following gradient separation (Ficoll-Paque PREMIUM; GE Healthcare, Little Chalfont, Buckinghamshire, UK). Drug sensitivity and resistance testing (DSRT) was performed based on methods described previously (Pemovska et al., 2013). CD138+ cells derived from myeloma patients were tested against 308 compounds at 5 concentrations overin 10-fold dilutions covering a 10,000-fold concentration range (1–10,000 nM). The drug panel included approved oncology drugs (n = 141) and investigational compounds (n = 167) targeting multiple signalling networks and molecular targets. In brief, 5µl of cell culture medium comprised of RPMI 1640 medium supplemented with 10% fetal bovine serum, 2 mM L-glutamine, penicillin (100 U/ml), streptomycin (100 µg/ml) and 25% conditioned medium from the HS-5 human BM stromal cell line was added to 384 well drug plates and shaken for 5 min to dissolve the compounds. CD138+ cells were diluted in the culture medium and 20µl of the cell suspension containing 5000 cells was transferred to each well using a MultiDrop Combi peristaltic dispenser (Thermo Scientific, Waltham, MA, USA). The plates were incubated in a humidified environment at 37°C and 5% CO2. Cell viability was measured after 72 h using the CellTiter-Glo assay (Promega, Madison, WI, USA) with a PHERAstar® microplate reader (BMG-Labtech, Offenburg, Germany) to measure luminescence. The mean viability of untreated cells at day three was 124 ± 10.40%. The data was normalized to negative (DMSO only) and positive control wells (containing 100 µM benzethonium chloride). This analysis was carried out by the Institute of Molecular Medicine, Helsinki, Finland (Majumder et al., 2017).

4.1.1.3 Phosphopeptide Enrichment

CD138+ lysed plasma cells were enriched for phosphopeptides using a Pierce Magnetic Titanium Dioxide Phosphopeptide Enrichment Kit to identify potential phosphopeptide biomarkers for treatment resistance using label-free LC-MS/MS. 25µl of sample was used for phosphopeptide enrichment. Manufacturers guidelines were followed exactly, as detailed in Chapter 2.

4.1.1.4 Label-free LC-MS/MS Analysis of Phosphopeptide Enriched Patient Samples.

After phosphopeptide enrichment and vacuum centrifugation, samples were re-suspended in loading buffer (2% ACN, 0.05% TFA in LC-MS grade water) (Murphy et al., 2015a). Peptide suspensions were vortexed and sonicated to aid full re-suspension. Samples were centrifuged briefly at 14,000 x g and the supernatant transferred to mass spectrometry vials. Peptides were eluted using the following binary gradient: solvent A [2% (v/v) ACN and 0.1% (v/v) formic acid in LC-MS grade water] and 0-90% solvent B [80% (v/v) ACN and 0.1% (v/v) formic acid in LC-MS grade water]: 2% solvent B for 10.5 min, 2-40% solvent B for 110 min, 40-90% solvent B for 2.5 min, 90% solvent B for 9 min and 2% solvent B for 43 min.

4.1.1.5 Qualitative Data Analysis of Enriched Phosphopeptides

Qualitative data analysis was used for protein identification. Mass spectrometry raw files were processed using the Proteome Discoverer 1.4 (Thermo Fisher Scientific) software with Sequest HT as the search engine and the UniProt sequence database. The following search parameters were used for protein identification: (i) peptide mass tolerance set to 10 ppm, (ii) MS/MS mass tolerance set to 0.02 Da, (iii) up to two missed cleavages, (iv) carbamidomethylation set as a fixed modification and (v)

methionine oxidation set as a variable modification. Mass spectrometry raw files were searched against *Homo Sapiens* database. Peptides were filtered using a minimum XCorr score of 1.5 for +1, 2.0 for +2, 2.25 for +3 and 2.5 for +4 charge states, with peptide probability set to high confidence.

4.1.1.6 Validation of Enriched Phosphopeptide Samples using Human Phospho-Kinase Array

A Human Phospho-Kinase Array was used to validate potential target phosphopeptide biomarkers as identified by label-free LC-MS/MS after phosphopeptide enrichment. 50μg of protein was used for analysis. The array was carried out as per the manufacturer's guidelines using two highly sensitive and two highly resistant lysed CD138+ plasma cell samples to treatment (Table 4.2), with zero alterations.

Table 4.2: Sample details for samples used in Human Phospho-Kinase Array.

Sample Number	Patient Identifier (As per Chapter 3)	DSS Grouping
MM024	R_MM_3001	Group 1
MM023	R_MM_882	Group 1
MM021	R_MM_584	Group 4
MM039	R_MM_1994	Group 4

4.2 Results

4.2.1 Qualitative Proteomic Analysis of Phosphopeptide Enriched CD138+ Cell Lysates.

The enrichment for phosphopeptides in sample preparation led to sufficient reduced sample complexity for in-depth proteomic analysis with LC-MS/MS. Of the 32 CD138+ lysed samples, 417 phosphorylation sites with an XCorr value greater than 2. 135 of these phosphorylation sites were found to have a XCorr value greater than 3.5 (Table 4.3). Percentage coverage ranged from 42.37% to 0.95% in the group with XCorr value greater than 3.5, the highest of these being for 26S proteasome non-ATPase regulatory subunit 2 with an S8 phosphorylation residue (42.37%), Lymphocyte-specific protein 1 with an S3 phosphorylation residue (33.33%), Galectin-related protein with a S11 phosphorylation residue (28.57%) and Small acidic protein with a S3 phosphorylation site (27.91%).

Table 4.3: List of Identified Proteins with >3.5 XCorr score determined by LC-MS/MS and Proteome Discoverer.

Accession	Description	Coverage	Modifications	XCorr
F8VZJ2	Nascent polypeptide-associated complex subunit alpha, muscle-specific form	25.74	S22(Phospho)	9.25
H0YE72	Elongation factor 1-delta (Fragment)	20.51	S19(Phospho)	9.15
H0YDD8	60S acidic ribosomal protein P2 (Fragment)	18.48	S4(Phospho); M11(Oxidation)	7.86
Q9H3N1	Thioredoxin-related transmembrane protein 1	7.5	S13(Phospho)	7.76
E9PK09	Bcl-2-associated transcription factor 1 (Fragment)	6.21	S15(Phospho)	7.53
O15173	Membrane-associated progesterone receptor component 2	19.28	T12(Phospho)	6.67
E5RJU9	Protein LYRIC	5.51	S12(Phospho)	6.46
Q5JSH3	WD repeat-containing protein 44	8.11	S10(Phospho)	6.22
Q5STZ8	ATP-binding cassette sub-family F member 1 (Fragment)	12.09	S6(Phospho)	6.22
Q86U12	Full-length cDNA clone CS0CAP007YF18 of Thymus of Homo sapiens (human)	5.81	S13(Phospho)	6.15
E9PS34	Nucleosome assembly protein 1-like 4 (Fragment)	18.8	S18(Phospho)	6.08
Q8IYB3	Serine/arginine repetitive matrix protein 1	1.77	S5(Phospho)	6.06
Q9H3N1	Thioredoxin-related transmembrane protein 1	7.5	S14(Phospho)	5.92
F8W7S5	Ribosome-binding protein 1	3.86	S14(Phospho)	5.81
H0YDD8	60S acidic ribosomal protein P2 (Fragment)	18.48	S4(Phospho)	5.76
E9PQA1	Small acidic protein	27.91	S3(Phospho)	5.57
B5MCB4	Methyl-CpG-binding protein 2	12.21	S19(Phospho)	5.52
P08238	Heat shock protein HSP 90-beta	4.42	S6(Phospho)	5.52

Accession	Description	Coverage	Modifications	XCorr
H7C2Y0	Septin-2 (Fragment)	10.64	S9(Phospho)	5.43
Q86U12	Full-length cDNA clone CS0CAP007YF18 of Thymus of Homo sapiens (human)	5.81	S13(Phospho)	5.36
O95218	Zinc finger Ran-binding domain-containing protein 2	16.36	S7(Phospho)	5.27
Q9Y2W1	Thyroid hormone receptor-associated protein 3	7.64	S13(Phospho)	5.08
A8K8G0	Hepatoma-derived growth factor	16.35	S8(Phospho)	5.02
J3KSH8	Hematological and neurological-expressed 1 protein (Fragment)	16.13	S3(Phospho)	5.02
O43719	HIV Tat-specific factor 1	13.11	S6(Phospho)	5.01
B3KXW9	Dedicator of cytokinesis protein 2	1.91	S8(Phospho)	4.96
P53999	Activated RNA polymerase II transcriptional coactivator p15	25.2	S12(Phospho)	4.96
O15173	Membrane-associated progesterone receptor component 2	19.28	T12(Phospho)	4.96
H7C1J8	Heterogeneous nuclear ribonucleoprotein A3 (Fragment)	19.13	S4(Phospho)	4.95
J3KQ96	Treacle protein (Fragment)	2.19	S12(Phospho)	4.95
P14625	Endoplasmin	4.11	S6(Phospho)	4.91
C9JID5	Transmembrane protein 40	10.19	S3(Phospho)	4.90
F5GZU3	Scaffold attachment factor B1	3.48	S21(Phospho)	4.76
P52756	RNA-binding protein 5	2.33	S10(Phospho)	4.76
O43719	HIV Tat-specific factor 1	13.11	S7(Phospho)	4.76
Q9HCN4	GPN-loop GTPase 1	5.35	S12(Phospho)	4.73
B1ALG5	Probable global transcription activator SNF2L2	14.29	S10(Phospho)	4.72
B4E2T8	Calnexin	7.02	S11(Phospho)	4.71
Q7Z6P5	DNA replication licensing factor MCM3 (Fragment)	7.32	T13(Phospho); M17(Oxidation)	4.71

Accession	Description	Coverage	Modifications	XCorr
Q9NTI5	Sister chromatid cohesion protein PDS5 homolog B	1.24	S3(Phospho)	4.70
O00264	Membrane-associated progesterone receptor component 1	10.26	S9(Phospho)	4.69
H0YL55	SAFB-like transcription modulator (Fragment)	6.55	S9(Phospho)	4.66
O95400	CD2 antigen cytoplasmic tail-binding protein 2	5.28	S5(Phospho)	4.61
O94804	Serine/threonine-protein kinase 10	1.55	S10(Phospho)	4.56
Q9BUH6	Uncharacterized protein C9orf142	5.88	S10(Phospho)	4.54
B4E2T8	Calnexin	7.02	S13(Phospho)	4.53
Q9UIG0	Tyrosine-protein kinase BAZ1B	1.15	S8(Phospho)	4.51
F8WBS8	26S proteasome non-ATPase regulatory subunit 2	42.37	S8(Phospho)	4.49
H7C446	Suppressor of SWI4 1 homolog (Fragment)	6.73	S4(Phospho)	4.46
Q9Y2W1	Thyroid hormone receptor-associated protein 3	7.64	S13(Phospho)	4.46
O60841	Eukaryotic translation initiation factor 5B	3.03	S9(Phospho)	4.42
Q9UEY8	Gamma-adducin	2.41	S16(Phospho)	4.42
P08238	Heat shock protein HSP 90-beta	4.42	S6(Phospho)	4.41
P08559	Pyruvate dehydrogenase E1 component subunit alpha, somatic form, mitochondrial	5.9	M6(Oxidation); S7(Phospho); S12(Phospho)	4.35
O43719	HIV Tat-specific factor 1	13.11	S6(Phospho)	4.35
P08238	Heat shock protein HSP 90-beta	4.42	S5(Phospho)	4.30
D6R9L5	Protein DEK (Fragment)	13.91	S3(Phospho)	4.30
Q9Y385	Ubiquitin-conjugating enzyme E2 J1	4.72	S3(Phospho)	4.29
E5RIS7	Transcription elongation factor A protein 1	13.51	S11(Phospho)	4.28

Accession	Description	Coverage	Modifications	XCorr
O60841	Eukaryotic translation initiation factor 5B	3.03	S8(Phospho)	4.25
G3V1K1	Coiled-coil-helix-coiled-coil-helix domain containing 3, isoform CRA_b	10.87	Y1(Phospho)	4.23
Q00839	Heterogeneous nuclear ribonucleoprotein U	3.88	S22(Phospho)	4.20
Q5JSH3	WD repeat-containing protein 44	8.11	S5(Phospho)	4.20
G3V529	ATP-dependent RNA helicase DDX24	1.72	S5(Phospho)	4.16
A2ABK4	Negative elongation factor E (Fragment)	19.5	S3(Phospho)	4.15
F8W646	Heterogeneous nuclear ribonucleoprotein A1 (Fragment)	17.31	S3(Phospho)	4.15
E5RJU9	Protein LYRIC	5.51	X1(L); S6(Phospho)	4.15
E9PIJ1	AMP deaminase 2 (Fragment)	12.64	S3(Phospho)	4.12
Q9Y2W1	Thyroid hormone receptor-associated protein 3	7.64	S7(Phospho)	4.09
B3KM87	Matrin-3	4.72	S10(Phospho)	4.09
Q9H6F5	Coiled-coil domain-containing protein 86	17.5	S17(Phospho)	4.08
H3BQZ7	HCG2044799	2.95	S9(Phospho)	4.07
H0Y579	UV excision repair protein RAD23 homolog B (Fragment)	25.44	S16(Phospho)	4.07
Q5VSL9	Striatin-interacting protein 1	4.54	S3(Phospho)	4.07
S4R359	Heterogeneous nuclear ribonucleoprotein K (Fragment)	19	S2(Phospho)	4.06
G3V5V7	Heterogeneous nuclear ribonucleoproteins C1/C2 (Fragment)	21.11	S10(Phospho)	4.05
Q9BUB1	PRKAR2A protein	10.21	S3(Phospho); C5(Carbamidomethyl)	4.05
Q86U12	Full-length cDNA clone CS0CAP007YF18 of Thymus of Homo sapiens (human)	5.81	S13(Phospho)	4.05

Accession	Description	Coverage	Modifications	XCorr
B4E2T8	Calnexin	7.02	S10(Phospho)	4.02
B7ZKW8	CapZ-interacting protein	10.62	S18(Phospho)	4.00
Q5T757	Serine/arginine-rich-splicing factor 11	3.54	S11(Phospho)	3.97
A8K8G0	Hepatoma-derived growth factor	16.35	S7(Phospho)	3.96
Q6UN15	Pre-mRNA 3'-end-processing factor FIP1	2.53	S3(Phospho)	3.96
B4E2T8	Calnexin	7.02	S3(Phospho); S13(Phospho)	3.95
A2AB27	Guanine nucleotide-binding protein-like 1 (Fragment)	6.44	S7(Phospho)	3.95
H3BUH7	Fructose-bisphosphate aldolase A (Fragment)	20.65	S11(Phospho)	3.94
E9PC28	Receptor-type tyrosine-protein phosphatase C	1.04	S4(Phospho)	3.94
E9PNJ4	Stromal interaction molecule 1	5.86	S3(Phospho)	3.91
Q9H6F5	Coiled-coil domain-containing protein 86	17.5	S20(Phospho)	3.91
J3KP29	Nuclear pore complex protein Nup98-Nup96	1.77	S6(Phospho)	3.88
B4E2T8	Calnexin	7.02	S11(Phospho)	3.85
F8VRE4	Processed lymphoid-restricted membrane protein (Fragment)	22.03	S3(Phospho)	3.82
Q96KC8	DnaJ homolog subfamily C member 1	8.48	S16(Phospho)	3.82
C9J7Y7	DNA mismatch repair protein Msh6 (Fragment)	10.6	S9(Phospho)	3.81
O95218	Zinc finger Ran-binding domain-containing protein 2	16.36	S6(Phospho)	3.80
Q09666	Neuroblast differentiation-associated protein AHNAK	0.95	S6(Phospho)	3.80
H0YFY6	Nuclear mitotic apparatus protein 1 (Fragment)	1.97	S14(Phospho)	3.79

Accession	Description	Coverage	Modifications	XCorr
E9PK09	Bcl-2-associated transcription factor 1 (Fragment)	6.21	S2(Phospho); S4(Phospho)	3.78
F5H8D7	DNA repair protein XRCC1	3.65	T4(Phospho); T17(Phospho)	3.78
O43649	Lymphocyte-specific protein 1 (Fragment)	33.33	S3(Phospho); M9(Oxidation)	3.78
F8WF17	Galectin-related protein	28.57	S11(Phospho)	3.78
Q9Y6X9	MORC family CW-type zinc finger protein 2	1.55	S5(Phospho)	3.77
H3BMF6	Ubiquitin carboxyl-terminal hydrolase 7	26.37	S7(Phospho); M12(Oxidation); M14(Oxidation)	3.76
H7C2Y0	Septin-2 (Fragment)	10.64	S9(Phospho)	3.74
K7EMU2	cAMP-dependent protein kinase type I-alpha regulatory subunit (Fragment)	15.93	S5(Phospho)	3.73
C9JBL0	Nuclear autoantigen Sp-100 (Fragment)	8.85	S6(Phospho)	3.70
F8WF45	TATA element modulatory factor	1.81	S7(Phospho)	3.70
M0R300	Unconventional myosin-IXb (Fragment)	1.83	S7(Phospho)	3.68
P49756	RNA-binding protein 25	1.66	S6(Phospho)	3.68
F5GYV5	ADP-ribosylation factor-like protein 6-interacting protein 4 (Fragment)	7.58	S1(Phospho)	3.68
G3V5V7	Heterogeneous nuclear ribonucleoproteins C1/C2 (Fragment)	21.11	M1(Oxidation); S10(Phospho)	3.67
Q08945	FACT complex subunit SSRP1	3.39	S13(Phospho)	3.67
Q96KC8	DnaJ homolog subfamily C member 1	8.48	S11(Phospho)	3.66
P08238	Heat shock protein HSP 90-beta	4.42	S3(Phospho)	3.66
P28715	DNA repair protein complementing XP-G cells	1.18	S12(Phospho)	3.66
Q09666	Neuroblast differentiation-associated protein AHNAK	0.95	S3(Phospho)	3.66

Accession	Description	Coverage	Modifications	XCorr
E7EQF0	Nexilin	8.81	M2(Oxidation); S5(Phospho)	3.65
P08559	Pyruvate dehydrogenase E1 component subunit alpha, somatic form, mitochondrial	5.9	Y1(Phospho); S12(Phospho)	3.64
E5RIS7	Transcription elongation factor A protein 1	13.51	S9(Phospho)	3.63
Q9Y2W1	Thyroid hormone receptor-associated protein 3	7.64	S7(Phospho); S18(Phospho)	3.62
H0YA82	La-related protein 7 (Fragment)	8.68	S8(Phospho)	3.60
J3KQ96	Treacle protein (Fragment)	2.19	S14(Phospho)	3.60
O75396	Vesicle-trafficking protein SEC22b	6.51	S4(Phospho)	3.59
O95218	Zinc finger Ran-binding domain-containing protein 2	16.36	S11(Phospho)	3.57
P29966	Myristoylated alanine-rich C-kinase substrate	5.42	S14(Phospho)	3.57
P06748	Nucleophosmin	6.46	M11(Oxidation); S16(Phospho)	3.56
P40222	Alpha-taxilin	2.56	S11(Phospho)	3.55
O00264	Membrane-associated progesterone receptor component 1	10.26	S9(Phospho)	3.55
H0YNE5	Regulator of microtubule dynamics protein 3 (Fragment)	7.17	S3(Phospho)	3.54
H0YJ03	Proteasome subunit alpha type-3 (Fragment)	16.87	S9(Phospho); M14(Oxidation)	3.54
Q9H1E3	Nuclear ubiquitous casein and cyclin-dependent kinase substrate 1	14.81	M2(Oxidation); M4(Oxidation); S9(Phospho)	3.53
J3QTP8	E3 ubiquitin-protein ligase RNF213	1.16	S10(Phospho)	3.52
Q8TAQ2	SWI/SNF complex subunit SMARCC2	1.15	S8(Phospho)	3.51
Q9UQ35	Serine/arginine repetitive matrix protein 2	2.58	T13(Phospho)	3.51
Q29RF7	Sister chromatid cohesion protein PDS5 homolog A	1.27	S7(Phospho)	3.50

4.2.2 Distribution of Proteins and Phosphorylation Sites Identified by Qualitative analysis.

Standard bioinformatic analysis was used to visualise the biological processes associated with the phosphorylated proteins in the BM aspirates of the 32 patients, identified by LC-MS/MS. PANTHER analysis was carried out to identify these biological functions. Cellular processes had the highest related proteins (29.4%), followed by metabolic processes (26.5%) and biological regulation (20.6%).

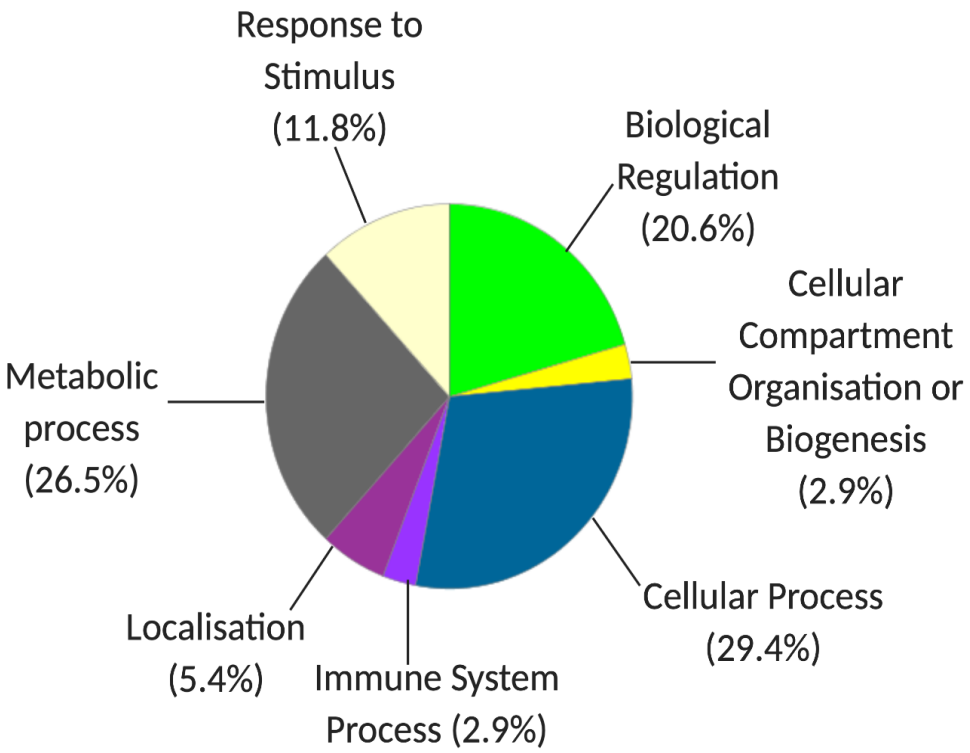

Figure 4.2: Biological processes of all qualitatively identified phosphopeptides analysed by PANTHER analysis.

The 135 proteins, identified using Proteome Discoverer, were grouped into retrospective biological processes using freely available PANTHER software (Thomas et al., 2003). Cellular processes were identified as the process with the most related proteins identified in phosphopeptide enriched BM aspirates.

4.2.3 Quantitative Proteomic Analysis of Phosphopeptide Enriched CD138+ Cell Lysates and Bioinformatic Analysis of individual DSS Groups.

The removal of non-phosphorylated proteins sufficiently reduced the abundance of proteins, allowing for the identification of distinct phosphoproteomic signatures in each group of drug sensitivity scored patients. 18 phosphorylated proteins were identified for group 1 (Table 4.4), 61 phosphorylated proteins were identified for group 2 (Table 4.5), 11 phosphorylated proteins identified for group 3 (Table 4.6) and 81 phosphorylated proteins were identified for group 4 (Table 4.7) by quantitative analysis after LC-MS/MS. PANTHER analysis was carried out on each individual group of proteins, identifying the most abundant biological processes within the identified phosphorylated proteins. The majority of group one is comprised of 37.5% metabolic process proteins, 25% biological regulation proteins and 18.8% cellular process related proteins (Figure 4.3). Group 2 exhibits a vast array of phosphorylated proteins, the majority of which are related to metabolic processes (28.6%), cellular processes (28.6%) and biological regulation (17.9%) (Figure 4.4). Group 3 has the most limited abundance of phosphorylated proteins, with only 11 identified phosphorylated proteins. 33.3% of phosphoproteins identified are metabolic related proteins, 22.2% are biological regulation proteins and 22.2% are cellular process proteins (Figure 4.5). Group 4 shows the most diverse range of abundant proteins, with 81 identified phosphoproteins. 34.5% of these identified proteins are cellular process proteins, 20.7% biological regulation proteins and 20.7% metabolic process proteins (Figure 4.6). A comparative study of the abundant proteins revealed that 48% of the identified proteins are, expectedly, identified within group 4. Interesting, the second most diverse group of abundant proteins are identified in the samples related to group 2 (35%), with group 1 and group 3 associated with 11% and 8% of the total abundant proteins respectively (Figure 4.7).

Table 4.4: Phosphoproteins identified in Group 1 patients by Perseus analysis.

Accession	Protein ID
H7C2Y0	Septin-2 (Fragment)
A8K8G0	Hepatoma-derived growth factor
B4DDC6	Prostaglandin E synthase 3
P08238	Heat shock protein HSP 90-beta
M0R088	Serine/arginine repetitive matrix protein 1 (Fragment)
Q9Y2W1	Thyroid hormone receptor-associated protein 3
Q92922	SWI/SNF complex subunit SMARCC1
E9PQA1	Small acidic protein
P29692	Elongation factor 1-delta
Q9H3N1	Thioredoxin-related transmembrane protein 1
P27824	Calnexin
Q9H1E3	Nuclear ubiquitous casein and cyclin-dependent kinase substrate 1
B3KV94	Jumonji, AT rich interactive domain 1B (RBP2-like), isoform CRA_a (Fragment)
P05387	60S acidic ribosomal protein P2
B4DDC6	Prostaglandin E synthase 3
Q9Y2W1	Thyroid hormone receptor-associated protein 3
P62995	Transformer-2 protein homolog beta
E9PQA1	Small acidic protein

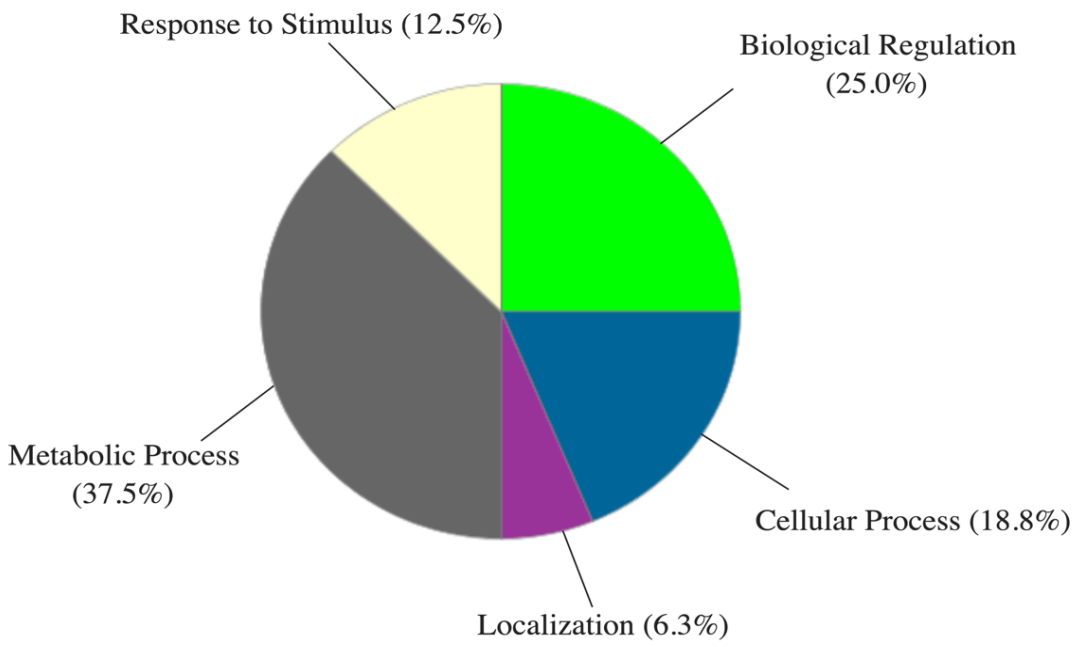

Figure 4.3: Biological processes represented in Group 1

The 18 proteins, identified using Perseus software, were grouped into retrospective biological processes using freely available PANTHER software (Thomas et al., 2003). Metabolic processes were identified as the process with the most related proteins identified in phosphopeptide enriched BM aspirates.

Table 4.5: Phosphoproteins identified in Group 2 patients by Perseus analysis.

Accession	Protein ID
D3DNX8	Membrane-associated progesterone receptor component 2
P14625	Endoplasmin
D3DNX8	Membrane-associated progesterone receptor component 2
O00264	Membrane-associated progesterone receptor component 1
H7C2Y0	Septin-2 (Fragment)
K7EMU2	cAMP-dependent protein kinase type I-alpha regulatory subunit (Fragment)
Q8ND56	Protein LSM14 homolog A
Q8TCJ2	Dolichyl-diphosphooligosaccharide--protein glycosyltransferase subunit STT3B
A8K8G0	Hepatoma-derived growth factor
P08238	Heat shock protein HSP 90-beta
H3BRV0	Eukaryotic translation initiation factor 3 subunit C
P49736	DNA replication licensing factor MCM2
B4DDC6	Prostaglandin E synthase 3
P46821	Microtubule-associated protein 1B
P14625	Endoplasmin
H3BPZ1	Very-long-chain (3R)-3-hydroxyacyl-[acyl-carrier protein] dehydratase 3
Q969E4	Transcription elongation factor A protein-like 3
Q8IYB3	Serine/arginine repetitive matrix protein 1
B8ZZB6	Protein IWS1 homolog (Fragment)
B7ZKW8	CapZ-interacting protein
O75396	Vesicle-trafficking protein SEC22b
J3KQ45	Trans-Golgi network integral membrane protein 2
E9PK09	Bcl-2-associated transcription factor 1 (Fragment)
Q9Y2W1	Thyroid hormone receptor-associated protein 3
P34910	Protein EVI2B
H7BXF3	Transformer-2 protein homolog beta (Fragment)
B4E2T8	Calnexin
F8VTQ5	Heterogeneous nuclear ribonucleoprotein A1 (Fragment)
D6REM6	Matrin-3
P05455	Lupus La protein
P14625	Endoplasmin
B7ZKW8	CapZ-interacting protein
H0Y4X3	RNA-binding protein 39 (Fragment)
P16403	Histone H1.2
O95218	Zinc finger Ran-binding domain-containing protein 2

Q9Y385	Ubiquitin-conjugating enzyme E2 J1
P48681	Nestin
E9PK09	Bcl-2-associated transcription factor 1 (Fragment)
H3BPD0	Zinc finger CCCH domain-containing protein 18 (Fragment)
P16403	Histone H1.2
H0YE72	Elongation factor 1-delta (Fragment)
B7ZKW8	CapZ-interacting protein]
Q9H3N1	Thioredoxin-related transmembrane protein 1
P54725	UV excision repair protein RAD23 homolog A
F8W7S5	Ribosome-binding protein 1
E5RJU9	Protein LYRIC
Q9H1E3	Nuclear ubiquitous casein and cyclin-dependent kinase substrate 1
B4E2T8	Calnexin
O95218	Zinc finger Ran-binding domain-containing protein 2
C9JZW3	Elongation factor 1-beta (Fragment)
F5GXU9	2-oxoisovalerate dehydrogenase subunit alpha, mitochondrial (Fragment)
E9PQA1	Small acidic protein
C9JKF7	Lymphocyte-specific protein 1 (Fragment)
P48681	Nestin
D3DNX8	Membrane-associated progesterone receptor component 2
P35579	Myosin-9
Q58FF8	Putative heat shock protein HSP 90-beta 2
H0YDD8	60S acidic ribosomal protein P2 (Fragment)

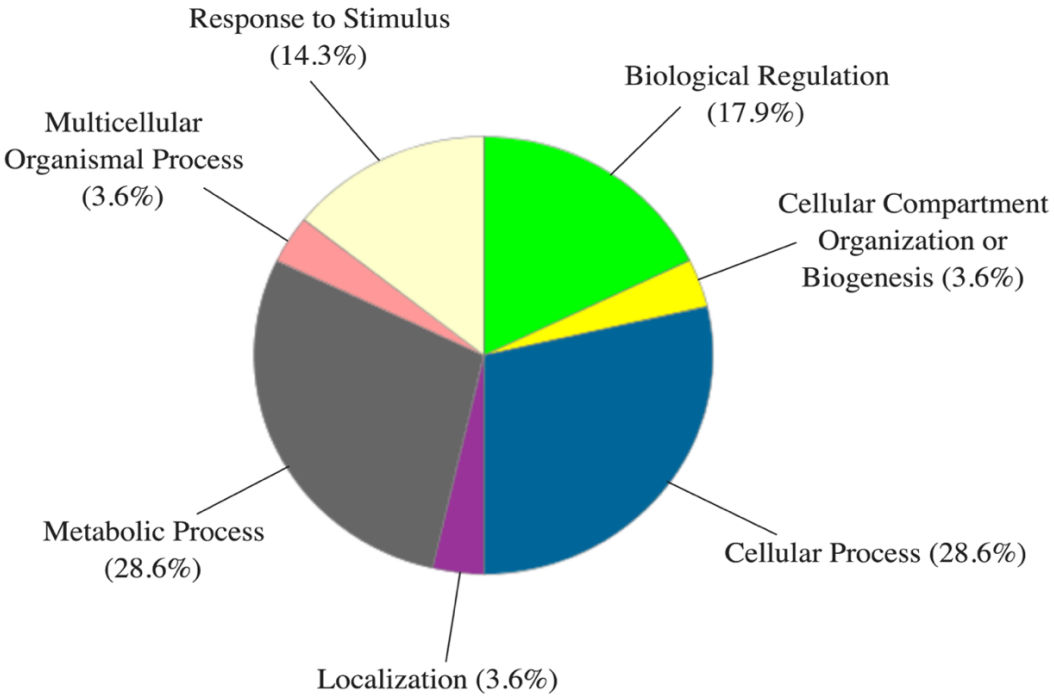

Figure 4.4: Biological processes represented in Group 2.

The 61 proteins, identified using Perseus, were grouped into retrospective biological processes using freely available PANTHER software (Thomas et al., 2003). Cellular processes and metabolic processes were identified as the process with the most related proteins identified in phosphopeptide enriched BM aspirates.

Table 4.6: Phosphoproteins identified in Group 3 patients by Perseus analysis.

Accession	Protein ID
O95218	Zinc finger Ran-binding domain-containing protein 2
Q9H1E3	Nuclear ubiquitous casein and cyclin-dependent kinase substrate 1
H7C2Y0	Septin-2 (Fragment)
A8K8G0	Hepatoma-derived growth factor
B4DDC6	Prostaglandin E synthase 3
H7BXF3	Transformer-2 protein homolog beta (Fragment)
F8WE04	Heat shock protein beta-1
F8VTQ5	Heterogeneous nuclear ribonucleoprotein A1 (Fragment)
F5GXU9	2-oxoisovalerate dehydrogenase subunit alpha, mitochondrial (Fragment)]
E9PHF0	Filamin-A
H7C1X9	CCR4-NOT transcription complex subunit 10 (Fragment)

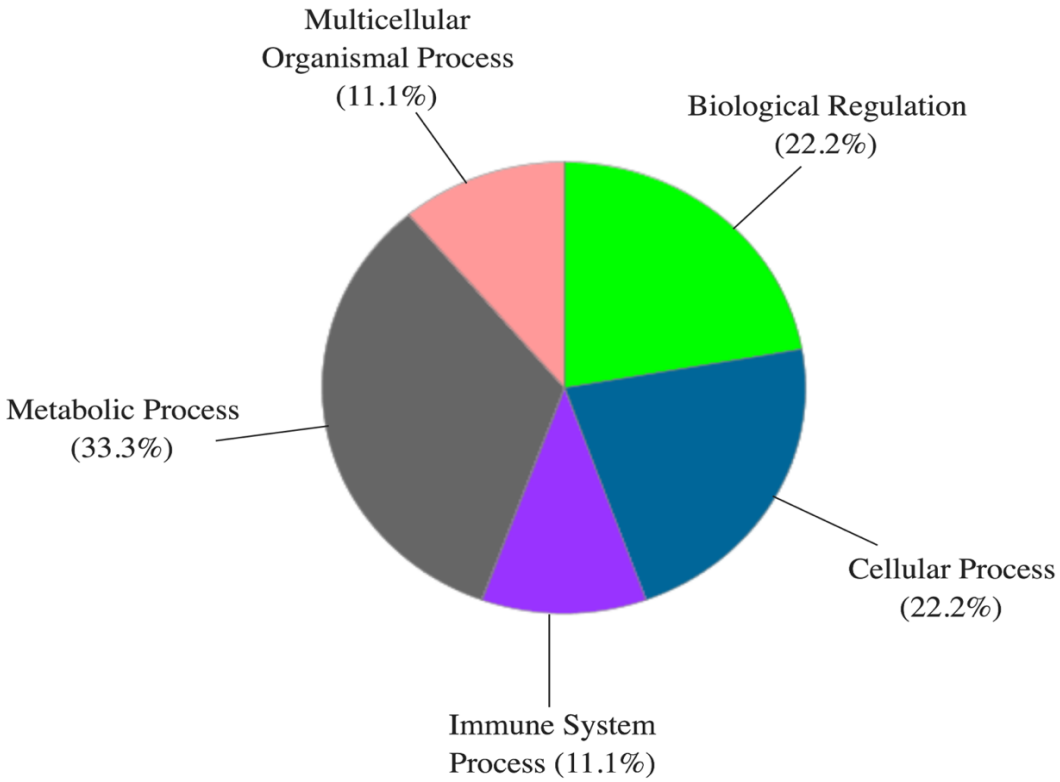

Figure 4.5: Biological processes represented in Group 3

The 11 proteins, identified using Perseus, were grouped into retrospective biological processes using freely available PANTHER software (Thomas et al., 2003). Metabolic processes were identified as the process with the most related proteins identified in phosphopeptide enriched BM aspirates.

Table 4.7: Phosphoproteins identified in Group 4 patients by Perseus analysis.

Accession	Protein ID
A6PVS8	Leucine-rich repeat and IQ domain-containing protein 3
D3DNX8	Membrane-associated progesterone receptor component 2
Q6IPX3	Transcription elongation factor A protein-like 6
H0Y579	UV excision repair protein RAD23 homolog B (Fragment)
B4E2T8	Calnexin
O00264	Membrane-associated progesterone receptor component 1
H7C2Y0	Septin-2 (Fragment)
Q8TCJ2	Dolichyl-diphosphooligosaccharide--protein glycosyltransferase subunit STT3B
A8K8G0	Hepatoma-derived growth factor
Q05209	Tyrosine-protein phosphatase non-receptor type 12
P05387	60S acidic ribosomal protein P2
Q99523	Sortilin
O43852	Calumenin
B4DF77	Phosphofurin acidic cluster sorting protein 1
B4DDC6	Prostaglandin E synthase 3
P08238	Heat shock protein HSP 90-beta
P49736	DNA replication licensing factor MCM2
Q5W011	Splicing factor 45 (Fragment)
M0R2H7	Cdc42-interacting protein 4
Q9UDY2	Tight junction protein ZO-2
Q14761	Protein tyrosine phosphatase receptor type C-associated protein
E7EQF0	Nexilin
C9JEN3	Protein lifeguard 3 (Fragment)
M0R088	Serine/arginine repetitive matrix protein 1 (Fragment)
Q5HY54	Filamin-A
P53999	Activated RNA polymerase II transcriptional coactivator p15
H3BS66	Small integral membrane protein 1
E9PEM5	Lipopolysaccharide-responsive and beige-like anchor protein
Q9H2G2	STE20-like serine/threonine-protein kinase
Q9Y2W1	Thyroid hormone receptor-associated protein 3
E5RJ61	Dematin (Fragment)
P34910	Protein EVI2B
F8VTQ5	Heterogeneous nuclear ribonucleoprotein A1 (Fragment)
C9JID5	Transmembrane protein 40
P37802	Transgelin-2
Q8ND76	Cyclin-Y
C9JSU1	Leucine-rich repeat flightless-interacting protein 2 (Fragment)

D6RAM3	Docking protein 3
E9PQA1	Small acidic protein OS=Homo sapiens GN=C11orf58 PE=2 SV=1 - [E9PQA1_HUMAN]
H7BXT7	BET1-like protein
P05455	Lupus La protein
Q13283	Ras GTPase-activating protein-binding protein 1
Q5QP22	RNA-binding protein 39 (Fragment)
P16403	Histone H1.2
A2ABK4	Negative elongation factor E (Fragment)
H0YF00	Bcl-2-associated transcription factor 1 (Fragment)
E9PNR6	Rho GTPase-activating protein 1 (Fragment)
C9JID5	Transmembrane protein 40
F5GYK6	ATP-binding cassette sub-family F member 1 (Fragment)
P13224	Platelet glycoprotein Ib beta chain
P16403	Histone H1.2
E9PS34	Nucleosome assembly protein 1-like 4 (Fragment)
F8W7S5	Ribosome-binding protein 1
P53999	Activated RNA polymerase II transcriptional coactivator p15
Q9H3N1	Thioredoxin-related transmembrane protein 1
Q5RHP9	Glutamate-rich protein 3
H0YBJ8	Protein LYRIC (Fragment)
B4E2T8	Calnexin
O00264	Membrane-associated progesterone receptor component 1
C9JZW3	Elongation factor 1-beta (Fragment)
B1ALG5	Probable global transcription activator SNF2L2
H0YDB2	Stromal interaction molecule 1 (Fragment)
Q9Y3C5	RING finger protein 11
C9JKF7	Lymphocyte-specific protein 1 (Fragment)
P12931	Proto-oncogene tyrosine-protein kinase Src
H0YJ73	Tandem C2 domains nuclear protein (Fragment)
F5GXU9	2-oxoisovalerate dehydrogenase subunit alpha, mitochondrial (Fragment)
D3DNX8	Membrane-associated progesterone receptor component 2
Q5VUB5	Protein FAM171A1
J3KQ98	Protein phosphatase 1 regulatory subunit 37
Q86YF9	Zinc finger protein DZIP1
H7C2Y0	Septin-2 (Fragment)
H0YDD8	60S acidic ribosomal protein P2 (Fragment)
P08238	Heat shock protein HSP 90-beta
E9PHF0	Filamin-A
H0YI14	Neuron navigator 3 (Fragment)
P05455	Lupus La protein]
Q5QP22	RNA-binding protein 39 (Fragment)

F8W7S5	Ribosome-binding protein 1
D6RC37	Activated RNA polymerase II transcriptional coactivator p15 (Fragment)
B4E2T8	Calnexin

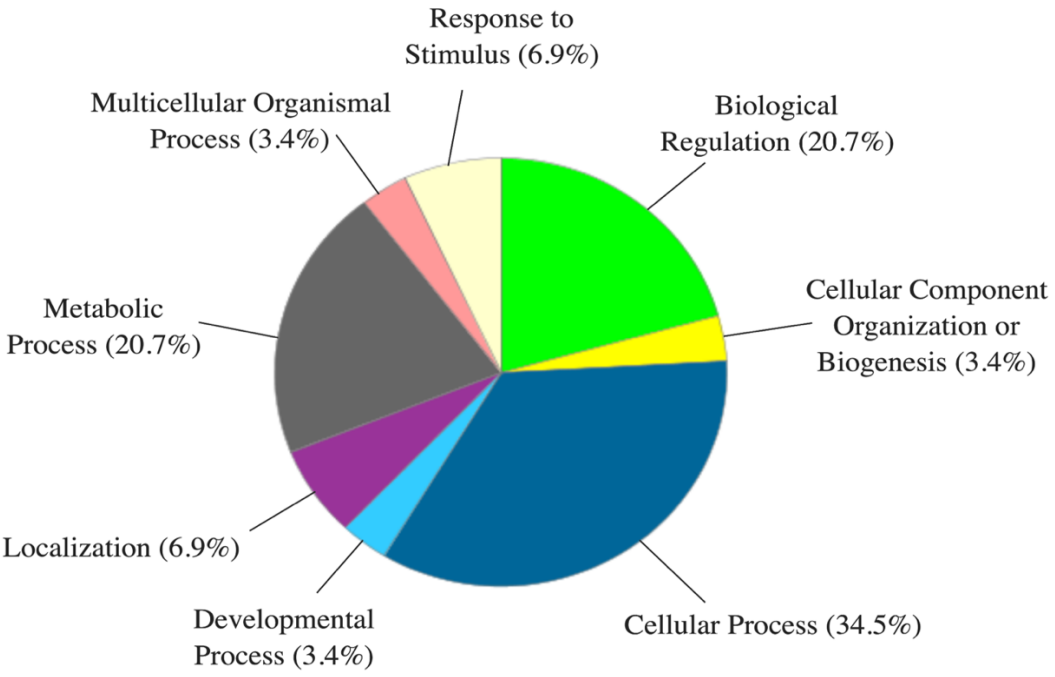

Figure 4.6: Biological processes represented in Group 4.

The 81 proteins, identified using Perseus, were grouped into retrospective biological processes using freely available PANTHER software (Thomas et al., 2003). Cellular processes were identified as the process with the most related proteins identified in phosphopeptide enriched BM aspirates.

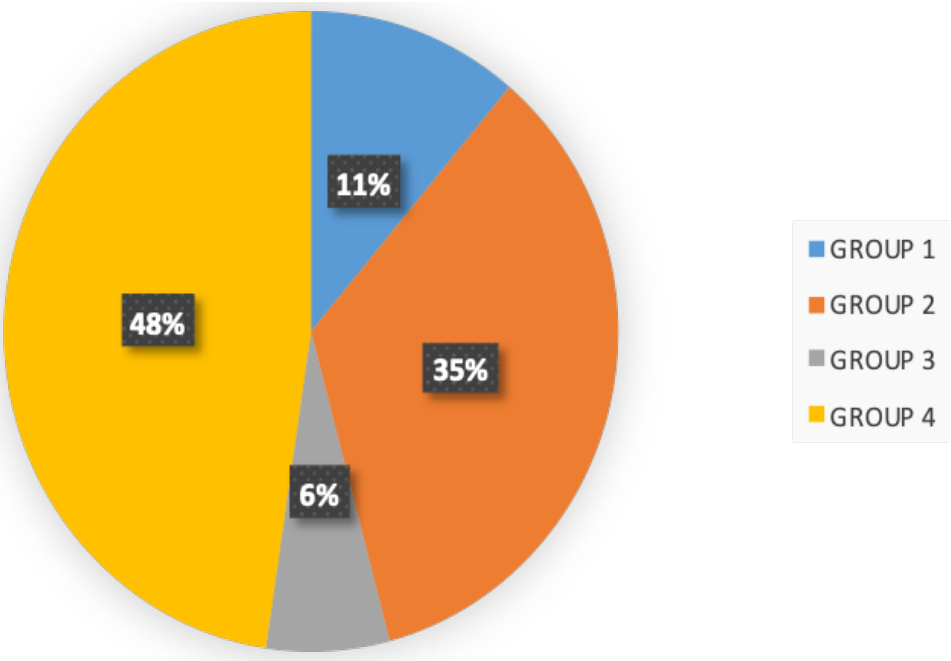

Figure 4.7: Percentage of phosphopeptides observed per DSS group

The pie chart depicts the percentage of differentially abundant phosphorylated proteins exhibited in each group established by the FIMM drug sensitivity scoring method, ranging from group 1 being sensitive to treatment and group 4 being drug resistant.

4.2.4 Comparative analysis of Biological Processes Related to Protein Signatures Abundant in Each DSS Group and Bioinformatic Analysis using Perseus.

After bioinformatic analysis, using PANTHER software, a comparison was carried out on the biological processes related to all of the identified phosphorylated proteins in each DSS groupings. Cellular process related proteins were the most abundant biological process with respect to group 4, closely followed by metabolic processes. The abundance of cellular process proteins present in group 4, which is a 5-fold increase from the number of cellular process proteins in group 3 and a 3.3-fold increase from that of group 1. Interestingly, group 2 exhibit the most metabolic proteins related proteins in comparison to the other DSS groups. Group 2 exhibits

equal amounts of proteins related to cellular processes as metabolic processes (Figure 4.8). Perseus software was used to compile a heatmap, comprised of the proteins with altered abundance from group 1 to group 4 (Figure 4.9). All proteins were found to be statistically significant ($p<0.05$) using a Student's *t*-test.

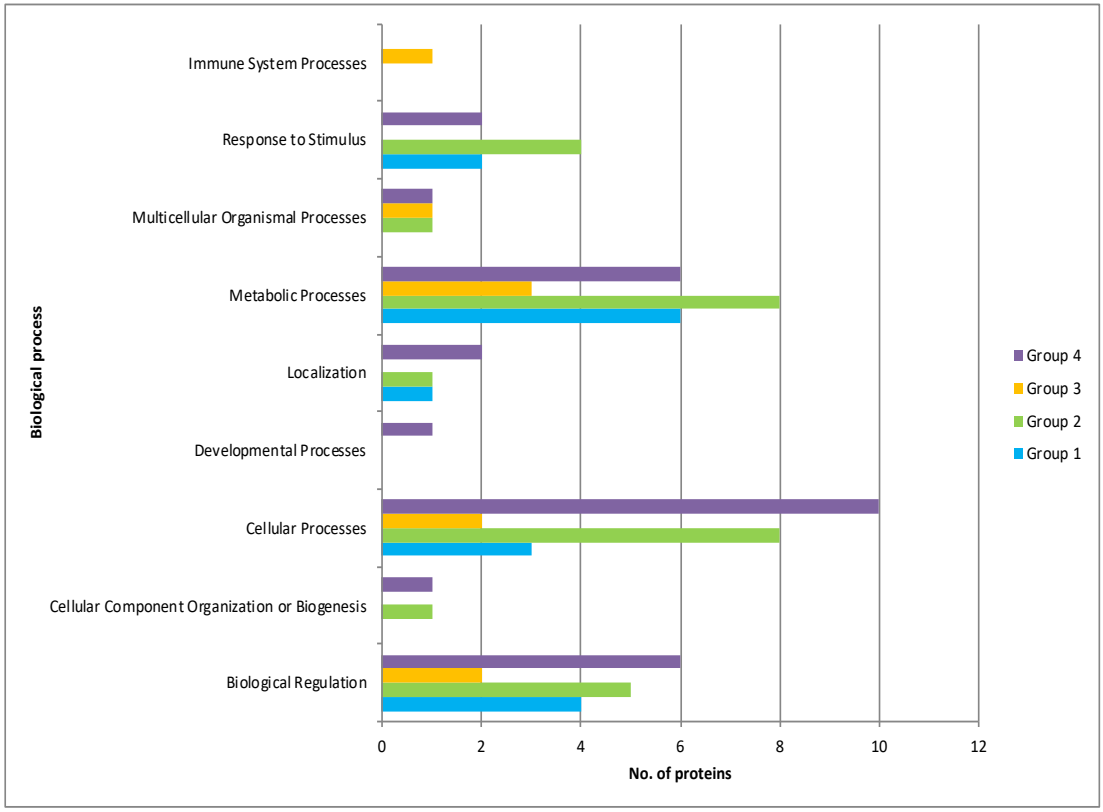

Figure 4.8: Comparison between biological processes.

This figure depicts a comparison of the number of phosphorylated proteins associated with specific biological processes, identified by Perseus analysis. Each group was established by the FIMM drug sensitivity scoring method, ranging from group 1 being sensitive to treatment and group 4 being drug resistant.

A

Accession Number	Protein IDs	Student's T-test significant	Phospho site IDs	Sequence
P16403	H12_HUMAN	G1_G4		ALAAAGYDVEK
P01857	IGHG1_HUMAN	G1_G4		ALPAPIEK
P16403	H12_HUMAN	G1_G4	223	ASGPPVSELITK
P01876	IGHA1_HUMAN	G1_G4		DASGVTFTWTPSSGK
Q14696	MESD_HUMAN	G1_G4		DDDIEEGDLPEHK
P01609	KV117_HUMAN	G1_G4		DIQMTQSPSSLSASVGDR
P14625	ENPL_HUMAN	G1_G4		DISTNYYASQK
Q8NBS9	TXND5_HUMAN	G1_G4		DLDSLHR
Q71U36	TBA1A_HUMAN	G1_G4		DYEEVGVDSVEGEGEEEGEEY
P67809	YBOX1_HUMAN	G1_G4		EDGNEEDKENQGDETQGQQPPQR
P14625	ENPL_HUMAN	G1_G4		EEEAIQLDGLNASQIR
P53999	TCP4_HUMAN	G1_G4	395	EQISDIDDAVR
P55060	XPO2_HUMAN	G1_G4		IIIPEIQK
P25705	ATPA_HUMAN	G1_G4		ILGADTSVDLEETGR
P08670	VIME_HUMAN	G1_G4		ILLAELEQLK
P62805	H4_HUMAN	G1_G4		ISGLIYEETR
Q8NBS9	TXND5_HUMAN	G1_G4		LQPTWNDLGDK
P14866	HNRPL_HUMAN	G1_G4		TDNAGDQHGGGGGGGGGAGAAGGGGGGENYDDPHK
P62987	RL40_HUMAN	G1_G4		TITLEVEPSDTIENVK
P62805	H4_HUMAN	G1_G4		VFLENVIR

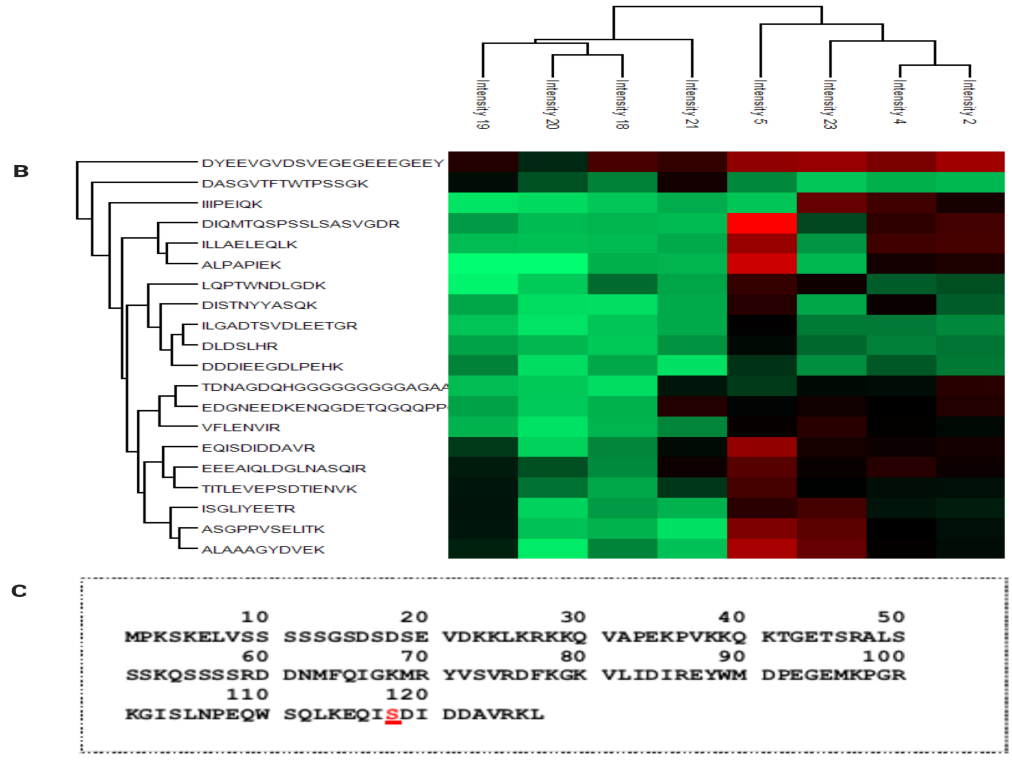

Figure 4.9: Heatmap of proteins with changed abundance from Group 1 to Group 4 patients.

A) Depicted is all proteins found to be significant from Group 1 to Group 4. The intensity of red indicates increased abundance of individual proteins and green indicating a decreased abundance of individual proteins. B) a heatmap compiled from all statistically significant proteins with altered abundance from Group 1 to Group 4 through Student's *t*-test. C) Focus on the TCP4 and the particular phosphorylation site identified by LC-MS/MS.

4.2.5 Comparative Human Phospho-Kinase Array using Enriched Phosphopeptide Samples.

For the further identification of potential phosphorylated sites related to drug resistance in the DSS patients, a Human Phospho-Kinase Array was carried out. The nitrocellulose membrane contained 43 different capture antibodies, in duplicate, allowing for the identification of changed abundance in each of these phosphorylated proteins (Figure 4.10A). This analysis was carried out solely on four patient samples, two samples from the groups with the largest disparity in drug sensitivity, Group 1 and Group 4. Sample 23 and 24 were from patients considered as group 1, with a strong sensitivity towards treatment, and sample 21 and 39 were obtained from patients with strong resistance to treatment (Group 4). Individual patient details are available in Table 4.1. The 2.3 fold increase in pHSP27 was identified in the comparative study, with the increase being noted with relation to drug resistant i.e. there was a 2.3 fold increase of pHSP27 noted in Group 4 in comparison to Group 1 (Figure 4.10B). The increased abundance was graphed to indicate the change between group 1 and group 4 (Figure 4.11).

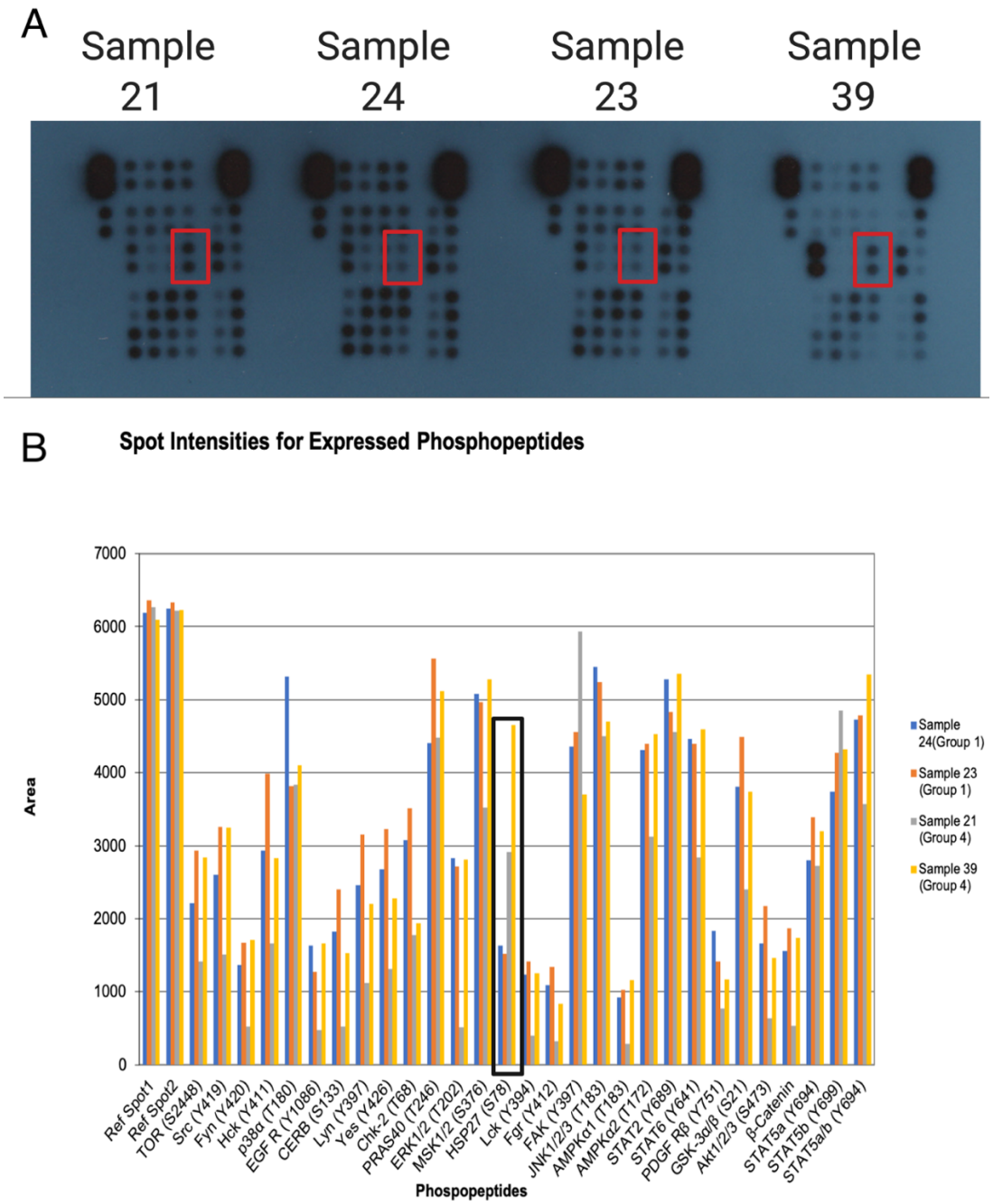

Figure 4.10: Comparative Immunoblotting of group 1 and group 4 samples with varying phosphorylated targets using a phosphor-kinase array.

A representative immunoblot array with immune-decorated bands representing multiple phosphorylation targets, with focus of HSP27 (marked in red). B is the graphical analysis of the immune-decoration for each individual target, again, with focus on HSP27 (marked in black).

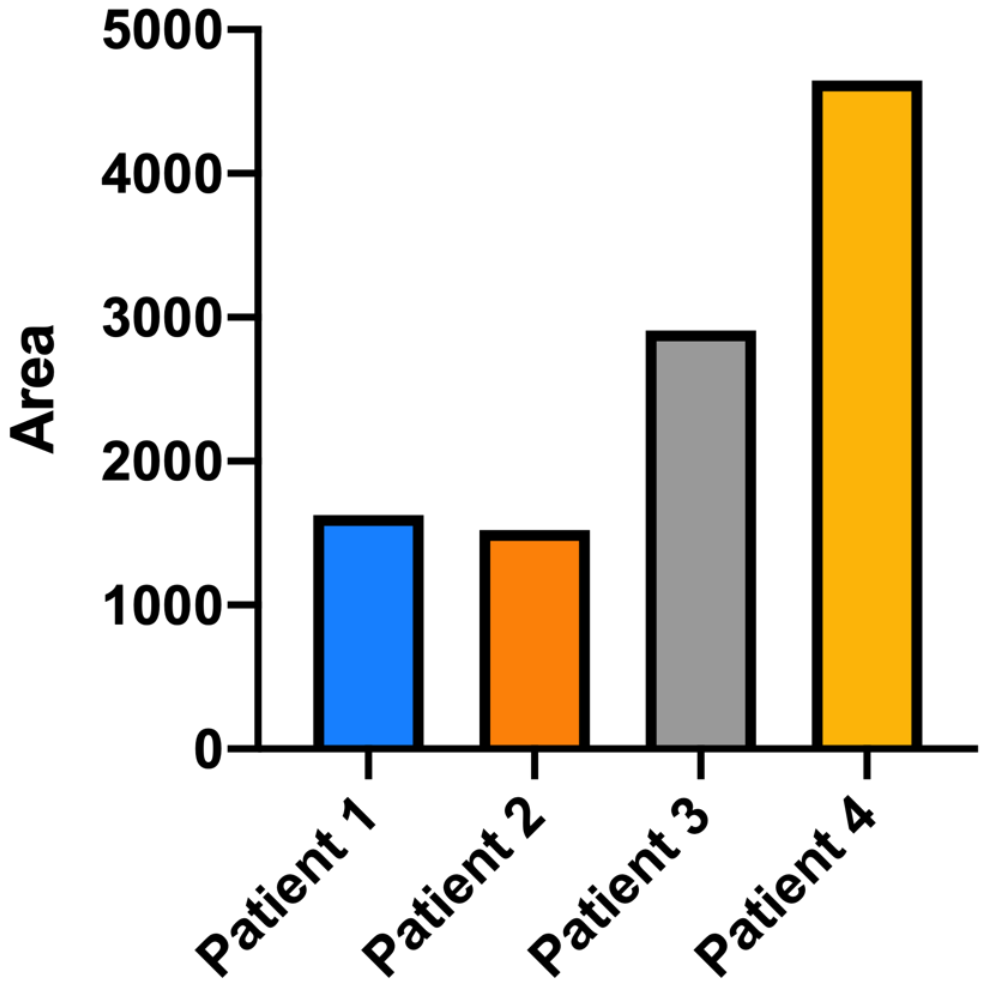

Figure 4.11: A focused comparison in the abundance of HSP27 in samples from group 1 and group 4 from Figure 4.9.

This figure depicts the change in abundance of HSP27 (s78) in Group 4 resistant patients in comparison to Group 1 sensitive patients. Sample 24 (blue) and sample 23 (orange) are Group 1 patients and sample 21 (grey) and sample 39 (yellow) are Group 4 patients.

4.3 Discussion

Phosphorylation, a reversible PTM, has proven to play a significant role in molecular mechanisms especially those governing tumour proliferation, growth and survival. In understanding phosphopeptides, their mechanisms and the manner in which they interact with a tumour microenvironment, the potential identification of effective therapeutic targets is endless. As phosphorylation has been identified as playing a significant role in the onset and progression of almost all cancer types, the potential of targeting specific kinase signalling pathways is a logical advance in therapeutic development. With promising kinase inhibitors in use for treatment of multiple cancer types and kinase inhibitor experimental treatments for MM, including PF-04691502, targeting kinase to inhibit phosphorylation can lead to cancer cell apoptosis, inhibition of cancer cell proliferation and antitumour effects.

To carry out in-depth analysis of phosphorylation and phosphopeptide involvement in cancer cell proliferation, with the intention of developing therapeutics to target phosphorylation manipulation, advanced proteomic approaches must be utilised. As there is an abundance of information to be extrapolated from peptides in normal human biofluids, saliva, urine, serum, plasma etc., the study of phosphoproteomics must involve enriching samples for phosphorylated proteins. Utilising techniques such as magnetic titanium dioxide beads, as used in this study, on-plate enrichment or monolithic columns (Vyse et al., 2017) allows to isolate phosphorylated proteins, while still maintaining the integrity of the original sample for analysis of non-phosphorylated proteins. This allows the identification of two distinct proteomic profiles from one set of samples.

The analysis of LC-MS/MS results can be analysed by two methods, quantitative and qualitative proteomic analysis. Quantitative proteomics is based on the relative or absolute quantities of target molecules present in samples, i.e. the quantity of the molecule. This form of proteomic analysis allows for the identification of the variability

of proteins within a sample cohort, as well as identifying the relevance of these changes in abundance using bioinformatic software (Välikangas et al., 2018). However, the quantification of proteins by mass spectrometry can be effected by factors such as sample and instrument related sensitivities. Qualitative proteomics allows the analysis of the mass spectra by different means, such as the percentage of protein sequence coverage from the identified peptides (%coverage), the quality of fit of the identified peptide fragments to the theoretical spectra created by the sequence b and y ions (Xcorr value) and minimal false discovery rate at which the identification is taken as correct (q-value). The change of proteomic profile generally, as opposed to the change in abundance of particular proteins, can lead to the identification of changes in PTMs, pathways and processes that may be overlooked when focusing on individual proteins (Mayya and Han, 2009). This method can, therefore, identify predicted drug resistance and the response to treatment by a patient without focusing on one or two particular biomarkers, allowing a more decisive decision to be made about the correct course of treatment for a patient.

The comparison between the phosphorylated protein abundance in Group 1 to Group 4 is vastly different. 81 phosphorylated proteins were identified in group 4, in comparison to 18 phosphorylated proteins in group 1. Group 1 is responsible for 11% of the overall identified phosphorylated proteins and Group 4 is responsible for 48% of the overall identified phosphorylated proteins (Figure 4.7). As group 4 are classed as the patients with prominent resistance to drug treatments, both established and investigational drugs, and group 1 are grouped due to their significant sensitivity to established and investigational drug treatments for MM. This leads to the conclusion that the phosphorylation of proteins drives drug resistance in MM. Phosphorylation has previously been implicated in drug resistance in MM. As in the analysis of the biological processes associated with the identified phosphorylated proteins, the most prevalent processes associated with Group 4 are cellular process (34.5%), metabolic process (20.7%) and biological regulation (20.7%) (Figure 4.6). Biological processes

associated with Group 1 are metabolic process (37.5%) and biological regulation (25%). The increase in metabolic process-related proteins in Group 1 directly correlates with the increase in abundance of metabolic process related proteins observed in the most sensitive patients in Chapter 3, leading to the conclusion that metabolism is upregulated in drug sensitive patients.

From the comparative study carried out on the statistically significant phosphorylated proteins with altered abundance from Group 1 to Group 4, 20 proteins were identified using a Student's *t*-test. Of these 20 identified phosphopeptides, two phosphorylation sites were identified. Activated RNA polymerase II transcriptional coactivator p15 (TCP4) 118 Phosphoserine, was identified as having a significantly increased abundance in Group 1 in comparison to Group 4 (Figure 4.9A). TCP4 is a general coactivator that functions cooperatively with TAFs and mediates functional interactions between upstream activators and the general transcriptional machinery. Activity is controlled by protein kinases that target the regulatory region. Phosphorylation inactivates both ds DNA-binding and cofactor function (Olsen et al., 2010). Recent studies have identified the decreased abundance of this particular phosphorylation residue having an implication in cancer progression (Zhou et al., 2013). As a decreased abundance has been identified in Group 4 in comparison to Group 1, there is less phosphorylation of this particular residue in Group 4 than observed in Group 1. The decreased phosphorylation means that there is more activity from the transcription factor associated with this particular phosphorylation residue, and therefore there is more activity in the drug resistant cohort. This leads to the hypothesis that the decreased amount of phosphorylation is leading to the increased activation of these transcription factors, switching on genes aiding in drug resistance in Group 4 patients. The identification of this particular phosphorylation residue, coupled with evidence in the literature, strengthens the importance in phosphoproteomics.

pHSP27 was noted to have a 2.3 fold increase in group 4 patients, in comparison to group 1, which was identified using a human phosphor-kinase array. Although the array identified other potential targets (Figure 4.10A), phosphorylated heat shock protein 27 showed the most consistent increased abundance from treatment sensitive group 1 patients to resistant group 4 patients. Heat shock proteins are observed in response to stresses, such as chemical, physical and environmental stress and are expressed in multiple parts of a cell (Kregel, 2002). Their primary function is protection, allowing cell survival when subjected to extreme stress, which has led to HSPs being implicated in drug resistance and poor prognosis in cancer patients. The abnormal phosphorylation of HSP27 has been strongly linked to cancer progression (Katsogiannou et al., 2014). In breast cancer it has been observed that an increased abundance directly correlates with reduced anti-cancer drug activity and, furthermore, increases Her-2 stability (Kang et al., 2008). It was noted that the increased abundance of pHSP27 is expressed in advanced stage lung cancer patients and is an indication of shorter OS (Liu et al., 2016). This correlation between increased abundance of HSP27 was also observed in pancreatic cancer cells with known resistance to treatment in comparison to treatment sensitive cells (Mori-Iwamoto et al., 2007).

To sum up, phosphorylation events can be used to predict drug resistance in MM, as has been shown previously in various types of cancer treatment. Although the identification of individual biomarkers has been proven to be an invaluable tool in cancer treatment, proliferation, diagnosis and prognosis, a general look at protein characterisation and pathways can be just as beneficial to cancer patients. Examining the consequences of PTMs such as phosphorylation, ubiquitination, acetylation etc. can give in-depth insight into cancer proliferative methods, processes and pathways and can, therefore, provide more informed strategies in fighting cancer.

Chapter 5

Proteomic Evaluation of Saliva Throughout disease Progression in Multiple Myeloma

5.1 Introduction

Biomarkers have proven themselves as an invaluable tool in the areas of early detection, diagnostics and predicting disease progression of multiple cancer types, including MM. With multiple verified biomarkers for MM, very little research has been conducted in the area of salivary biomarkers for the disease. It has been observed that approximately 40% of cancer, stroke and cardiovascular disease biomarkers are present in whole saliva (Loo et al., 2010). Due to the invasiveness of serum collection, saliva biomarkers seem to be the logical progression in disease detection and diagnosis. Salivary biomarkers have revealed significant promise in the area of cancer detection over recent years. In a study carried out by Agha-Hosseini and colleagues it was noted that CA15-3 levels, in both serum and saliva, was significantly increased in stage 2 breast cancer patients. This was evidence to establish CA15-3 as a salivary biomarker for breast cancer, along with the 65% detection in saliva of CA15-3 in breast cancer seen by (Streckfus et al., 2000) and a 62% sensitivity noted by (Bigler et al., 2002) CA 15-3 is hypothesised to play a role in cell adhesion, is a significant transmembrane glycoprotein and has been observed to often overexpressed in cancer (Duffy et al., 2000).

Epidermal growth factor (EGF) has been noted as being significantly higher in the saliva of women with primary or recurrent breast cancer in comparison with healthy controls. The most significant increased expression was noted in the saliva of women with local recurrence (Navarro et al., 1997). As this protein has been seen to play an important role in tumorigenesis, invasiveness and is known to be responsible for a variety of tissue growth and repair associated with poor prognosis, EGF is seen to be a potential salivary biomarker for breast cancer, especially since therapeutic target pharmaceuticals have already been approved by the FDA in the treatment of multiple cancer types (Kabbinavar et al., 2003). This increased expression of EGF, along with increased vascular endothelial growth factor (VEGF) and carcinoembryonic antigen

(CEA), was more recently observed by Brooks et al., 2008. Increased EGF has shown close links to cancer progression, due to its pro-migratory properties, and it's overexpression has been recorded in multiple cancer types such as gastric (Zhen et al., 2014), oral (Xu et al., 2017), lung (Kuo et al., 2012) and head and neck cancer (Chang et al., 2015).

Saliva has proven itself useful in the detection and diagnosis of oral cancer (OC), a malignancy referring to the oral cavity, lip and pharynx. The majority of oral cancers are referred to as oral squamous cell carcinoma (OSCC). Interleukins such as IL-6, IL-8 and IL-1β have shown a significant increase in the saliva of OC patients in comparison with healthy controls. IL-8, specifically, has shown great promise in the search for early detection biomarkers in saliva for OC, with a mean copy for IL-8 mRNA being $1.1x10^8$ in OSCC in comparison to $2.6x10^6$ in the control patients and a difference of statistical significance of $P<0.001$ (St John et al., 2004). Metalloproteinases (MMP-1, MMP-3, MMP-10, MMP-12) have been commonly associated with multiple cancer types, including OSCC, in recent years and are thought to play a role in metastases and tumour invasion (Kurahara et al., 1999). The over expression of MMP-1 and MMP-3 have been noted as over expressed in OSCC patients in comparison to cancer free control patients, with an observed trend towards higher expression with increasing disease severity (Stott-Miller et al., 2011). A 75% increase in the expression of MMP-2 was observed by (Shpitzer et al., 2007) in the saliva of OSCC patients in comparison to healthy controls.

A recent pilot study, carried out by (Katz et al., 2017) , observed that increased levels of salivary AGEs (advanced glycation endproducts) may act as a good way to determine biomarkers regarding the development of bone lesions in MM patients, especially those who have decreased marker expression for the progression of bone lesions. It was noted that patients who show multiple bone lesions also exhibit a significantly higher concentration of AGEs in both plasma (Gangemi et al., 2012) and saliva (Katz et al., 2017). AGEs are proteins that are post-translationally modified and

are known to act as markers of oxidative stress. They have been previously implicated in the proliferation of multiple types of cancer, such as prostate, OSCC, brain, breast and ovarian cancer by triggering proliferation, angiogenesis and inflammatory reactions during cancer progression (Yamagishi et al., 2015). These findings show great promise in the use of salivary biomarkers for disease diagnosis and bone lesion formation in MM.

BMTs are considered the gold standard in MM diagnosis, allowing an insight into bone structure, cell distribution, focal lymphoid infiltrates and BM granulomas. This procedure is vital for base-line diagnosis and repeat biopsies must be obtained during follow up consultations. BMTs are considered superior to bone marrow aspirates (sampling the liquid of the soft tissue inside the bone (Bain, 2001a)) as the indication of more prevalent MM. Extensive infiltration can be observed in trephines, along with the identification of light chain associated amyloidosis more readily from BMTS than aspirates (Bain, 2001b). This procedure, however, is excruciatingly uncomfortable for patients, useful biopsies should measure at least 1.6 cm, and is vastly invasive for patients. Along with discomfort to patients, BMTs carry risk of infection and, in rare cases, death due to haemorrhage (Ben-Chetrit et al., 1984). This, therefore, leads to the requirement of reliable biomarkers for indication of when a BMT needs to be performed as opposed to immediately carrying out such an invasive and painful procedure regularly.

Salivaomics has become an area of great interest in disease diagnosis over the last number of years, following the footsteps of the other “omics” based diagnostic tools. Saliva has been referred to as “the mirror of the body” as it gives an insight into the internal pathological state (Lee and Wong, 2009). As saliva is considered a fast, inexpensive and non-invasive method of sample collection, the future of diagnosis, early detection, monitoring and prediction of progression of disease has been thought to lie here. Unfortunately, the development of saliva biomarkers has taken time and more research is still required for the clinical use of these biomarkers.

5.1.1 Experimental Design

5.1.1.1 Patients and Samples

91 saliva samples were provided by the Mater Misericordiae University Hospital, Dublin 7, Ireland. No exclusion criteria were applied to both patients and samples collected. Samples were collected and stored on-site at the Mater Misericordiae University Hospital. Samples were received from patients at varying diagnosis and at varying treatment stages (Table 5.1). Saliva sample collection was carried out using the GBO Saliva Collection System, requiring patients to thoroughly rinse the oral cavity for 2 minutes using the saliva extraction solution. The solution was then collected into sterile collection tubes and stored at -80ºC.

Table 5.1: MM Patient Cohort Clinical Information.

ID	Disease Status	Status	Subtype
MMA 01	MM	Newly Dx	IgG kappa
MMA 02	MM	Newly Dx	IgA lambda
MMA 03	MM	Newly Dx	IgG kappa
MMA 04	MM	Early Relapse (on Len/Dex)	IgG kappa
MMA 05	MM	VGPR (Elotuzumab/Len/Dex)	IgA lambda
MMA 06	MM	PR (post 8x Len/Dex)	IgG kappa
MMA 07	MGUS		
MMA 08	MM	Stable disease	IgA lambda
MMA 09	MM	VGPR (post 4x RVD)	IgG kappa
MMA 10	MM	PR (had Tha/Dex EOT 6/2010)	IgG lambda
MMA 11	SMM		
MMA 12	MM	VGPR	IgA lambda
MMA 13	Plasma cell leukaemia		
MMA 14	MM	Newly Dx	IgG kappa

ID	Disease Status	Status	Subtype
MMA 15	MM	Newly Dx	IgG kappa
MMA 16	MM	Relapse (previously tx CTD to VGPR)	IgG kappa
MMA 17	SMM		
MMA 18	Solitary plasmacytoma	Newly Dx	
MMA 19	MM	Relapse Refractory	IgG kappa
MMA 20	MM	Relapse	IgG kappa
MMA 21	MM	Newly Dx	IgA kappa
MMA 22	Neutropenia	Control	
MMA 23	MM	Relapse	IgG lambda
MMA 24	MM	Relapse	IgG lambda
MMA 25	MM	Relapse	IgG kappa
MMA 26	MM	CR (post ASCT)	IgG lambda
MMA 27	SMM		IgG kappa
MMA 28	MM	Newly Dx	
MMA 29	MM	PR (post 4x Vel/Dex)	IgG kappa
MMA 30	MM	VGPR (post ASCT, 8x VTD induction)	IgG lambda
MMA 31	MM	VGPR (Elotuzumab)	IgA lambda
MMA 32	MM		IgG kappa
MMA 33	MM	PD (on Vel/Dex)	IgG lambda
MMA 34	MM	Relapse	IgA kappa
MMA 35	MGUS	Newly Dx	IgG
MMA 36	MM	VGPR (on VTD)	lambda LC
MMA 37	MGUS	Newly Dx	IgG
MMA 38	MGUS	Newly Dx	IgA kappa
MMA 39	MM	VGPR	IgG kappa
MMA 40	MM	Newly Dx	IgG lambda

ID	Disease Status	Status	Subtype
MMA 41	MM	VGPR (post 4x Vel/Dex)	IgA kappa
MMA 42	MM	Relapse (previously on Len/Dex)	IgA kappa
MMA 43	MGUS		IgG
MMA 44	MM	Relapse	IgG lambda
MMA 45	MGUS		
MMA 46	MM	MGUS transformed to MM	
MMA 47	MM	PR (6x Vel/Dex)	IgG kappa
MMA 48	MGUS		
MMA 49	MM	VGPR (4x CyBorD)	IgG lambda
MMA 50	MM	Relapse	IgG kappa
MMA 51	MM	CR (post ASCT)	IgG kappa
MMA 52	MM	relapse (previous 4x CTD, ?VGPR)	IgA lambda
MMA 53	MM	Newly Dx	IgG lambda
MMA 54	SMM		IgG kappa
MMA 55	MM	relapse (previous RVD, then ASCT, VGPR)	IgD kappa
MMA 56	MM	relapse (previous 5x Vel/Dex, 9x RVD, VGPR)	IgG lambda
MMA 57	MGUS		
MMA 58	MM	PR (previous Vel/Dex, switched to RVD)	IgG kappa
MMA 59	MM	? Relapse refractory (6x RVD)	IgG lambda
MMA 60	MM	Relapse Refractory	
MMA 61	MM	?relapse	IgA kappa
MMA 62	Plasmacytoma	Newly Dx	
MMA 63	MGUS		
MMA 64	MM	VGPR (6x RVD)	IgG lambda
MMA 65			
MMA 66	MM	Newly Dx	
MMA 67	MM	Relapse Refractory	
MMA 68	MM	Relapse	Light chain

ID	Disease Status	Status	Subtype
MMA 69	MM	Newly Dx	Light chain
MMA 70	MM	Relapse	IgG kappa
MMA 71	MM	VGPR	IgA lambda
MMA 72	MM	Newly Dx	kappa LC
MMA 73	MGUS	Newly Dx	
MMA 74	SMM	Progressing to MM	IgG
MMA 75	MM	Remission	IgG kappa
MMA 76	MM	Newly Dx	
MMA 77			
MMA 78	MGUS	Newly Dx	
MMA 79	MGUS	Newly Dx	
MMA 80	PRV	Control	
MMA 81	MM	Newly Dx	
MMA 82	MM	Relapse	
MMA 83	MGUS	Newly Dx	
MMA 84	Amyloidosis		
MMA 85			
MMA 86	Amyloidosis		
MMA 87	Mantle cell lymphoma	Newly Dx	
MMA 88	Follicular lymphoma		
MMA 89	Amyloidosis		
MMA 90	MM	Newly Dx	IgA
MMA 91	MM	Remission	

5.1.1.2 Label-free LC-MS/MS Analysis of Patient Saliva Samples.

Prior to mass spectrometric analysis, samples were purified by acetone precipitation. Five times the sample volume of cold 100% acetone was added to each sample and stored overnight at -20℃. Samples were centrifuged at 15,000 x g for 15 min at 4℃. The supernatant was decanted, and samples centrifuged again at 15,000 x g for 5 min. The supernatant was discarded, excess supernatant was removed and the resulting pellet was allowed to air-dry for 10 min. The pellets were re-suspended in appropriate volume of label-free solubilisation buffer and vortexed and sonicated to

ensure full re-suspension. The protein amount was estimated using an RC/DC protein assay from Bio-Rad. BSA was used as a standard. Protein concentrations were equalised with label-free solubilisation buffer and 30 µg of protein was processed by the filter aided sample preparation (FASP) method (Wiśniewski et al., 2009) using a trypsin to protein ratio of 1:25 (protease: protein). Following overnight digestion and elution of peptides from the spin filter, 2% TFA in 20% ACN was added to the filtrates (3:1 (v/v) dilution).

5.1.1.3 Data Analysis of all Statistically Significantly Proteins with Altered Abundance Observed in Patient Saliva.

Protein identification and label-free quantification (LFQ) normalisation of MS/MS data was performed using MaxQuant v1.5.2.8 (http://www.maxquant.org). The Andromeda search algorithm incorporated in the MaxQuant software was used to correlate MS/MS data against the *Homo sapiens* Uniprot reference proteome database and a contaminant sequence set provided by MaxQuant. Perseus v.1.5.6.0 (www.maxquant.org/) was used for data analysis, processing and visualisation. Normalised LFQ intensity values were used as the quantitative measurement of protein abundance for subsequent analysis. The data matrix was first filtered for the removal of contaminants and peptides identified by site. LFQ intensity values were log2 transformed and each sample was assigned to its corresponding group. ANOVA-based multisample t-test were performed using a cut-off of $p<0.05$ on the post imputated dataset to identify statistically significant differentially abundant proteins.

5.1.1.4 ELISA for Validation of Decreased Abundance of FABP5 from Newly Diagnosed MM to Remission

50µl of crude saliva and serum samples were added to antibody-coated microtiter wells and incubated at room temperature for 2h, as directed by the manufacturers' recommendations. All manufacturers guidelines were followed, unaltered.

5.1.1.5 Immunoblotting for Validation of Increased Abundance of FABP5 throughout Disease Progression

20µg of acetone precipitated protein, quantified using a Bradford assay, from MGUS and newly diagnosed MM patient samples were loaded into each lane and an SDS-PAGE gel was run. 20µl of the resuspended protein was also loaded into each lane for samples from multiple patients and different time points (serial samples). Anti-FABP5 was used at a concentration stated in Chapter 2 and anti-goat secondary antibody was used at 1:1000. Transfer was carried out as previously detailed in Chapter 2 (Materials and Methods). For coomassie staining loading controls, proteins were run on 10% SDS gels and incubated in fixing solution (50% methanol, 10% glacial acetic acid) for 1 hour with gentle shaking. Gels were then incubated in staining solution (0.1% Coomassie Brilliant Blue R-250, 50% methanol, 10% glacial acetic acid) for 20 minutes, followed by incubation in de-staining solution (40% methanol, 10% glacial acetic acid) solution. This solution was renewed 3 times before exposure of gels using the G:BOX Chemi XRQ (Syngene). Densitometric analysis of each blot was carried out using ImageJ software.

5.1.1.6 Immunohistochemistry for Validation of Increased Abundance of FABP5 from MGUS to Newly Diagnosed MM.

Immunohistochemistry analysis for validation of FABP5 as a potential salivary biomarker was carried out as stated in detail in Chapter 2. Anti-FABP5 was used at a concentration of 1:250 on BMTs of patients diagnosed with MGUS and MM.

5.2 Results

5.2.1 Quantitative Proteomic Analysis of Patient Saliva with MGUS and Newly Diagnosed MM.

In-depth proteomic analysis of 8 MGUS saliva samples and 18 Newly diagnosed MM samples identified 152 proteins with altered abundance when comparing the proteomic signature of saliva samples MGUS and newly diagnosed MM patients. Of these 152 proteins, 42 of which have an increased abundance from MGUS to MM and 110 of which have a decreased abundance from MM to MGUS. Of the 152 proteins with changed abundance, six statistically significant ($p<0.05$) proteins with an increase in abundance in disease progression from non-malignant to malignant disease (Table 5.2) have been identified. Interestingly, there were no statistically significant proteins recorded with a decreased abundance from MGUS to newly diagnosed MM. A fold change increase in abundance as high as 35.25 was recorded for FABP5 abundance.

Table 5.2: Significant proteins with increased abundance from MGUS to newly diagnosed MM.

Accession Number	Protein Name	Fold Change	p-value
P01034	Cystatin C	1.890035303	0.0434095
P11021	78 kDa Glucose-Regulated Protein	3.442115345	0.0230914
P27482	Calmodulin-like Protein 3	3.30620761	0.0214094
P37802	Transgelin-2	5.222278045	0.0466408
P47989	Xanthine Dehydrogenase/Oxidase	1.58996479	0.0334987
Q01469	Fatty Acid-Binding Protein, Epidermal	35.25038341	0.00191934

5.2.2 Quantitative Proteomic Analysis of Patient Saliva Samples at Multiple Time Points (Serial Samples).

In-depth proteomic analysis of saliva samples from 7 patients, 6 of which had two time points and 1 of which had three time points. Patient samples ranged from MGUS, newly diagnosed MM, post treatment and remission (Table 5.2). The in-depth analysis identified 74 proteins with a common altered abundance when comparing the proteomic signature of the serial saliva samples (Table 5.3). 23 proteins were identified with a changed abundance in patient one (Pt.1), 19 of which were identified as significant. 64 proteins were identified with altered abundance in patient 2 (Pt.2), 52 were identified as statistically significant. 43 proteins were identified with a changed abundance in patient three (Pt.3), 31 of which were identified as significant. 45 proteins were identified with a changed abundance in patient four (Pt.4), 32 of which were identified as significant. 23 proteins were identified with a changed abundance in patient five (Pt.5), 17 of which were identified as significant. 32 proteins

were identified with a changed abundance in patient six (Pt.6), 23 of which were identified as significant. 26 proteins were identified with a changed abundance in patient seven (Pt.7), 25 of which were identified as significant. As patient 7 had three serial samples, three comparisons were made for the change in abundance between each sample. Pt. 7A compares newly diagnosed to partial response, Pt. 7B compares partial response and remission and Pt. 7C compares newly diagnosed to remission in patient 7 (Table 5.4).

Table 5.3: Serial Sample Patient Diagnosis

Patient ID	1st sample	2nd sample	3rd sample
Pt.1	Newly Diagnosed MM	Remission	
Pt. 2	Newly Diagnosed MM	Remission	
Pt. 3	Newly Diagnosed MM	Post Treatment	
Pt. 4	Post Treatment	Relapse	
Pt.5	Newly Diagnosed MM	Remission	
Pt. 6	Remission	Post-Transplant	
Pt. 7	Newly Diagnosed MM	Partial Response	Remission

Table 5.4: Compiled list of identified proteins with significantly changed abundances common across serial samples identified by LC-MS/MS.

Accession number	Protein	Pt. 1	Pt. 2	Pt. 3	Pt. 4	Pt. 5	Pt. 6	Pt. 7A	Pt. 7B	Pt. 7C
P07355	Annexin A2	↓	↓	-	↓	↑	↑	↓	↑	↓
P01036	Cystatin-S	↓	↑	↑	↑	↓	↓	↑	↓	↑
Q96DA0	Zymogen granule protein 16 homolog B	↑	↑	-	↑	-	↑	↓	↑	↑
P31025	Lipocalin-1	↓	↑	-	-	-	↓	↑	↓	↓
P02788	Lactotransferrin	↑	↓	↓	-	↑	-	↓	↑	↑
P01876	Ig alpha-1 chain C region	↑	↑	↑	↑	↑	↓	↑	↑	↑
P04083	Annexin A1	↓	↓	↑	↑	↑	-	↓	↑	↓
Q04118	Basic salivary proline-rich protein 3	↓	↑	-	↑	↓	↑	↑	↓	↑
P04745	Alpha-amylase 1	↑	-	↑	↑	-	↑	↓	↑	↓
P02812	Basic salivary proline-rich protein 2	↓	-	-	↑	-	-	↑	↓	↑
P25311	Zinc-alpha-2-glycoprotein	↓	↑	↓	-	-	↓	↓	↑	↑
P04280	Basic salivary proline-rich protein 1	↓	-	-	-	-	-	↑	↓	↓
P01833	Polymeric immunoglobulin receptor	↑	↓	↓	-	-	-	↓	↑	↑
P04080	Cystatin-B	↓	-	-	-	↑	-	↑	↓	↓
Q9UGM3	Deleted in malignant brain tumors 1 protein	↓	↓	-	-	-	↓	↓	↑	↑
P02810	Salivary acidic proline-rich phosphoprotein 1/2	↓	-	-	↑	↓	↓	↑	↑	↑
Q9UBC9	Small proline-rich protein 3	↓	↑	↑	↑	-	-	↑	↓	↓
P10163	Basic salivary proline-rich protein 4	↓	-	↑	↑	↓	-	↑	↓	↓
P06702	Protein S100-A9	↓	↓	↓	-	↑	-	↓	↑	↑
Q9HC84	Mucin-5B	-	↑	↑	↓	-	↓	↓	↑	↑
P10599	Thioredoxin	-	↓	-	-	-	-	-	-	-
P63261	Actin, cytoplasmic 2	-	↑	↓	-	-	↑	↑	↑	↑

Accession number	Protein	Pt. 1	Pt. 2	Pt. 3	Pt. 4	Pt. 5	Pt. 6	Pt. 7A	Pt. 7B	Pt. 7C
P02675	Fibrinogen beta chain	-	↑	↓	↓	-	-	-	-	-
P01834	Ig kappa chain C region	-	↑	-	-	-	↑	-	-	-
P01591	Immunoglobulin J chain	-	↑	-	-	-	-	-	-	-
P00738	Haptoglobin	-	↑	-	-	-	-	-	-	-
P11684	Uteroglobin	-	↓	-	-	-	-	-	-	-
P01857	Ig gamma-1 chain C region	-	↑	↓	↓	-	-	-	-	-
Q08188	Protein-glutamine gamma-glutamyltransferase E	-	↓	↓	↓	-	↓	↑	↓	↓
Q9NZT1	Calmodulin-like protein 5	-	↓	-	-	-	-	-	-	-
P01023	Alpha-2-macroglobulin	-	↓	↓	↓	-	-	-	-	-
P02647	Apolipoprotein A-I	-	↓	↓	↓	-	-	-	-	-
P02679	Fibrinogen gamma chain	-	↑	-	-	-	-	-	-	-
P05109	Protein S100-A8	-	↓	-	-	-	↓	-	-	-
P05164	Myeloperoxidase	-	↓	↓	↓	-	-	-	-	-
P02814	Submaxillary gland androgen-regulated protein 3B	-	↑	↑	↑	↓	-	-	-	-
P07737	Profilin-1	-	↓	-	-	-	-	-	-	-
P12273	Prolactin-inducible protein	-	↓	-	↑	↓	↓	↑	↑	↑
P09211	Glutathione S-transferase P	-	↓	-	-	-	-	-	-	-
P12429	Annexin A3	-	↓	-	↓	-	-	-	-	-
P23528	Cofilin-1	-	↑	-	-	-	-	-	-	-
P08311	Cathepsin G	-	↓	-	-	-	-	-	-	-
P61626	Lysozyme C	-	↓	-	-	-	-	-	-	-
P22079	Lactoperoxidase	-	↓	↓	↑	↓	↑	↓	↑	↑
B9A064	Immunoglobulin lambda-like polypeptide 5	-	↑	-	-	-	-	-	-	-
A8K2U0	Alpha-2-macroglobulin-like protein 1	-	↓	-	-	-	-	-	-	-
P52566	Rho GDP-dissociation inhibitor 2	-	↑	-	-	-	-	-	-	-

Accession number	Protein	Pt. 1	Pt. 2	Pt. 3	Pt. 4	Pt. 5	Pt. 6	Pt. 7A	Pt. 7B	Pt. 7C
Q96DR5	BPI fold-containing family A member 2	-	↓	↓	↑	↓	↑	↑	↑	↑
P13796	Plastin-2	-	↑	↓	↓	-	↑	-	-	-
Q8TDL5	BPI fold-containing family B member 1	-	↑	-	-	-	-	-	-	-
P02671	Fibrinogen alpha chain	-	↑	↓	-	-	-	-	-	-
P80723	Brain acid soluble protein 1	-	↑	-	-	-	-	-	-	-
Q6UWP8	Suprabasin	-	↑	↓	-	-	-	-	-	-
P06733	Alpha-enolase	-	↑	-	-	-	-	-	-	-
P00338	L-lactate dehydrogenase A chain	-	↑	-	-	-	-	-	-	-
P11021	78 kDa glucose-regulated protein	-	↓	-	-	-	-	-	-	-
P04206	Ig kappa chain V-III region GOL	-	↑	-	-	-	-	-	-	-
Q9BQE3	Tubulin alpha-1C chain	-	↓	-	-	-	-	-	-	-
P16401	Histone H1.5	-	-	↓	-	-	-	-	-	-
P02790	Hemopexin	-	-	↓	-	-	-	-	-	-
Q8TAX7	Mucin-7	-	-	↓	-	-	-	-	-	-
P61769	Beta-2-microglobulin	-	-	↓	-	↓	↓	-	-	-
P35908	Keratin, type II cytoskeletal 2 epidermal	-	-	↑	-	-	-	-	-	-
P14618	Pyruvate kinase PKM	-	-	↓	↓	-	-	-	-	-
P01024	Complement C3	-	-	↓	↓	-	↓	-	-	-
P01037	Cystatin-SN	-	-	-	↑	↑	-	-	-	-
P07108	Acyl-CoA-binding protein	-	-	-	↓	-	-	-	-	-
P01859	Ig gamma-2 chain C region	-	-	-	↓	-	-	-	-	-
P60709	Actin, cytoplasmic 1	-	-	-	↓	-	-	-	-	-
P30740	Leukocyte elastase inhibitor	-	-	-	↓	-	-	-	-	-
A8K2U0	Alpha-2-macroglobulin-like protein 1	-	-	-	↓	-	-	-	-	-
P23280	Carbonic anhydrase 6	-	-	-	-	↓	-	-	-	-
P10909	Clusterin	-	-	-	-	-	↓	-	-	-

Q08380	Galectin-3-binding protein	-	-	-	-	-	↓	-	-	-

5.2.3 Comparative Immunoblotting Analysis of Increased Abundance of FABP5 for MGUS Verses Newly Diagnosed MM.

For verification of an increased abundance of potential targets from MGUS to newly diagnosed MM from the mass spectrometric data, comparative immunoblotting of four MGUS and four newly diagnosed MM acetone precipitated saliva samples was preformed, investigating the abundance of FABP5. The overall trend of an increased abundance of FABP5 in saliva from MGUS to newly diagnosed MM was confirmed by the comparative immunoblotting analysis (Figure 5.1)

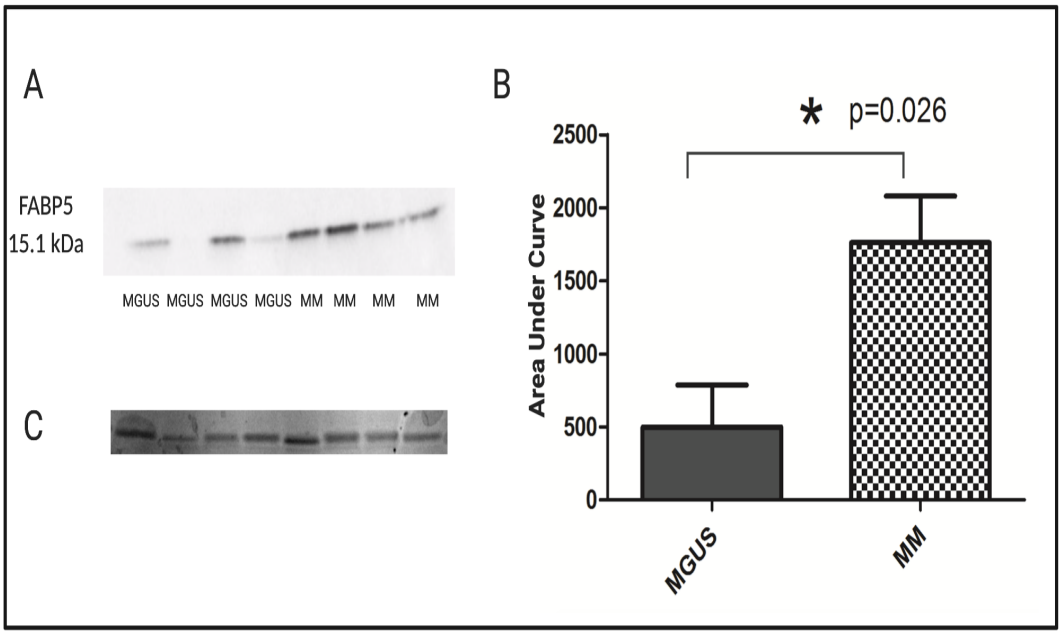

Figure 5.1: Comparative immunoblot analysis of FABP5 Abundance from MGUS to Newly Diagnosed MM.

Shown is a representative immunoblot with immuno-decorated bands labelled with an antibody specific to FABP5 (A). B is the graphical analysis of the immuno-decoration (MGUS n=4, MM n=4). C depicts a coomassie stained SDS-gel to indicate equal loading of each individual saliva sample for immunoblotting.

5.2.4 ELISA analysis of the increased abundance of FABP5 throughout disease progression of patient saliva samples.

ELISA analysis was carried out on crude saliva samples of five patients to identify an increased abundance of FABP5 throughout disease progression. Three of five patients exhibited a decreased abundance of FABP5 from newly diagnosed MM to remission. A decreased abundance was also observed from newly diagnosed MM to post VMP treatment (x8). Interestingly, an increased abundance of FABP5 was observed from newly diagnosed MM to remission for one of the five serial patients (Figure 5.2).

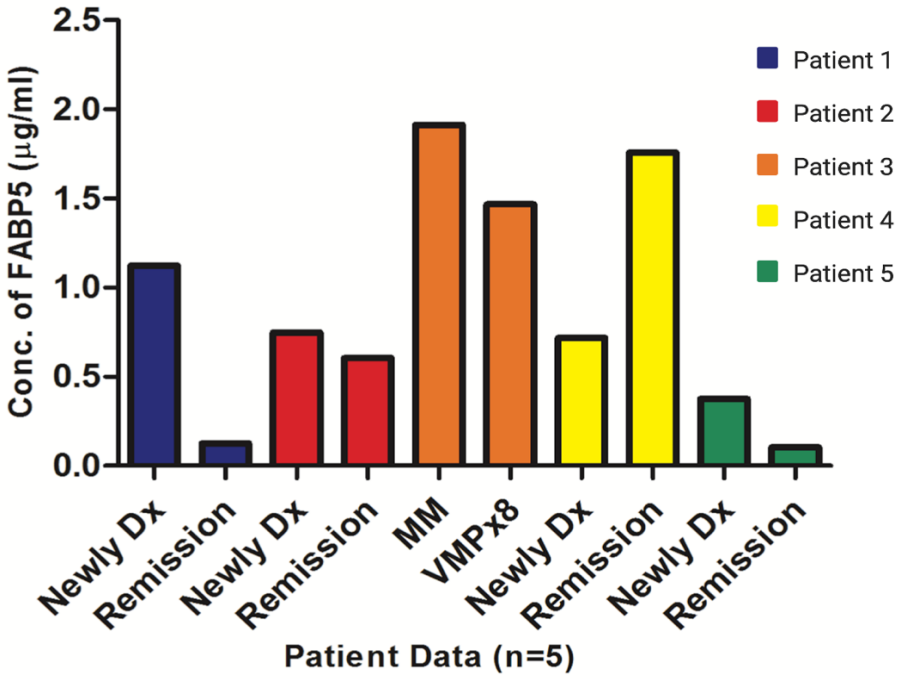

Figure 5.2: Bar Chart of ELISA Analysis Comparing Abundance of FABP5 in Saliva of Serial Sample Patients.

Figure depicts a comparative bar chart of the change in abundance of FABP5 in serial saliva from five patients. Each colour represents an individual patient at each of two time points. VMP x8 indicates eight cycles of treatment using Bortezomib, Melphalan and Prednisone.

5.2.5 Immunohistochemical Analysis of FABP5 abundance in Bone Marrow Trephines of MGUS and Newly Diagnosed MM Patients.

Comparative IHC was carried out with the use of an FABP5 to identify the change in abundance of FABP5 from premalignant MGUS to malignant newly diagnosed MM. FABP5 was identified as a potential biomarker in saliva for disease progression in MM, identified by LC-MS/MS (Table 5.2). This increase in abundance was verified using immunoblotting analysis in saliva samples (Figure 5.1), however, a bone marrow trephine is considered the gold standard for patient diagnosis of MM. Evaluating the change in abundance in BMTs can lead to the verification of reliability of the potential biomarker. Independent, blind scoring of stained slides was carried out, to ensure an unbiased evaluation of the staining intensity. Staining was observed to be negative in the MGUS sample (0) and weak positive staining was observed in the newly diagnosed MM sample (+1) (Figure 5.3).

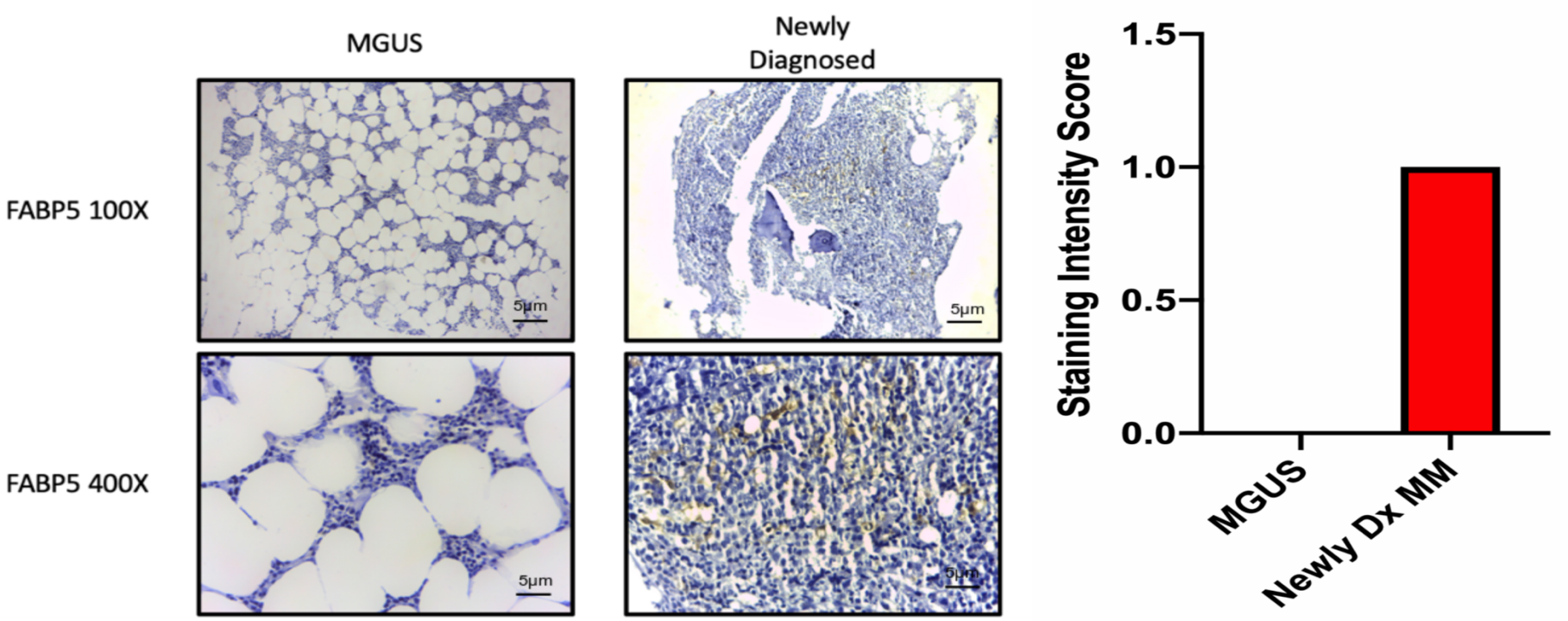

Figure 5.3: Comparative Immunohistochemistry (IHC) staining of FABP5 in BM trephines from MGUS to Newly Diagnosed.

The figure depicts the comparative IHC staining of BMTs using an antibody specific for FABP5. the increased abundance of FABP5 from MGUS to newly diagnosed MM is noted in staining of the sectioned tissue, the scoring of which is depicted in the corresponding graph.

5.3 Discussion

Serum biomarkers have become an important tool in the diagnosis of multiple myeloma, increasing the criteria for diagnosis to include three vital biomarkers for the disease (Rajkumar et al., 2014). All verified biomarkers for MM are, however, serum biomarkers. The collection of serum is an invasive process, which has been noted to cause varying levels of stress/discomfort to patients. The logical progression in the search for new biomarkers is to consider saliva as a biofluid for analysis as saliva collection is a non-invasive process, it is inexpensive and a fast biofluid to collect. Limited research has been published, to date, based on salivaomics in relation to cancer biomarkers in general, especially in MM.

Cystatin C (CysC) is a cysteine protease inhibitor produced by the majority of nucleated cells (Filler et al., 2005) that is filtered by the glomerulus, reabsorbed and metabolizes by the proximal tubule and is considered an accurate endogenous maker of glomerular filtration rate (GFR) in chronic kidney disease (Stevens et al., 2008). It has been noted in MM studies that CysC is one of the most highly upregulated genes expressed (De Vos et al., 2002) and has been recognised as a potential serum marker for prognosis in MM. One of the key diagnostic criteria of MM is renal failure, explaining the increased expression in CysC (Rajkumar et al., 2014). A significantly increased abundance of CysC has been noted in multiple studies of MM progression and, interestingly, a reduction in expression has been noted in patients after treatment using bortezomib (Terpos et al., 2009). As treatment with bortezomib has shown a direct correlation with decreased kidney damage, in some cases the improvement was seen in numbers as high as 77% of patients treated (Zannetti et al., 2015), the reduction in the over expression of CysC shows positive results from bortezomib. In the study presented above, the results exhibited an expression of CysC in the progression of disease from MGUS to MM. The statistically significant increase ($P<0.05$) exhibited in disease progression samples leads to the prediction

that salivary CysC may be considered as reliable as serum CysC at predicting disease from MGUS to MM.

Fatty Acid Binding Protein 5 (FABP5) is one of several isoforms of FABP (Coe and Bernlohr, 1998) and is known to enhance the transcriptional activity of nuclear receptor peroxisome proliferator-activated receptor β/δ (Adhikary et al., 2013) and promotes cell proliferation, survival and migration (Wang et al., 2006). FABP5 has been observed to be implicated in the proliferation of cancer and has been seen to be increased in abundance in multiple cancer types such as breast (Levi et al., 2013), prostate (Nitschke et al., 2019), cervical (Zhan et al., 2019) and HCC (Ohata et al., 2017). Interestingly, in a study carried out by Waheed and colleagues, FABP5 in MM patients was associated with poor outcome and unfavourable clinical parameters. FABP5 has been observed, in this study, to be statistically significant in comparisons between MGUS and MM. The abundance is significantly higher ($P<0.002$) of FABP5 in the newly diagnosed MM patient samples in comparison with the MGUS patient samples (Table 5.2). This would lead us to believe that FABP5 levels increase as the disease progresses. Based on the data in this study, FABP5 is predicted to be a useful salivary marker in the determination of disease progression as this information correlates with multiple distinct types of cancer. Using ELISA analysis, a decrease in the abundance of FAPB5 was noted in serial samples from newly diagnosed to remission in four of the five patients tested (Figure 5.2). This, again, leads us to believe that an increase in FABP5 is directly linked to disease progression and severity. The IHC analysis of BMT trephines from premalignant MGUS to newly diagnosed MM revealed an increased abundance of FABP5 in disease progression. As the increase is not determined to be vast in abundance and, due to limitations from small BMT sample size, no strong conclusions could be based on this analysis alone. However, due to the nature of diagnosis of MM, BMTs are considered the gold standard in diagnosis and the fact that there is an increased abundance of FABP5 in

the bone marrow, along with the ELISA and immunoblotting data (Figure 5.1), it is evident that an increase in FABP5 in MM patients may indicate disease progression. An increased abundance of multiple proteins during disease progression at different time points has been noted, and specifically a significant down regulation from newly diagnosed to remission in patient samples. Protein-glutamine gamma-glutamyltransferase E or Tranglutaminase-3 (TGM3) was seen to have a significantly decreased abundance in five of the seven patients studied. TGM3 has been noted as being vital for the formation of cornified cell envelope (Kalinin et al., 2002) and epidermal terminal differentiation. Expressed in the suprabasal layers of stratified squamous epithelium in skin and mucosa, and regularly expressed in small intestine and brain (Hitomi et al., 1999), TGM3 has been implemented in multiple cancer types such as oral squamous cell carcinoma (Wu et al., 2018), head and neck squamous cell carcinoma (Wu et al., 2013) and oesophageal cancer (Li et al., 2016).

β2M (Beta-2-microglobulin) was significantly decreased in abundance in three of seven patients from diagnosis to remission. β2M, in combination with albumin, has been established since 2005 as a predictive biomarker for disease progression and stage according to the ISS. The ISS uses serum β2M to provide three stage classifications with three different median survival periods, establishing that lower expression of β2M is directly correlated with increased overall survival (Palumbo et al., 2009). The significant decreased abundance noted in this study further supports the finding of the ISS (the increased expression of β2M indicates decreased overall survival) and strengthens the use of saliva as a biofluid for prediction of disease progression as it mirrors the findings in serum. β2M is a widely known housekeeping gene and interacts and stabilizes “tertiary structures of the major histocompatibility complex class I α-chain for presenting antigenic peptides from intracellular proteins to cytotoxic T lymphocytes” (Bjorkman and Burmeister, 1994). In a study carried out by Rajpal and colleagues, the significant upregulation of β2M in non-responders, in comparison to responders to thalidomide-based therapy was recorded, providing a

link to over expression of β2M and drug resistance in multiple myeloma. This β2M increase in drug resistance has also been linked to resistance using bortezomib for treatment of MM (Ting et al., 2017). The presence of β2M, with increased abundance in the saliva of MM patients again solidifies the relevance of carrying out proteomic analysis on patient samples for predictive markers for disease progression.

Saliva has been observed to have undetermined potential as a biomarker for disease diagnosis, prognosis and progression. However, saliva also has infinite potential as a source of biomarkers for patient monitoring. MM patients must undergo a BMT biopsy, a hugely invasive, uncomfortable process, for diagnosis of disease. Saliva has proven to show a direct, reliable correlation between protein abundance of the proteins profile and disease progression from non-malignant to malignant malignancy. This proves saliva potential to predict the need for a BMT procedure to be carried out, as opposed to initially carrying out the traumatic procedure making diagnosis and disease monitoring much less invasive on the patients involved.

Chapter 6

The Proteomic Analysis of Disease Burden from RsqVD Clinical Trial Samples

6.1 Introduction

Translational research is considered the movement of “basic scientific research from the lab bench to the patients’ bedside”. This encompasses the transfer of knowledge from basic to clinical research and the transfer of these findings from trials to practical use in the clinic (Rubio et al., 2010). Traditionally, the progression from basic research to clinical use has taken arduous amounts of time with minimal cross over between the two. This gap, however, has been shortened over recent years with the identification of potential biomarkers for disease progression, diagnosis and treatment management being developed for clinic use. Knowledge of tumour microenvironment, molecular characterisation of tumours, tumour-driving molecular pathways, the establishment of new treatment targets and immuno-oncology have all vastly changed the way in which cancer is treated (Shrager and Tenenbaum, 2014). Using translational oncology approaches to clinical trials, patients can be monitored more closely than previously, allowing for the early identification of adverse side effects from the trial or disease progression, allowing the early discontinuation of treatment. This chapter combines proteomic analysis and early clinical trial samples for the identification of potential biomarkers indicating patient response, further closing the gap between basic research and clinical use.

The clinical trial in question, RsqVD, is a Phase Ⅱ multi-centre, transatlantic study of MM patients. The study involves treatment using standard RVD treatment regime (Lenalidomide, Bortezomib and Dexamethasone), however the Bortezomib is administered subcutaneously (sq), as opposed to the standard method of administration via Intravenous (IV) line (Attal et al., 2017). Bortezomib administration through an IV has notoriously been linked with peripheral neuropathy and toxicity in patients, leading to the need for alternative administration methods to improve patient health. Sq administration of Bortezomib has shown equal effectiveness to that of IV

administration and has been seen to be less time consuming and more convenient for both patients and hospital staff (Barbee et al., 2013). Bortezomib, through standard administration methods, has been linked extensively to peripheral neuropathy (Richardson et al., 2009), anaemia, vomiting, diarrhoea, leukopenia and thrombocytopenia (Lonial et al., 2005). The prevalence of peripheral nerve damage associated with IV bortezomib is a worrying trend, which leads to painful sensory neuropathy seriously affecting patients over all standard of living (Richardson et al., 2006). This neuropathy is predicted as due to metabolic changes from the accumulation of bortezomib in dorsal root ganglia cells, dysregulation of neurotrophins and Ca++ homeostasis dysregulation mediated by mitochondria (Argyriou et al., 2008). Sq administration of bortezomib has been observed as vastly decreasing the incidences of peripheral neuropathy, leukopenia and thrombocytopenia (Ye et al., 2019). As studies are still being carried out on the effectiveness of IV versus sq administrative methods for bortezomib, a direct correlation between sq bortezomib and decreased prevalence of adverse side effects such as peripheral neuropathy, leukopenia, thrombocytopenia, anaemia, nausea, vomiting and diarrhoea is becoming more apparent (Hu et al., 2017). The establishment of sq bortezomib as standard practice seems to be the logical answer in combatting adverse side effects.

Serum, the most commonly used biofluid for proteomic analysis, is collected after coagulation and is centrifuged to remove any clotting agents from the blood sample (Yu et al., 2011). With the abundance of proteins present within serum, the minimally invasive collection method and the fact that serum comes into direct contact with all tissues within the body, the information available from proteomic analysis of serum is endless. Serum is, generally, more stable than plasma after storage due to the removal of coagulation material and is also less contaminated with free cells and platelets. However, serum must be left to coagulate for 30 minutes after collection, to allow clot formation, whereas plasma can be directly used for analysis (Oddoze et

al., 2012). Serum is comprised of proteins, lipids, electrolytes, antibodies, hormones, as well as exogenous substances with proteins such as albumin, transferrins, immunoglobulins and complement factors making up 99% of the serum proteome. The remaining 1% of lower abundance circulatory are considered the proteins of interest in terms of their potential as prognostic and diagnostic biomarkers (Betgovargez et al., 2005).

To date, ELISA has been considered the most efficient assay based technology for low abundant target detection in patient samples. However, in recent years, the development of Luminex screening technologies, using multiplex arrays, has allowed the identification of multiple analytes in the same sample at the same time. Utilising this technology has a number of distinct advantages over ELISA such as less sample volume required and higher efficiency in terms of cost and time. The maximum number of analytes that can be analysed at one time using this multiplex assay is 500 and the maximum number of samples that can be analysed at once is dependent on the plate used, either 96 samples or 384 samples (Purohit et al., 2015). Among these advantages, multiplex assays also give the opportunity to evaluate levels of the analyte in the context of multiple other analytes, allows reproducibility across assays and allows the detection of analytes across a broad range of concentrations (Leng et al., 2008). Luminex multi-analyte profiling is based on the use of antibody coated beads, which are distinguishable using flow cytometry. Each antibody coated bead contains a fluorescence or streptavidin-labelled detection antibody that binds to specific targets, leading to the identification and measurement of multiple targets from one biological sample. The chromogenic or fluorogenic emission is detected by flow cytometric analysis (Leng et al., 2008).

6.1.1 Experimental Design

6.1.1.1 Patients and Samples

The ethics committees of the participating hospitals approved the study in compliance with the Declaration of Helsinki. A total of 70 serum samples were collected from patients enrolled in the clinical study. Patient characteristics and details of response are stated in Table 6.1. No exclusion criteria were applied to the patients and the samples were collected prospectively.

Table 6.1: Clinical details of patients involved in RsqVD study.

Patient	Visit	Sample ID	Post C4 Response	On treatment	Reason discontinued
1	Screening	01-1	CR	Yes	N/A
2	Screening	02-1	PR	Yes	N/A
3	Screening	03-1			
4	Screening	04-1	VGPR	No	Progression
5	Screening	05-1	PR	Yes	N/A
6	Screening	06-1	PR	Yes	N/A
7	Screening	07-1	VGPR	No	Toxicity
8	Screening	08-1	PR	No	Progression
	EoT	08-2			
11	Screening	11-1	CR	Yes	N/A
12	Screening	12-1	Unevaluable	Yes	N/A
14	Screening	14-1	VGPR	Yes	N/A
15	Screening	15-1	PR	No	Progression
17	Screening	17-1	PR	No	Progression
18	Screening	18-1	PR	No	Progression
	EoT	18-2			
	EoT	18-3			
19	Screening	19-1	VGPR	No	Progression

Patient	Visit	Sample ID	Post C4 Response	On treatment	Reason discontinued
	MC5	19-2			
20	Screening	20-1	PR	Yes	N/A
21	Screening	21-1		Yes	N/A
	MC5	21-2			
23	Screening	23-1	VGPR	No	Progression
	Pre-Maintenance	23-2			
25	Screening	25-1	CR	Yes	N/A
	MC2	25-2			
	MC2	25-3			
27	Screening	27-1	Did not complete 4 cycles	No	Toxicity
	C4	27-2			
28	Screening	28-1	Unevaluable	Yes	N/A
	C8	28-2			
	MC2	28-3			
29	Screening	29-1	PR	Yes	N/A
	MC1	29-2			
	MC2	29-3			
30	Screening	30-1	PR	No	Progression
	Pre-Maintenance	30-2			
	MC2	30-3			
32	Screening	32-1	PR	Yes	N/A
	C8	32-2			
	Pre-Maintenance	32-3			
	MC2	32-4			
33	Screening	33-1	PR	No	Withdrew consent
34	Screening	34-1	VGPR	No	Toxicity
	C2	34-2			

Patient	Visit	Sample ID	Post C4 Response	On treatment	Reason discontinued
	C6	34-3			
	C8	34-4			
	C6	34-5			
35	Screening	35-1	CR	No	Withdrew consent
36	Screening	36-1	PR	Yes	N/A
	Post C4	36-2			
37	Screening	37-1	CR	Yes	N/A
	C4	37-2			
	C6	37-3			
39	Screening	39-1	PR	Yes	N/A
	Post C4	39-2			
41	Screening	41-1	SD	Yes	N/A
	C2	41-2			
42	Screening	42-1	CR	Yes	N/A
43	C4	43-2	PR	Yes	N/A
	Post C4	43-3			
	Post C4	43-4			
44	C4	44-1	VGPR	Yes	N/A
	Post C4	44-2			
45	Screening	45-1	PR	No	Progression
	C2	45-2			
	C4	45-3			
46	Screening	46-1	VGPR	Yes	N/A
	C2	46-2			

6.1.1.2 MILLIPLEX® MAP Kit analysis using Luminex technology of RsqVD clinical trial patient serum.

MILLIPLEX® MAP Kit: Human Cytokine/Chemokine Magnetic Bead Panel Ⅰ, MILLIPLEX® MAP Kit: Human Cytokine/Chemokine Panel Ⅱ and MILLIPLEX® MAP Kit: Human Circulating Cancer Biomarker Magnetic Bead Panel 4 were all used in the targeted analysis of all patient serum samples. 25µl crude serum was used per sample and all manufacturers guidelines were followed, with variations stated in Chapter 2.

6.2 Results

6.2.1 Luminex Technology Analysis of Clinical Trial Patient Serum Samples.

For further identification of changes in the proteomic profile of varying RsqVD clinical trial serum samples, MILLIPLEX® MAP Kit: Human Cytokine/Chemokine Magnetic Bead Panel Ⅰ, MILLIPLEX® MAP Kit: Human Cytokine/Chemokine Panel Ⅱ and MILLIPLEX® MAP Kit: Human Circulating Cancer Biomarker Magnetic Bead Panel 4 were utilised. The analysis of the changed abundance of targeted proteins in 70 serum samples allowed the identification of previously established biomarkers, implicated previously in multiple types of cancer, in trial patient serum. Comparative bar charts were compiled with the use of the concentration of each individual potential target abundant in each sample. Trends in decreased/increased concentrations were analysed in-depth in samples from individual patients at multiple timepoints, allowing a more comprehensive study of the changed abundance throughout the trial (Table 6.2). In-depth analysis of the results obtained from the multiplex assays revealed several established biomarkers exhibiting trends in RsqVD patients. Of the 62 potential biomarkers analysed, CD44, Eotaxin, EGF, MIP-1α and L1CAM all exhibited

trends in changed abundance. CD44 showed an obvious increase in abundance in 5 of the patients with multiple samples in the cohort. This increase was observed as significant as the initial sample failed to record a value for CD44 abundance (Figure 6.1). The most significant increase in abundance in Eotaxin was observed in three of the serial samples, with vastly different abundances of Eotaxin recorded from sample one to sample two (Figure 6.2). A significant increase in abundance of EGF was noted in two of the serial sample patients, again with a significant increase of abundance recorded from sample one to sample two (Figure 6.3). MIP-1α (Figure 6.4) and L1CAM (Figure 6.5) were both observed to have significant changes in two of the serial patient samples. MIP-1α exhibits vastly different abundances from sample one to sample two for each patient.

Table 6.2: Patient details of focused study

Patient	Visit	Sample ID	Post C4 Response	On treatment	Reason discontinued
8	Screening	08-1	PR	No	Progression
	EoT	08-2			
18	Screening	18-1	PR	No	Progression
	EoT	18-2			
	EoT	18-3			
19	Screening	19-1	VGPR	No	Progression
	MC5	19-2			
21	Screening	21-1		Yes	N/A
	MC5	21-2			
23	Screening	23-1	VGPR	No	Progression
	Pre-Maintenance	23-2			
25	Screening	25-1	CR	Yes	N/A
	MC2	25-2			
	MC2	25-3			

Patient	Visit	Sample ID	Post C4 Response	On treatment	Reason discontinued
27	Screening	27-1	Did not complete 4 cycles	No	Toxicity
	C4	27-2			
28	Screening	28-1	Unevaluable	Yes	N/A
	C8	28-2			
	MC2	28-3			
29	Screening	29-1	PR	Yes	N/A
	MC1	29-2			
	MC2	29-3			
30	Screening	30-1	PR	No	Progression
	Pre-Maintenance	30-2			
	MC2	30-3			
32	Screening	32-1	PR	Yes	N/A
	C8	32-2			
	Pre-Maintenance	32-3			
	MC2	32-4			
34	Screening	34-1	VGPR	No	Toxicity
	C2	34-2			
	C6	34-3			
	C8	34-4			
	C6	34-5			
36	Screening	36-1	PR	Yes	N/A
	Post C4	36-2			
37	Screening	37-1	CR	Yes	N/A
	C4	37-2			
	C6	37-3			
39	Screening	39-1	PR	Yes	N/A
	Post C4	39-2			
41	Screening	41-1	SD	Yes	N/A
	C2	41-2			

Patient	Visit	Sample ID	Post C4 Response	On treatment	Reason discontinued
43	C4	43-2	PR	Yes	N/A
	Post C4	43-3			
	Post C4	43-4			
44	C4	44-1	VGPR	Yes	N/A
	Post C4	44-2			
45	Screening	45-1	PR	No	Progression
	C2	45-2			
	C4	45-3			
46	Screening	46-1	VGPR	Yes	N/A
	C2	46-2			

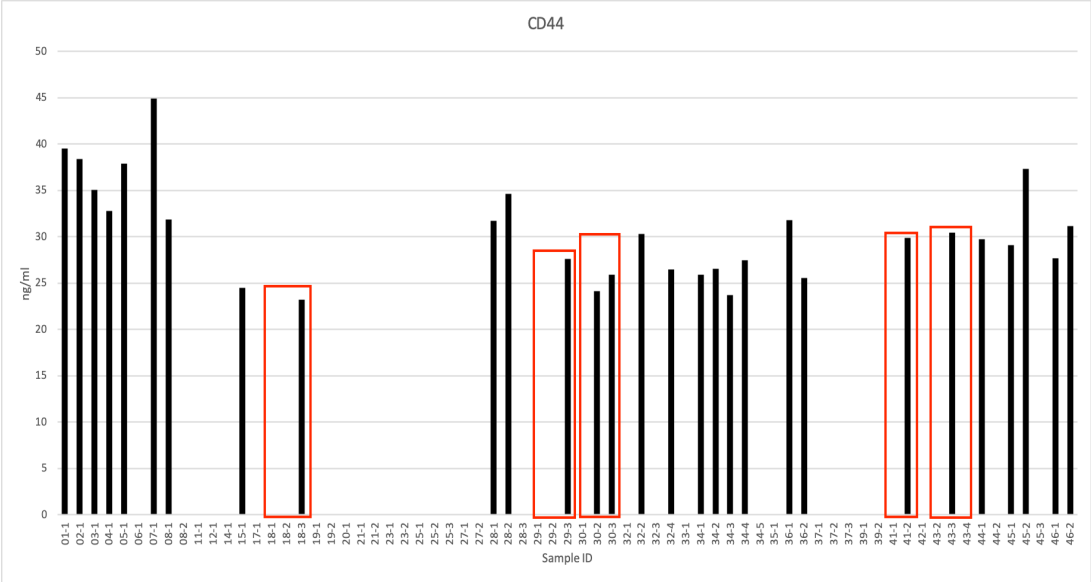

Figure 6.1: Comparative bar chart of change in abundance of CD44.

Depicted is the change in abundance of CD-44 across all RsqVD trial samples. A clear increase in abundance in trends outlined in red.

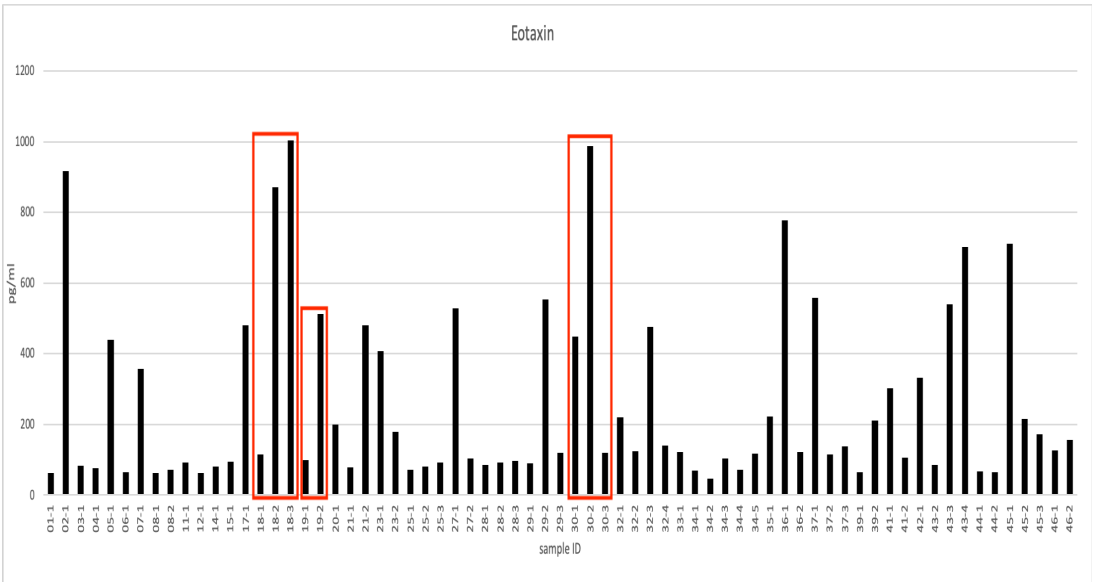

Figure 6.2: Comparative bar chart of changed abundance in Eotaxin.

Depicted is the change in abundance of Eotaxin across all RsqVD trial samples. Clear trends in increased abundance are outlined in red.

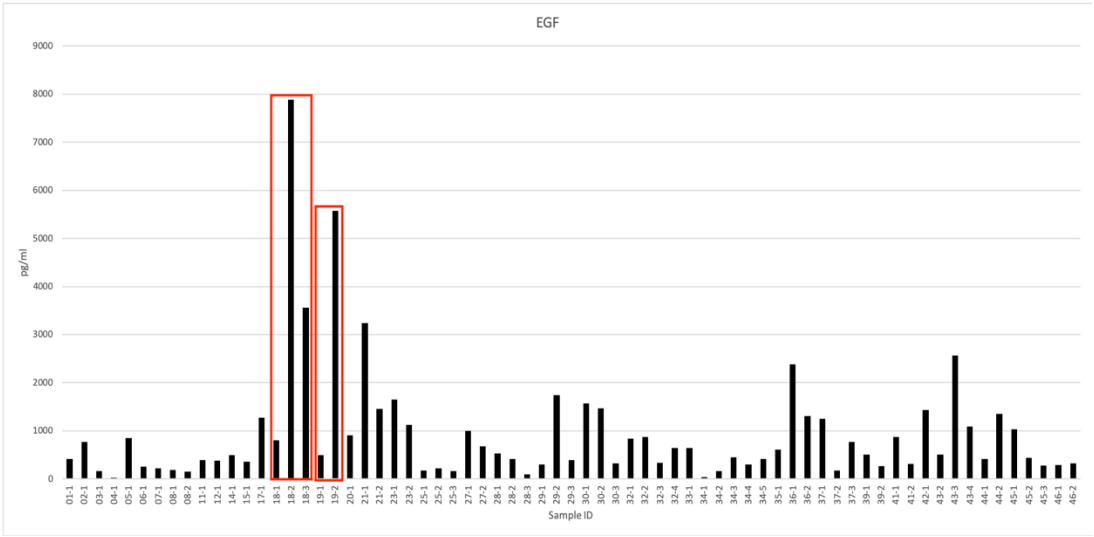

Figure 6.3: Comparative bar chart of changed abundance in EGF.

Depicted is the change in abundance of EGF across all RsqVD trial samples. Clear trends in increased abundance are outlined in red.

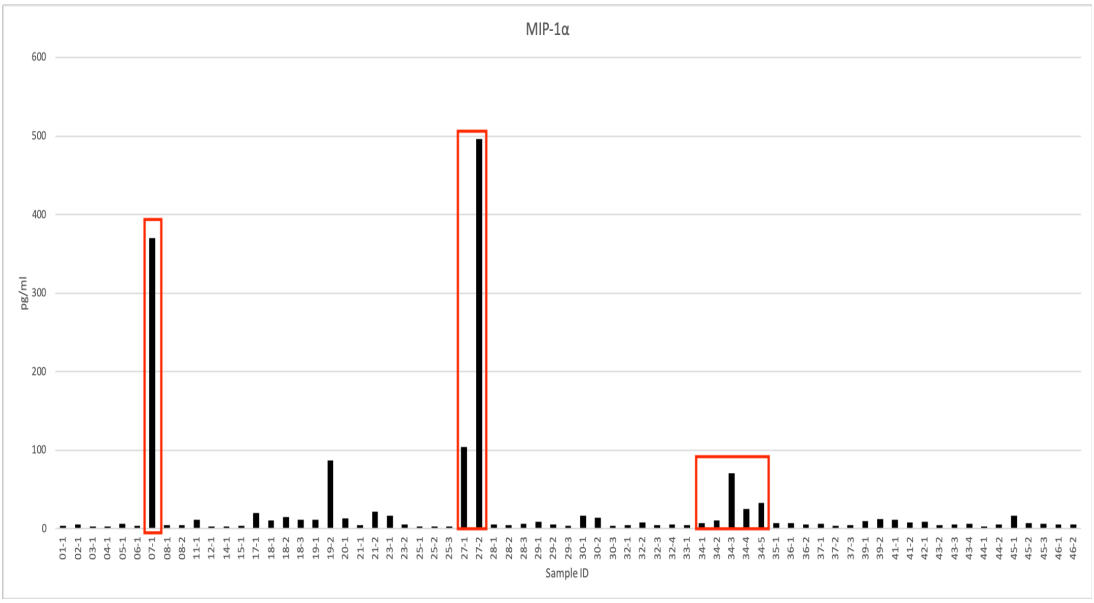

Figure 6.4: Comparative bar chart of changed abundance in MIP-1α.

Depicted is the change in abundance of MIP-1α across all RsqVD trial samples. Clear trends in increased abundance are outlined in red.

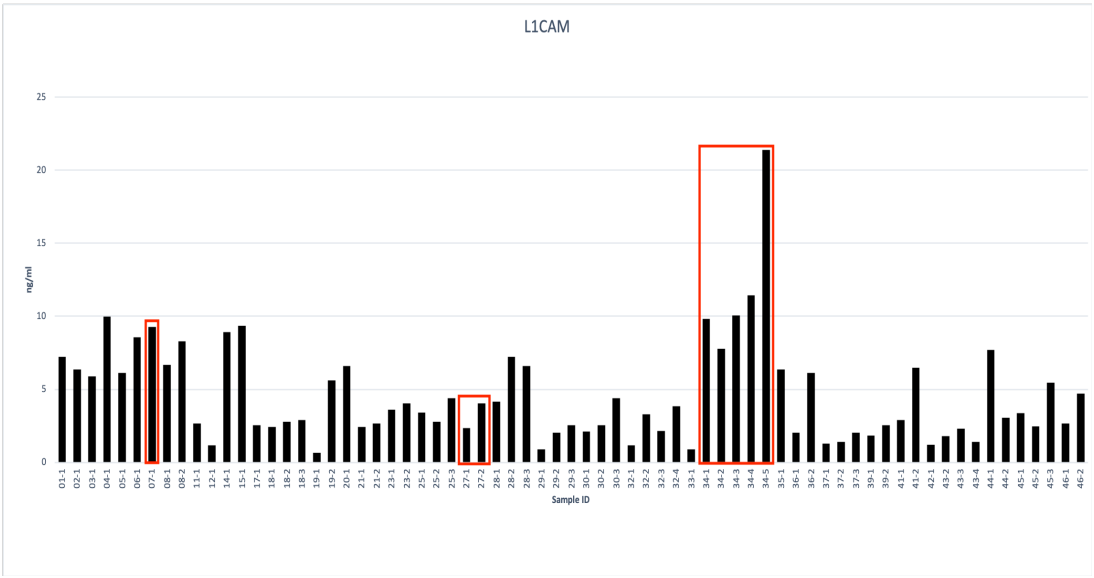

Figure 6.5: Comparative bar chart of changed abundance in L1CAM.

Depicted is the change in abundance of L1CAM across all RsqVD trial samples. Clear trends in increased abundance are outlined in red.

6.3 Discussion

Translational oncology is the combination of basic scientific research and clinical application to improve the treatment of cancer, improve diagnosis, aid in prognosis prediction and monitoring disease progression. Bridging the gap between the lab bench to the patient bedside has seen rapid improvement in cancer diagnosis. The establishment of molecular level changes through different disease timepoints have been acknowledged as being the route to improved treatment, combining the application of basic science with patient resources available. In this study we combine the applications of basic science via proteomics to RsqVD clinical trial samples to establish potential markers for disease progression, treatment response and, importantly, markers for disease related adverse effects from treatment.

Through high throughput, multiple target multiplex assays, 5 potential disease related biomarkers have been identified using a combination of MILLIPLEX® MAP Kit: Human Cytokine/Chemokine Magnetic Bead Panel Ⅰ, MILLIPLEX® MAP Kit: Human Cytokine/Chemokine Panel Ⅱ and MILLIPLEX® MAP Kit: Human Circulating Cancer Biomarker Magnetic Bead Panel 4 and Luminex technologies. CD44 was identified as being increased in abundance in 5 patients who underwent treatment with Lenalidomide, Dexamethasone and subcutaneous Bortezomib. On further analysis, all 5 patients were identified as having a partial response (PR) to the treatment administered. No evidence of the presence of CD44 was observed in all 5 screening samples but an increased abundance was observed in the second sample taken, the lowest of which being 23.2 ng/ml for sample 18.3 (Figure 6.1). This trend indicates that CD44 may elude to partial response in patients after initial treatment. CD44, as discussed in detail in Chapter 3, is a cell surface receptor that plays a role in cell-cell interactions, cell migration, response to tissue microenvironment changes and cell adhesion (Crosby et al., 2009). CD44 functions

in recirculation, inflammation, haematopoiesis, activation and T-lymphocytes homing (Funaro et al., 1994). The decreased abundance of CD44 has been observed as sensitising myeloma cells to treatment using Lenalidomide (Canella et al., 2015) and the increased abundance has shown a direct correlation to both Dexamethasone and Bortezomib resistance (Ohwada et al., 2008). Interestingly, of the 5 patients with an observed increased abundance, 2 of those patients had to be discontinued from the trial due to disease progression. This increased CD44 could be an early indicator of disease progression while receiving RsqVD treatment. Eotaxin is a chemokine which has been implicated in the inflammatory response by the recruitment of both eosinophils and neutrophils (Menzies-Gow et al., 2002). Through interaction with CC chemokine receptor-3 (CCR3), Eotaxin has been seen to promote cell growth and survival, especially of anaplastic large cell lymphoma cells (Miyagaki et al., 2011). Eotaxin has previously been confirmed as a biomarker for prostate cancer (Ugge et al., 2019), along with ovarian cancer (Nolen and Lokshin, 2010) and colorectal cancer (Johdi et al., 2017). The significantly increased abundance observed in 3 patients with multiple samples enrolled in the RsqVD trial of Eotaxin was noted as being linked to disease progression in patients. Notably, all 3 of the patients exhibiting the increase were removed from the clinical trial due to progression of MM (Table 6.2). Epidermal Growth Factor (EGF), in combination with the EGF receptor control cell proliferation, differentiation, motility and survival by downstream activation (Massagué and Pandiella, 1993). Significant levels of EGF have previously been noted in both MM cell lines and in the BM microenvironment in comparison to healthy donors (Cao et al., 2010). Two patients exhibited a significant increase in the abundance of EGF from screening sample to second sample taken (Figure 6.3). Interestingly, both patients were withdrawn from the clinical trial due to disease progression. These findings elude to significant increases of EGF have the

potential to be considered a marker for disease progression in RsqVD administration.

Generally, bortezomib is the first line of treatment for patients diagnosed with MM. Bortezomib, a proteasome inhibitor, has vastly improved the treatment of MM, with the use of its treatment directly correlating with increased OS in MM patients. Bortezomib, however, has shown important links to adverse side effects, classed as toxicity, such as leukopenia, thrombocytopenia and peripheral neuropathy (Richardson et al., 2009). These side effects have been observed as a complication from IV administration of bortezomib, the prevalence of which has been observed to decrease significantly with subcutaneous administration of bortezomib (Hu et al., 2017). As these adverse side effects cause a significant decrease to a patient's quality of life, predictive markers for the early detection of these are needed. MIP-1α and L1CAM were both chosen as potential targets for unique reasons. Both potential targets show a significant increase in patients discontinued from the clinical trial due to toxicity. A significant increase in the abundance of MIP-1α in patient 27 was observed from initial screening sample to the second sample, with a less drastic increase observed in patient 34 from initial screening sample to subsequent samples. Although there is only one sample within the study for patient 07, a significant peak in abundance is observed in comparison to all other patient samples. As the abundance of MIP-1α is very low in all other patient samples in comparison to patient 07, patient 27 and patient 34, it is being hypothesised that MIP-1α plays a role in toxicity in patients. Patient 07, patient 27 and patient 34 are the only patients in the study that exhibited adverse effects to treatment and, subsequently, are the only patients exhibiting a high abundance of MIP-1α (Figure 6.4). MIP-1α is an inflammatory CC chemokine, known for promoting cell migration against immune cells (Lee et al., 2000). With direct inhibitory activity on normal hematopoietic stem/progenitor cells (HSPC) growth (Graham et al., 1990), MIP-1α has previously been implicated in the proliferation of chronic myeloid leukaemia (Baba et al., 2013)

and MM (Tsubaki et al., 2007). Interestingly, the direct correlation between MIP-1α and adverse side effects from bortezomib has previously been identified, linking the adverse effects to the inhibition of ERK1/2, Akt and mTOR activation (Tsubaki et al., 2018). L1CAM (L1 cell adhesion molecule) plays a role in cell migration, cell adhesion, cell survival and myelination (Maness and Schachner, 2007) and has previously been linked with poor prognosis, advanced tumour stage and metastasis in multiple cancer types (Tangen et al., 2017). L1CAM has been considered as a suitable biomarker for disease progression in a number of cancer types, such as ovarian (Fogel et al., 2003), gastrointestinal (Zander et al., 2011) and breast cancer (Wu et al., 2018). Figure 6.5 depicts the increased abundance of L1CAM in all patients samples from the RsqVD clinical trial. It's increased abundance has been noted specifically in patient 07, 27 and 34. A significant increase in the abundance has been observed specifically in patient 34, but an increase has also been noted in both other patients. All three patients have been withdrawn from the clinical trial due to toxicity, leading the prediction that L1CAM plays a role in the development of adverse side effects in patients treated with bortezomib.

As the RsqVD clinical trial develops, more information and samples will become readily available for proteomic analysis. This resource has the potential to form panels of biomarkers for all MM related complications, such as disease progression, adverse side effects of treatment, prognosis prediction etc. The establishment of these panels of biomarkers, via proteomics, is hugely important as it will allow the identification of disease related complications at early stages, allowing the appropriate action to be taken. As the clinical trial is on-going, further analysis and validation of the potential biomarkers mentioned above can be done with less restriction on patient details, patient response and sample volume.

Chapter Seven

The Proteomic Characterization of Acute Myeloid Leukaemia Cells and Serum with Ranging Prognostic Risk Grouping.

7.1 Introduction

With approximately 20,000 diagnosis per year in the USA alone, acute myeloid leukaemia (AML) is considered the most common acute leukaemia in adults. This rate of diagnosis accounts for approximately 80% of all acute leukaemia diagnosed in adults annually (Siegel et al., 2015). Similarly to MM, AML is considered a disease of old age, with only 1.3 per 100,000 patients diagnosed with AML being aged under 65. The trend in age leads to difficulty in disease treatment and, therefore, leads to a short OS for AML patients. Younger patients tend to have significant improvements in clinical outcomes due to advances in treatment. In patients over 65, it has been observed that the average survival rate after diagnosis is less than one year. Interestingly, AML comprises 15-20% of leukaemia cases in patients aged ≤15 years, with highest incidence occurring in the first year from birth and declining until the age of 4 years. Disease diagnosis has been observed to plateau throughout childhood and early adulthood, with risk increasing again in later life (Aquino, 2002).

The abnormal proliferation and differentiation of a clonal population of myeloid stem cells, derived from differing chromosomal translocations characteristic of AML, leads to the formation of chimeric proteins (RUNX1-RUNX1T1 and PML-RARA) therefore altering the normal maturation process of myeloid precursor cells. Some of the physical manifestations of AML are anaemia, leukocytosis (an increased abundance of white blood cells in the blood), thrombocytopenia (a low blood platelet count), fatigue and severe weight loss or anorexia. Swollen or enlarged lymph nodes (lymphadenopathy) and enlargement of organs (organomegaly) are rarely observed in AML patients but cases of this have been recorded (De Kouchkovsky and Abdul-Hay, 2016). The proliferation of myeloid stem cells results in the accumulation of malignant myeloid cells in the BM, peripheral blood and, in some rare cases, in other organs. Further diagnosis is established by demonstrating the origin of the myeloid stem cells, determined by myeloperoxidase activity. Minimal requirements for AML

diagnosis combine immunophenotyping, morphology, cytochemistry and molecular/cytogenetic screening of patients bone marrow aspirate. A peripheral blood diagnostic test is sufficient if patient conditions contraindicates a bone marrow aspirate, along with a cerebrospinal fluid biopsy for all patients indicating central nervous system (CNS) involvement (Creutzig et al., 2012). Immunophenotyping is carried out in diagnosis, as AML patients show distinct cytogenetic and molecular abnormalities. One of the chromosomal translocations related to AML is t(8;12), resulting in the formation of chimeric proteins. These chimeric proteins change normal maturation of myeloid precursor cells. The presence of Auer rods, azurophilic, needle-shaped cytoplasmic inclusion bodies, are present predominately in AML with t(8;21) and diagnosis can also be established due to the presence of extramedullary tissue infiltration (Vardiman et al., 2009).

Three separate classification systems have been employed for the characterisation of AML: the French-American British (FAB) classification system, the World Health Organisation (WHO) classification system (Table 7.1) and the European LeukemiaNet (ELN) Classification system (Table 7.2). The FAB system identifies 30% blast infiltration as the cut off for diagnosis and classifies AML into 9 sub categories, M0-M7. Subject to cell morphology, cytochemical characteristics and cell type in which AML cells in question have been derived. This classification system focuses on the routine use of microscopy to identify stained, malignant blast cells (Bennett et al., 1991). This system aimed to provide a means to distinguish between individual cases easily but was noted as unable to differentiate immunophenotypic characteristics, failed to identify myelodysplastic alterations and cytogenetic defects related to AML. The WHO developed a more inclusive classification system for AML, combining genetic information, immunophenotyping, clinical aspects and morphological observations to define disease. This classification system divides AML into distinct sub categories, combining all recent scientific findings relating to the disease (Arber et al., 2016) (Table 7.1). A revised cut off point of ≤20% blast cell

infiltration in peripheral blood or BM was also established by the WHO for a more well-rounded classification method (Döhner et al., 2010).

Table 7.1: WHO Classification of AML.

*Table was modified from (Arber et al., 2016)

AML Type	Genetic Abnormalities
AML with recurrent genetic abnormalities	AML with t(8;21)(q22;q22); RUNX1-RUNX1T1
	AML with inv(16)(p13.1q22) t(16;16|)(p13.1;q22); CBFB-MYH11
	APL with PML-RARA
	AML with t(9;1)(p21.3;q23.3); MLLT3-KMT2A
	ML with t(6;9)(p23;q34.1); DEK-NUP214
	AML with inv(3)(q21.3q26.2) or t(3;3)(q21.2;q26.2); GATA2, MECOM
	AML (megakaryoblastic) with t(1;22)(p13.3;q13.3); RBM15-MKL1
	AML with BCR-ABL1 (provisional entity)
	AML with mutated NPM1
	AML with biallelic mutations of CEBPA
	AML with mutated RUNX1 (provisional entity)
AML with myelodysplasia-related changes	
Therapy-related myeloid neoplasms	
AML not otherwise specified	AML with minimal differentiation
	AML without maturation
	AML with maturation
	Acute myelomonocytic leukemia
	Acute monoblastic/monocytic leukemia
	Acute erythroid leukemia
	Pure erythroid leukemia
	Acute megakaryoblastic leukemia
	Acute basophilic leukaemia

	Acute panmyelosis with myelofibrosis
Myeloid Sarcoma	
Myeloid proliferations related to Down syndrome	Transient abnormal myelopoiesis
	ML associated with Down syndrome

The final classification system, established by the ELN, links cytogenetic aberrations with prognosis and therapeutic response, establishing 3 distinct groups: Favourable (Group 1), Intermediate (Group 2) and Adverse (Group 3) (Table 7.2). By grouping patients by prognosis risk group, it allows more informed clinical decisions to be made regarding treatment strategies such as standard or increased intensity courses, consolidation chemotherapy or ASCT and choosing between conventional therapies or investigational therapies (Döhner et al., 2017). Favourable group 1s are observed in approximately 15% of diagnosis cases of AML and have a survival rate of approximately 65%, intermediate group 2 patients make up approximately 55% of AML cases and have a survival rate of 50% and adverse group 3 patients are observed in 30% of AML diagnosis and have a survival rate of 20% (Döhner et al., 2010). The ELN system also allows the incorporation of patient associated risk factors, such as old age, co-existing illnesses and predicted treatment related early death to make treatment decisions for a more effective clinical course of action (Walter et al., 2011).

Table 7.2: AML Prognostic Risk Grouping Based on Cytogenetics and Molecular Profile.

*Table was modified from (De Kouchkovsky and Abdul-Hay, 2016)

Prognostic-risk Group	Cytogenetic Profile	Cytogenetic profile and Molecular Profile
Favourable (Group 1)	t(8;21)(q22;q22)	t(8;21)(q22;q22) with no c-KIT mutation
	inv(16)(p13;1q22)	inv(16)(p13;1q22)
	t(15;17)(q22;q12)	t(15;17)(q22;q12)
		Mutated NPM1 without FLT3-ITD (CN-AML)
		Mutated biallelic CEBPA (CN-AML)
Intermediate (Group 2)	CN-AML	t(8;21)(q22;q22) with muted c-KIT
	t(9;11)(p22;q23)	CN-AML other than those included in either favourable or adverse risk group.
	Cytogenetic abnormalities not included in either favourable or adverse risk group.	t(9;11)(p22;q23)
		Cytogenetic abnormalities not included in either favourable or adverse risk group.
Adverse (Group 3)	inv(3)(q21q26.2)	TP53 mutation, regardless of cytogenetic profile
	t(6;9)(p23;q34)	CN with FLT3-ITD
		CN with DNMT3A
		CN with KMT2A-PTD
	11q abnormalities other than t(9;11)	inv(3)(q21q26.2)
	-5 or del(5q)	t(6;9)(p23;q34)
		11q abnormalities other than t(9;11)
	-7	5 or del(5q)
	Complex karyotype	-7

Clinical decisions on the treatment of AML are made according to disease prognostic risk group, age and overall health status of the patient. Induction therapy is the first line of action in treatment, usually employing a “7+3” treatment regime. This course entails a patient undergoing treatment using a combination of 7 days infusion cytarabine, followed by 3 days of anthracycline (Dombret and Gardin, 2016) and is prescribed to patients with prognostic group 1 or 2 and patients with a low risk of treatment related mortality (Estey, 2014). Complete Remission (CR) is obtained by 60-80% of patients less than 60 years of age and 40-60% in patients over the age of 60 after “7+3” treatment regime (Büchner et al., 2012). As with MM, AML is a disease linked with extensive amounts of relapse cases. The inevitability of relapse in AML is linked to minimal residual disease (MRD) persisting in CR (defined as <5% blast count in total nonerythroid cells in the BM) (Chen et al., 2015). After induction therapy, patients who reach CR have been noted as having significantly increased OS in comparison to those who are noted as treatment resistant. This increased survival does, however, depend on the presence of persistent thrombocytopenia, which has been observed as directly correlating with a shorter OS (Walter et al., 2010). The detection of MRD, by flow cytometry, is an indicator of disease relapse and subsequent survival for both favourable and intermediate prognostic risk groups (Buccisano et al., 2012). When relapse occurs in patients, consolidation therapy is utilised in one of three methods: high dose chemotherapy paired with allogeneic HLA-matched stem cell transplant from biological sibling, high dose chemotherapy paired with ASCT or conventional dose chemotherapy (Löwenberg, 2013).

7.1.1 Experimental Design

7.1.1.1 Patients and Samples

Both plasma cell and serum AML samples were collected from 49 patients with varying grade of disease, ranging from grade 1 to grade 3. This grading was carried out by the participating hospitals and the study was approved in compliance with the Declaration of Helsinki. These samples were obtained from the Finnish Haematology Registry and Clinical Biobank (FHRB). Patient details for plasma cell samples used (40 samples) are detailed on Table 7.3 and patient details for serum samples used (49) are detailed in Table 7.4.

Table 7.3: Patient details of cell lysate samples analysed by LC-MS/MS

Sample ID	Gender	Diagnosis Age	Risk Class	Diagnosis Type
1266	Female	46.4	1	9871 Ac. myelomonocytic leuk. w abn. mar. eosinophils
1497	Female	35.3	1	9896 Acute myeloid leukemia, t(8;21)(q22;q22)
1644	Male	21.6	1	9896 Acute myeloid leukemia, t(8;21)(q22;q22)
2688	Female	67.3	1	9861 Acute myeloid leukemia
2788	Female	68.8	1	9861 Acute myeloid leukemia
2908	Male	16.8	1	9896 Acute myeloid leukemia, t(8;21)(q22;q22)
3101	Female	55.5	1	9873 Acute myeloid leukemia without maturation
3708	Female	44.8	1	9861 Acute myeloid leukemia
3786	Female	53.5	1	9874 Acute myeloid leukemia with maturation
3884	Male	72.8	1	9861 Acute myeloid leukemia

Sample ID	Gender	Diagnosis Age	Risk Class	Diagnosis Type
3893	Female	48.7	1	9891 Acute monocytic leukemia
1219	Male	76.9	2	9861 Acute myeloid leukemia
1712	Female	62.9	2	9874 Acute myeloid leukemia with maturation
1886	Male	56.5	2	9861 Acute myeloid leukemia
2035	Female	63.8	2	9861 Acute myeloid leukemia
2067	Female	78.1	2	9891 Acute monocytic leukemia
2098	Female	24.3	2	9861 Acute myeloid leukemia
2774	Male	67.3	2	9895 Acute myeloid leuk. with multilineage dysplasia
2796	Female	48.6	2	9873 Acute myeloid leukemia without maturation
2889	Male	72.6	2	9874 Acute myeloid leukemia with maturation
3298	Male	16.5	2	9891 Acute monocytic leukemia
3520	Female	62.9	2	9861 Acute myeloid leukemia
3730	Female	61.5	2	9891 Acute monocytic leukemia
3822	Female	66.7	2	9897 Acute myeloid leukemia, 11q23 abnormalities
3869	Male	57	2	9874 Acute myeloid leukemia with maturation
4021	Female	35.4	2	9920 Therapy-related acute myeloid leukemia, NOS
4980	Female	68.2	2	
1314	Female	76.6	3	9873 Acute myeloid leukemia without maturation
1320	Female	54.3	3	9867 Acute myelomonocytic leukemia
1413	Male	28.6	3	9891 Acute monocytic leukemia

Sample ID	Gender	Diagnosis Age	Risk Class	Diagnosis Type
2095	Male	66.7	3	9873 Acute myeloid leukemia without maturation
2294	Female	52	3	9896 Acute myeloid leukemia, t(8;21)(q22;q22)
3443	Female	21.8	3	9873 Acute myeloid leukemia without maturation
3490	Male	44.6	3	9873 Acute myeloid leukemia without maturation
3591	Female	71.1	3	9873 Acute myeloid leukemia without maturation
3600	Female	39.7	3	9891 Acute monocytic leukemia
3630	Male	40.6	3	9861 Acute myeloid leukemia
3853	Female	59.4	3	9865 Acute myeloid leukemia with t(6;9)(p23;q34) DEK-NUP214
4000	Male	77.7	3	9895 Acute myeloid leuk. with multilineage dysplasia
4919	Male	62.5	3	9727 Precursor cell lymphoblastic lymphoma, NOS
5034	Female	64.7	3	9920 Therapy-related acute myeloid leukemia, NOS

Table 7.4: Patient details of serum samples included in Luminex study

Sample ID	Gender	Diagnosis Age	Risk Class	Diagnosis Type
1266	Female	46.4	1	9871 Ac. myelomonocytic leuk. w abn. mar. eosinophils
1497	Female	35.3	1	9896 Acute myeloid leukemia, t(8;21)(q22;q22)
1644	Male	21.6	1	9896 Acute myeloid leukemia, t(8;21)(q22;q22)
2688	Female	67.3	1	9861 Acute myeloid leukemia
2788	Female	68.8	1	9861 Acute myeloid leukemia
2908	Male	16.8	1	9896 Acute myeloid leukemia, t(8;21)(q22;q22)
3101	Female	55.5	1	9873 Acute myeloid leukemia without maturation
3708	Female	44.8	1	9861 Acute myeloid leukemia
3769	Male	50	1	9861 Acute myeloid leukemia
3786	Female	53.5	1	9874 Acute myeloid leukemia with maturation
3884	Male	72.8	1	9861 Acute myeloid leukemia
3893	Female	48.7	1	9891 Acute monocytic leukemia
1219	Male	76.9	2	9861 Acute myeloid leukemia
1690	Female	63.2	2	9861 Acute myeloid leukemia
1712	Female	62.9	2	9874 Acute myeloid leukemia with maturation
1886	Male	56.5	2	9861 Acute myeloid leukemia
2035	Female	63.8	2	9861 Acute myeloid leukemia
2067	Female	78.1	2	9891 Acute monocytic leukemia
2098	Female	24.3	2	9861 Acute myeloid leukemia
2448	Male	72.6	2	9874 Acute myeloid leukemia with maturation
2774	Male	67.3	2	9895 Acute myeloid leuk. with multilineage dysplasia

Sample ID	Gender	Diagnosis Age	Risk Class	Diagnosis Type
2796	Female	48.6	2	9873 Acute myeloid leukemia without maturation
2889	Male	72.6	2	9874 Acute myeloid leukemia with maturation
3298	Male	16.5	2	9891 Acute monocytic leukemia
3520	Female	62.9	2	9861 Acute myeloid leukemia
3730	Female	61.5	2	9891 Acute monocytic leukemia
3822	Female	66.7	2	9897 Acute myeloid leukemia, 11q23 abnormalities
3869	Male	57	2	9874 Acute myeloid leukemia with maturation
4021	Female	35.4	2	9920 Therapy-related acute myeloid leukemia, NOS
4980	Female	68.2	2	
5184	Female	78.7	2	9897 Acute myeloid leukemia, 11q23 abnormalities
1314	Female	76.6	3	9873 Acute myeloid leukemia without maturation
1320	Female	54.3	3	9867 Acute myelomonocytic leukemia
1413	Male	28.6	3	9891 Acute monocytic leukemia
1867	Male	70	3	9891 Acute monocytic leukemia
2095	Male	66.7	3	9873 Acute myeloid leukemia without maturation
2294	Female	52	3	9896 Acute myeloid leukemia, t(8;21)(q22;q22)
3443	Female	21.8	3	9873 Acute myeloid leukemia without maturation
3490	Male	44.6	3	9873 Acute myeloid leukemia without maturation

Sample ID	Gender	Diagnosis Age	Risk Class	Diagnosis Type
3529	Male	54.1	3	9891 Acute monocytic leukemia
3591	Female	71.1	3	9873 Acute myeloid leukemia without maturation
3600	Female	39.7	3	9891 Acute monocytic leukemia
3630	Male	40.6	3	9861 Acute myeloid leukemia
3853	Female	59.4	3	9865 Acute myeloid leukemia with t(6;9)(p23;q34) DEK-NUP214
4000	Male	77.7	3	9895 Acute myeloid leuk. with multilineage dysplasia
4690	Male	52.3	3	9874 Acute myeloid leukemia with maturation
4919	Male	62.5	3	9727 Precursor cell lymphoblastic lymphoma, NOS
4991	Male	64	3	9873 Acute myeloid leukemia without maturation
5034	Female	64.7	3	9920 Therapy-related acute myeloid leukemia, NOS

7.1.1.2 Label-free LC-MS/MS Analysis of AML Cell Lysates.

AML patient cells were initially lysed in RIPA buffer (25mM Tris, pH 7 – 8; 150 mM NaCl; 0.1% SDS; 0.5% sodium deoxycholate and 1% NP-40). The lysates were buffer exchanged using the 'filter aided sample preparation' (FASP) method in a buffer containing 8M urea/50 mM NH4HCO3/0.1% ProteaseMax. The protein amount was estimated using an RC/DC protein assay from Bio-Rad. BSA was used as a standard. After dithiothreitol reduction and iodoacetic acid-mediated alkylation, a double digestion was performed using Lys-C (for 4 hours at 37°C) and Trypsin (overnight at 37°C) on 10µg of protein. Digested samples were desalted prior to analysis using

C18 spin columns (Thermo Scientific, UK). 500 ng of each digested sample was loaded onto a Q-Exactive (ThermoFisher Scientific, Hemel Hempstead, UK) high-resolution accurate mass spectrometer connected to a Dionex Ultimate 3000 (RSLCnano) chromatography system (ThermoFisher Scientific, Hemel Hempstead, UK). Peptides were separated using a 2% to 40% gradient of acetonitrile on a Biobasic C18 Picofrit column (ThermoFisher Scientific, Hemel Hempstead, UK) (100mm length, 75mm ID) over 65 min at a flow rate of 250nl/min. Data was acquired with the mass spectrometer operating in automatic data dependent switching mode. A full MS scan at 140,000 resolution and a range of 300–1700 m/z was followed by an MS/MS scan, resolution 17,500 and a range of 200–2000 m/z, selecting the 10 most intense ions prior to MS/MS.

7.1.1.3 Data analysis of all statistically significantly proteins with altered abundance for each diagnostic group.

Protein identification and label-free quantification (LFQ) normalisation of MS/MS data was performed using MaxQuant v1.5.2.8 (http://www.maxquant.org). The Andromeda search algorithm incorporated in the MaxQuant software was used to correlate MS/MS data against the *Homo sapiens* Uniprot reference proteome database and a contaminant sequence set provided by MaxQuant. Perseus v.1.5.6.0 (www.maxquant.org/) was used for data analysis, processing and visualisation. Normalised LFQ intensity values were used as the quantitative measurement of protein abundance for subsequent analysis. The data matrix was first filtered for the removal of contaminants and peptides identified by site. LFQ intensity values were log2 transformed and each sample was assigned to its corresponding group. ANOVA-based multisample *t*-tests were performed using a cut-off of $p<0.05$ on the post imputated dataset to identify statistically significant differentially abundant proteins.

7.1.1.4 Bioinformatic analysis of all statistically significantly proteins with altered abundance for each treatment.

In order to group identified proteins based on their protein class and to identify potential protein targets with increased abundance in all three patient prognostic risk groups, publicly available bioinformatics software programmes were employed. The programs used were the PANTHER database of protein families (http://pantherdb.org/). KEGG colour pathway analysis was carried out with a focus on proteins increased in abundance in both patient groupings using the Kyoto Encyclopaedia of Genes and Genomes databank (https://www.genome.jp/kegg).

7.1.1.5 MILLIPLEX® MAP Kit analysis using Luminex technology of AML patient serum.

MILLIPLEX® MAP Kit: Human Cytokine/Chemokine Magnetic Bead Panel Ⅰ, MILLIPLEX® MAP Kit: Human Cytokine/Chemokine Panel Ⅱ and MILLIPLEX® MAP Kit: Human Circulating Cancer Biomarker Magnetic Bead Panel 4 were all used in the targeted analysis of patient serum samples, ranging in prognostic risk grouping from group 1 to group 3. 25µl crude serum was used per sample and all manufacturers guidelines were followed, with variations stated in Chapter 2.

7.2 Results

7.2.1 Quantitative Proteomic Analysis of AML Cell Lysates using Label-Free LC-MS/MS for Group 1 (Favourable) versus Group 3 (Adverse).

In-depth proteomic analysis of 11 Group 1 samples and 13 Group 3 samples identified 65 statistically significantly changed proteins ($p>0.05$). Of these 65 statistically significant proteins, 8 were observed to have an increased abundance in group 1 patients, in comparison to group 3, and 57 proteins were observed to have an increased abundance in group 3, in comparison to group 1. Fold changes as high as 1.978 times were recorded for Receptor-type tyrosine-protein phosphatase C in group 1 to group 3 and fold changes as high as 6.954 were recorded for Transcription intermediary factor 1-beta in group 3 compared to group 1 (Table 7.5).

Table 7.5: List of proteins with statistically significant altered abundance between Group 1 and Group 3, identified by label-free LC-MS/MS and Perseus analysis.

Gene name	Protein ID	ANOVA p value	↑ in Gr1 (fold-change)	↑ in Gr3 (fold-change)
LA	Lupus La protein	0.001		4.138
OTUB1	Ubiquitin thioesterase	0.001		2.212
CNDP2	Cytosolic non-specific dipeptidase	0.001		5.283
RAN	GTP-binding nuclear protein	0.001		2.531
HNRPC	Heterogeneous nuclear ribonucleoproteins C1/C2	0.002		4.106
HNRPQ	Heterogeneous nuclear ribonucleoprotein Q	0.003		4.228

Gene name	Protein ID	ANOVA p value	↑ in Gr1 (fold-change)	↑ in Gr3 (fold-change)
CH60	60 kDa heat shock protein, mitochondrial	0.003		6.610
PRDX6	Peroxiredoxin-6	0.004		2.927
TBA1B	Tubulin alpha-1B chain	0.005		3.711
TERA	Transitional endoplasmic reticulum ATPase	0.006		2.235
SET	Protein SET	0.006		2.172
ROA2	Heterogeneous nuclear ribonucleoproteins A2/B1	0.006		2.839
CAPZB	F-actin-capping protein subunit beta	0.007	1.419	
RCC2	Protein RCC2	0.007		2.001
ECHA	Trifunctional enzyme subunit alpha, mitochondrial	0.007		4.205
ARPC4	Actin-related protein 2/3 complex subunit 4	0.007	1.267	
PTPRC	Receptor-type tyrosine-protein phosphatase C	0.007	1.978	
NONO	Non-POU domain-containing octamer-binding protein	0.008		2.475
THIO	Thioredoxin	0.009		2.897
ILF3	Interleukin enhancer-binding factor 3	0.011		1.981
VIME	Vimentin	0.011		3.464
TALDO	Transaldolase	0.012		2.122
LDHA	L-lactate dehydrogenase A chain	0.013		1.990
TCPH	T-complex protein 1 subunit eta	0.013		2.322
NUCL	Nucleolin	0.014		2.828

Gene name	Protein ID	ANOVA p value	↑ in Gr1 (fold-change)	↑ in Gr3 (fold-change)
NAGK	N-acetyl-D-glucosamine kinase	0.016	1.672	
DHX9	ATP-dependent RNA helicase A	0.016		4.069
PRDX4	Peroxiredoxin-4	0.016		1.041
TCP4	Activated RNA polymerase II transcriptional coactivator p15	0.017		2.524
HS90A	Heat shock protein HSP 90-alpha	0.018		1.919
ROA1	Heterogeneous nuclear ribonucleoprotein A1	0.018		2.548
LDHB	L-lactate dehydrogenase B chain	0.019		2.609
EF1A3	Putative elongation factor 1-alpha-like 3	0.020		2.408
FEN1	Flap endonuclease 1	0.020		1.805
EF2	Elongation factor 2	0.021		1.925
NPM	Nucleophosmin	0.024		2.604
F10A1	Hsc70-interacting protein	0.025		2.431
1433Z	14-3-3 protein zeta/delta	0.026		1.593
TIF1B	Transcription intermediary factor 1-beta	0.027		6.954
ESTD	S-formylglutathione hydrolase	0.028		2.092
HNRH1	Heterogeneous nuclear ribonucleoprotein H	0.029		2.369
LC7L2	Putative RNA-binding protein Luc7-like 2	0.030		2.108
TCPZ	T-complex protein 1 subunit zeta	0.030		1.745
GANAB	Neutral alpha-glucosidase AB	0.030		2.254

Gene name	Protein ID	ANOVA p value	↑ in Gr1 (fold-change)	↑ in Gr3 (fold-change)
PGAM1	Phosphoglycerate mutase 1	0.031	1.298	
ACTB	Actin, cytoplasmic 1	0.031		1.694
PARP1	Poly [ADP-ribose] polymerase 1	0.032		2.879
RUVB2	RuvB-like 2	0.032		2.135
NPS3A	Protein NipSnap homolog 3A	0.034	1.192	
NDKB	Nucleoside diphosphate kinase B	0.034		2.163
RHOA	Transforming protein RhoA	0.035		1.599
SFPQ	Splicing factor, proline- and glutamine-rich	0.035		1.949
IF4A3	Eukaryotic initiation factor 4A-III	0.035		2.311
HNRPU	Heterogeneous nuclear ribonucleoprotein U	0.037		2.430
DLDH	Dihydrolipoyl dehydrogenase, mitochondrial	0.039		2.613
RSSA	40S ribosomal protein SA	0.041		3.584
ROA3	Heterogeneous nuclear ribonucleoprotein A3	0.042		2.377
G3P	Glyceraldehyde-3-phosphate dehydrogenase	0.042		2.775
RS3	40S ribosomal protein S3	0.042		4.481
FSCN1	Fascin	0.044		1.014
RL40	Ubiquitin-60S ribosomal protein L40	0.046	1.219	
PDIA3	Protein disulfide-isomerase A3	0.049		1.687
HSP7C	Heat shock cognate 71 kDa protein	0.049		1.743
TSN	Translin	0.050	1.167	

7.2.2 Quantitative Proteomic Analysis of AML Cell Lysates using Label-Free LC-MS/MS for Group 1 (Favourable) versus Group 2 (Intermediate).

The in-depth proteomic analysis of 11 Group 1 samples and 16 Group 2 samples revealed 18 statistically significantly changed ($p>0.05$) proteins with altered abundance between group 1 and group 2. Of these identified proteins, 7 were confirmed to have an increased abundance in group 1 and 9 were noted as having an increase abundance in group 2. Fold changes as high as 2.263 for Spectrin alpha chain, non-erythrocytic 1 were noted in group 1, in comparison to group 2, and fold changes as high as 5.218 were observed in group 2 in comparison to group 1 for Carbonic anhydrase 1 (Table 7.6)

Table 7.6: List of Proteins with Altered Abundance between Group 1 and Group 2, Identified by Label-free LC-MS/MS and Perseus Analysis.

Gene name	Protein ID	ANOVA p value	↑ in Gr1 (fold-change)	↑ in Gr2 (fold-change)
UBP7	Ubiquitin carboxyl-terminal hydrolase 7	0.001	1.424	
HS105	Heat shock protein 105 kDa	0.004		2.017
DPYL2	Dihydropyrimidinase-related protein 2	0.006		1.165
SRSF2	Serine/arginine-rich splicing factor 2	0.007		1.130
FUS	RNA-binding protein FUS	0.010	1.581	
RTCB	tRNA-splicing ligase RtcB homolog	0.012	1.448	
ANM1	Protein arginine N-methyltransferase 1	0.017	1.251	
PSA1	Proteasome subunit alpha type-1	0.020	1.212	

HNRL1	Heterogeneous nuclear ribonucleoprotein U-like protein 1	0.020		1.067
RAB5C	Ras-related protein Rab-5C	0.022		1.314
SYVC	Valine--tRNA ligase	0.030	1.267	
1433Z	14-3-3 protein zeta/delta	0.032		1.244
CAH1	Carbonic anhydrase 1	0.035		5.218
SPTN1	Spectrin alpha chain, non-erythrocytic 1	0.035	2.263	
LDHA	L-lactate dehydrogenase A chain	0.043		1.317
FLNA	Filamin-A	0.045		1.461
ANXA6	Annexin A6	0.046		1.290
G6PD	Glucose-6-phosphate 1-dehydrogenase	0.048		1.815

7.2.3 Quantitative Proteomic Analysis of AML Cell Lysates using Label-Free LC-MS/MS for Group 2 (Intermediate) versus Group 3 (Adverse).

The in-depth proteomic analysis of 16 Group 2 samples and 13 Group 3 samples revealed 41 statistically significantly changed ($p>0.05$) proteins with altered abundance between group 2 and group 3 patients. Of these 41 proteins, 31 were seen to be differentially abundant in group 2 and 10 were found to have an altered abundance in group 3. Fold changes as high as 11.978 were observed for DNA-dependent protein kinase catalytic subunit in group 2 and fold changes as high as 8.187 for Haemoglobin subunit delta were recorded for the abundance change from group 3 to group 2 (Table 7.7).

Table 7.7: List of proteins with altered abundance between Group 2 and Group 3, identified by label-free LC-MS/MS and Perseus analysis.

Gene name	Protein ID	ANOVA p value	↑ in Gr2 (fold-change)	↑ in Gr3 (fold-change)
DHX9	ATP-dependent RNA helicase A	0.000	3.410	
ATPB	ATP synthase subunit beta, mitochondrial	0.001	6.149	
GSTK1	Glutathione S-transferase kappa 1	0.001	6.689	
AHNK	Neuroblast differentiation-associated protein AHNAK	0.004	6.487	
SYNC	Asparagine--tRNA ligase, cytoplasmic	0.004	1.390	
TCPA	T-complex protein 1 subunit alpha	0.005	2.220	
1433G	14-3-3 protein gamma	0.007	1.337	
CH60	60 kDa heat shock protein, mitochondrial	0.010	2.924	
VATA	V-type proton ATPase catalytic subunit A	0.010	2.286	
PRKDC	DNA-dependent protein kinase catalytic subunit	0.010	11.978	
TAGL2	Transgelin-2	0.011	1.733	
RPN1	Dolichyl-diphosphooligosaccharide--protein glycosyltransferase subunit 1	0.012	1.873	
TCPH	T-complex protein 1 subunit eta	0.013	1.679	
UB2V1	Ubiquitin-conjugating enzyme E2 variant 1	0.013		1.357
PA2G4	Proliferation-associated protein 2G4	0.016		1.067

Gene name	Protein ID	ANOVA p value	↑ in Gr2 (fold-change)	↑ in Gr3 (fold-change)
ROA2	Heterogeneous nuclear ribonucleoproteins A2/B1	0.016	1.457	
ATPA	ATP synthase subunit alpha, mitochondrial	0.018	5.940	
UBA1	Ubiquitin-like modifier-activating enzyme 1	0.020	1.559	
FUBP1	Far upstream element-binding protein 1	0.020	1.917	
TCPG	T-complex protein 1 subunit gamma	0.020	1.642	
TBB4B	Tubulin beta-4B chain	0.021	4.392	
FUBP2	Far upstream element-binding protein 2	0.022	2.836	
PNPH	Purine nucleoside phosphorylase	0.023		2.214
GSTO1	Glutathione S-transferase omega-1	0.025		1.909
CAN1	Calpain-1 catalytic subunit	0.026	1.469	
HBB	Haemoglobin subunit beta	0.029		4.749
BAX	Apoptosis regulator BAX	0.029	1.854	
EF2	Elongation factor 2	0.030	1.362	
DDX1	ATP-dependent RNA helicase DDX1	0.031	3.311	
URP2	Fermitin family homolog 3	0.031	1.791	
HBA	Haemoglobin subunit alpha	0.032		5.373
ESTD	S-formylglutathione hydrolase	0.032		1.372
HBD	Haemoglobin subunit delta	0.034		8.187
ACTZ	Alpha-centractin	0.038	1.899	
TCPB	T-complex protein 1 subunit beta	0.039	1.635	
CBX3	Chromobox protein homolog 3	0.040		1.237

Gene name	Protein ID	ANOVA p value	↑ in Gr2 (fold-change)	↑ in Gr3 (fold-change)
TIF1B	Transcription intermediary factor 1-beta	0.043	2.774	
PGM1	Phosphoglucomutase-1	0.045		1.139
IF4A1	Eukaryotic initiation factor 4A-I	0.045	2.943	
CPNS1	Calpain small subunit 1	0.047	3.485	
TCPE	T-complex protein 1 subunit epsilon	0.048	1.643	

7.2.4 Comparative Analysis of Biological Processes Related to Protein Signatures Abundant in Group 1 and Group 3.

Bioinformatic analysis, using KEGG software, was carried out on each individual prognostic risk group, identifying the pathways associated with the proteins with changed abundance. The proteins with altered abundance Group 1, in comparison to Group 3, was most associated with metabolic pathways and glycolysis/gluconeogenesis. Group 3 also showed an increased abundance of proteins associated with metabolic pathways and glycolysis/gluconeogenesis, in comparison to Group 1. Unsurprisingly, the amount of protein related pathways for group 3 is vastly more than that of group 1, with proteins related to microRNAs in cancer, tight junction and endocytosis pathways (Figure 7.1).

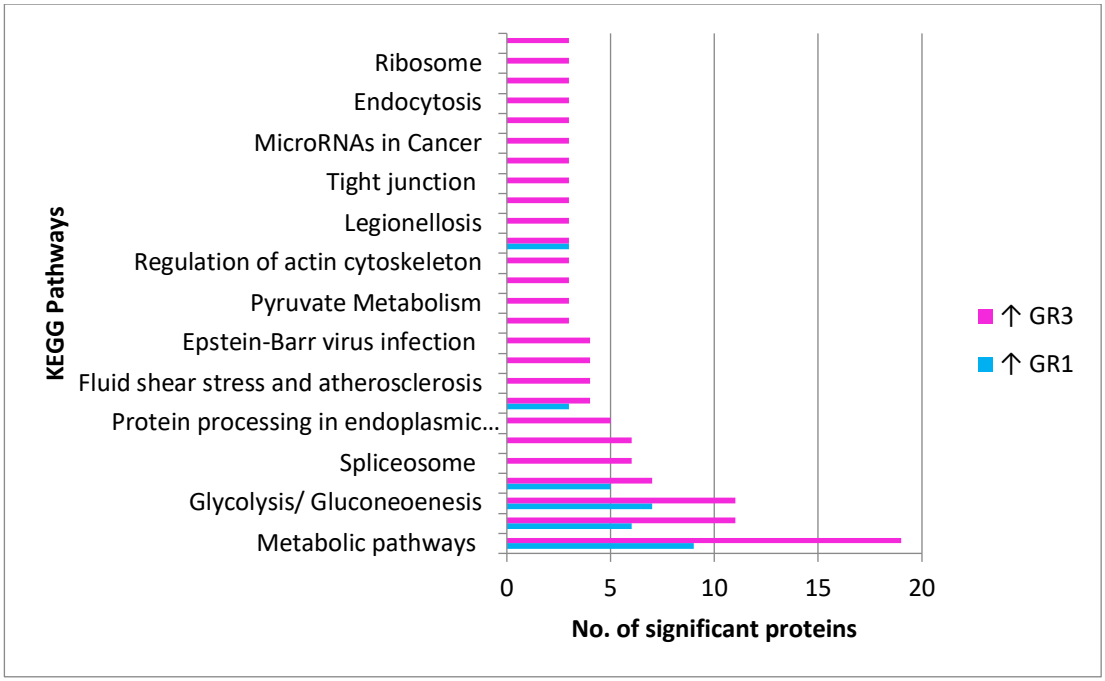

Figure 7.1: Comparative bar chart of KEGG Pathway associated with differentially abundant proteins from Group 1 to Group 3.

This figure depicts a comparison of the number of proteins, identified by Perseus analysis, associated with each individual KEGG pathway. Group 1 is depicted in blue and Group 3 is depicted in pink.

7.2.5 Comparative Analysis of Biological Processes Related to Protein Signatures Abundant in Group 1 and Group 2.

Bioinformatic analysis, using KEGG software, was carried out on each individual prognostic risk group, identifying the pathways associated with the proteins with changed abundance. The proteins with altered abundance Group 1, in comparison to Group 2, was most associated with metabolic pathways and glycolysis/gluconeogenesis, followed by carbon metabolism. Group 2 also showed an increased abundance of proteins associated with metabolic pathways, glycolysis/gluconeogenesis and carbon metabolism, in comparison to Group 1.

Group 1 also showed an increased abundance of proteins related to HIF-1 signalling pathway, which was not recorded in Group 2 (Figure 7.2).

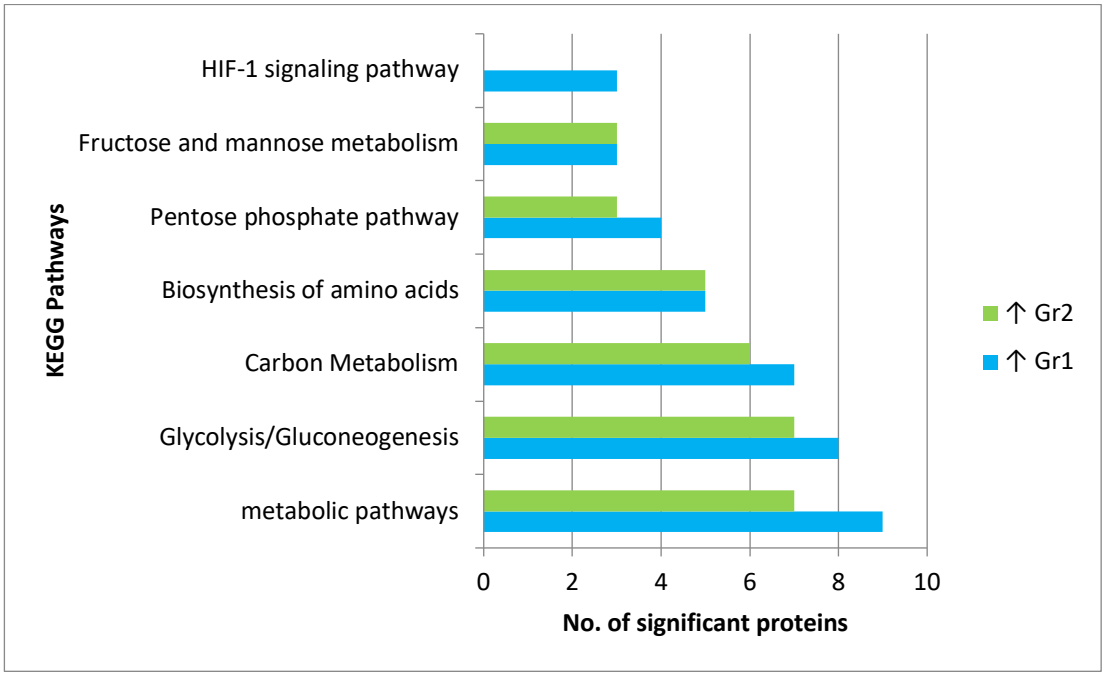

Figure 7.2: Comparative bar chart of KEGG Pathway associated with differentially abundant proteins from Group 1 to Group 3.

This figure depicts a comparison of the number of proteins, identified by Perseus analysis, associated with each individual KEGG pathway. Group 1 is depicted in blue and Group 2 is depicted in green.

7.2.6 Comparative Analysis of Biological Processes Related to Protein Signatures Abundant in Group 2 and Group 3.

Bioinformatic analysis, using KEGG software, was carried out on each individual prognostic risk group, identifying the pathways associated with the proteins with changed abundance. The proteins with altered abundance Group 2, in comparison to Group 3, was most associated with metabolic pathways,

glycolysis/gluconeogenesis and carbon metabolism. Group 3 also showed an increased abundance of proteins associated with metabolic pathways, glycolysis/gluconeogenesis and carbon metabolism, in comparison to Group 2. Group 2 showed an increased abundance in proteins related to Protein processing in endoplasmic reticulum and oxidative phosphorylation pathways, neither of which were recorded in Group 3 proteins (Figure 7.3).

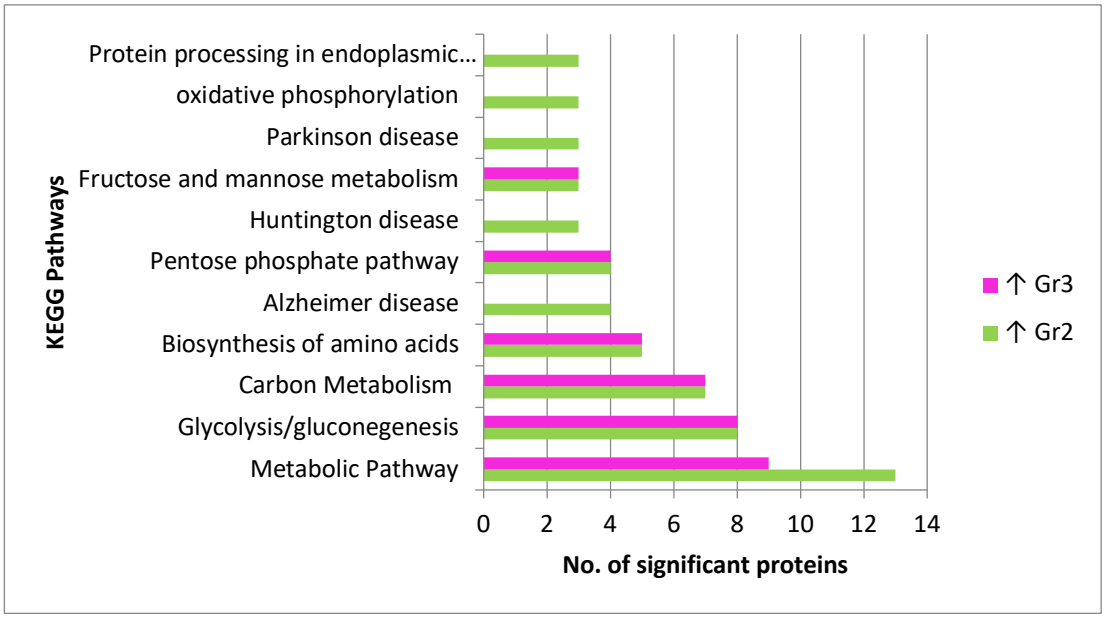

Figure 7.3: Comparative bar chart of KEGG Pathway associated with differentially abundant proteins from Group 2 to Group 3.

This figure depicts a comparison of the number of proteins, identified by Perseus analysis, associated with each individual KEGG pathway. Group 2 is depicted in green and Group 3 is depicted in pink.

7.2.7 Luminex Technology Analysis of AML Patient Serum Samples with Varying Prognostic Risk Grouping.

For further identification of changes in the proteomic profile of varying prognostic risk groups in AML MILLIPLEX® MAP Kit: Human Cytokine/Chemokine Magnetic Bead Panel Ⅰ, MILLIPLEX® MAP Kit: Human Cytokine/Chemokine Panel Ⅱ and MILLIPLEX® MAP Kit: Human Circulating Cancer Biomarker Magnetic Bead Panel 4 were utilised. The analysis of the changed abundance of targeted proteins in 49 AML serum from Group 1 (Favourable), Group 2 (Intermediate) and Group 3 (Adverse) patients allowed the identification of previously established biomarkers, implicated in multiple types of cancers, in AML serum. Box and whisker plots were constructed from the findings of all three MILLIPLEX® MAP Kits, to illustrate the range, median and quartiles for the specific markers used. Of the 62 potential biomarkers tested, Interleukin-17A (IL-17A), Interleukin -1 receptor (IL-1RA), Interleulin-1 alpha (IL-1α) and Stromal cell-derived factor 1 (SDF1Aβ) were found to have statistically significant changes in abundance over the three prognostic risk groups. IL-17A exhibits an increase with statistical significance of 0.03 from group 2 to group 3 and a significant increase of 0.025 from group 1 to group 3 (Figure 7.4). Analysis of IL-1RA indicates a significant increase in abundance of $p=0.032$ for group 1 versus group 2 and $p=0.045$ for group 2 versus group 3 (Figure 7.5). IL-1α was observed to have a significant increase of $p=0.039$ in group 2 versus group 1 only (Figure 7.6) and SDF1Aβ was observed to have a significantly changed abundance from group 1 to group 2 of $p=0.025$ and group 1 versus group 3 of $p=0.029$ (Figure 7.7). All p values were calculated using the Mann Whitney U Test, where $p \leq 0.05$.

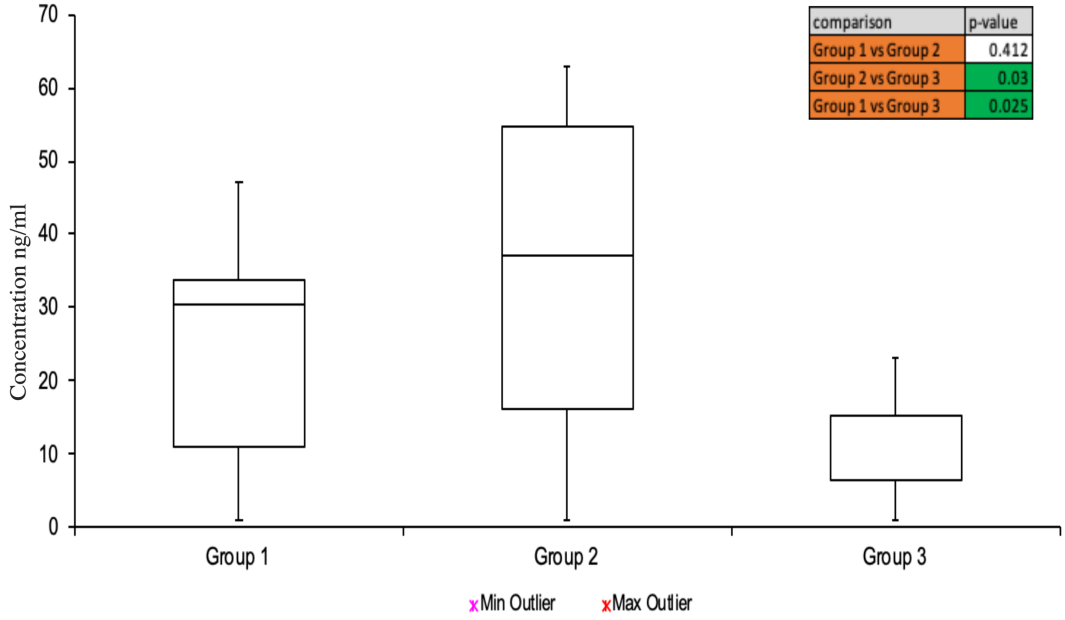

Figure 7.4: Box and Whisker plot for IL-17A abundance in AML serum samples.

Shown is a box and whisker plot from Luminex analysis carried out using AML serum samples from favourable, intermediate and adverse prognostic risk groups for IL-17A. Green indicates statistical significance ($p \leq 0.05$). There are no minimum or maximum outliers observed in the changed abundance of IL-17A.

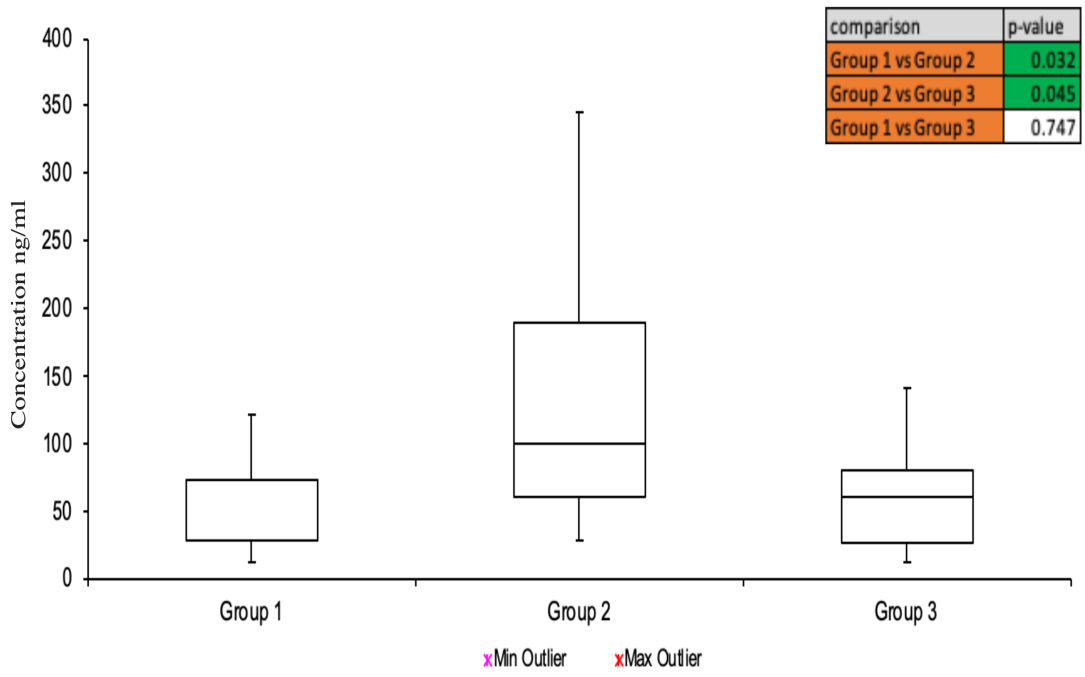

Figure 7.5: Box and Whisker plot for IL-1RA abundance in AML serum samples.

Shown is a box and whisker plot from Luminex analysis carried out using AML serum samples from favourable, intermediate and adverse prognostic risk groups for IL-1RA. Green indicates statistical significance ($p \leq 0.05$). There are no minimum or maximum outliers observed in the changed abundance of IL-1RA.

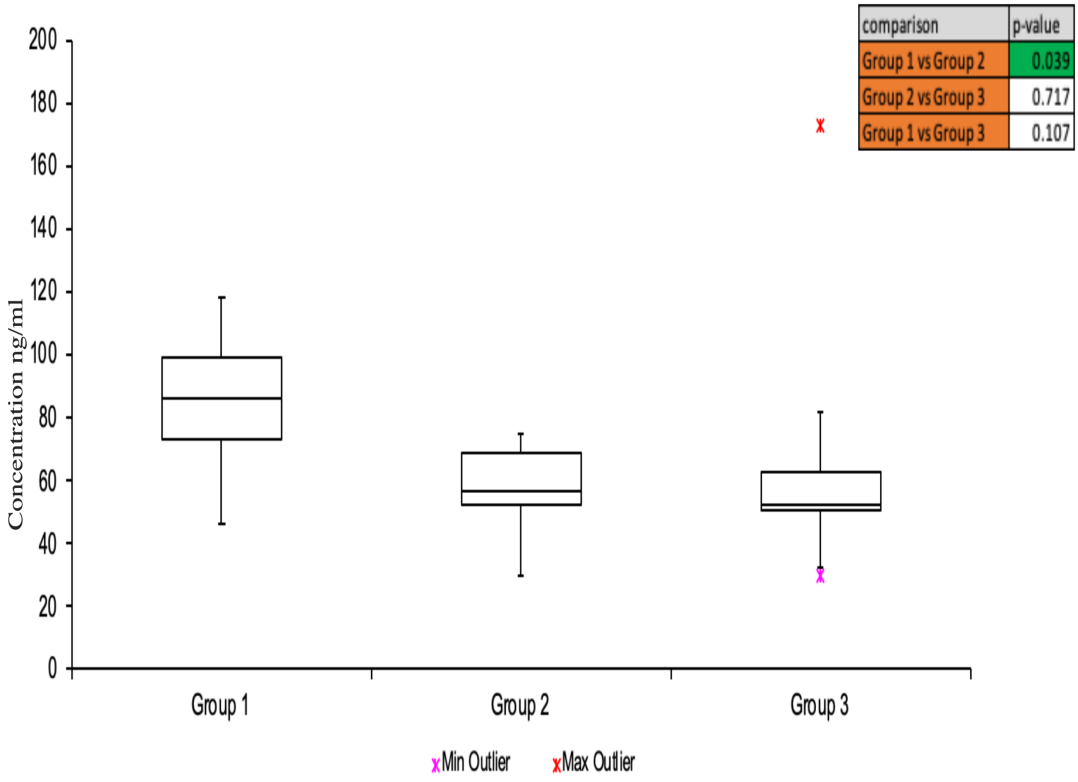

Figure 7.6: Box and Whisker Plot for IL-1α abundance in AML serum samples.

Shown is a box and whisker plot from Luminex analysis carried out using AML serum samples from favourable, intermediate and adverse prognostic risk groups for IL-1α. Green indicates statistical significance ($p \leq 0.05$).

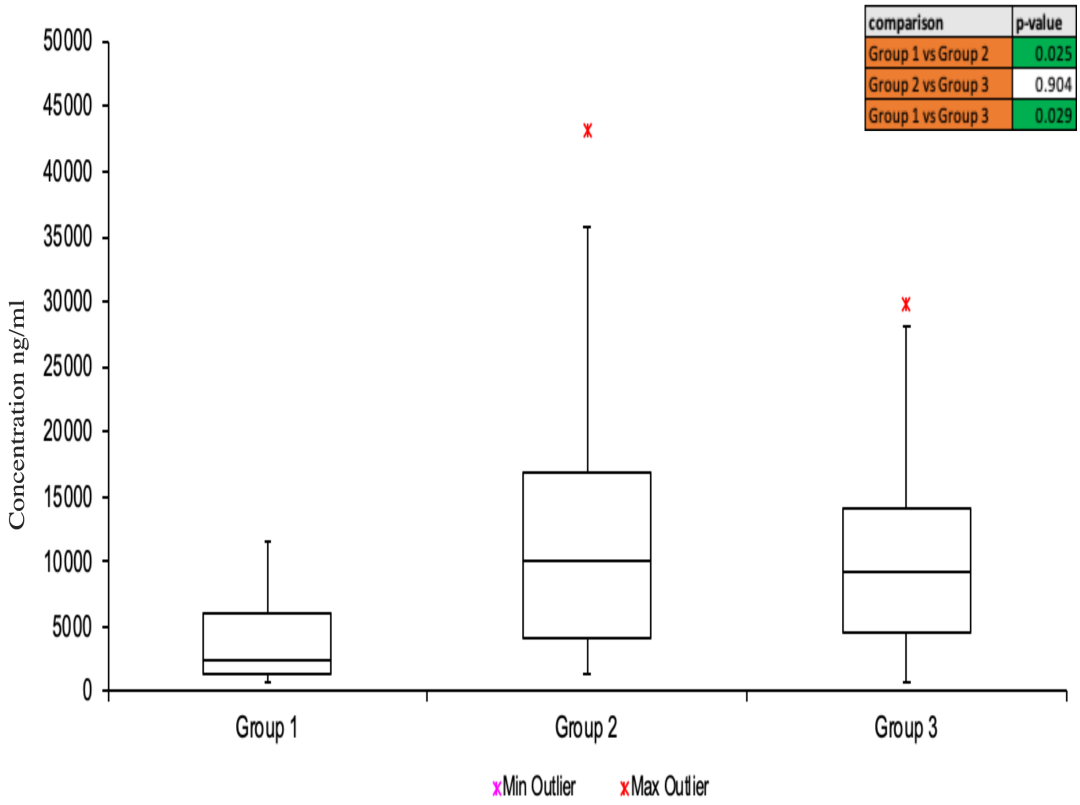

Figure 7.7: Box and Whisker Plot for SDF1αβ abundance in AML serum samples.

Shown is a box and whisker plot from Luminex analysis carried out using AML serum samples from favourable, intermediate and adverse prognostic risk groups for SDF1Aβ. Green indicates statistical significance ($p \leq 0.05$). There are no minimum observed in the changed abundance of SDF1Aβ.

7.3 Discussion

AML is a heterogeneous disorder, caused by the abnormal proliferation and differentiation of a clonal population of myeloid stem cells, due to the production of chimeric proteins which alter normal maturation of myeloid precursor cells. 97% of AML patients present genetic abnormalities (Patel et al., 2012), the prevalence of which led to the ELN classification system for prognostic determination. The formation of these grouping guidelines led to more efficient diagnosis of AML and faster determination of treatment course for patients.

With little proteomic analysis carried out for AML, the identification of potential protein biomarkers for disease diagnosis, treatment response, prognosis and progression is a novel area with much needed work. The in-depth analysis of both lysed AML cell samples by label-free LC-MS/MS and AML serum samples by Luminex technologies revealed multiple potential target proteins with altered abundance across favourable group 1, intermediate group 2 and adverse group 3. The LC-MS/MS analysis revealed the potential of multiple markers with altered abundance between each prognostic risk groups. The 65 statistically significant, differentially abundant proteins in favourable to adverse groups revealed the increased abundance of Receptor-type tyrosine-protein phosphatase C from group 1 to group 3, with a fold increase of 1.978 (Table 7.5). Receptor-type tyrosine-protein phosphatase C is a tyrosine-protein phosphatase essential for T-cell activation, acting as a positive regulator of T-cell coactivation after binding to Dipeptidyl peptidase 4 (Charbonneau et al., 1988). The increased abundance of Transcription intermediary factor 1-beta was recorded in group 3 in comparison to group 1, with a fold increase of 6.954 (Table 7.5). Transcription intermediary factor 1-beta has previously been noted as being required for the transcriptional repressor activity of FOXP3 and has been observed as functionally supressing regulator T-cells (Huang et al., 2013). Interestingly, transcription intermediary factor 1-beta has been implicated in the progressive

chronic lymphocytic leukaemia (Huang et al., 2016), indicating a similarity between the two haematological malignancies. The 18 statistically significant, differentially abundant proteins when comparing group 1 and group 2 revealed a differing proteomic signature between favourable and intermediate AML prognostic risk groups (Table 7.6). Spectrin alpha chain, non-erythrocytic 1 was noted as being increased in abundance in favourable prognostic group in comparison to intermediate prognostic group, with a fold increase of 2.263. Spectrin alpha chain, non-erythrocytic 1 is noted as being a significant component of neuronal cytoskeletal and has been previously implicated in atypical chronic myeloid leukaemia in patients presenting with t(1;9)(p34;q34) aberration (Sheng et al., 2017). Carbonic anhydrase 1 was noted as being significantly increased in group 2 in comparison to group 1, exhibiting a 5.218 fold abundance increase. Carbonic anhydrase 1 (CA1) is a cytoplasmic protein. It is the most abundant of the CA family in adult red blood cells (Pocker and Sarkanen, 1978) and has been linked to hypertension. Decreased abundance is also linked to anaemia and type Ⅱ diabetes (Gambhir et al., 2007), with CA Ⅸ and CA Ⅻ having already been identified as biomarkers for disease diagnosis, staging and progression in multiple cancer types (Zamanova et al., 2019). Of the 41 statistically significant proteins with altered abundance between group 2 and group 3 (Intermediate and adverse) the proteins with the most drastically altered abundance are DNA-dependent protein kinase catalytic subunit, with an 11.978 fold increase from group 2 to group 3, and Haemoglobin subunit delta, with a noted fold increase of 8.187 from group 3 to group 2 (Table 7.7). DNA-dependent protein kinase catalytic subunit (DNA-PK) is a serine/threonine-protein kinase which exhibits molecular sensor like functions for DNA damage, high levels of which have been implicated in breast cancer (Zhang et al., 2019b), gastric cancer (Zhang et al., 2019a) and radiation resistance in thyroid cancer (Ihara et al., 2019). Haemoglobin subunit delta is involved in the transport of oxygen to the lungs and other peripheral tissue.

The analysis of serum samples using Luminex technologies, in conjunction with MILLIPLEX® MAP Kits, lead to the identification of 4 potential, already established, biomarkers by using targeted analysis. Interleukin 17A, a pro-inflammatory cytokine encoded by the IL-17A gene and secreted by Th17/CD4+/CD8+ cells (Parker, et al., 2015) is reported to exhibit significant concentration differences between AML and normal cells, indicating a pathophysiological significance for AML (Abousamra, et al., 2013). IL-17A acts as a hematopoietic stimulatory cytokine, aiding blast development and the proliferation of neutrophils. It has also been observed functioning in T-cell mediated angiogenesis and shows evidence promoting MDSC formation (Yazawa, et al., 2013). A statistically significant increase of IL-17A was recorded from both group 1 vs group 3 and group 2 vs group 3, with p=0.025 and 0.03 respectively (Figure 7.5). Notably, group 3 has the lowest average concentration value and hence poorest prognosis, correlating with findings that IL-17A abundance is increased with favourable prognosis/survival rate (Abousamra, et al., 2013). Interleukin-1 receptor antagonist is an IL-1 family member protein encoded by the ILR1N gene (Arend, et al., 1998). IL-1RA non-productively binds to the cell surface interleukin-1 receptor (IL-1R), inhibiting IL-1α/IL-1β interaction with IL-1R. This prevents downstream signalling cascade initiation and other agonistic activities that provoke inflammation and chronic diseases (Carter, et al., 1990). It has been observed that IL-1RA can stimulate suppression of AML blast replication in the presence of various growth factors and reduction of GM-CSF in AML cells (Estrov, et al., 1992). A statistically significant increased abundance of IL-1RA is noted in group 2, in comparison to group 1, with p=0.039. Interestingly, this statistical significance is not noted in either of the comparisons from group 2 to group 3 or group 1 to group 3. The increased abundance of IL-1RA may be attributed to an attempt to regain cell differentiation/proliferation control by the immune system. Interleukin-1α is an interleukin-1 family cytokine encoded by the IL-1A gene with immune and haematopoietic functions and is produced by macrophages, neutrophils, endothelial and epithelial cells (Bankers-

Fulbright, et al., 1996). In most AML cases, the pro-inflammatory cytokines IL-1α and IL-1β inhibit normal progenitor growth while eliciting abnormal growth of blasts (Cozzolino, et al., 1989). IL-1α improves p38 MAPK phosphorylation while stimulating growth factor and inflammatory cytokine secretion to promote AML cell development (Carey, et al., 2017). A statically significant increase in the abundance of IL-1α from group 1 in comparison to group 2, where p=0.039, suggests IL-1α may be necessary for favourable prognostic risk stratification in AML.

Encoded by the CXCL12 gene, SDF-1 alpha and beta (CXCL12) are commonly expressed cytokines in many tissue/cell types (Janowski, 2009). CXCL12 binding to CXCR4 activates intracellular signalling events which initiate chemotaxis, proliferation, cell survival and kick-starts gene transcription. CXCR4 is expressed on numerous cell types including lymphocytes and haemopoietic stem cells (HSCs) (Moore et al., 2017). In the immune system, the binding of CXCL12 to CXCR4 induces intracellular signalling through several divergent pathways (phospholipase C, MAPK, and PI3K-Akt-mTOR), pathways involved in chemotaxis, cell survival, cell proliferation and gene transcription. CXCR4 is expressed on multiple cell types including lymphocytes, hematopoietic stem cells, endothelial and epithelial cells, together with cancer cells, where the ligand/receptor complex is involved in tumour progression, angiogenesis, metastasis, and survival. Upregulation of CXCL12 by hypoxia also occurs during cancer development to promote angiogenesis, as has been demonstrated for ovarian cancer (Kryczek et al., 2005). Recently, it was reported that 56.7% of pancreatic cancer tissues, 50.0% of para-cancerous tissues, and 53.3% of pancreas surrounding lymph nodes express CXCR4 compared to 18.3% of the normal pancreatic tissues using immunohistochemistry data (Zhang et al., 2018). Analysis of breast cancer data sets uncovered a role for CXCL12 over-expression correlating with better prognosis in breast cancer (Liu et al., 2018). Additionally, higher CXCL12/SDF1 expression was related to positive ER status, negative HER2 status and small tumour size. The bone marrow microenvironment

facilitates the survival, differentiation, and proliferation of both normal and malignant hematopoietic cells. Bone marrow factors produced, such as CXCL12, mediate homing, survival and proliferation of tumour cells. Integrin-mediated adhesion sequesters tumour cells to this niche, as exemplified in acute lymphoid leukaemia and acute myeloid leukaemia (Juarez et al., 2007); (Nervi et al., 2009)). The chemokine receptor CXCR4 facilitates cell anchorage in the bone marrow microenvironment and is overexpressed in 25–30% of patients with AML (Spoo et al., 2007). Lately, researchers have shown how a new CXCR4 receptor antagonist IgG1 antibody (PF-06747143) binds strongly to AML cell lines and to AML primary cells inhibiting their chemotaxis in response to CXCL12 (Zhang et al., 2017). Previously, Rombouts and co-workers found that patients with a high CXCR4 expression in the CD34+ subset of cells have a significantly reduced overall survival and have a greater risk of leukaemia relapse (Rombouts et al., 2004). This data supports the role for CXCL12 in the risk profile associated with different cohorts of AML patients, and the increase in CXCL12 found in the adverse risk group in this study (serum levels) and the increase in metabolism seen at the cellular level in the adverse risk group. Schelker and colleagues demonstrated that human mesenchymal stromal cells (MSC) are effective feeder cells, able to maintain AML cells in long-term culture, due in part to key molecules (including TGF-β1 and CXCL12) that are important for intercellular communication within the niche (Schelker et al., 2018). Blockade of the CXCL12 pathway (using a commercially available CXCR4 antagonist (plerixafor)) modulated AML cell proliferation and chemotherapy resistance.

Although AML is a different haematological malignancy to MM, the same proteomic techniques can be utilised to identify disease changes and potential biomarkers. As stated above, a plethora of potential biomarkers have been identified by the use of label-free LC-MS/MS and a targeted approach using Luminex technologies, which can be used in conjunction with the prognostic risk classification improving patient

diagnosis rates, increasing speed to treatment and reducing uncertainty within prognostic grouping.

Chapter 8

General Discussion

8.1 Discussion

Haematological malignancies are typically based on four broad categories: Leukaemia, Hodgkin's lymphoma, non-Hodgkin's lymphoma and myeloma, and account for approximately 9% of all cancers diagnosed yearly (Smith et al., 2011). As the fourth most commonly diagnosed cancer type worldwide, in both men and women, approximately 1,186,598 people were diagnosed with one of the aforementioned categories in 2018 alone (Bray et al., 2018). Of this figure, MM was reported to be diagnosed approximately 159,985 times. As haematological malignancies are considered complex cancers, diagnosis must be carried out using a multitude of differing techniques including histology, cytology, immunophenotyping and cytogenetics, to name but a few (Sabattini et al., 2010).

The use of proteomic analysis to determine individual protein signatures to understand disease was utilised in Chapter 3, where label-free LC-MS/MS technology was combined with commonly used bioinformatic software to determine unique proteomic signatures to help determine the molecular mechanisms with which drug resistance occurs. A cohort of 35 MM patients were used to determine a drug sensitivity score for each of six established/investigational drugs. These patients were then grouped into the ten most sensitive and ten least sensitive to each individual drug. After bioinformatic analysis of the established groups, a clear link between drug resistance and the focal adhesion pathway became clear for four of the six drugs tested. Bortezomib, Carfilzomib, Quizinostat and PF-04691502 all exhibited a statistically significant increased abundance in proteins related to the focal adhesion pathway, namely Vinculin, Talin-1, Integrin β3 and Filamin-A (Figure 8.1). All of the aforementioned proteins interact in the focal adhesion pathway, with downstream activation of actin polymerization. The activation of this section of the focal adhesion pathway subsequently leads to cell motility.

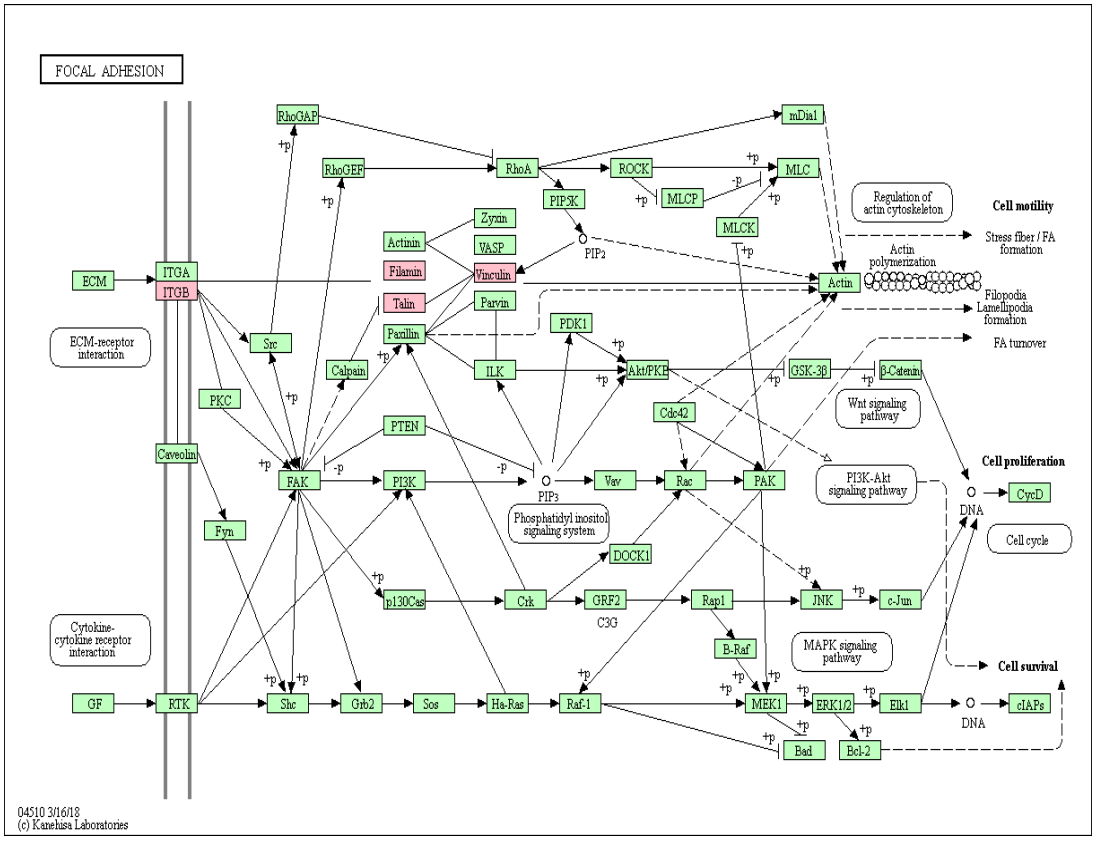

Figure 8.1: Focal Adhesion Pathway

Depicted is the focal adhesion pathway with highlighted (in pink) the proteins observed to have an increased abundance in the least sensitive patients to Bortezomib, Carfilzomib, Quizinostat and PF-04691502, discussed in Chapter 3.

Further investigation into the peptides identified by LC-MS/MS revealed multiple interesting potential targets indicating drug resistance, such as CD44 and CD68. The abundance of both potential targets, along with Vinculin, Talin-1 and Integrin β3 was further investigated using immunohistochemistry on patient bone marrow trephines. Both CD44 and CD68 showed an increased abundance in active MM, in comparison to other disease stages, indicating a role in disease homeostasis.

Phosphoproteomics is an area of great interest for understanding cancer and its survival enhancing molecular mechanisms. The manipulation of the phosphorylation “on/off’ switch, which is observed in a multitude of different cancers, aids in cancer survival and proliferation (Ardito et al., 2017). To examine this manipulation in MM, Chapter 4 involved the enrichment of 32 CD138+ lysed cells for phosphopeptides. These enriched samples were analysed using label-free LC-MS/MS, in combination with commonly used bioinformatic software, to determine unique phosphoproteomic signatures for drug resistant MM patients. With the combination of quantitative and qualitative proteomic approaches, it became clear that the manipulation of phosphorylation is used to drive drug resistance in the non-responding patients to treatment. In a direct comparison between Group 1 (drug sensitive patients) and Group 4 (drug resistant patients), the increased abundance of one particular phosphorylation site in TCP4, 118 Phosphoserine residue, was observed as significantly increased in Group 1 patients. This particular phosphorylation site has a decreased abundance in the resistant cohort of patients, leading to the increased activation of dsDNA-binding and its cofactor function in Group 4 patients. A Human Phospho-Kinase array was used to identify further phosphorylation residues with a changed abundance in drug resistance. HSP27 phosphoserine 78 was identified as having an increased abundance in Group 4 patients in comparison to Group 1 patients, indicating that increased phosphorylation of HSP27 at serine 78 is helping to drive drug resistance in MM patients.

In combining the information obtained from Chapter 3 and Chapter 4, it becomes apparent that MM uses multiple molecular mechanisms to develop drug resistance against multiple established/investigational drugs. In resistance against Bortezomib, Carfilzomib, Quizinostat and PF-04691502, the least sensitive patients exhibit an increased abundance of a combination of focal adhesion related proteins, all of which combine for downstream actin production activation. Phosphorylation events were also observed to drive drug resistance in this cohort of patients, such as increased

phosphorylation of phosphoserine 78 in HSP27 and decreased phosphorylation of phosphoserine 118 in TCP4. The combination of this information, along with drug sensitivity screens carried out on CD138+ MM cells in patients allows the identification of drug resistance in patients before starting a treatment regime (Figure 8.2). The combination of these sample analysis techniques is predicted to allow more informed clinical decisions to be made about treatment, ensuring better outcomes for patients and eventually increased OS.

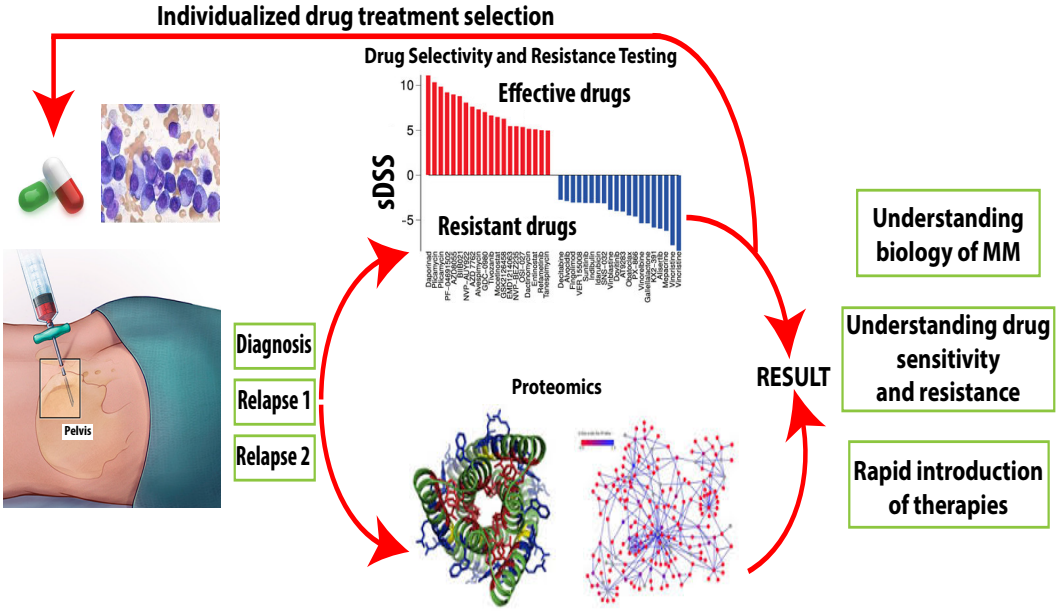

Figure 8.2: Workflow for Personalised Course of Treatment Combining DSS and Proteomic Approaches.

Depicted is the workflow for combining the drug sensitivity screening approaches, developed by the Institute of Molecular Medicine, Helsinki, Finland (Majumder et al., 2017), and proteomic approaches established in chapter 3 and 4 for the development of personalised treatment for individual patients depending on their proteomic profile and DSS score.

Although saliva has been considered the mirror of the body, minimal research has been carried out in the area of salivaomics. Approximately 3000 differentially abundant proteins have previously been identified in the salivary proteome (Grassl et al., 2016), and thus, saliva is a biofluid with huge disease marker potential. Chapter 5 explores the differentially abundant proteins present in saliva during MM disease progression, from pre-malignant MGUS to malignant newly diagnosed MM and from newly diagnosed MM to remission in patients. Through label-free LC-MS/MS and bioinformatic analysis, six statically significant proteins were identified with altered abundance from MGUS to MM. Of these six proteins, in-depth validation was carried out with focus on the increased abundance of FABP5 from MGUS to MM and through disease progression. The increased abundance of this protein was identified using immunoblotting (MGUS to newly diagnosed comparison) and ELISA (disease progression analysis using serial samples). Further analysis of this change in abundance of FABP5 was carried out using immunohistochemical techniques in BMTs of MGUS and newly diagnosed MM patients. The increase in abundance of FABP5 was observed in the BM microenvironment, with a non-existent presence in MGUS BM and a visible abundance in newly diagnosed MM. As BM is considered the gold standard of MM diagnosis, the change in abundance of FABP5 in the BM microenvironment further validates FABP5 potential as a salivary biomarker for disease progression in MM. The potential of this biomarker does not eradicate the need for BM samples to be taken but could be used alongside this diagnostic sample as an indicator for the need for re-staging of MM patients and monitoring disease progression. The identification of β2-microglobulin within patient saliva via label-free LC-MS/MS analysis further evaluates the use of saliva as a source of potential biomarkers. β2-microglobulin is considered an important biomarker for MM, which is already established and integrated into CRAB criteria for diagnosis. Used in diagnosis and staging of MM, the identification of β2-microglobulin within the saliva of patient samples is an extremely important finding.

Intravenous RVD (Lenalidomide, Bortezomib and Dexamethasone) is considered as a standard treatment regime for all MM patients, regardless of diagnosis, prognosis or general health (Roussel et al., 2014). Although the worldwide use of this three-drug combination is standard practice, a multitude of adverse side effects have been strongly linked to the intravenous administration of Bortezomib. These side effects include vomiting, diarrhoea, anaemia, thrombocytopenia (a low blood platelet count), leukopenia (reduction in white blood cell count) and peripheral neuropathy (Richardson et al., 2009). In the hopes of eradicating these adverse side effects, a multicentre clinical trial has been established with the administration of Bortezomib through subcutaneous tissue as opposed to through IV. Chapter 6 examines the proteomic profile of 70 samples from this Phase Ⅱ clinical trial, obtained from the Dana Farber Cancer Institute, Boston. The use of three multiplex assays allowed the identification of trends exhibited by patients with a targeted approach. This proteomic approach included the use of MILLIPLEX® MAP Kit: Human Cytokine/Chemokine Magnetic Bead Panel Ⅰ, MILLIPLEX® MAP Kit: Human Cytokine/Chemokine Panel Ⅱ and MILLIPLEX® MAP Kit: Human Circulating Cancer Biomarker Magnetic Bead Panel 4, analysed using Luminex technologies. Of the 62 potential targets included in these multiplex assays, five proteins were identified as showing significant trends across patients enrolled in the trial. CD44 showed a spike in abundance in patients with partial response to treatment, 2 of which withdrew from the clinical trial due to disease progression. This observed increase in abundance correlates with the findings in immunohistochemistry in Chapter 3, where an increased abundance was observed in the BMT of active MM in comparison to other disease states. This correlation leads to the prediction that CD44 is more highly abundant in patients with active disease or partial response to treatment and therefore may be considered a predictive biomarker for disease progression or lack of satisfactory response to

Bortezomib treatment. This finding was also observed in a study by Ohwada et al., who established a link between increased CD44 and disease progression associated with Bortezomib treatment in MM. The most significant finding of the Rsq-VD proteomic analysis was a significant increase in the abundance of MIP-1α and its direct correlation to toxicity in patients enrolled in this clinical trial. Each of the three patients included in the clinical trial with toxicity exhibited a significantly increased abundance of MIP-1α. All other patients included in the trial showed a minimum abundance of MIP-1α. This finding is considered extremely important as it indicates that MIP-1α may play a direct role in the development of adverse side effects. The potential to monitor a patients well-being during treatment, using a biomarker specific for adverse side effects, is highly sought after. Moreover, MIP-1α has previously been implicated in MM, exhibiting links to poorer prognosis than patients with a low level abundance of MIP-1α (Terpos et al., 2005), along with the observation that MIP-1α promotes cell proliferation in MM cell lines (Lentzsch et al., 2003) and promotes drug resistance in MM (Tsubaki et al., 2016). The finding that MIP-1α is directly correlated with the development of adverse side effects has previously been observed, linking this with ERK1/2, Akt and mTOR inhibition (Tsubaki et al., 2018).

Acute myeloid leukaemia (AML) is attributed to the abnormal differentiation and proliferation of myeloid stem cells. This proliferation leads to the formation of chimeric proteins which alter the normal maturation of myeloid precursor cells (De Kouchkovsky and Abdul-Hay, 2016). This further leads to the accumulation of malignant myeloid cells in the BM and peripheral blood. To date, a minimal amount of proteomic analysis has been carried out in AML. Chapter 7 is comprised of the discovery (40 lysed cell samples) and targeted (49 serum samples) proteomic analysis of AML samples from patients with differing prognostic risk grouping. This grouping ranges from favourable Group 1, Intermediate Group 2 and Adverse Group 3. Discovery analysis was carried out using label-free LC-MS/MS in combination with

a variety of bioinformatic techniques. This analysis revealed 65 statistically significant, differentially abundant proteins when comparing Favourable prognosis to Adverse prognosis, 18 statistically significant, differentially abundant proteins from Favourable to Intermediate prognosis and 41 statistically significant, differentially abundant proteins from Intermediate to Adverse prognosis. Interestingly, an increased abundance has been noted in Intermediate patients in comparison to Adverse patients of Transgelin-2. Transgelin-2 had an increased abundance in chapter 5 from MGUS to MM and an increased abundance was observed in the least sensitive patients after treatment with Bortezomib and Carfilzomib in chapter 3. Transgelin-2 is an actin-binding protein with a basic function of regulating the actin cytoskeleton through actin binding, stabilizing actin filaments. This regulation is involved in cell proliferation, differentiation apoptosis and migration related to cytoskeleton remodelling (Dvorakova et al., 2014). Transgelin-2 has been observed as being highly abundant in BM mesenchymal stem cells (MSCs) showing links to proliferation and differentiation of these MSCs (Kuo et al., 2011) and has previously been implicated in B-cell chronic lymphocytic leukaemia and B-cell lymphoma, suggesting that Trangelin-2 plays a significant role in B cell development (Gez et al., 2007). Evidence of an increased abundance of Transgelin-2 in patient saliva from MGUS to MM and in drug resistant groups after treatment with bortezomib and carfilzomib further links trangelin-2 and B-cell development, specifically monoclonal B-cells. The transcriptional and translational alteration of Transgelin-2 has been identified as playing a role in a plethora of different cancer types, with the increased abundance noted in tumour-derived lung cancer endothelial cells and lung cancer tissue. This increased abundance directly correlated with tumour size, clinical stage and histological neural invasion (Jin et al., 2016). It was also observed that Transgelin-2 suppression inhibited cancer cell migration and proliferation in uterine cancer squamous cell carcinoma (Fukushima et al., 2011). The increased abundance of Transgelin-2 has been observed to play a role in chemoresistance in two specific

chemotherapies, methotrexate and paclitaxel (Chen et al., 2004), with the suppression of Transgelin-2 resulting in restored sensitivity to the treatment, while leading to inhibited invasion, migration and proliferation (Cai et al., 2014). The analysis of the targeted proteomic approach, carried out using the three multiple assays mentioned in chapter 7 on 49 serum samples, revealed 4 potential biomarkers of interest. The most interesting of these 4 potential biomarkers was SDF-1. SDF-1 has previously been implicated in AML OS, with patients showing an increased abundance of SDF-1αβ correlating with reduced OS and greater risk of leukaemia relapse .

8.1.1 Concluding Remarks and Future Direction

"OMIC" based technologies have become the future of patient monitoring, diagnostics and prognosis. With disease prevalence increasing in the modern era, proteomics and the study of altered protein abundances in disease has the potential to increase OS, identify potential drug targets, develop predictive biomarkers for varying disease states and give a better understanding of disease and its molecular mechanisms. Here we analysed a multitude of patients samples with different haematological malignancies using standard proteomic approaches, to identified predictive markers, aiding in the treatment and diagnosis of both MM and AML. In the analysis of drug resistant patient samples, we identified multiple different predictive markers for drug resistance to four established/investigational treatments. These predictive biomarkers included Vinculin, Talin-1, Filamin A and Integrin β3, all of which interact within the focal adhesion pathway. CD44 and CD68 were also identified as having the potential to monitor drug resistance. Multiple different phosphorylation sites were also identified as playing a role in drug resistance across four groups scored from sensitive to resistant, namely Activated RNA polymerase II transcriptional coactivator p15 118 phosphoserine and heat shock protein 27

phosphoserine 78. The evaluation of saliva as a potential biofluid for MM disease progression identified multiple potential targets with altered abundance, with focus on FABP5. It was determined that FABP5 exhibits an increased abundance in saliva throughout disease progression in MM, revealing saliva as a source of potential biomarkers. Subcutaneous bortezomib, along with lenalidomide and dexamethasone, is predicted to be the optimum administration method for the three-drug based regime. The evaluation of patient serum from this clinical trial identified potential markers for disease progression (CD44) and adverse side effects (MIP-1α) from subcutaneous Bortezomib. Multiple isoforms of Interleukin, along with stromal derived growth factor 1 were identified as potential biomarkers to aid in prognostic risk grouping in AML. To conclude, proteomic approaches to sample analysis provides a huge amount of information regarding disease, along with holding the potential to predict drug resistance, disease progression, treatment outcome, prediction of treatment side effects and relevant diagnostic biomarkers for both MM and AML.

Future work would involve further validation of the identified potential biomarkers throughout this project. A more extensive patient cohort would be needed to truly verify these findings as biomarkers population-wide. 308 compounds, both investigational and established, were used to group patients into drug sensitive to drug resistant cohorts, with in-depth proteomic analysis carried out on six of the 308 compounds. Analysis of the 302 compounds to identify potential biomarkers for drug resistance in the remaining compounds is future work of interest. Further immunohistochemistry, including CD138 staining to identify plasma cells, is essential future work to verify the increased abundance of potential targets expressed by mutated plasma cells. Saliva samples have been collected alongside the serum samples from the multicentre clinical trial. Proteomic analysis of these saliva samples to identify potential biomarkers for disease response, disease progression and adverse side effects to the Rsq-VD trial is an area of great interest as further

validation for the use of saliva as a biomarker source. The research presented in this thesis has provided the first steps to marker discovery for both MM and AML, with further work being required before these markers can be considered for clinical use.

Chapter 9

Bibliography

Anderson, K. C., R. A. Kyle, S. V. Rajkumar, A. K. Stewart, D. Weber, P. Richardson, and A. F. P. o. C. E. i. M. Myeloma, 2008, Clinically relevant end points and new drug approvals for myeloma: Leukemia, v. 22, p. 231-9.

Aquino, V. M., 2002, Acute myelogenous leukemia: Curr Probl Pediatr Adolesc Health Care, v. 32, p. 50-8.

Arber, D. A., A. Orazi, R. Hasserjian, J. Thiele, M. J. Borowitz, M. M. Le Beau, C. D. Bloomfield, M. Cazzola, and J. W. Vardiman, 2016, The 2016 revision to the World Health Organization classification of myeloid neoplasms and acute leukemia: Blood, v. 127, p. 2391-405.

Ardito, F., M. Giuliani, D. Perrone, G. Troiano, and L. Lo Muzio, 2017, The crucial role of protein phosphorylation in cell signaling and its use as targeted therapy (Review): Int J Mol Med, v. 40, p. 271-280.

Argyriou, A. A., G. Iconomou, and H. P. Kalofonos, 2008, Bortezomib-induced peripheral neuropathy in multiple myeloma: a comprehensive review of the literature: Blood, v. 112, p. 1593-9.

Attal, M., V. Lauwers-Cances, C. Hulin, X. Leleu, D. Caillot, M. Escoffre, B. Arnulf, M. Macro, K. Belhadj, L. Garderet, M. Roussel, C. Payen, C. Mathiot, J. P. Fermand, N. Meuleman, S. Rollet, M. E. Maglio, A. A. Zeytoonjian, E. A. Weller, N. Munshi, K. C. Anderson, P. G. Richardson, T. Facon, H. Avet-Loiseau, J. L. Harousseau, P. Moreau, and I. Study, 2017, Lenalidomide, Bortezomib, and Dexamethasone with Transplantation for Myeloma: N Engl J Med, v. 376, p. 1311-1320.

Baba, T., K. Naka, S. Morishita, N. Komatsu, A. Hirao, and N. Mukaida, 2013, MIP-1α/CCL3-mediated maintenance of leukemia-initiating cells in the initiation process of chronic myeloid leukemia: J Exp Med, v. 210, p. 2661-73.

Bain, B. J., 2001a, Bone marrow aspiration: J Clin Pathol, v. 54, p. 657-63.

Bain, B. J., 2001b, Bone marrow trephine biopsy: J Clin Pathol, v. 54, p. 737-42.

Barbee, M. S., R. D. Harvey, S. Lonial, J. L. Kaufman, N. M. Wilson, T. McKibbin, D. A. Hutcherson, M. Surati, K. Valla, and K. S. Shah, 2013, Subcutaneous versus intravenous bortezomib: efficiency practice variables and patient preferences: Ann Pharmacother, v. 47, p. 1136-42.

Barber, T. D., B. Vogelstein, K. W. Kinzler, and V. E. Velculescu, 2004, Somatic mutations of EGFR in colorectal cancers and glioblastomas: N Engl J Med, v. 351, p. 2883.

Barford, D., 1996, Molecular mechanisms of the protein serine/threonine phosphatases: Trends Biochem Sci, v. 21, p. 407-12.

Becker, N., 2011, Epidemiology of multiple myeloma: Recent Results Cancer Res, v. 183, p. 25-35.

Ben-Chetrit, E., D. Flusser, and Y. Assaf, 1984, Severe bleeding complicating percutaneous bone marrow biopsy: Arch Intern Med, v. 144, p. 2284.

Bennett, J. M., D. Catovsky, M. T. Daniel, G. Flandrin, D. A. Galton, H. R. Gralnick, and C. Sultan, 1991, Proposal for the recognition of minimally differentiated acute myeloid leukaemia (AML-MO): Br J Haematol, v. 78, p. 325-9.

Betgovargez, E., V. Knudson, and M. H. Simonian, 2005, Characterization of proteins in the human serum proteome: J Biomol Tech, v. 16, p. 306-10.

Bollag, G., J. Tsai, J. Zhang, C. Zhang, P. Ibrahim, K. Nolop, and P. Hirth, 2012, Vemurafenib: the first drug approved for BRAF-mutant cancer: Nat Rev Drug Discov, v. 11, p. 873-86.

Bray, F., J. Ferlay, I. Soerjomataram, R. L. Siegel, L. A. Torre, and A. Jemal, 2018, Global cancer statistics 2018: GLOBOCAN estimates of incidence and mortality worldwide for 36 cancers in 185 countries: CA Cancer J Clin, v. 68, p. 394-424.

Buccisano, F., L. Maurillo, M. I. Del Principe, G. Del Poeta, G. Sconocchia, F. Lo-Coco, W. Arcese, S. Amadori, and A. Venditti, 2012, Prognostic and therapeutic implications of minimal residual disease detection in acute myeloid leukemia: Blood, v. 119, p. 332-41.

Büchner, T., R. F. Schlenk, M. Schaich, K. Döhner, R. Krahl, J. Krauter, G. Heil, U. Krug, M. C. Sauerland, A. Heinecke, D. Späth, M. Kramer, S. Scholl, W. E. Berdel, W. Hiddemann, D. Hoelzer, R. Hehlmann, J. Hasford, V. S. Hoffmann, H. Döhner, G. Ehninger, A. Ganser, D. W. Niederwieser, and M. Pfirrmann, 2012, Acute Myeloid Leukemia (AML): different treatment strategies versus a common standard arm--combined prospective analysis by the German AML Intergroup: J Clin Oncol, v. 30, p. 3604-10.

Cai, J., S. Chen, W. Zhang, S. Hu, J. Lu, J. Xing, and Y. Dong, 2014, Paeonol reverses paclitaxel resistance in human breast cancer cells by regulating the expression of transgelin 2: Phytomedicine, v. 21, p. 984-91.

Califf, R. M., 2018, Biomarker definitions and their applications: Exp Biol Med (Maywood), v. 243, p. 213-221.

Canella, A., H. Cordero Nieves, D. W. Sborov, L. Cascione, H. S. Radomska, E. Smith, A. Stiff, J. Consiglio, E. Caserta, L. Rizzotto, N. Zanesi, V. Stefano, B. Kaur, X. Mo, J. C. Byrd, Y. A. Efebera, C. C. Hofmeister, and F. Pichiorri, 2015, HDAC inhibitor AR-42 decreases CD44 expression and sensitizes myeloma cells to lenalidomide: Oncotarget, v. 6, p. 31134-50.

Cao, Y., T. Luetkens, S. Kobold, Y. Hildebrandt, M. Gordic, N. Lajmi, S. Meyer, K. Bartels, A. R. Zander, C. Bokemeyer, N. Kröger, and D. Atanackovic, 2010, The

cytokine/chemokine pattern in the bone marrow environment of multiple myeloma patients: Exp Hematol, v. 38, p. 860-7.

Carvajal-Hausdorf, D. E., K. A. Schalper, L. Pusztai, A. Psyrri, K. T. Kalogeras, V. Kotoula, G. Fountzilas, and D. L. Rimm, 2015, Measurement of Domain-Specific HER2 (ERBB2) Expression May Classify Benefit From Trastuzumab in Breast Cancer: J Natl Cancer Inst, v. 107.

Catherman, A. D., O. S. Skinner, and N. L. Kelleher, 2014, Top Down proteomics: facts and perspectives: Biochem Biophys Res Commun, v. 445, p. 683-93.

Chang, M. J., F. Zhong, A. R. Lavik, J. B. Parys, M. J. Berridge, and C. W. Distelhorst, 2014, Feedback regulation mediated by Bcl-2 and DARPP-32 regulates inositol 1,4,5-trisphosphate receptor phosphorylation and promotes cell survival: Proc Natl Acad Sci U S A, v. 111, p. 1186-91.

Chapman, M. A., M. S. Lawrence, J. J. Keats, K. Cibulskis, C. Sougnez, A. C. Schinzel, C. L. Harview, J. P. Brunet, G. J. Ahmann, M. Adli, K. C. Anderson, K. G. Ardlie, D. Auclair, A. Baker, P. L. Bergsagel, B. E. Bernstein, Y. Drier, R. Fonseca, S. B. Gabriel, C. C. Hofmeister, S. Jagannath, A. J. Jakubowiak, A. Krishnan, J. Levy, T. Liefeld, S. Lonial, S. Mahan, B. Mfuko, S. Monti, L. M. Perkins, R. Onofrio, T. J. Pugh, S. V. Rajkumar, A. H. Ramos, D. S. Siegel, A. Sivachenko, A. K. Stewart, S. Trudel, R. Vij, D. Voet, W. Winckler, T. Zimmerman, J. Carpten, J. Trent, W. C. Hahn, L. A. Garraway, M. Meyerson, E. S. Lander, G. Getz, and T. R. Golub, 2011, Initial genome sequencing and analysis of multiple myeloma: Nature, v. 471, p. 467-72.

Charbonneau, H., N. K. Tonks, K. A. Walsh, and E. H. Fischer, 1988, The leukocyte common antigen (CD45): a putative receptor-linked protein tyrosine phosphatase: Proc Natl Acad Sci U S A, v. 85, p. 7182-6.

Chen, X., H. Xie, B. L. Wood, R. B. Walter, J. M. Pagel, P. S. Becker, V. K. Sandhu, J. L. Abkowitz, F. R. Appelbaum, and E. H. Estey, 2015, Relation of clinical response and minimal residual disease and their prognostic impact on outcome in acute myeloid leukemia: J Clin Oncol, v. 33, p. 1258-64.

Chen, Y. X., X. Xie, and Q. Cheng, 2004, [cDNA microarray analysis of gene expression in acquired methotrexate-resistant of human choriocarcinoma]: Zhonghua Fu Chan Ke Za Zhi, v. 39, p. 396-9.

Cherry, B. M., N. Korde, M. Kwok, E. E. Manasanch, M. Bhutani, M. Mulquin, D. Zuchlinski, M. A. Yancey, I. Maric, K. R. Calvo, R. Braylan, M. Stetler-Stevenson, C. Yuan, P. Tembhare, A. Zingone, R. Costello, M. J. Roschewski, and O. Landgren, 2013, Modeling progression risk for smoldering multiple myeloma: results from a prospective clinical study: Leuk Lymphoma, v. 54, p. 2215-8.

Chipuk, J. E., T. Moldoveanu, F. Llambi, M. J. Parsons, and D. R. Green, 2010, The BCL-2 family reunion: Mol Cell, v. 37, p. 299-310.

Chistiakov, D. A., M. C. Killingsworth, V. A. Myasoedova, A. N. Orekhov, and Y. V. Bobryshev, 2017, CD68/macrosialin: not just a histochemical marker: Lab Invest, v. 97, p. 4-13.

Corral, L. G., P. A. Haslett, G. W. Muller, R. Chen, L. M. Wong, C. J. Ocampo, R. T. Patterson, D. I. Stirling, and G. Kaplan, 1999, Differential cytokine modulation and T cell activation by two distinct classes of thalidomide analogues that are potent inhibitors of TNF-alpha: J Immunol, v. 163, p. 380-6.

Courtney, K. D., R. B. Corcoran, and J. A. Engelman, 2010, The PI3K pathway as drug target in human cancer: J Clin Oncol, v. 28, p. 1075-83.

Crawford, J., M. K. Eye, and H. J. Cohen, 1987, Evaluation of monoclonal gammopathies in the "well" elderly: Am J Med, v. 82, p. 39-45.

Creutzig, U., M. M. van den Heuvel-Eibrink, B. Gibson, M. N. Dworzak, S. Adachi, E. de Bont, J. Harbott, H. Hasle, D. Johnston, A. Kinoshita, T. Lehrnbecher, G. Leverger, E. Mejstrikova, S. Meshinchi, A. Pession, S. C. Raimondi, L. Sung, J. Stary, C. M. Zwaan, G. J. Kaspers, D. Reinhardt, and A. C. o. t. I. B. S. Group, 2012, Diagnosis and management of acute myeloid leukemia in children and adolescents: recommendations from an international expert panel: Blood, v. 120, p. 3187-205.

Crosby, H. A., P. F. Lalor, E. Ross, P. N. Newsome, and D. H. Adams, 2009, Adhesion of human haematopoietic (CD34+) stem cells to human liver compartments is integrin and CD44 dependent and modulated by CXCR3 and CXCR4: J Hepatol, v. 51, p. 734-49.

Czarnecka, A. M., W. Solarek, A. Kornakiewicz, and C. Szczylik, 2016, Tyrosine kinase inhibitors target cancer stem cells in renal cell cancer: Oncol Rep, v. 35, p. 1433-42.

D'Amato, R. J., M. S. Loughnan, E. Flynn, and J. Folkman, 1994, Thalidomide is an inhibitor of angiogenesis: Proc Natl Acad Sci U S A, v. 91, p. 4082-5.

Dancey, J. E., 2006, Therapeutic targets: MTOR and related pathways: Cancer Biol Ther, v. 5, p. 1065-73.

De Kouchkovsky, I., and M. Abdul-Hay, 2016, 'Acute myeloid leukemia: a comprehensive review and 2016 update': Blood Cancer J, v. 6, p. e441.

de Weers, M., R. G. Mensink, M. E. Kraakman, R. K. Schuurman, and R. W. Hendriks, 1994, Mutation analysis of the Bruton's tyrosine kinase gene in X-linked agammaglobulinemia: identification of a mutation which affects the same codon as is altered in immunodeficient xid mice: Hum Mol Genet, v. 3, p. 161-6.

Demetri, G. D., A. T. van Oosterom, C. R. Garrett, M. E. Blackstein, M. H. Shah, J. Verweij, G. McArthur, I. R. Judson, M. C. Heinrich, J. A. Morgan, J. Desai, C. D. Fletcher, S. George, C. L. Bello, X. Huang, C. M. Baum, and P. G. Casali, 2006,

Efficacy and safety of sunitinib in patients with advanced gastrointestinal stromal tumour after failure of imatinib: a randomised controlled trial: Lancet, v. 368, p. 1329-38.

Döhner, H., E. Estey, D. Grimwade, S. Amadori, F. R. Appelbaum, T. Büchner, H. Dombret, B. L. Ebert, P. Fenaux, R. A. Larson, R. L. Levine, F. Lo-Coco, T. Naoe, D. Niederwieser, G. J. Ossenkoppele, M. Sanz, J. Sierra, M. S. Tallman, H. F. Tien, A. H. Wei, B. Löwenberg, and C. D. Bloomfield, 2017, Diagnosis and management of AML in adults: 2017 ELN recommendations from an international expert panel: Blood, v. 129, p. 424-447.

Döhner, H., E. H. Estey, S. Amadori, F. R. Appelbaum, T. Büchner, A. K. Burnett, H. Dombret, P. Fenaux, D. Grimwade, R. A. Larson, F. Lo-Coco, T. Naoe, D. Niederwieser, G. J. Ossenkoppele, M. A. Sanz, J. Sierra, M. S. Tallman, B. Löwenberg, C. D. Bloomfield, and E. LeukemiaNet, 2010, Diagnosis and management of acute myeloid leukemia in adults: recommendations from an international expert panel, on behalf of the European LeukemiaNet: Blood, v. 115, p. 453-74.

Dombret, H., and C. Gardin, 2016, An update of current treatments for adult acute myeloid leukemia: Blood, v. 127, p. 53-61.

Dowling, P., C. Hayes, K. R. Ting, A. Hameed, J. Meiller, C. Mitsiades, K. C. Anderson, M. Clynes, C. Clarke, P. Richardson, and P. O'Gorman, 2014a, Identification of proteins found to be significantly altered when comparing the serum proteome from Multiple Myeloma patients with varying degrees of bone disease: BMC Genomics, v. 15, p. 904.

Dowling, P., A. Holland, and K. Ohlendieck, 2014b, Mass Spectrometry-Based Identification of Muscle-Associated and Muscle-Derived Proteomic Biomarkers of Dystrophinopathies: J Neuromuscul Dis, v. 1, p. 15-40.

Dredge, K., R. Horsfall, S. P. Robinson, L. H. Zhang, L. Lu, Y. Tang, M. A. Shirley, G. Muller, P. Schafer, D. Stirling, A. G. Dalgleish, and J. B. Bartlett, 2005, Orally administered lenalidomide (CC-5013) is anti-angiogenic in vivo and inhibits endothelial cell migration and Akt phosphorylation in vitro: Microvasc Res, v. 69, p. 56-63.

Durie, B. G., and S. E. Salmon, 1975, A clinical staging system for multiple myeloma. Correlation of measured myeloma cell mass with presenting clinical features, response to treatment, and survival: Cancer, v. 36, p. 842-54.

Dvorakova, M., R. Nenutil, and P. Bouchal, 2014, Transgelins, cytoskeletal proteins implicated in different aspects of cancer development: Expert Rev Proteomics, v. 11, p. 149-65.

Estey, E. H., 2014, Acute myeloid leukemia: 2014 update on risk-stratification and management: Am J Hematol, v. 89, p. 1063-81.

Farrah, T., E. W. Deutsch, G. S. Omenn, Z. Sun, J. D. Watts, T. Yamamoto, D. Shteynberg, M. M. Harris, and R. L. Moritz, 2014, State of the human proteome in 2013 as viewed through PeptideAtlas: comparing the kidney, urine, and plasma proteomes for the biology- and disease-driven Human Proteome Project: J Proteome Res, v. 13, p. 60-75.

Fogel, M., P. Gutwein, S. Mechtersheimer, S. Riedle, A. Stoeck, A. Smirnov, L. Edler, A. Ben-Arie, M. Huszar, and P. Altevogt, 2003, L1 expression as a predictor of progression and survival in patients with uterine and ovarian carcinomas: Lancet, v. 362, p. 869-75.

Fonseca, R., P. L. Bergsagel, J. Drach, J. Shaughnessy, N. Gutierrez, A. K. Stewart, G. Morgan, B. Van Ness, M. Chesi, S. Minvielle, A. Neri, B. Barlogie, W. M. Kuehl, P. Liebisch, F. Davies, S. Chen-Kiang, B. G. Durie, R. Carrasco, O. Sezer, T. Reiman, L. Pilarski, H. Avet-Loiseau, and I. M. W. Group, 2009, International Myeloma Working Group molecular classification of multiple myeloma: spotlight review: Leukemia, v. 23, p. 2210-21.

Fukami, Y., and F. Lipmann, 1983, Reversal of Rous sarcoma-specific immunoglobulin phosphorylation on tyrosine (ADP as phosphate acceptor) catalyzed by the src gene kinase: Proc Natl Acad Sci U S A, v. 80, p. 1872-6.

Fukushima, C., A. Murakami, K. Yoshitomi, K. Sueoka, S. Nawata, K. Nakamura, and N. Sugino, 2011, Comparative proteomic profiling in squamous cell carcinoma of the uterine cervix: Proteomics Clin Appl, v. 5, p. 133-40.

Funaro, A., G. C. Spagnoli, M. Momo, W. Knapp, and F. Malavasi, 1994, Stimulation of T cells via CD44 requires leukocyte-function-associated antigen interactions and interleukin-2 production: Hum Immunol, v. 40, p. 267-78.

Gambhir, K. K., J. Ornasir, V. Headings, and A. Bonar, 2007, Decreased total carbonic anhydrase esterase activity and decreased levels of carbonic anhydrase 1 isozyme in erythrocytes of type II diabetic patients: Biochem Genet, v. 45, p. 431-9.

Gez, S., B. Crossett, and R. I. Christopherson, 2007, Differentially expressed cytosolic proteins in human leukemia and lymphoma cell lines correlate with lineages and functions: Biochim Biophys Acta, v. 1774, p. 1173-83.

Gilmore, T. D., 2007, Multiple myeloma: lusting for NF-kappaB: Cancer Cell, v. 12, p. 95-7.

Gonzalez de Castro, D., P. A. Clarke, B. Al-Lazikani, and P. Workman, 2013, Personalized cancer medicine: molecular diagnostics, predictive biomarkers, and drug resistance: Clin Pharmacol Ther, v. 93, p. 252-9.

Graham, G. J., E. G. Wright, R. Hewick, S. D. Wolpe, N. M. Wilkie, D. Donaldson, S. Lorimore, and I. B. Pragnell, 1990, Identification and characterization of an inhibitor of haemopoietic stem cell proliferation: Nature, v. 344, p. 442-4.

Grassl, N., N. A. Kulak, G. Pichler, P. E. Geyer, J. Jung, S. Schubert, P. Sinitcyn, J. Cox, and M. Mann, 2016, Ultra-deep and quantitative saliva proteome reveals dynamics of the oral microbiome: Genome Med, v. 8, p. 44.

Greipp, P. R., J. San Miguel, B. G. Durie, J. J. Crowley, B. Barlogie, J. Bladé, M. Boccadoro, J. A. Child, H. Avet-Loiseau, J. L. Harousseau, R. A. Kyle, J. J. Lahuerta, H. Ludwig, G. Morgan, R. Powles, K. Shimizu, C. Shustik, P. Sonneveld, P. Tosi, I. Turesson, and J. Westin, 2005, International staging system for multiple myeloma: J Clin Oncol, v. 23, p. 3412-20.

Group, F.-N. B. W., 2016, BEST (Biomarkers, EndpointS, and other Tools) Resource.

Group, I. M. W., 2003, Criteria for the classification of monoclonal gammopathies, multiple myeloma and related disorders: a report of the International Myeloma Working Group: Br J Haematol, v. 121, p. 749-57.

Group., B. D. W., 2001, Biomarkers and surrogate endpoints: preferred definitions and conceptual framework: Clin Pharmacol Ther, v. 69, p. 89-95.

Hari, P. N., M. J. Zhang, V. Roy, W. S. Pérez, A. Bashey, L. B. To, G. Elfenbein, C. O. Freytes, R. P. Gale, J. Gibson, R. A. Kyle, H. M. Lazarus, P. L. McCarthy, G. A. Milone, S. Pavlovsky, D. E. Reece, G. Schiller, J. Vela-Ojeda, D. Weisdorf, and D. Vesole, 2009, Is the International Staging System superior to the Durie-Salmon staging system? A comparison in multiple myeloma patients undergoing autologous transplant: Leukemia, v. 23, p. 1528-34.

Heinrich, R., B. G. Neel, and T. A. Rapoport, 2002, Mathematical models of protein kinase signal transduction: Mol Cell, v. 9, p. 957-70.

Hideshima, T., C. Mitsiades, G. Tonon, P. G. Richardson, and K. C. Anderson, 2007, Understanding multiple myeloma pathogenesis in the bone marrow to identify new therapeutic targets: Nat Rev Cancer, v. 7, p. 585-98.

Hu, B., Q. Zhou, T. Wu, L. Zhuang, L. Yi, J. Cao, X. Yang, and J. Wang, 2017, Efficacy and safety of subcutaneous versus intravenous bortezomib in multiple myeloma: a meta-analysis: Int J Clin Pharmacol Ther, v. 55, p. 329-338.

Huang, C., S. Martin, C. Pfleger, J. Du, J. H. Buckner, J. A. Bluestone, J. L. Riley, and S. F. Ziegler, 2013, Cutting Edge: a novel, human-specific interacting protein couples FOXP3 to a chromatin-remodeling complex that contains KAP1/TRIM28: J Immunol, v. 190, p. 4470-3.

Huang, P. Y., S. Mactier, N. Armacki, O. Giles Best, L. Belov, K. L. Kaufman, D. Pascovici, S. P. Mulligan, and R. I. Christopherson, 2016, Protein profiles distinguish stable and progressive chronic lymphocytic leukemia: Leuk Lymphoma, v. 57, p. 1033-43.

Hungria, V. T., A. Maiolino, G. Martinez, G. W. Colleoni, E. O. Coelho, L. Rocha, R. Nunes, R. Bittencourt, L. C. Oliveira, R. M. Faria, R. Pasquini, S. M. Magalhães, C.

A. Souza, J. V. Pinto Neto, L. Barreto, E. Andrade, M. o. S. Portella, V. Bolejack, B. G. Durie, and I. M. W. G. L. America, 2008, Confirmation of the utility of the International Staging System and identification of a unique pattern of disease in Brazilian patients with multiple myeloma: Haematologica, v. 93, p. 791-2.

Ihara, M., K. Ashizawa, K. Shichijo, and T. Kudo, 2019, Expression of the DNA-dependent protein kinase catalytic subunit is associated with the radiosensitivity of human thyroid cancer cell lines: J Radiat Res, v. 60, p. 171-177.

Imai, Y., E. Ohta, S. Takeda, S. Sunamura, M. Ishibashi, H. Tamura, Y. H. Wang, A. Deguchi, J. Tanaka, Y. Maru, and T. Motoji, 2016, Histone deacetylase inhibitor panobinostat induces calcineurin degradation in multiple myeloma: JCI Insight, v. 1, p. e85061.

Janowski, M., 2009, Functional diversity of SDF-1 splicing variants: Cell Adh Migr, v. 3, p. 243-9.

Jin, H., X. Cheng, Y. Pei, J. Fu, Z. Lyu, H. Peng, Q. Yao, Y. Jiang, L. Luo, and H. Zhuo, 2016, Identification and verification of transgelin-2 as a potential biomarker of tumor-derived lung-cancer endothelial cells by comparative proteomics: J Proteomics, v. 136, p. 77-88.

Johdi, N. A., L. Mazlan, I. Sagap, and R. Jamal, 2017, Profiling of cytokines, chemokines and other soluble proteins as a potential biomarker in colorectal cancer and polyps: Cytokine, v. 99, p. 35-42.

Juarez, J., A. Dela Pena, R. Baraz, J. Hewson, M. Khoo, A. Cisterne, S. Fricker, N. Fujii, K. F. Bradstock, and L. J. Bendall, 2007, CXCR4 antagonists mobilize childhood acute lymphoblastic leukemia cells into the peripheral blood and inhibit engraftment: Leukemia, v. 21, p. 1249-57.

Kang, S. H., K. W. Kang, K. H. Kim, B. Kwon, S. K. Kim, H. Y. Lee, S. Y. Kong, E. S. Lee, S. G. Jang, and B. C. Yoo, 2008, Upregulated HSP27 in human breast cancer cells reduces Herceptin susceptibility by increasing Her2 protein stability: BMC Cancer, v. 8, p. 286.

Katsogiannou, M., C. Andrieu, and P. Rocchi, 2014, Heat shock protein 27 phosphorylation state is associated with cancer progression: Front Genet, v. 5, p. 346.

Klose, J., 1975, Protein mapping by combined isoelectric focusing and electrophoresis of mouse tissues. A novel approach to testing for induced point mutations in mammals: Humangenetik, v. 26, p. 231-43.

Kovacs, J. J., P. J. Murphy, S. Gaillard, X. Zhao, J. T. Wu, C. V. Nicchitta, M. Yoshida, D. O. Toft, W. B. Pratt, and T. P. Yao, 2005, HDAC6 regulates Hsp90 acetylation and chaperone-dependent activation of glucocorticoid receptor: Mol Cell, v. 18, p. 601-7.

Kregel, K. C., 2002, Heat shock proteins: modifying factors in physiological stress responses and acquired thermotolerance: J Appl Physiol (1985), v. 92, p. 2177-86.

Kryczek, I., A. Lange, P. Mottram, X. Alvarez, P. Cheng, M. Hogan, L. Moons, S. Wei, L. Zou, V. Machelon, D. Emilie, M. Terrassa, A. Lackner, T. J. Curiel, P. Carmeliet, and W. Zou, 2005, CXCL12 and vascular endothelial growth factor synergistically induce neoangiogenesis in human ovarian cancers: Cancer Res, v. 65, p. 465-72.

Kumar, S. K., M. A. Dimopoulos, E. Kastritis, E. Terpos, H. Nahi, H. Goldschmidt, J. Hillengass, X. Leleu, M. Beksac, M. Alsina, A. Oriol, M. Cavo, E. M. Ocio, M. V. Mateos, E. K. O'Donnell, R. Vij, H. M. Lokhorst, N. W. C. J. van de Donk, C. Min, T. Mark, I. Turesson, M. Hansson, H. Ludwig, S. Jagannath, M. Delforge, C. Kyriakou, P. Hari, U. Mellqvist, S. Z. Usmani, D. Dytfeld, A. Z. Badros, P. Moreau, K. Kim, P. R. Otero, J. H. Lee, C. Shustik, D. Waller, W. J. Chng, S. Ozaki, J. J. Lee, J. de la Rubia, H. S. Eom, L. Rosinol, J. J. Lahuerta, A. Sureda, J. S. Kim, and B. G. M. Durie, 2017, Natural history of relapsed myeloma, refractory to immunomodulatory drugs and proteasome inhibitors: a multicenter IMWG study: Leukemia, v. 31, p. 2443-2448.

Kumar, S. K., J. H. Lee, J. J. Lahuerta, G. Morgan, P. G. Richardson, J. Crowley, J. Haessler, J. Feather, A. Hoering, P. Moreau, X. LeLeu, C. Hulin, S. K. Klein, P. Sonneveld, D. Siegel, J. Bladé, H. Goldschmidt, S. Jagannath, J. S. Miguel, R. Orlowski, A. Palumbo, O. Sezer, S. V. Rajkumar, B. G. Durie, and I. M. W. Group, 2012, Risk of progression and survival in multiple myeloma relapsing after therapy with IMiDs and bortezomib: a multicenter international myeloma working group study: Leukemia, v. 26, p. 149-57.

Kuo, H. C., C. C. Chiu, W. C. Chang, J. M. Sheen, C. Y. Ou, R. F. Chen, T. Y. Hsu, J. C. Chang, C. C. Hsaio, F. S. Wang, C. C. Huang, H. Y. Huang, and K. D. Yang, 2011, Use of proteomic differential displays to assess functional discrepancies and adjustments of human bone marrow- and Wharton jelly-derived mesenchymal stem cells: J Proteome Res, v. 10, p. 1305-15.

Kyle, R. A., 1984, 'Benign' monoclonal gammopathy. A misnomer?: JAMA, v. 251, p. 1849-54.

Kyle, R. A., B. G. Durie, S. V. Rajkumar, O. Landgren, J. Blade, G. Merlini, N. Kröger, H. Einsele, D. H. Vesole, M. Dimopoulos, J. San Miguel, H. Avet-Loiseau, R. Hajek, W. M. Chen, K. C. Anderson, H. Ludwig, P. Sonneveld, S. Pavlovsky, A. Palumbo, P. G. Richardson, B. Barlogie, P. Greipp, R. Vescio, I. Turesson, J. Westin, M. Boccadoro, and I. M. W. Group, 2010, Monoclonal gammopathy of undetermined significance (MGUS) and smoldering (asymptomatic) multiple myeloma: IMWG consensus perspectives risk factors for progression and guidelines for monitoring and management: Leukemia, v. 24, p. 1121-7.

Kyle, R. A., T. M. Therneau, S. V. Rajkumar, D. R. Larson, M. F. Plevak, and L. J. Melton, 2004, Long-term follow-up of 241 patients with monoclonal gammopathy of undetermined significance: the original Mayo Clinic series 25 years later: Mayo Clin Proc, v. 79, p. 859-66.

Kyle, R. A., T. M. Therneau, S. V. Rajkumar, D. R. Larson, M. F. Plevak, J. R. Offord, A. Dispenzieri, J. A. Katzmann, and L. J. Melton, 2006, Prevalence of monoclonal gammopathy of undetermined significance: N Engl J Med, v. 354, p. 1362-9.

Lander, E. S., 2011, Initial impact of the sequencing of the human genome: Nature, v. 470, p. 187-97.

Lane, C. S., 2005, Mass spectrometry-based proteomics in the life sciences: Cell Mol Life Sci, v. 62, p. 848-69.

Laubach, J., L. Garderet, A. Mahindra, G. Gahrton, J. Caers, O. Sezer, P. Voorhees, X. Leleu, H. E. Johnsen, M. Streetly, A. Jurczyszyn, H. Ludwig, U. H. Mellqvist, W. J. Chng, L. Pilarski, H. Einsele, J. Hou, I. Turesson, E. Zamagni, C. S. Chim, A. Mazumder, J. Westin, J. Lu, T. Reiman, S. Kristinsson, D. Joshua, M. Roussel, P. O'Gorman, E. Terpos, P. McCarthy, M. Dimopoulos, P. Moreau, R. Z. Orlowski, J. S. Miguel, K. C. Anderson, A. Palumbo, S. Kumar, V. Rajkumar, B. Durie, and P. G. Richardson, 2016, Management of relapsed multiple myeloma: recommendations of the International Myeloma Working Group: Leukemia, v. 30, p. 1005-17.

Leal, T. B., S. C. Remick, C. H. Takimoto, R. K. Ramanathan, A. Davies, M. J. Egorin, A. Hamilton, P. A. LoRusso, S. Shibata, H. J. Lenz, J. Mier, J. Sarantopoulos, S. Mani, J. J. Wright, S. P. Ivy, R. Neuwirth, L. von Moltke, K. Venkatakrishnan, and D. Mulkerin, 2011, Dose-escalating and pharmacological study of bortezomib in adult cancer patients with impaired renal function: a National Cancer Institute Organ Dysfunction Working Group Study: Cancer Chemother Pharmacol, v. 68, p. 1439-47.

Lee, S. C., M. E. Brummet, S. Shahabuddin, T. G. Woodworth, S. N. Georas, K. M. Leiferman, S. C. Gilman, C. Stellato, R. P. Gladue, R. P. Schleimer, and L. A. Beck, 2000, Cutaneous injection of human subjects with macrophage inflammatory protein-1 alpha induces significant recruitment of neutrophils and monocytes: J Immunol, v. 164, p. 3392-401.

Lee, S. D., D. Yu, D. Y. Lee, H. S. Shin, J. H. Jo, and Y. C. Lee, 2019, Upregulated microRNA-193a-3p is responsible for cisplatin resistance in CD44(+) gastric cancer cells: Cancer Sci, v. 110, p. 662-673.

Leng, S. X., J. E. McElhaney, J. D. Walston, D. Xie, N. S. Fedarko, and G. A. Kuchel, 2008, ELISA and multiplex technologies for cytokine measurement in inflammation and aging research: J Gerontol A Biol Sci Med Sci, v. 63, p. 879-84.

Lentzsch, S., M. Gries, M. Janz, R. Bargou, B. Dörken, and M. Y. Mapara, 2003, Macrophage inflammatory protein 1-alpha (MIP-1 alpha) triggers migration and signaling cascades mediating survival and proliferation in multiple myeloma (MM) cells: Blood, v. 101, p. 3568-73.

Lewis, C., P. Doran, and K. Ohlendieck, 2012, Proteomic analysis of dystrophic muscle: Methods Mol Biol, v. 798, p. 357-69.

Lind, J., F. Czernilofsky, S. Vallet, and K. Podar, 2019, Emerging protein kinase inhibitors for the treatment of multiple myeloma: Expert Opin Emerg Drugs, p. 1-20.

Lisch, W., J. Wasielica-Poslednik, T. Kivelä, U. Schlötzer-Schrehardt, J. M. Rohrbach, W. Sekundo, U. Pleyer, C. Lisch, A. Desuki, H. Rossmann, and J. S. Weiss, 2016, The Hematologic Definition of Monoclonal Gammopathy of Undetermined Significance in Relation to Paraproteinemic Keratopathy (An American Ophthalmological Society Thesis): Trans Am Ophthalmol Soc, v. 114, p. T7.

Liu, C. L., S. F. Chen, M. Z. Wu, S. W. Jao, Y. S. Lin, C. Y. Yang, T. Y. Lee, L. W. Wen, G. L. Lan, and S. Nieh, 2016, The molecular and clinical verification of therapeutic resistance via the p38 MAPK-Hsp27 axis in lung cancer: Oncotarget, v. 7, p. 14279-90.

Liu, H., Z. Li, M. Deng, Q. Liu, T. Zhang, W. Guo, P. Li, and W. Qiao, 2018, Prognostic and clinicopathological value of CXCL12/SDF1 expression in breast cancer: A meta-analysis: Clin Chim Acta, v. 484, p. 72-80.

Lonial, S., E. K. Waller, P. G. Richardson, S. Jagannath, R. Z. Orlowski, C. R. Giver, D. L. Jaye, D. Francis, S. Giusti, C. Torre, B. Barlogie, J. R. Berenson, S. Singhal, D. P. Schenkein, D. L. Esseltine, J. Anderson, H. Xiao, L. T. Heffner, K. C. Anderson, and S. C. Investigators, 2005, Risk factors and kinetics of thrombocytopenia associated with bortezomib for relapsed, refractory multiple myeloma: Blood, v. 106, p. 3777-84.

LoRusso, P. M., K. Venkatakrishnan, R. K. Ramanathan, J. Sarantopoulos, D. Mulkerin, S. I. Shibata, A. Hamilton, A. Dowlati, S. Mani, M. A. Rudek, C. H. Takimoto, R. Neuwirth, D. L. Esseltine, and P. Ivy, 2012, Pharmacokinetics and safety of bortezomib in patients with advanced malignancies and varying degrees of liver dysfunction: phase I NCI Organ Dysfunction Working Group Study NCI-6432: Clin Cancer Res, v. 18, p. 2954-63.

Löwenberg, B., 2013, Sense and nonsense of high-dose cytarabine for acute myeloid leukemia: Blood, v. 121, p. 26-8.

Majumder, M. M., R. Silvennoinen, P. Anttila, D. Tamborero, S. Eldfors, B. Yadav, R. Karjalainen, H. Kuusanmäki, J. Lievonen, A. Parsons, M. Suvela, E. Jantunen, K. Porkka, and C. A. Heckman, 2017, Identification of precision treatment strategies for relapsed/refractory multiple myeloma by functional drug sensitivity testing: Oncotarget, v. 8, p. 56338-56350.

Maness, P. F., and M. Schachner, 2007, Neural recognition molecules of the immunoglobulin superfamily: signaling transducers of axon guidance and neuronal migration: Nat Neurosci, v. 10, p. 19-26.

Manning, G., D. B. Whyte, R. Martinez, T. Hunter, and S. Sudarsanam, 2002, The protein kinase complement of the human genome: Science, v. 298, p. 1912-34.

Massagué, J., and A. Pandiella, 1993, Membrane-anchored growth factors: Annu Rev Biochem, v. 62, p. 515-41.

Mayya, V., and D. K. Han, 2009, Phosphoproteomics by mass spectrometry: insights, implications, applications and limitations: Expert Rev Proteomics, v. 6, p. 605-18.

Menzies-Gow, A., S. Ying, I. Sabroe, V. L. Stubbs, D. Soler, T. J. Williams, and A. B. Kay, 2002, Eotaxin (CCL11) and eotaxin-2 (CCL24) induce recruitment of eosinophils, basophils, neutrophils, and macrophages as well as features of early- and late-phase allergic reactions following cutaneous injection in human atopic and nonatopic volunteers: J Immunol, v. 169, p. 2712-8.

Michigami, T., N. Shimizu, P. J. Williams, M. Niewolna, S. L. Dallas, G. R. Mundy, and T. Yoneda, 2000, Cell-cell contact between marrow stromal cells and myeloma cells via VCAM-1 and alpha(4)beta(1)-integrin enhances production of osteoclast-stimulating activity: Blood, v. 96, p. 1953-60.

Minami, K., K. Hiwatashi, S. Ueno, M. Sakoda, S. Iino, H. Okumura, M. Hashiguchi, Y. Kawasaki, H. Kurahara, Y. Mataki, K. Maemura, H. Shinchi, and S. Natsugoe, 2018, Prognostic significance of CD68, CD163 and Folate receptor-β positive macrophages in hepatocellular carcinoma: Exp Ther Med, v. 15, p. 4465-4476.

Miyagaki, T., M. Sugaya, T. Murakami, Y. Asano, Y. Tada, T. Kadono, H. Okochi, K. Tamaki, and S. Sato, 2011, CCL11-CCR3 interactions promote survival of anaplastic large cell lymphoma cells via ERK1/2 activation: Cancer Res, v. 71, p. 2056-65.

Moore, N., M. Moreno Gonzales, K. Bonner, B. Smith, W. Park, and M. Stegall, 2017, Impact of CXCR4/CXCL12 Blockade on Normal Plasma Cells In Vivo: Am J Transplant, v. 17, p. 1663-1669.

Mori-Iwamoto, S., Y. Kuramitsu, S. Ryozawa, K. Mikuria, M. Fujimoto, S. Maehara, Y. Maehara, K. Okita, K. Nakamura, and I. Sakaida, 2007, Proteomics finding heat shock protein 27 as a biomarker for resistance of pancreatic cancer cells to gemcitabine: Int J Oncol, v. 31, p. 1345-50.

Murphree, A. L., and W. F. Benedict, 1984, Retinoblastoma: clues to human oncogenesis: Science, v. 223, p. 1028-33.

Nervi, B., P. Ramirez, M. P. Rettig, G. L. Uy, M. S. Holt, J. K. Ritchey, J. L. Prior, D. Piwnica-Worms, G. Bridger, T. J. Ley, and J. F. DiPersio, 2009, Chemosensitization of acute myeloid leukemia (AML) following mobilization by the CXCR4 antagonist AMD3100: Blood, v. 113, p. 6206-14.

Nishi, H., K. Hashimoto, and A. R. Panchenko, 2011, Phosphorylation in protein-protein binding: effect on stability and function: Structure, v. 19, p. 1807-15.

Nishi, H., A. Shaytan, and A. R. Panchenko, 2014, Physicochemical mechanisms of protein regulation by phosphorylation: Front Genet, v. 5, p. 270.

Nolen, B. M., and A. E. Lokshin, 2010, Targeting CCL11 in the treatment of ovarian cancer: Expert Opin Ther Targets, v. 14, p. 157-67.

O'Farrell, P. H., 1975, High resolution two-dimensional electrophoresis of proteins: J Biol Chem, v. 250, p. 4007-21.

Obeng, E. A., L. M. Carlson, D. M. Gutman, W. J. Harrington, K. P. Lee, and L. H. Boise, 2006, Proteasome inhibitors induce a terminal unfolded protein response in multiple myeloma cells: Blood, v. 107, p. 4907-16.

Oddoze, C., E. Lombard, and H. Portugal, 2012, Stability study of 81 analytes in human whole blood, in serum and in plasma: Clin Biochem, v. 45, p. 464-9.

Ohlendieck, K., 2011, Skeletal muscle proteomics: current approaches, technical challenges and emerging techniques: Skelet Muscle, v. 1, p. 6.

Ohlendieck, K., 2013, Proteomic identification of biomarkers of skeletal muscle disorders: Biomark Med, v. 7, p. 169-86.

Ohwada, C., C. Nakaseko, M. Koizumi, M. Takeuchi, S. Ozawa, M. Naito, H. Tanaka, K. Oda, R. Cho, M. Nishimura, and Y. Saito, 2008, CD44 and hyaluronan engagement promotes dexamethasone resistance in human myeloma cells: Eur J Haematol, v. 80, p. 245-50.

Olsen, J. V., B. Blagoev, F. Gnad, B. Macek, C. Kumar, P. Mortensen, and M. Mann, 2006, Global, in vivo, and site-specific phosphorylation dynamics in signaling networks: Cell, v. 127, p. 635-48.

Olsen, J. V., M. Vermeulen, A. Santamaria, C. Kumar, M. L. Miller, L. J. Jensen, F. Gnad, J. Cox, T. S. Jensen, E. A. Nigg, S. Brunak, and M. Mann, 2010, Quantitative phosphoproteomics reveals widespread full phosphorylation site occupancy during mitosis: Sci Signal, v. 3, p. ra3.

Parlati, F., S. J. Lee, M. Aujay, E. Suzuki, K. Levitsky, J. B. Lorens, D. R. Micklem, P. Ruurs, C. Sylvain, Y. Lu, K. D. Shenk, and M. K. Bennett, 2009, Carfilzomib can induce tumor cell death through selective inhibition of the chymotrypsin-like activity of the proteasome: Blood, v. 114, p. 3439-47.

Patel, J. P., M. Gönen, M. E. Figueroa, H. Fernandez, Z. Sun, J. Racevskis, P. Van Vlierberghe, I. Dolgalev, S. Thomas, O. Aminova, K. Huberman, J. Cheng, A. Viale, N. D. Socci, A. Heguy, A. Cherry, G. Vance, R. R. Higgins, R. P. Ketterling, R. E. Gallagher, M. Litzow, M. R. van den Brink, H. M. Lazarus, J. M. Rowe, S. Luger, A. Ferrando, E. Paietta, M. S. Tallman, A. Melnick, O. Abdel-Wahab, and R. L. Levine, 2012, Prognostic relevance of integrated genetic profiling in acute myeloid leukemia: N Engl J Med, v. 366, p. 1079-89.

Paulovich, A. G., J. R. Whiteaker, A. N. Hoofnagle, and P. Wang, 2008, The interface between biomarker discovery and clinical validation: The tar pit of the protein biomarker pipeline: Proteomics Clin Appl, v. 2, p. 1386-1402.

Pearse, R. N., E. M. Sordillo, S. Yaccoby, B. R. Wong, D. F. Liau, N. Colman, J. Michaeli, J. Epstein, and Y. Choi, 2001, Multiple myeloma disrupts the TRANCE/ osteoprotegerin cytokine axis to trigger bone destruction and promote tumor progression: Proc Natl Acad Sci U S A, v. 98, p. 11581-6.

Pemovska, T., M. Kontro, B. Yadav, H. Edgren, S. Eldfors, A. Szwajda, H. Almusa, M. M. Bespalov, P. Ellonen, E. Elonen, B. T. Gjertsen, R. Karjalainen, E. Kulesskiy, S. Lagström, A. Lehto, M. Lepistö, T. Lundán, M. M. Majumder, J. M. Marti, P. Mattila, A. Murumägi, S. Mustjoki, A. Palva, A. Parsons, T. Pirttinen, M. E. Rämet, M. Suvela, L. Turunen, I. Västrik, M. Wolf, J. Knowles, T. Aittokallio, C. A. Heckman, K. Porkka, O. Kallioniemi, and K. Wennerberg, 2013, Individualized systems medicine strategy to tailor treatments for patients with chemorefractory acute myeloid leukemia: Cancer Discov, v. 3, p. 1416-29.

Pocker, Y., and S. Sarkanen, 1978, Carbonic anhydrase: structure catalytic versatility, and inhibition: Adv Enzymol Relat Areas Mol Biol, v. 47, p. 149-274.

Purohit, S., A. Sharma, and J. X. She, 2015, Luminex and other multiplex high throughput technologies for the identification of, and host response to, environmental triggers of type 1 diabetes: Biomed Res Int, v. 2015, p. 326918.

Rabilloud, T., and C. Lelong, 2011, Two-dimensional gel electrophoresis in proteomics: a tutorial: J Proteomics, v. 74, p. 1829-41.

Rajkumar, S. V., 2016, Updated Diagnostic Criteria and Staging System for Multiple Myeloma: Am Soc Clin Oncol Educ Book, v. 35, p. e418-23.

Rajkumar, S. V., M. A. Dimopoulos, A. Palumbo, J. Blade, G. Merlini, M. V. Mateos, S. Kumar, J. Hillengass, E. Kastritis, P. Richardson, O. Landgren, B. Paiva, A. Dispenzieri, B. Weiss, X. LeLeu, S. Zweegman, S. Lonial, L. Rosinol, E. Zamagni, S. Jagannath, O. Sezer, S. Y. Kristinsson, J. Caers, S. Z. Usmani, J. J. Lahuerta, H. E. Johnsen, M. Beksac, M. Cavo, H. Goldschmidt, E. Terpos, R. A. Kyle, K. C. Anderson, B. G. Durie, and J. F. Miguel, 2014, International Myeloma Working Group updated criteria for the diagnosis of multiple myeloma: Lancet Oncol, v. 15, p. e538-48.

Ramasamy, P., C. C. Murphy, M. Clynes, N. Horgan, P. Moriarty, D. Tiernan, S. Beatty, S. Kennedy, and P. Meleady, 2014, Proteomics in uveal melanoma: Exp Eye Res, v. 118, p. 1-12.

Richardson, P. G., H. Briemberg, S. Jagannath, P. Y. Wen, B. Barlogie, J. Berenson, S. Singhal, D. S. Siegel, D. Irwin, M. Schuster, G. Srkalovic, R. Alexanian, S. V. Rajkumar, S. Limentani, M. Alsina, R. Z. Orlowski, K. Najarian, D. Esseltine, K. C. Anderson, and A. A. Amato, 2006, Frequency, characteristics, and reversibility of peripheral neuropathy during treatment of advanced multiple myeloma with bortezomib: J Clin Oncol, v. 24, p. 3113-20.

Richardson, P. G., W. Xie, C. Mitsiades, A. A. Chanan-Khan, S. Lonial, H. Hassoun, D. E. Avigan, A. L. Oaklander, D. J. Kuter, P. Y. Wen, S. Kesari, H. R. Briemberg, R. L.

Schlossman, N. C. Munshi, L. T. Heffner, D. Doss, D. L. Esseltine, E. Weller, K. C. Anderson, and A. A. Amato, 2009, Single-agent bortezomib in previously untreated multiple myeloma: efficacy, characterization of peripheral neuropathy, and molecular correlations with response and neuropathy: J Clin Oncol, v. 27, p. 3518-25.

Rifai, N., M. A. Gillette, and S. A. Carr, 2006, Protein biomarker discovery and validation: the long and uncertain path to clinical utility: Nat Biotechnol, v. 24, p. 971-83.

Rombouts, E. J., B. Pavic, B. Löwenberg, and R. E. Ploemacher, 2004, Relation between CXCR-4 expression, Flt3 mutations, and unfavorable prognosis of adult acute myeloid leukemia: Blood, v. 104, p. 550-7.

Roskoski, R., 2012, ERK1/2 MAP kinases: structure, function, and regulation: Pharmacol Res, v. 66, p. 105-43.

Roussel, M., V. Lauwers-Cances, N. Robillard, C. Hulin, X. Leleu, L. Benboubker, G. Marit, P. Moreau, B. Pegourie, D. Caillot, C. Fruchart, A. M. Stoppa, C. Gentil, S. Wuilleme, A. Huynh, B. Hebraud, J. Corre, M. L. Chretien, T. Facon, H. Avet-Loiseau, and M. Attal, 2014, Front-line transplantation program with lenalidomide, bortezomib, and dexamethasone combination as induction and consolidation followed by lenalidomide maintenance in patients with multiple myeloma: a phase II study by the Intergroupe Francophone du Myélome: J Clin Oncol, v. 32, p. 2712-7.

Rubio, D. M., E. E. Schoenbaum, L. S. Lee, D. E. Schteingart, P. R. Marantz, K. E. Anderson, L. D. Platt, A. Baez, and K. Esposito, 2010, Defining translational research: implications for training: Acad Med, v. 85, p. 470-5.

Sabattini, E., F. Bacci, C. Sagramoso, and S. A. Pileri, 2010, WHO classification of tumours of haematopoietic and lymphoid tissues in 2008: an overview: Pathologica, v. 102, p. 83-7.

Sacco, F., L. Perfetto, L. Castagnoli, and G. Cesareni, 2012, The human phosphatase interactome: An intricate family portrait: FEBS Lett, v. 586, p. 2732-9.

Sawyer, J. R., 2011, The prognostic significance of cytogenetics and molecular profiling in multiple myeloma: Cancer Genet, v. 204, p. 3-12.

Scheele, G. A., 1975, Two-dimensional gel analysis of soluble proteins. Charaterization of guinea pig exocrine pancreatic proteins: J Biol Chem, v. 250, p. 5375-85.

Schelker, R. C., S. Iberl, G. Müller, C. Hart, W. Herr, and J. Grassinger, 2018, TGF-β1 and CXCL12 modulate proliferation and chemotherapy sensitivity of acute myeloid leukemia cells co-cultured with multipotent mesenchymal stromal cells: Hematology, v. 23, p. 337-345.

Schuringa, J. J., A. T. Wierenga, W. Kruijer, and E. Vellenga, 2000, Constitutive Stat3, Tyr705, and Ser727 phosphorylation in acute myeloid leukemia cells caused by the autocrine secretion of interleukin-6: Blood, v. 95, p. 3765-70.

Schwartz, P. A., and B. W. Murray, 2011, Protein kinase biochemistry and drug discovery: Bioorg Chem, v. 39, p. 192-210.

Seminerio, I., N. Kindt, G. Descamps, J. Bellier, J. R. Lechien, Q. Mat, C. Pottier, F. Journé, and S. Saussez, 2018, High infiltration of CD68+ macrophages is associated with poor prognoses of head and neck squamous cell carcinoma patients and is influenced by human papillomavirus: Oncotarget, v. 9, p. 11046-11059.

Sheng, G., J. Zhang, Z. Zeng, J. Pan, Q. Wang, L. Wen, Y. Xu, D. Wu, and S. Chen, 2017, Identification of a novel CSF3R-SPTAN1 fusion gene in an atypical chronic myeloid leukemia patient with t(1;9)(p34;q34) by RNA-Seq: Cancer Genet, v. 216-217, p. 16-19.

Shrager, J., and J. M. Tenenbaum, 2014, Rapid learning for precision oncology: Nat Rev Clin Oncol, v. 11, p. 109-18.

Siegel, R. L., K. D. Miller, and A. Jemal, 2015, Cancer statistics, 2015: CA Cancer J Clin, v. 65, p. 5-29.

Smith, A., D. Howell, R. Patmore, A. Jack, and E. Roman, 2011, Incidence of haematological malignancy by sub-type: a report from the Haematological Malignancy Research Network: Br J Cancer, v. 105, p. 1684-92.

Sonneveld, P., 2017, Management of multiple myeloma in the relapsed/refractory patient: Hematology Am Soc Hematol Educ Program, v. 2017, p. 508-517.

Spoo, A. C., M. Lübbert, W. G. Wierda, and J. A. Burger, 2007, CXCR4 is a prognostic marker in acute myelogenous leukemia: Blood, v. 109, p. 786-91.

Stephens, P., S. Edkins, H. Davies, C. Greenman, C. Cox, C. Hunter, G. Bignell, J. Teague, R. Smith, C. Stevens, S. O'Meara, A. Parker, P. Tarpey, T. Avis, A. Barthorpe, L. Brackenbury, G. Buck, A. Butler, J. Clements, J. Cole, E. Dicks, K. Edwards, S. Forbes, M. Gorton, K. Gray, K. Halliday, R. Harrison, K. Hills, J. Hinton, D. Jones, V. Kosmidou, R. Laman, R. Lugg, A. Menzies, J. Perry, R. Petty, K. Raine, R. Shepherd, A. Small, H. Solomon, Y. Stephens, C. Tofts, J. Varian, A. Webb, S. West, S. Widaa, A. Yates, F. Brasseur, C. S. Cooper, A. M. Flanagan, A. Green, M. Knowles, S. Y. Leung, L. H. Looijenga, B. Malkowicz, M. A. Pierotti, B. Teh, S. T. Yuen, A. G. Nicholson, S. Lakhani, D. F. Easton, B. L. Weber, M. R. Stratton, P. A. Futreal, and R. Wooster, 2005, A screen of the complete protein kinase gene family identifies diverse patterns of somatic mutations in human breast cancer: Nat Genet, v. 37, p. 590-2.

Strimbu, K., and J. A. Tavel, 2010, What are biomarkers?: Curr Opin HIV AIDS, v. 5, p. 463-6.

Tangen, I. L., R. K. Kopperud, N. C. Visser, A. C. Staff, S. Tingulstad, J. Marcickiewicz, F. Amant, L. Bjørge, J. M. Pijnenborg, H. B. Salvesen, H. M. Werner, J. Trovik, and C. Krakstad, 2017, Expression of L1CAM in curettage or high L1CAM level in preoperative blood samples predicts lymph node metastases and poor outcome in endometrial cancer patients: Br J Cancer, v. 117, p. 840-847.

Tannu, N. S., and S. E. Hemby, 2006, Two-dimensional fluorescence difference gel electrophoresis for comparative proteomics profiling: Nat Protoc, v. 1, p. 1732-42.

Terpos, E., M. Politou, N. Viniou, and A. Rahemtulla, 2005, Significance of macrophage inflammatory protein-1 alpha (MIP-1alpha) in multiple myeloma: Leuk Lymphoma, v. 46, p. 1699-707.

Thomas, G. V., C. Tran, I. K. Mellinghoff, D. S. Welsbie, E. Chan, B. Fueger, J. Czernin, and C. L. Sawyers, 2006, Hypoxia-inducible factor determines sensitivity to inhibitors of mTOR in kidney cancer: Nat Med, v. 12, p. 122-7.

Thomas, P. D., M. J. Campbell, A. Kejariwal, H. Mi, B. Karlak, R. Daverman, K. Diemer, A. Muruganujan, and A. Narechania, 2003, PANTHER: a library of protein families and subfamilies indexed by function: Genome Res, v. 13, p. 2129-41.

Tsubaki, M., C. Kato, M. Manno, M. Ogaki, T. Satou, T. Itoh, T. Kusunoki, Y. Tanimori, K. Fujiwara, H. Matsuoka, and S. Nishida, 2007, Macrophage inflammatory protein-1alpha (MIP-1alpha) enhances a receptor activator of nuclear factor kappaB ligand (RANKL) expression in mouse bone marrow stromal cells and osteoblasts through MAPK and PI3K/Akt pathways: Mol Cell Biochem, v. 304, p. 53-60.

Tsubaki, M., T. Takeda, Y. Tomonari, K. Mashimo, Y. I. Koumoto, S. Hoshida, T. Itoh, M. Imano, T. Satou, K. Sakaguchi, and S. Nishida, 2018, The MIP-1α autocrine loop contributes to decreased sensitivity to anticancer drugs: J Cell Physiol, v. 233, p. 4258-4271.

Tsubaki, M., T. Takeda, M. Yoshizumi, E. Ueda, T. Itoh, M. Imano, T. Satou, and S. Nishida, 2016, RANK-RANKL interactions are involved in cell adhesion-mediated drug resistance in multiple myeloma cell lines: Tumour Biol, v. 37, p. 9099-110.

Ugge, H., M. K. Downer, J. Carlsson, M. Bowden, S. Davidsson, L. A. Mucci, K. Fall, S. O. Andersson, and O. Andrén, 2019, Circulating inflammation markers and prostate cancer: Prostate, v. 79, p. 1338-1346.

Unlü, M., M. E. Morgan, and J. S. Minden, 1997, Difference gel electrophoresis: a single gel method for detecting changes in protein extracts: Electrophoresis, v. 18, p. 2071-7.

Välikangas, T., T. Suomi, and L. L. Elo, 2018, A systematic evaluation of normalization methods in quantitative label-free proteomics: Brief Bioinform, v. 19, p. 1-11.

Vardiman, J. W., J. Thiele, D. A. Arber, R. D. Brunning, M. J. Borowitz, A. Porwit, N. L. Harris, M. M. Le Beau, E. Hellström-Lindberg, A. Tefferi, and C. D. Bloomfield, 2009, The 2008 revision of the World Health Organization (WHO) classification of myeloid neoplasms and acute leukemia: rationale and important changes: Blood, v. 114, p. 937-51.

Vogler, M., D. Dinsdale, M. J. Dyer, and G. M. Cohen, 2009, Bcl-2 inhibitors: small molecules with a big impact on cancer therapy: Cell Death Differ, v. 16, p. 360-7.

Vyse, S., H. Desmond, and P. H. Huang, 2017, Advances in mass spectrometry based strategies to study receptor tyrosine kinases: IUCrJ, v. 4, p. 119-130.

Walter, R. B., H. M. Kantarjian, X. Huang, S. A. Pierce, Z. Sun, H. M. Gundacker, F. Ravandi, S. H. Faderl, M. S. Tallman, F. R. Appelbaum, and E. H. Estey, 2010, Effect of complete remission and responses less than complete remission on survival in acute myeloid leukemia: a combined Eastern Cooperative Oncology Group, Southwest Oncology Group, and M. D. Anderson Cancer Center Study: J Clin Oncol, v. 28, p. 1766-71.

Walter, R. B., M. Othus, G. Borthakur, F. Ravandi, J. E. Cortes, S. A. Pierce, F. R. Appelbaum, H. A. Kantarjian, and E. H. Estey, 2011, Prediction of early death after induction therapy for newly diagnosed acute myeloid leukemia with pretreatment risk scores: a novel paradigm for treatment assignment: J Clin Oncol, v. 29, p. 4417-23.

Wang, Z., S. Sau, H. O. Alsaab, and A. K. Iyer, 2018, CD44 directed nanomicellar payload delivery platform for selective anticancer effect and tumor specific imaging of triple negative breast cancer: Nanomedicine, v. 14, p. 1441-1454.

Whiteaker, J. R., H. Zhang, L. Zhao, P. Wang, K. S. Kelly-Spratt, R. G. Ivey, B. D. Piening, L. C. Feng, E. Kasarda, K. E. Gurley, J. K. Eng, L. A. Chodosh, C. J. Kemp, M. W. McIntosh, and A. G. Paulovich, 2007a, Integrated pipeline for mass spectrometry-based discovery and confirmation of biomarkers demonstrated in a mouse model of breast cancer: J Proteome Res, v. 6, p. 3962-75.

Whiteaker, J. R., L. Zhao, H. Y. Zhang, L. C. Feng, B. D. Piening, L. Anderson, and A. G. Paulovich, 2007b, Antibody-based enrichment of peptides on magnetic beads for mass-spectrometry-based quantification of serum biomarkers: Anal Biochem, v. 362, p. 44-54.

Wu, J. D., C. Q. Hong, W. H. Huang, X. L. Wei, F. Zhang, Y. X. Zhuang, Y. Q. Zhang, and G. J. Zhang, 2018, L1 Cell Adhesion Molecule and Its Soluble Form sL1 Exhibit Poor Prognosis in Primary Breast Cancer Patients: Clin Breast Cancer, v. 18, p. e851-e861.

Yaccoby, S., M. J. Wezeman, A. Henderson, M. Cottler-Fox, Q. Yi, B. Barlogie, and J. Epstein, 2004, Cancer and the microenvironment: myeloma-osteoclast interactions as a model: Cancer Res, v. 64, p. 2016-23.

Yan, Y., X. Zuo, and D. Wei, 2015, Concise Review: Emerging Role of CD44 in Cancer Stem Cells: A Promising Biomarker and Therapeutic Target: Stem Cells Transl Med, v. 4, p. 1033-43.

Yang, C., C. Wei, S. Wang, D. Shi, C. Zhang, X. Lin, R. Dou, and B. Xiong, 2019, Elevated CD163: Int J Biol Sci, v. 15, p. 984-998.

Yang, J., Z. Wang, Y. Fang, J. Jiang, F. Zhao, H. Wong, M. K. Bennett, C. J. Molineaux, and C. J. Kirk, 2011, Pharmacokinetics, pharmacodynamics, metabolism, distribution, and excretion of carfilzomib in rats: Drug Metab Dispos, v. 39, p. 1873-82.

Yang, X., A. K. Iyer, A. Singh, E. Choy, F. J. Hornicek, M. M. Amiji, and Z. Duan, 2015, MDR1 siRNA loaded hyaluronic acid-based CD44 targeted nanoparticle systems circumvent paclitaxel resistance in ovarian cancer: Sci Rep, v. 5, p. 8509.

Ye, Z., J. Chen, Z. Xuan, and W. Yang, 2019, Subcutaneous bortezomib might be standard of care for patients with multiple myeloma: a systematic review and meta-analysis: Drug Des Devel Ther, v. 13, p. 1707-1716.

Yu, Z., G. Kastenmüller, Y. He, P. Belcredi, G. Möller, C. Prehn, J. Mendes, S. Wahl, W. Roemisch-Margl, U. Ceglarek, A. Polonikov, N. Dahmen, H. Prokisch, L. Xie, Y. Li, H. E. Wichmann, A. Peters, F. Kronenberg, K. Suhre, J. Adamski, T. Illig, and R. Wang-Sattler, 2011, Differences between human plasma and serum metabolite profiles: PLoS One, v. 6, p. e21230.

Zamanova, S., A. M. Shabana, U. K. Mondal, and M. A. Ilies, 2019, Carbonic anhydrases as disease markers: Expert Opin Ther Pat, v. 29, p. 509-533.

Zander, H., T. Rawnaq, M. von Wedemeyer, M. Tachezy, M. Kunkel, G. Wolters, M. Bockhorn, M. Schachner, J. R. Izbicki, and J. Kaifi, 2011, Circulating levels of cell adhesion molecule L1 as a prognostic marker in gastrointestinal stromal tumor patients: BMC Cancer, v. 11, p. 189:1-7.

Zaytseva, Y. Y., P. G. Rychahou, P. Gulhati, V. A. Elliott, W. C. Mustain, K. O'Connor, A. J. Morris, M. Sunkara, H. L. Weiss, E. Y. Lee, and B. M. Evers, 2012, Inhibition of fatty acid synthase attenuates CD44-associated signaling and reduces metastasis in colorectal cancer: Cancer Res, v. 72, p. 1504-17.

Zhang, J., C. Liu, X. Mo, H. Shi, and S. Li, 2018, Mechanisms by which CXCR4/CXCL12 cause metastatic behavior in pancreatic cancer: Oncol Lett, v. 15, p. 1771-1776.

Zhang, Y., E. Saavedra, R. Tang, Y. Gu, P. Lappin, D. Trajkovic, S. H. Liu, T. Smeal, V. Fantin, S. De Botton, O. Legrand, F. Delhommeau, F. Pernasetti, and F. Louache, 2017, Targeting primary acute myeloid leukemia with a new CXCR4 antagonist IgG1 antibody (PF-06747143): Sci Rep, v. 7, p. 7305.

Zhang, Y., G. M. Wen, C. A. Wu, Z. L. Jing, D. Z. Li, G. L. Liu, X. X. Wei, M. S. Tang, Y. H. Li, Y. Zhong, Y. J. Deng, and W. K. Yang, 2019a, PRKDC is a prognostic marker

for poor survival in gastric cancer patients and regulates DNA damage response: Pathol Res Pract, v. 215, p. 152509.

Zhang, Y., W. K. Yang, G. M. Wen, H. Tang, C. A. Wu, Y. X. Wu, Z. L. Jing, M. S. Tang, G. L. Liu, D. Z. Li, Y. H. Li, and Y. J. Deng, 2019b, High expression of PRKDC promotes breast cancer cell growth via p38 MAPK signaling and is associated with poor survival: Mol Genet Genomic Med, p. e908.

Zhou, H., S. Di Palma, C. Preisinger, M. Peng, A. N. Polat, A. J. Heck, and S. Mohammed, 2013, Toward a comprehensive characterization of a human cancer cell phosphoproteome: J Proteome Res, v. 12, p. 260-71.

Zhou, J., K. Mauerer, L. Farina, and J. G. Gribben, 2005, The role of the tumor microenvironment in hematological malignancies and implication for therapy: Front Biosci, v. 10, p. 1581-96.